EDITORIAL

A COMPARATIVE STUDY OF BIPOLAR DISORDER AND ATTENTION DEFICIT HYPERACTIVITY DISORDER THROUGH THE MEASUREMENT OF REGIONAL CEREBRAL BLOOD FLOW

M.C. DI TOMMASO

McLean Hospital, Harvard University, Cambridge, USA

Received March 26, 2011 – Accepted November 8, 2011

Attention Deficit Hyperactivity Disorder (ADHD) and Bipolar Disorder (BPD) are two common neuropsychological disorders which are often present in a comorbid state. I used the results of cerebral blood flow studies made with Single Photon Emission Computer Tomography (SPECT), Positron Emission Tomography (PET) and Functional Magnetic Resonance Imaging (fMRI), to investigate a possible relationship between ADHD and BPD. The common areas of the brain involved in both BPD and ADHD appears to be the prefrontal cortex in its various components, the basal ganglia and possibly the cerebellum which, especially in the past, has been little studied by researchers in relation to ADHD and BPD. Among the differences the blood flow lateralization, present in BPD in states of altered mood, is evident with left hypoperfusion and right hyperperfusion during depression, the opposite in the case of manic state; in ADHD, the lateralization is less constant and of questionable interpretation. In BPD the involvement of a greater number of brain areas, especially the temporal lobe, is common. I advance the hypothesis that BPD progresses from ADHD secondary to expansion of perturbation in cerebral blood flow.

The possibility of a relationship between Attention Deficit Hyperactivity Disorder (ADHD) and Bipolar Disorder (BPD) has of late been attracting great interest (1, 2). Some areas of deficit typical of ADHD, such as impairment in sustained attention, motor inhibition, verbal learning, memory, organization and problem solving (3) have been reported in BPD (4, 5).

Many of the diagnostic criteria for ADHD overlap with those of BPD, possibly resulting in mistaken diagnosis of mania. Likewise, hyperactivity in ADHD may be mistakenly diagnosed as BPD (6). Conversely, incidence of BPD co-diagnosed in children with ADHD (11% to 22% in outpatient and hospitalized patients, respectively) is also higher than that expected in comparison to the basal rate in an isolated sample population (1). Moreover, evidence has supported the assertion that the comorbid diagnosis of BPD in ADHD children is not due to artefact from overlapping symptoms: following the removal from the diagnostic procedure of overlapping symptoms such as hyperactivity and distractibility which could contribute to both diagnoses (7) argues that a significant proportion of individuals retain both diagnoses.

Though the diagnostic criteria for ADHD and BPD per the DSM-IV appear to be unrelated, there is evidence to suggest that a relationship may exist. Three hypotheses exist suggesting 1) the two conditions may be completely distinct and unrelated in any way to one another 2) the conditions may be distinct manifestations deriving from the

Key words: cerebral blood flow, attention deficit hyperactivity disorder, bipolar disorder, fMRI, SPECT

Mailing address:
Maria Cristina Di Tommaso M.D
80 Lakeside Ave
Cranston RI 02910, USA
Tel: +1 857 413 9128
Fax: +11 401 444 7146
e-mail: mditommaso@mclean.harvard.edu

0393-974X (2012)

same disorder or 3) there may be a more complex relationship between ADHD and BPD, somewhere therein.

The aim of this study is to determine the possible alteration in neuropsychological functioning in patients with BPD and in ones with ADHD, by relating the cerebral blood flow, and to establish a relationship, as yet not formulated, between the two illnesses.

MATERIALS AND METHODS

Papers were reviewed through 2009 using the NIH PubMed literature search system. Additionally, references from identified papers were evaluated for inclusion in this review. Inclusion criteria were that manuscripts: 1) use research diagnostic criteria(RDC) or DSM-III, DSM-III-R or DSM-IV to diagnose BPD and/or ADHD; 2) Directly compare ADHD or BPD with healthy subjects; 3) be published in English. For select manuscripts these criteria were relaxed to allow the inclusion of studies that were particularly useful.

I reviewed papers in which regional cerebral blood flow had been valued as an objective index of functional brain activity. I considered trials made with Single Photon Emission Computer Tomography (SPECT) and Positron Emission Tomography (PET). Also, it seemed to be appropriate to mention some studies, among the few existing on this topic in ADHD, conducted with Functional Magnetic Resonance Imaging (fMRI) as that added some interesting findings.

Limits

A considerable amount of limitations of published functional imaging literature limit the conclusions of this review. These studies exhibit a number of methodological limitations that preclude clear conclusions. For example, different diagnostic groups (e.g. unipolar and bipolar depressed) and different active states within diagnoses (e.g. depressed and manic) are often lumped into a single patient sample. Similarly, the statistical methods utilized in each manuscript are often incompletely described and important confounders are not controlled. Additionally, many of the studies do not report whether investigators were blinded to group assignment prior to beginning measurements. Moreover, there is a considerable variability among studies in institutional dependent image acquisition and post-processing methods as well as region-of-interest identification, making direct comparative analysis difficult.

The matching of population is also crucial for ensuring valid results, but is difficult to control.

Rarely the studied subjects were similar for sociodemographic conditions, ethnicity or even age or gender, though there can be profound effects on all brain measures and cognitive functional performance.

Attention deficit/hyperactivity disorder

Initially, ADHD studies focused on the frontal lobe, often seen as the origin of this disorder (8, 3). Others, hypothesizing insufficient frontal cortical inhibitory control, focused on a fronto-limbic dysfunction (9, 10). This view drew support from studies of stimulant medications and animal models (both of which implicated dopaminergic and noradrenergic influences on prefrontal cortex) (11, 12). These early hypotheses have now expanded as cognitive neuroscience has determined that distributed networks of brain regions underlie attention, cognition, and behavioral self-regulation (13) and that dysfunction in various components of this network can be associated with ADHD (14-16). Studies of functional imaging, in agreement with the structural ones, have revealed the involvement of the prefrontal cortex (17-19) and in particular the dorso lateral prefrontal cortex (DLPFC) (20) and the ventral lateral prefrontal cortex VLPFC (19). These two areas were thought to be involved in functions such as selective attention, planning, executive control and working memory (13, 21).

The anterior cingulate dorsal cortex (dACC), which from earlier studies of cerebral blood flow did not appear to be involved in ADHD, was found to be hypofunctional in other types of functional studies. In a focused study on dACC, in which the Counting Stroop task was used as a cognitive activation index, Bush et al. (22) reported that dACC was hypofunctional in adults with ADHD. Similarly, Rubia et al. (23),using stop-signal and motor timing tasks, also found mesial prefrontal hypofunction in the vicinity of dACC in patients with ADHD. Rubia et al. (23) attributed to the hypoactivation of this area a deficit of attention regulation of the motor output and to the hypofunction of the right inferior prefrontal cortex the poor inhibitory control. More recently, Durston et al. (24) and Tamm et al. (25), using Go-NoGo tasks, respectively, in children and adolescents, reported that healthy subjects activated dACC, whereas ADHD subjects did not. Additionally, Tamm et al. (25) also reported that dACC was hypoactive in the ADHD group relative to the control group.

The alteration of dACC, especially on the right hemisphere, could itself justify all the symptoms of ADHD, as it has been shown that it has an important role in attention, motor control, response inhibition and decision-making based on reward (13, 26-28). Thus, hypoperfusion, or less activity, in this region would necessarily decrease attentiveness, the result of which is

manifested as attention deficit.

The frontal cortex is obviously a very complex structure, and its specific areas are connected with several subcortical structures. Alterations in prefrontal cortex and subcortical structures can be the basis not only of ADHD, but also of BPD (29).

In animals it has been demonstrated that lesions of the striatum (30), or of the prefrontal cortex, yield a picture very similar to ADHD, with hyperactivity and attention deficit. Lou et al. (31, 32) reporting a striatal hypoperfusion in ADHD children, hypothesize that the caudate nucleus, through the connections with the thalamus, modulate (mainly inhibitory) the polisensory activity. This did not occur in ADHD because of the striatal lesions.

Studies concerning the functional abnormalities of the cerebellum in ADHD are a relatively recent phenomenon. Structural imaging studies have reported the involvement of the cerebellar inferior- posterior lobe while more recent functional studies (17, 19) have demonstrated the cerebellar alteration in ADHD patients. In these studies a relevant role is attributed to the cerebellum, not only to the prefrontal cortex, in the cognitive processes and the executive functioning changes in ADHD.

I can conclude that the hypofunctionality of the cerebellum, the striatum, and the prefrontal cortex in its various components (orbital, mesial, lateral) is associated with ADHD. However the frontal cortex appears to be the structure most intricately involved in this disorder: in that regard any injury, even isolated, of the frontal lobe may cause ADHD.

Bipolar disorder

The findings regarding the BPD appear to be quite complex though one result remains almost constant in all studies: the involvement of the prefrontal cortex. Another element nearly universally present is asymmetry of perfusion. Commonly, in patients with structural brain damage from stroke or cancer, depression occurs when lesions are located in the left hemisphere. When the right hemisphere is injured, however, manifestations of mania appear instead. Delvenne et al. (33) reported for the first time a hypoperfusion in the left hemisphere (basal ganglia and frontal and occipital lateral cortex) in bipolar patients with major depression. In 1993 Migliorelli et al. (34) showed in manic patients a reduced regional cerebral blood flow (rCBF) in the ventral basal area of the right temporal lobe, with hyperperfusion in the same area in the left hemisphere. In 1995, Rubin et al. (35) published a more significant trial where they compared 22 patients with BPD (11 depressed, 11 manic) with 11 controls. In the prefrontal and temporal cortex right hyperperfusion and left hypoperfusion was shown in manic subjects, the opposite in depressed patients. Later, almost all researchers with functional neuroimaging confirmed the blood flow asymmetry in BPDin brain areas (36, 37).

Culha et al. (38) reported in euthymic bipolar subjects a bilateral low rCBF in the medial-basal temporal region, in the medial frontal region, in the occipital lobe and in the cingulate gyrus; there were no differences for the hemisphere. This paper seems to show not only that in bipolar patients there are alterations in the euthymic state, but also that the lateralization and inversion of perfusion state in the BPD is a phenomenon which occurs during periods of depression or mania. Six of the papers here presented yielded the involvement of the temporal lobe in the BPD (34-36, 37). While most of the studies reported a hypoperfusion in the temporal lobe, in a group of bipolar subjects, without distinguishing between depressed, manic and euthymic patients, found a high rCBF in the anterior temporal region, correlated with low psychomotor and executive performance (37). The basal ganglia are surely involved in the BPD, given their close connections with the frontal cortex and given that the injuries of the ventral-medial caudate may produce a secondary bipolar syndrome. Delvenne et al. (33) and Benabarre et al. (40) demonstrated a low rCBF in the basal ganglia in depressed bipolar patients. O'Connell (39) showed hypo and hyperperfusion in the basal ganglia in manic subjects; Benabarre et al. (37) also found a striatal hypoperfusion in bipolar patients during the execution of the Wisconsin Card Sorting Test (executive functions) and a right striatum hyperperfusion during the Stroop test (attention task), related to a worse performance in memory and in attention and executive tasks. The right parietal cortex, which has a role in the spatial attention was hypoperfused in depressed bipolar patients (36, 38), while in the Benabarre trial (37) a high rCBF was shown in the left parietal lobe. Only in this last paper the cerebellum appears, which in the bipolar subjects has a low rCBF and is related to low executive performance. The occipital lobe was hypoperfused in the trials of Delvenne et al. (33), Bonne et al. (36), and Culha et al. (38), while in the work of Benabarre et al. (37), there is a hyperperfusion in the occipital cortex.

CONCLUSION

There appears to be an overall asymmetry of focal change in cerebral perfusion that occurs more clearly in BPD than ADHD. In depression associated with BPD, hypoperfusion is often reported in the left frontal, sometimes also left temporal, lobes, while in manic patients a right prefrontal lobe hypoperfusion appears. This was exemplified by the work of Rubin et al. (35), contributing to the understanding of

asymmetrical flow in BPD. This asymmetry was shown not to be a constant alteration, but linked to the state of depression and mania (38). In fact, in euthymic patients, even with significant anomalies, there were no differences of CBF by side.

In the ADHD the asymmetry is less evident and thus less relevant, and, when present, it is more frequently associated with right frontal lobe hyperperfusion. However, it is of note that in studies describing and reporting on ADHD, in contrast to those of BPD, the mood state is not explicitly discriminated.

Changes in cerebral perfusion and CBF appear more robust in patients with BPD. In addition to changes in the prefrontal cortex and the striatum, which are common to either disorder, in BPD the involvement of the temporal lobe occurs much more frequently. Moreover, in BPD there often is a hypoperfusion of the parietal lobe, which in ADHD is instead hyperperfused. Likewise, in the BPD there is evidence of involvement of insula which is not seen in ADHD.

The existence of common areas of change in cerebral perfusion, such as the prefrontal cortex, the striatum, and, possibly, the cerebellum, might explain the frequent comorbidity that occurs between the two diseases. Alternatively, the characteristics shared between the diseases may derive from these areas. It is plausible that, in a brain diseased with BPD or ADHD, when changes occur in additional areas of the brain the disease associated with those areas manifests.

Children with ADHD and comorbid BPD more often have a severe disease consistent with extensive changes on functional imaging. However, the symptoms of ADHD are always identifiable, even with concurrent BPD, suggesting the two diseases have their symptomatological and organic peculiarities. This hypothesis is in agreement with the results of other studies that have verified that children with severe symptoms of ADHD are more likely to develop BPD. The mechanism for this hypothesis remains, as of yet, unelicited. I, however, suggest that relative change in perfusion may affect brain acclimated to a pathological perfusion state resulting in precipitation of a new disease despite relative normality of perfusion at that time. This subsequently results in further pathological changes in brain and perfusion.

REFERENCES

1. Faraone SV, Biederman J, Wozniak J, Mundy D, Mennin D, O'Donnell D. Is comorbidity with ADHD a marker for juvenile-onset mania? J Am Acad Child Adolesc Psychiatry 36:1046-55.
2. Faraone SV, Biederman J, Mennin D, Wozniak J, Spencer T. Attention-deficit hyperactivity disorder with bipolar disorder: a familial subtype? J Am Acad Child Adolesc Psychiatry 1997; 36(10):1378-87.
3. Barkley RA, Grodzinsky G, DuPaul GJ. Frontal lobe functions in attention deficit disorder with and without hyperactivity: a review and research report. J Abnorm Child Psychol 1992; 20(2):163-88.
4. McKay AP, Tarbuck AF, Shapleske J, McKenna PJ. Neuropsychological function in manic-depressive psychosis. Evidence for persistent deficits in patients with chronic, severe illness. Br J Psychiatry 1995; 167:51-7.
5. Ferrier IN, Stanton BR, Kelly TP, Scott J. Neuropsychological function in euthymic patients with bipolar disorder.Br J Psychiatry 1999; 175:246-51.
6. Kent L, Craddock N. Is there a relationship between attention deficit hyperactivity disorder and bipolar disorder? J Affect Disord 2003; 73(3):211-21.
7. Biederman J. Resolved: mania is mistaken for ADHD in prepubertal children: affirmative. J Am Acad Child Adolesc Psychiatry 1998; 37:1091-3.
8. Mattes JA. The role of frontal lobe dysfunction in childhood hyperkinesis. Compr Psychiatry 1980; 21(5):358-69.
9. Satterfield JH, Dawson ME. Electrodermal correlates of hyperactivity in children. Psychophysiology 1971; 8(2):191-7.
10. Casey BJ, Castellanos FX, Giedd JN, et al. Implication of right frontostriatal circuitry in response inhibition and attention-deficit/hyperactivity disorder. J Am Acad Child Adolesc Psychiatry 1997; 36(3):374-83.
11. Arnsten AF, Steere JC, Hunt RD. The contribution of alpha 2-noradrenergic mechanisms of prefrontal cortical cognitive function. Potential significance for attention-deficit hyperactivity disorder.Arch Gen

Psychiatry 1996; 53(5):448-55.
12. Shaywitz BA, Fletcher JM, Shaywitz SE. Attention-deficit/hyperactivity disorder. Adv Pediatr 1997; 44:331-67.
13. Posner MI, Petersen SE. The attention system of the human brain. Annu Rev Neurosci 1990; 13:25-42.
14. Denckla MB. Executive function, the overlap zone between attention-deficit/ hyperactivity disorder and learning disabilities. Int Pediatr 1989; 4:155-60.
15. Seidman LJ, Valera EM, Bush G. Brain function and structure in adults with attention-deficit/hyperactivity disorder. Psychiatr Clin North Am 2004; 27(2):323-47.
16. Sergeant JA, Geurts H, Oosterlaan J. How specific is a deficit of executive functioning for attention-deficit/ hyperactivity disorder? Behav Brain Res 2002; 130(1-2):3-28.
17. Gustafsson P, Thernlund G, Ryding E, Rosen I, Cederblad M. Associations between cerebral blood-flow measured by single photon emission computed tomography (SPECT), electro-encephalogram (EEG), behaviour symptoms, cognition and neurological soft signs in children with attention-deficit hyperactivity disorder (ADHD). Acta Paediatr 2000; 89(7):830-5.
18. Schweitzer JB, Faber TL, Grafton ST, Tune LE, Hoffman JM, Kilts CD.Alterations in the functional anatomy of working memory in adult attention deficit hyperactivity disorder. Am J Psychiatry 2000; 157(2):278-80.
19. Kim BN, Lee JS, Shin MS, Cho SC, Lee DS. Regional cerebral perfusion abnormalities in attention deficit/ hyperactivity disorder. Statistical parametric mapping analysis. Eur Arch Psychiatry Clin Neurosci 2002; 252(5):219-25.
20. Spalletta G, Pasini A, Pau F, Guido G, Menghini L, Caltagirone C.Prefrontal blood flow dysregulation in drug naive ADHD children without structural abnormalities. J Neural Transm 2001; 108(10):1203-16.
21. Duncan J, Owen AM. Common regions of the human frontal lobe recruited by diverse cognitive demands. Trends Neurosci 2000; 23(10):475-83.
22. Bush G, Frazier JA, Rauch SL, Seidman LJ, Whalen PJ, Jenike MA, Rosen BR, Biederman J. Anterior cingulate cortex dysfunction in attention-deficit/ hyperactivity disorder revealed by fMRI and the Counting Stroop. Biol Psychiatry 1999; 45(12):1542-52.
23. Rubia K, Overmeyer S, Taylor E, Brammer M, Williams SC, Simmons A, Bullmore ET Hypofrontality in attention deficit hyperactivity disorder during higher-order motor control: a study with functional MRI. Am J Psychiatry 1999; 156(6):891-6.
24. Durston S, Tottenham NT, Thomas KM, Davidson MC, Eigsti IM, Yang Y, Ulug AM, Casey BJ.Differential patterns of striatal activation in young children with and without ADHD. Biol Psychiatry 2003; 53(10):871-8.
25. Tamm L, Menon V, Ringel J, Reiss AL. Event-related FMRI evidence of frontotemporal involvement in aberrant response inhibition and task switching in attention-deficit/hyperactivity disorder. J Am Acad Child Adolesc Psychiatry 2004; 43(11):1430-40.
26. Vogt BA, Finch DM, Olson CR. Functional heterogeneity in cingulate cortex: the anterior executive and posterior evaluative regions. Cereb Cortex 1992; 2(6):435-43.
27. Bush G, Luu P, Posner MI. Cognitive and emotional influences in anterior cingulate cortex. Trends Cogn Sci 2000; 4(6):215-22.
28. Bush G, Vogt BA, Holmes J, Dale AM, Greve D, Jenike MA, Rosen BR Dorsal anterior cingulate cortex: a role in reward-based decision making. Proc Natl Acad Sci USA 2002; 899(1):523-8.
29. Strakowski SM, DelBello MP, Adler C, Cecil DM, Sax KW. Neuroimaging in bipolar disorder. Bipolar Disord 2000; 2:148-64.
30. Iversen SD. Behavior after neostriatal lesions in anomals, in Divac I, Öberg RGE (eds): The neostriatum. Elmsford, NY, Pergamon Press Inc.1977; pp.195-210.
31. Lou HC, Henriksen L, Bruhn P, Børner H, Nielsen JB. Striatal dysfunction in attention deficit and hyperkinetic disorder. Arch Neurol 1989; 46(1):48-52.
32. Lou HC, Andresen J, Steinberg B, McLaughlin T, Friberg L.The striatum in a putative cerebral network activated by verbal awareness in normals and in ADHD children. Eur J Neurol 1998; 5(1):67-74.
33. Delvenne V, Delecluse F, Hubain PP, Schoutens A, De Maertelaer V, Mendlewicz J.Regional cerebral blood flow in patients with affective disorders. Br J Psychiatry 1990; 157:359-65.

34. Migliorelli R, Starkstein SE, Tesón A, de Quirós G, Vázquez S, Leiguarda R, Robinson RG. SPECT findings in patients with primary mania. J Neuropsychiatry Clin Neurosci 1993; 5(4):379-83.
35. Rubin E, Sackeim HA, Prohovnik I, Moeller JR, Schnur DB, Mukherjee S. Regional cerebral blood flow in mood disorders: IV. Comparison of mania and depression. Psychiatry Res 1995; 61(1):1-10.
36. Bonne O, Krausz Y, Gorfine M, Karger H, Gelfin Y, Shapira B, Chisin R, Lerer BJ. Cerebral hypoperfusion in medication resistant, depressed patients assessed by Tc99m HMPAO SPECT. BJ Affect Disord 1996; 41(3):163-71.
37. Benabarre A, Vieta E, Martínez-Arán A, et al.Neuropsychological disturbances and cerebral blood flow in bipolar disorder. Aust NZ J Psychiatry 2005; 39(4):227-34.
38. Culha AF, Osman O, Dogangün Y, Filiz K, Suna K, Kalkan ON, Gulfizar V, Beyza A. Changes in regional cerebral blood flow demonstrated by 99mTc-HMPAO SPECT in euthymic bipolar patients. Eur Arch Psychiatry Clin Neurosci 2007; 258(3):144-51.
39. O'Connell RA, Van Heertum RL, Luck D, Yudd AP, Cueva JE, Billick SB, Cordon DJ, Gersh RJ, Masdeu JC. Single-photon emission computed tomography of the brain in acute mania and schizophrenia. J Neuroimaging 1995; 5(2):101-4.
40. Benabarre A, Vieta E, Martín F, et al. Clinical value of 99mTc-HMPAO SPECT in depressed bipolar I patients. Psychiatry Res 2003; 132(3):285-9.

EDITORIAL

IL-36 A NEW MEMBER OF THE IL-1 FAMILY CYTOKINES

D. TRIPODI[1], F. CONTI[2], M. ROSATI[2], G. MACCAURO[3], A. SAGGINI[4], E. CIANCHETTI[5], D. ANGELUCCI[6], M. FULCHERI[7], S. TETÈ[1], V. SALINI[8], A. CARAFFA[9], P. ANTINOLFI[9], E. TONIATO[10], M.L. CASTELLANI[10], P. CONTI[10] and T.C. THEOHARIDES[11]

[1]Dental School, University of Chieti-Pescara, Italy; [2]Gynecology Division, Pescara Hospital, Pescara, Italy; [3]Department of Orthopedics, Catholic University of Rome, Rome, Italy; [4]Department of Dermatology, University of Rome Tor Vergata, Rome, Italy; [5]Ortona Hospital, Italy; [6]Pathological Anatomy, Chieti Hospital, Chieti, Italy; [7]Psychology Department, University of Chieti, Italy; [8]Department of Orthopedics, University of Chieti, Italy; [9]Department of Orthopedics, University of Perugia, Perugia, Italy; [10]Immunology Division, University of Chieti-Pescara, Italy; [11]Department of Physiology and Pharmacology, Tufts University School of Medicine, New England Medical Center, Boston, MA, USA

Received December 15, 2011 – Accepted February 20, 2012

Interleukin-36 (IL-36) is a pro-inflammatory cytokine which plays an important role in innate and adaptive immunity. IL-36 activates MAPK and NF-KB pathways and is produced by many different cells. This cytokine is a family member of interleukin-1 (IL-1) and plays an important role in the pathophysiology of several diseases. Here we summarise and review the new aspects of this important pro-inflammatory cytokine.

Cytokines are a large and heterogeneous group of proteins that modulate the immune system (1-5) and play an increasingly important role in immunology, immunopathology, and immunopharmacology. Cytokines are released by particular cells in response to a variety of stimuli, activate target cells after binding to specific cell surface receptors, and mediate communication between cells of the immune and inflammatory systems. Pro-inflammatory cytokines are important mediators of inflammation, proteolysis, and cell recruitment and proliferation (6-9). Interleukin 1 (IL-1)was discovered by Gery in 1972 and he named it lymphocyte-activating factor (LAF). It was not until 1985 that IL-1 was discovered to consist of two distinct proteins, now called interleukin-1 alpha (IL-1a) and interleukin-1 beta (IL-1b) (10-14). The most important regulatory molecule for IL-1α activity is IL-1RA, which is usually produced in a 10-100-fold molar excess. IL-1α (Fig. 1) possesses biological effects on cells in the picomolar to femtomolar range. Cytokines of the IL-1 family, such as IL-1 a/b, IL-18 and IL-33, have important functions in host defense, immune regulation, and inflammation. These cytokines play critical roles in the function of the innate and adaptive immune system. The IL-1 family cytokines include a noumber of interleukins such as IL-1α, IL-1β, IL-1 receptor antagonist (IL-1RA), IL-18, IL-33 and

Key words: IL -36, cytokines, interleukins, inflammation, immunity

Mailing address: Prof. Domenico Tripodi,
Dipartimento di Scienze Orali,
Università "G. d'Annunzio" Chieti- Pescara",
Via dei Vestini, 31
Chieti, Italy
Tel/Fax: +39 0871 3554063
e-mail: tripodi@unich.it

0393-974X (2012)

DISCLOSURE: ALL AUTHORS REPORT NO CONFLICTS OF INTEREST RELEVANT TO THIS ARTICLE.

now IL-36 has been added which is a newly-named cytokine family that comprises three members: IL-36α, IL-36β and IL-36γ (Table I) (15). IL-36, a pro-inflammatory cytokine that activates the MAPK and NF-kappaB pathways is an important player in innate and adaptive immune response (Table II) (16-19). Probably, many different cells are source of IL-36, and this cytokine may play an important role in the pathophysiology of several diseases, similar to other IL-1 family member cytokines (20-23).

IL-18 is a pleiotropic proinflammatory cytokine produced by monocyte/macrophage lineage as well as epithelial cells, such as human keratinocytes (24-27). IL-18 leads to increased immunoglobulin E production from B cells and enhanced production of IL-4 and IL-13 by basophils, mast cells, and CD4(+) T cells. Inflammation is thought to be initiated by over-release of IL-18 and accelerated by IL-1. Recent studies also demonstrate a convincing role for IL-18 in atopic responses, including atopic inflammatory diseases (28-32). Moreover, IL-18 directly stimulates basophils and mast cells to produce Th2 cytokines and histamine, independently of IgE. IL-18 also induces IL-13 and/or IL-4 production by NK cells, mast cells and basophils (33-36).

IL-1RA is a competitive inhibitor of IL-1 binding to IL-1RI, and promotes anti-inflammatory activity (37-43). IL-33 stimulates in mast cells arachidonic acid products release such as PGD2 and inflammatory cytokines including TNFa (44-47). However, these effects have shown neither induced nor enhanced mast cell degranulation. IL-33 induces biological effects on mast cells and T cells through its receptor IL-33Rb-chain and may have pro-inflammatory potential effects similar to the cytokines from the same family. This cytokine/receptor combination may therefore serve as novel target for the treatment and control of allergy, autoimmune diseases, and some cancers. Recently, it was found that IL-33 is a strong activator of mast cell lines (LAD II cells) capable of inducing MCP-1 (a C-C chemokine family member) release at transcriptional and translational level, IL-8 and VEGF, suggesting a possible role of this new cytokine in the inflammatory response and recruitment of inflammatory cells (48-52).

IL-36 cytokines, are expressed in a restrictive manner, primarily in the skin and epithelium. All these cytokines are similar to the classical IL-1 cytokines, and are involved in the initiation or regulation of immune responses and inflammation (53-57). However, little is known about the expression pattern and the biologic function of IL-36α, IL-36β, IL-36γ and IL-36 receptor antagonist (IL-36RA) *in vivo* and *in vitro*. In addition, their IL-36R ligands are also poorly understood. IL-1 family ligands signal through heterodimeric receptors which induce signaling and involve the activation of NF-κB and MAPK pathways (58-62).

IL-36 receptor (IL-36R), also called (IL-1R)-Related Protein 2 (IL-1RRP2), is a ligand for IL-

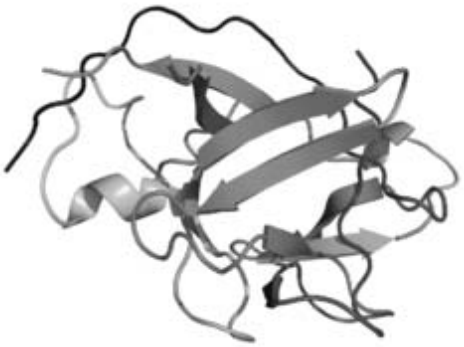

Fig. 1. *Interleukin 1 alpha.*

Table I. *The IL-1 family of cytokines is composed of 11 different ligands as shown below.*

Name	*Also termed*
IL-1α	IL-1F1
IL-1β	IL-1F2
IL-1RA	IL-1F3
IL-18	IL-1F4
IL-1F5	
IL-1F6	IL-36α
IL-1F7	
IL-1F8	IL-36β
IL-1F9	IL-36γ
IL-1F10	
IL-1F11	IL-33

Table II. *Biological effects of IL-36.*

- Activates the MAPK and NF-kappaB pathways
- An important player in innate and adaptive immune response
- Pathophysiology of several diseases
- Initiation or regulation of immune responses and inflammation
- IL-1F5 (renamed IL-36RA) exerts receptor antagonist activities
- IL-1F5 inhibits NF-κB in certain cell types
- Mediate lesional psoriasis skin
- Mediate epidermis and dermis inflammation
- Mediate the proliferation of keratinocytes and in activate epithelial tissues
- Strongly increased in psoriatic-like mouse skin plaques
- IL-36α and IL-36β, but not IL-36γ, directly induced TNF-α
- IL-36 can be induced by Th17 cytokines
- Direct regulates IL-8 and IL-6
- Regulates the expression and enhance the function of Th17
- Interelation with IL-22 in skin inflammation
- Mediate chronic kidney disease, and human rheumatoid synovial tissues

36α (IL-1F6), IL-36β (IL-1F8), and IL-36γ (IL-1F9). Moreover, IL-1F5, which has been shown to exert receptor antagonist activities, has been renamed IL-36RA. IL-36RA binds to IL-1RRP2 and inhibits IL-36. It has been reported that IL-36RA is a strong antagonist not only of IL-36γ but also of IL-36α and IL-36β and the authors demonstrated that this activity requires removal of the N-terminal methionine from IL-36RA (63-68).

It has been also shown that IL-36α, β and γ bind to IL-36R, and stimulate intracellular signals; while IL-1F5 inhibits NF-κB in certain cell types. IL-36α, IL-36β, IL-36γ and IL-36RA, probably act extracellularly, and it is unclear how they are generated. It has been reported that IL-36α, β and γ are important in dermatology, since they are produced in the skin, in lesional psoriasis skin, in both the epidermis and dermis, in IL-1β or TNF-α–stimulated human keratinocytes and in activated epithelial tissues, where the messenger RNAs are highly expressed. In the biopsies of psoriatic-like mouse skin plaques, gene and protein expression of IL-36 cytokines was strongly increased (69-75).

These authors also show that IL-22, IL-17A, and TNF-α induce the *ex vivo* production of all three IL-36 by human keratinocytes, whereas IFN-γ selectively induces IL-36β. In addition they found that IL-36α and IL-36β, but not IL-36γ, directly induced TNF-α mRNA and protein synthesis in keratinocytes demostrating that IL-36α and IL-36β could regulate TNF-α directly in these cells. Moreover, they show that IL-36 can be induced by Th17 cytokines and direct regulation of IL-8 and IL-6 by IL-36α and IL-36β, which synergized with IL-17A and TNF-α. IL-36s are not only regulated by Th17 cytokines, but they themselves can regulate the expression and enhance the function of Th17 cytokines. In addition, they reported that blockade of IL-22 signaling downregulated the gene expression of all IL-36 cytokines and skin inflammation in the psoriatic tissues, whereas injection of recombinant IL-22 protein into the skin had opposite results (69, 76-79)

In addition, in chronic kidney disease, and human rheumatoid synovial tissues, IL-36α is also expressed. These biological implications of IL-36 suggest a link between inflammatory skin lesions (psoriasis vulgaris biopsies) and rheumatoid arthritis (80-86).

This study show that IL-36α, IL-36β, and IL-36γ,

play an important role in inflammatory diseases and that IL-36RA is their natural antagonist. IL-36RA inhibits both the full-length and truncated ligands; the ratio of antagonist to agonist required for full inhibition is similar to that of IL-1RA to IL-1β (63, 87-89). In addition, it has been shown that IL-36R is expressed in dendritic cells (DCs) and $CD4^+$ T cells and that IL-36R agonist ligands are able to stimulate the production of several cytokines by DCs, whereas IL-36Ra exerts an inhibitory effect. In addition these authors shown that IL-36R agonist ligands are potent regulators of T-cell responses.

These studies amplify the concept of innate immune and describe the role of IL-36s in autoimmune disease, suggesting that IL-36 cytokines and their receptor represent a fundamental target for understanding inflammatory and autoimmune diseases.

REFERENCES

1. Dinarello CA. Interleukin-1 and the pathogenesis of the acute-phase response. N Engl J Med 1984; 311:1413-8.
2. Miura M, Hiwatashi N. Cytokine production in inflammatory bowel disease. J Clin Lab Immunol 1985; 18:81-6.
3. Dinarello CA. An update on human interleukin-1: from molecular biology to clinical relevance. J Clin Immunol 1985; 5:287-97.
4. Marzano AV, Cugno M, Trevisan V, Lazzari R, Fanoni D, Berti E, Crosti C. Inflammatory cells, cytokines and matrix metalloproteinases in amicrobial pustulosis of the folds and other neutrophilic dermatoses. Int J Immunopathol Pharmacol 2011; 24:451-60.
5. Scaramuzzo L, Manicone PF, Graci C, Muratori F, Spinelli MS, Damis G, Raffaelli L, Maccauro G. Morphological modifications in osteoarthritis: a scanning electron microscopy study Eur J Inflamm 2011; 9:73-78.
6. Maury CP. Interleukin 1 and the pathogenesis of inflammatory diseases. Acta Med Scand 1986; 220:291-4.
7. Rosato E, Rossi C, Molinaro I, Giovannetti A, Pisarri S, Salsano F. Long-term N-acetylcysteine therapy in systemic sclerosis interstitial lung disease: a retrospective study. Int J Immunopathol Pharmacol 2011; 24:727-33.
8. Rigante D, Zampetti A, Bersani G, Candelli M, Piras A, Rendeli C, Antuzzi D, Feliciani C, Stabile A. Serum interleukin-18 in children with Henoch-Schönlein purpura: a promising marker of disease activity. Eur J Inflamm 2011; 9:157-68.
9. Ciprandi G, De Amici M, Berardi L, Vignini M, Marseglia G. Serum IgE for Bet v 1 in patients affected by atopic dermatitis. Eur J Inflamm 2011; 9:205-7.
10. Bevilacqua MP, Pober JS, Wheeler ME, Cotran RS, Gimbrone MA Jr. Interleukin 1 acts on cultured human vascular endothelium to increase the adhesion of polymorphonuclear leukocytes, monocytes, and related leukocyte cell lines. J Clin Invest 1985; 76:2003-11.
11. Placido R, Auricchio G, Gabriele I, Galli E, Brunetti E, Colizzi V, Battistini L, Mancino G. Characterization of the immune response of human cord-blood derived gamma/delta T cells to stimulation with aminobisphosphonate compounds. Int J Immunopathol Pharmacol 2011; 24:101-10.
12. Belizário JE. Pathogens and dead cells cooperate with cytokines in activating the innate and adaptive response. Eur J Inflamm 2011; 9:1-11.
13. Angelini A, Centurione L, Sancilio SA, Castellani ML, Conti P, Di Ilio C, Porreca E, Cuccurullo F, Di Pietro R. The effect of the plasticizer diethylhexyl phthalate on transport activity and expression of P-glycoprotein in parental and doxo-resistant human sarcoma cell lines. J Biol Regul Homeost Agents 2011; 25:203-11
14. Suzuki K, Setoyama Y, Yoshimoto K, Tsuzaka K, Abe T, Takeuchi T. Decreased mRNA expression of two FOXP3 isoforms in peripheral blood mononuclear cells from patients with rheumatoid arthritis and systemic lupus erythematosus. Int J Immunopathol Pharmacol 2011; 24:7-14.
15. Dinarello C, Arend W, Sims J et al. IL-1 family nomenclature. Nat Immunol 2010; 11:973-6
16. Vigne S, Palmer G, Lamacchia C, Martin P, Talabot-Ayer D, Rodriguez E, Ronchi F, Sallusto F, Dinh H, Sims JE, Gabay C. IL-36R ligands are potent regulators of dendritic and T cells. Blood 2011; 118:5813-23.
17. Artini M, Scoarughi GL, Papa R, et al. A new anti-

infective strategy to reduce adhesion-mediated virulence in Staphylococcus aureus affecting surface proteins. Int J Immunopathol Pharmacol 2011; 24:661-72.
18. Torretta S, Marchisio P, Esposito S, Garavello W, Cappadona M, Clemente IA, Pignataro L. Exhaled nitric oxide levels in children with chronic adenotonsillar disease. Int J Immunopathol Pharmacol 2011; 24:471-80.
19. Belloli L, Carlo-Stella N, Ughi N, Marasini B. Cancer in Italian patients with systemic sclerosis. Eur J Inflamm 2011; 9:151-6.
20. Towne JE, Renshaw BR, Douangpanya J, Lipsky BP, Shen M, Gabel CA, Sims JE. Interleukin-36 (IL-36) ligands require processing for full agonist (IL-36α, IL-36β, and IL-36γ) or antagonist (IL-36Ra) activity. J Biol Chem 2011; 286:42594-602.
21. Cantarini L, Iacoponi F, Lucherini OM, et al. Validation of a diagnostic score for the diagnosis of autoinflammatory diseases in adults. Int J Immunopathol Pharmacol 2011; 24:695-702.
22. Kauffman MA, Sterin-Prync A, Papouchado M, et al. Immunogenicity of an interferon-beta1a product. Int J Immunopathol Pharmacol 2011; 24:499-504.
23. Tsoucalas G, Karamanou M, Androutsos G. Travelling through time with aspirin, a healing companion. Eur J Inflamm 2011; 9:13-16.
24. Matsumoto S, Tsuji-Takayama K, Aizawa Y, Koide K, Takeuchi M, Ohta T, Kurimoto M. Interleukin-18 activates NF-kappaB in murine T helper type 1 cells. Biochem Biophys Res Commun 1997; 234:454-7.
25. Nowakowska-Zajdel E, Mazurek U, Ziółko E, Niedworok E, Fatyga E, Kokot T, Muc-Wierzgoń M. Analysis of expression profile of gene encoding proteins of signal cascades activated by insulin-like growth factors in colorectal cancer. Int J Immunopathol Pharmacol 2011; 24:781-7.
26. Maghbooli Z, Hossein-Nezhad A, Shirzad M, Behzadi H. The role of osteoprotegrin/ nuclear factor kb ligand in coronary collateral development Eur J Inflamm 2011; 9:57-64.
27. Di Paola R, Mazzon E, Paterniti I, Impellizzeri D, Bramanti P, Cuzzocrea S. Apocynin, a plant-derived drug, might be useful in the treatment of myocardial ischemia reperfusion injury in rat hearts. Eur J Inflamm 2011; 9:169-74.
28. Zhang J, Li L, Lu Q, et al. Acute stress enhances contact dermatitis by promoting nuclear factor-kappaB DNA-binding activity and interleukin-18 expression in mice. J Dermatol 2010; 37:512-21.
29. Varricchio A, Capasso M, De Lucia A, Avvisati F, Varricchio AM, Bettoncelli G, Ciprandi G. Intranasal flunisolide treatment in patients with non-allergic rhinitis. Int J Immunopathol Pharmacol 2011; 24:401-9.
30. Wu KG, Li TH, Chen CJ, Cheng HI, Wang TY. Correlations of serum Interleukin-16, total IgE, eosinophil cationic protein and total eosinophil counts with disease activity in children with atopic dermatitis. Int J Immunopathol Pharmacol 2011; 24:15-23.
31. Meglio P, Giampietro PG, Gabriele I, Carello R, Avitabile S, Galli E. Oral desensitisation with food is food-specific and protein-specific. Int J Immunopathol Pharmacol 2011; 24:803-11.
32. Boita M, Garzaro M, Raimondo L, et al. The expression of TSLP receptor in chronic rhinosinusitis with and without nasal polyps. Int J Immunopathol Pharmacol 2011; 24:761-8.
33. Hayashi N, Yoshimoto T, Izuhara K, Matsui K, Tanaka T, Nakanishi K. T helper 1 cells stimulated with ovalbumin and IL-18 induce airway hyperresponsiveness and lung fibrosis by IFN-gamma and IL-13 production. Proc Natl Acad Sci USA 2007; 104:14765-70.
34. Nenna R, Papoff P, Moretti C, et al. Detection of respiratory viruses in the 2009 winter season in Rome: 2009 influenza A (H1N1) complications in children and concomitant type 1 diabetes onset. Int J Immunopathol Pharmacol 2011; 24:651-9.
35. Migueres M, Fontaine JF, Haddad T, Grosclaude M, Saint-Martin F, Bem David D, Crestani B. Characteristics of patients with respiratory allergy in France and factors influencing immunotherapy prescription: a prospective observational study (REALIS). Int J Immunopathol Pharmacol 2011; 24:387-400.
36. Guillén D, Millán O, Brunet M. *In vitro* studies of the immunomodulatory effects of statins alone and in combination with immunosuppressive drugs. Eur J Inflamm 2011; 9:117-24.
37. Seckinger P, Kaufmann MT, Dayer JM. An

interleukin 1 inhibitor affects both cell-associated interleukin 1-induced T cell proliferation and PGE2/collagenase production by human dermal fibroblasts and synovial cells. Immunobiology 1990; 180:316-27.

38. Cantarini L, Iacoponi F, Lucherini OM, et al. Validation of a diagnostic score for the diagnosis of autoinflammatory diseases in adults. Int J Immunopathol Pharmacol 2011; 24:695-702.
39. Devirgiliis V, Panasiti V, Fioriti D, et al. Antibacterial activity of methyl aminolevulinate photodynamic therapy in the treatment of a cutaneous ulcer. Int J Immunopathol Pharmacol 2011; 24:793-5.
40. Binici DN, Güneş N, Kayataş K, Pişkinpaşa N. The effects of interferon-α2b on intestinal flora in peritoneal fibrosis. Eur J Inflamm 2011; 9:135-9.
41. Silambarasan G, Ramanathan T, Nabeel MA, Kalaichelvan VK, Kathiresan K, Balasubramanian T. Anti-inflammatory activity of the marine cyanobacterium *trichodesmium erythraeum* against carrageenan-induced paw oedema in wistar albino rats. Eur J Inflamm 2011; 9:53-56.
42. Galliera E, De Girolamo L, Randelli P, et al. High articular levels of the angiogenetic factors VEGF and VEGF-receptor 2 as tissue healing biomarkers after single bundle anterior cruciate ligament reconstruction. J Biol Regul Homeost Agents 2011; 25:85-91.
43. Saggini A, Saraceno R, Chimenti S. Exaggerated imiquimod application site reactions in the context of systemic tumor necrosis factor-alpha inhibition: more than a coincidental occurrence? Int J Immunopathol Pharmacol 2011; 24:509-15.
44. Iikura M, Suto H, Kajiwara N, Oboki K, Ohno T, Okayama Y, Saito H, Galli SJ, Nakae S. IL-33 can promote survival, adhesion and cytokine production in human mast cells. Lab Invest 2007; 87:971-8.
45. Trellakis S, Farjah H, Bruderek K, Dumitru CA, Hoffmann TK, Lang S, Brandau S. Peripheral blood neutrophil granulocytes from patients with head and neck squamous cell carcinoma functionally differ from their counterparts in healthy donors. Int J Immunopathol Pharmacol 2011; 24:683-93.
46. Caccavo D, Pellegrino NM, Totaro I, Vacca MP, Selvaggi L, Depalo R. Anti-laminin-1 antibodies in sera and follicular fluid of women with endometriosis undergoing in vitro fertilization. Int J Immunopathol Pharmacol 2011; 24:481-8.
47. Dianzani C, Pizzuti A, Gaspardini F, Bernardini L, Rizzo B, Degener AM. Ulerythema ophryogenes, a rare and often misdiagnosed syndrome: analysis of an idiopathic case. Int J Immunopathol Pharmacol 2011; 24:523-7.
48. Hueber AJ, Alves-Filho JC, Asquith DL, et al. IL-33 induces skin inflammation with mast cell and neutrophil activation. Eur J Immunol 2011; 41:2229-37
49. Di Muzio G, Perricone C, Ballanti E, et al. Complement system and rheumatoid arthritis: relationships with autoantibodies, serological, clinical features, and anti-TNF treatment. Int J Immunopathol Pharmacol 2011; 24:357-66.
50. Hatzistilianou M, Antoniades D, Zournatzi V, Pappa S, Antoniades M, Koiou K, Frydas I, Tzafetas J. Isoenzymes of adenosine deaminase and metalloproteinases as biomarkers in *in vitro* fertilization and embryo transfer. Int J Immunopathol Pharmacol 2011; 24:25-31.
51. Tsoupras AB, Chini M, Tsogas N, Mangafas N, Demopoulos CA, Lazanas MC. *In vivo* effects of a *Ginkgo biloba* extract on platelet activating factor metabolism in two asymptomatic HIV-infected patients. Eur J Inflamm 2011; 9:107-116.
52. Melillo L, Valente D, D'Arena G, Dell'Olio M, Falcone A, Minervini MM, Nobile M, Rossi G, Sanpaolo G, Scalzulli PR, Cascavilla N. Combination treatment of flag with non-pegylated liposomal doxorubicin (MYOCET(TM)) in elderly patients with acute myeloid leukemia: a single center experience. Int J Immunopathol Pharmacol 2011; 24:703-9.
53. Sims JE, Smith DE. The IL-1 family: regulators of immunity. Nat Rev Immunol 2010; 10:89-102.
54. Tarantino G, Savastano S, Colao A, Polichetti G, Capone D. Urinary excretion of 5-hydroxy-3-indoleacetic acid in dystimic/depressed, adult obese women: what correlations to hepatic steatosis? Int J Immunopathol Pharmacol 2011; 24:769-79.
55. Mazzucchelli R, Scarpelli M, Lopez-Beltran A, Cheng L, Bartels H, Bartels PH, Alberts DS, Montironi R. Global acetylation and methylation changes predict papillary urothelial neoplasia of

low malignant potential recurrence: a quantitative analysis. Int J Immunopathol Pharmacol 2011; 24:489-97.
56. Saggini A, Anogeianaki A, Maccauro G, et al. What you should know about *Escherichia coli* infection. Eur J Inflamm 2011; 9:103-106.
57. Ruiz-Pérez MV, Sánchez-Jiménez F, Quesada AR, Medina MA. A re-evaluation of the mitogenic effect of serotonin on vascular endothelial cells. J Biol Regul Homeost Agents 2011; 25:13-20.
58. Osborn L, Kunkel S, Nabel GJ. Tumor necrosis factor alpha and interleukin 1 stimulate the human immunodeficiency virus enhancer by activation of the nuclear factor kappa B. Proc Natl Acad Sci USA 1989; 86:2336-40.
59. Wu KG, Li TH, Chen CJ, Cheng HI, Wang TY. A pilot study evaluating the clinical and immunomodulatory effects of an orally administered extract of *Dendrobium huoshanense* in children with moderate to severe recalcitrant atopic dermatitis. Int J Immunopathol Pharmacol 2011; 24:367-75.
60. Pannone G, Hindi SA, Santoro A, et al. Aurora B expression as a prognostic indicator and possible therapeutic target in oral squamous cell carcinoma. Int J Immunopathol Pharmacol 2011; 24:79-88.
61. Mirzaei K, Hossein-Nezhad A, Mokhtari F, Najmafshar A, Khoshniat Nikoo M. VISFATIN/NAMPT/PBCEF and cytokine concentration in multiple sclerosis patients compared to healthy subjects. Eur J Inflamm 2011; 9:31-37.
62. Santino I, Longobardi V. Clinical and serological features of patients with suspected Lyme borreliosis. Int J Immunopathol Pharmacol 2011; 24:797-801.
63. Towne JE. Interleukin-36 (IL-36) ligands require processing for full agonist (IL-36a, IL-36b, and IL-36g) or antagonist (IL-36Ra) Activity. J Biol Chem 2011; 286:42594-602.
64. Sakellaropoulou AV, Hatzistilianou MN, Emporiadou MN, Aivazis VT, Rousso I, Athanasiadou-Piperopoulou F. Evaluation of thyroid gland function in children with obstructive apnea hypopnea syndrome. Int J Immunopathol Pharmacol 2011; 24:377-86.
65. Veda P. Why are neutrophils polymorphonuclear? Eur J Inflamm 2011; 9:85-93.
66. Brazzelli V, Calcaterra V, Muzio F, Klersy C, Larizza D, Borroni G. Reduced sebum production in Turner syndrome: a study of twenty-two patients. Int J Immunopathol Pharmacol 2011; 24:789-92.
67. Armogida M, Spalloni A, Amantea D, Nutini M, Petrelli F, Longone P, Bagetta G, Nisticò R, Mercuri NB. The protective role of catalase against cerebral ischemia in vitro and in vivo. Int J Immunopathol Pharmacol 2011; 24:735-47.
68. Aslani S, Hossein-Nezhad A, Mirzaei K, Maghbooli Z, Asgarabad SN, Karimi F. Tandem repeats of the CATT element of macrophage migration inhibitory factor gene may predict gestational diabetes mellitus severity. Eur J Inflamm 2011; 9:193-7.
69. Carrier Y, Ma HL, Ramon HE, Napierata L, Small C, O'Toole M, Young DA, Fouser LA, Nickerson-Nutter C, Collins M, Dunussi-Joannopoulos K, Medley QG. Inter-regulation of Th17 cytokines and the IL-36 cytokines *in vitro* and *in vivo*: implications in psoriasis pathogenesis. J Invest Dermatol 2011; 131:2428-37.
70. Ricci G, Piccinno V, Giannetti A, Miniaci A, Specchia F, Masi M. Evolution of hypogammaglobulinemia in premature and full-term infants. Int J Immunopathol Pharmacol 2011; 24:721-6.
71. Hossein-Nezhad A, Mirzaei K, Aslani S, Tootee A, Karimi F. MIF expression in induced peripheral blood mononuclear cells by vitamin D3 and its potential correlation with resting metabolic rate in obesity. Eur J Inflamm 2011; 9:125-34.
72. Tripodi D, D'Ercole S, Pasini M, Nastasio S, Bonini S, Giuca MR. Inflammatory and immunitary modifications in saliva of subjects with labial and tongue piercing. Eur J Inflamm 2011; 9:185-91.
73. Shimizu Y, Dobashi K, Fueki N, Fueki M, Okada T, Tomioka S, Makino S, Mori M. Changes of immunomodulatory cytokines associated with omalizumab therapy for severe persistent asthma. J Biol Regul Homeost Agents 2011; 25:177-86.
74. Palumbo P, Cinque B, Miconi G, et al. Biological effects of low frequency high intensity ultrasound application on ex vivo human adipose tissue. Int J Immunopathol Pharmacol 2011; 24:411-22.
75. Caimmi S, Marseglia A, Caimmi D, Marseglia GL. Friday asthma crisis in the daughter of two bakers. Int J Immunopathol Pharmacol 2011; 24:517-8.
76. Failli A, Legitimo A, Mazzoni A, Urbani L, Scatena

F, Mosca F, Consolini R. The combination of immunosuppressive drugs with 8-methoxypsoralen and ultraviolet a light modulates the myeloid-derived dendritic cell function. Int J Immunopathol Pharmacol 2011; 24:89-99.

77. Romano G, Barbagli G, Lazzeri M. The use of topical hyaluronic acid and silver sulfadiazine (Altergen®) in patients undergoing two-stage anterior urethroplasty with oral mucosal graft. Eur J Inflamm 2011; 9:175-83.
78. Symeonidou I, Hatzistilianou M, Papadopoulos E, Dovas CI, Karagouni E, Pappa S, Pantzartzi CN, Kourelis A, Frydas S. Susceptibility and resistance to canine leishmaniosis is associated to polymorphisms of the canine TNF-α gene. Eur J Inflamm 2011; 9:23-9.
79. Pantalone A, Abate M, D'Ovidio C, Carnevale A, Salini V. Diagnostic failure of ciprofloxacin-induced spontaneous bilateral Achilles tendon rupture: case-report and medical-legal considerations. Int J Immunopathol Pharmacol 2011; 24:519-22.
80. Park JA, Pak JJ, Kim J, Lee EY, Lee YJ, Song YW, Lee EB. Adenosine A2A receptor polymorphisms in Korean patients with systemic sclerosis. Int J Immunopathol Pharmacol 2011; 24:505-8.
81. Racciatti D, Gorgoretti V, Sepede G, Gambi F, Pizzigallo E. An Italian study on health-related quality of life and fatigue in patients with chronic fatigue syndrome and patients with chronic HCV virus infection: similarities and differences. Int J Immunopathol Pharmacol 2011; 24:673-81.
82. Tammaro A, Narcisi A, Persechino S, De Marco G, Camplone G. Contact allergy to disperse blue dye in goggles for swimming-bath. Eur J Inflamm 2011; 9:83-84.
83. Zhang C-Y, Shao S-H, Chen X, Shi Y-L. Anti-frostbite effects of *prunus tomentosa thunb* total flavone Eur J Inflamm 2011; 9:65-71.
84. Sancilio S, Di Giacomo V, Quaglietta AM, et al. TRAIL promotes a pro-survival signal in erythropoietin-deprived human erythroblasts through the activation of an NF-κB/IκBα pathway. J Biol Regul Homeost Agents 2011; 25:375-86.
85. Frega A, Lorenzon L, Giovagnoli MR, De Sanctis L, Fabiano V, Lukic A, Moscarini M, Torrisi MR, French D. Prognostic implication of high risk human papillomavirus E6 and E7 mRNA in patients with intraepithelial lesions of the cervix in relationship to age. Int J Immunopathol Pharmacol 2011; 24:461-70.
86. Zhu J-S, Xu Z-P, Song M-Q, Zhang Q. Effect of oxymatrine combined with low dose 5-FU on lymphatic vessel and microvascular endothelial cell growth of gastric cancer in a severe combined immunodeficient mouse orthotopic implantation model. Eur J Inflamm 2011; 9:45-51.
87. Schiavone Panni A, Vasso M, Cerciello S, Maccauro G. Metallosis following knee arthroplasty: a histological and immunohistochemical study. Int J Immunopathol Pharmacol 2011; 24:711-9.
88. Ciprandi G, De Amici M, Quaglini S, et al., Workgroup "Allergy Project". Prediction of allergy by total serum IgE measurements in infancy: a 10-year follow-up. Eur J Inflamm 2011; 9:199-203.
89. De Amici M, Villani MA, Milanesi E, Rossini B, Barco S, Gerletti M, Ciprandi G. Adverse reactions to anaesthetics prevented by the use of specific laboratory tests Eur J Inflamm 2011; 9:79-81.

TREADMILL EXERCISE IMPROVED ADRIAMYCIN-INDUCED NEPHROPATHY

C.C. PENG[1,2,3], K.C. CHEN[4], H.Y. LU[3] and R.Y. PENG[5]

[1]Graduate Institute of Clinical Medicine, Taipei Medical University, Taipei, Taiwan; Department of Physical Therapy, [3]Graduate Institute of Rehabilitation Science, College of Health Care, China Medical University, Taichung, Taiwan; [4]Department of Urology, Taipei Medical University-Shuang Ho Hospital, Taipei Medical University, Taipei, Taiwan; [5]Research Institute of Biotechnology, Hungkuang University, Shalu County, Taichung Hsien, Taiwan

Received June 9, 2011 – Accepted November 4, 2011

Adriamycin nephropathy (AN) or doxorubicin-induced chronic kidney disease (DRCKD) has several strengths as an experimental model of renal diseases involving glomerulosclerosis, tubulointerstitial inflammation and fibrosis. Exercise has shown to be beneficial to many chronic diseases. We hypothesize that treadmill exercise may improve AN, and an investigation was carried out with the AN SD rat model. Treadmill exercise was conducted three times per week, each time for 30 and 60 min. DR induced swelling of glomeruli, collagen deposition in the interstitium and renal cortex, and increased the serum levels of MDA, IL-6, PDGF-BB, MMP-2, MMP-9, TGF-β, p-PDGFR, uric acid, serum cholesterol, triglycerides, BUN, creatinine, blood platelet count, ratio of kidney to body weight, glomerular volume, and urinary BUN and protein. Conversely, levels of serum SOD, TNF-α, p-PI3K, p-Akt, albumin, WBC, RBC, and urinary creatinine were decreased. Treadmill exercise ameliorated most of these damaging effects, better outcome was found for the 60-min exercise training. Conclusively, the endurance exercise is more associated with the normalization of signaling expressions involving TGF-β, PDGF-BB, *p*-PDGFR, *p*-PI3K, and *p*-Akt, which may help CKD patients to restore cell survival, proliferation, and growth. As rehabilitation is a personalized medicine, an appropriate design to fit individual feasibility has to be well figured out.

Adriamycin nephropathy (AN) (or doxorubicin nephropathy, DN) has several strengths as an experimental model of chronic kidney disease (CKD). Doxorubicin (DR) alters glomerular endothelium and exerts oxidative damage on cell structure through a direct reduction to a semiquinone radical or by producing reactive oxidative species (ROS) via the xanthine oxidase system (1). Oxidative stress (OS) and inflammation increase in normal aging and in CKD (2). DN is characterized by glomerulosclerosis, tubulointerstitial inflammation and fibrosis (3, 4). Fibrosis typically results from chronic inflammation. Emerging evidence has revealed that the mechanisms driving fibrogenesis are distinct from those regulating inflammation (5). Fibroblasts and myofibroblasts are considered to be the key mediators of fibrosis in the kidney and other organs (6). Fibroblasts in kidney fibrosis emerge via endothelial-to-mesenchymal (EMT-EndMT) transition (7). Activated myofibroblasts serve as the primary collagen-producing cells (5). The mice with DRCKD develop overt proteinuria from day 5, with

Key words: chronic kidney disease, doxorubicin (adriamycin), exercise, matrix metalloproteinases, renal fibrosis

Mailing address:
Chiung-Chi, Peng, Ph.D.
4F-3, No. 133, Song-Pin Rd, Taipei,
Taiwan, 110
Tel/Fax: +886 2 27585767
e-mail: misspeng@ms2.hinet.net

0393-974X (2012)

mild glomerosclerotic lesions starting by week 4, becoming extensive with associated tubulointerstitial fibrosis by week 6 (8).

Transforming growth factor (TGF)-β and platelet-derived growth factor (PDGF) are known to be important cytokines for mesangial proliferation and renal fibrogenesis in glomerulonephritis and anti-Thy1 nephritis. TGF-β and PDGF stimulate mesangial cell proliferation and the synthesis of extracellular matrix (ECM) proteins, leading to progressive matrix expansion changes (mesangial proliferation) and renal fibrosis (9, 10). Almost all experimental and human renal diseases are characterized by altered expression of components of the PDGF system. PDGF alpha-receptors (PDGFR-α) and beta-receptors (PDGFR-β) are induced during fibrogenesis, thereby amplifying biological responses to PDGF isoforms (11). MMP-2 may regulate collagen accumulation in CKD inflammatory sites, allowing cyst enlargement and limiting the severity of interstitial fibrosis (12). Much of the literature has shown that TGF-β1 is strongly implicated in the progression of renal fibrosis (13). However, some studies demonstrated TGF-β1 to be with duality, acting either as a pro-apoptotic or an anti-apoptotic depending on the cell type or circumstances (14). Akt and PI3K are related to the cell growth and proliferation (15). Numerous interventions including aerobic training, resistance exercise training, and combined training programs have been reported as beneficial to the end-stage renal disease (ESRD) (16).

Kidney is one of the major sites for elimination of many cytokines. The delicate equilibrium of pro-inflammatory cytokines and their inhibitors is clearly dysregulated in CKD patients, particularly seen in the altered immune response in uremia linking to a diversity of complications including activation of proinflammatory interleukin-6 (IL-6) (17). Exercise decreases IL-6 and TNF-alpha levels (18). Acute exercise increases adipose tissue interstitial adiponectin concentration in both overweight and lean subjects (19).

The severity and timing of renal injury in DN implicates it to be a model suitable for testing interventions that could either worsen or protect against renal injury. Moreover, DN has been shown in numerous studies to be modulated by both non-immune and immune factors, and has facilitated further study of mechanisms of tubulointerstitial injury (4). More importantly, the type of structural and functional injury is very similar to that of chronic proteinuric renal disease in humans (4), and it is a highly reproducible model.

Considering rehabilitation has improved many chronic diseases, we hypothesized that treadmill exercise may improve DN by modulating levels of some relevant cytokines (IL-6 and TNF-α), signaling proteins (Akt, PI3K, TGF-β1, and smooth muscle actin), certain enzymes (metalloproteinase-2, metalloproteinase-9 and superoxide dismutase), and the oxidative stress marker malondialdehyde.

MATERIALS AND METHODS

Chemicals and kits

All the biochemical tests were conducted using the enzymatic colorimetric assays by the specific kits provided by Roche, either located in Switzerland or USA. Collagen was assayed by Sirius Red staining. Doxorubicin was a product of Pfizer (Milano, Italia), Pro-PREP lysis buffer was purchased from iNtRON Biotechnology (Seongnam, Korea). The kit source for other determinations included SOD and TBARS from Cayman (MI, USA); Rat IL-6 EIA KIT from PeproTech (NJ, USA); Rat TNF-α KIT and Quantikine® Mouse/Rat PDGF-BB Immunoassay from R&D Systems Inc. (MN, USA). The source of the antibody used in this experiment was: phosphor-Akt (1:1000), phosphor-PDGF Receptor β (1:1000) and β-actin from Cell Signaling (MA, USA); phosphor-PI3K (1:500) from Santa Cruz (CA, USA); α-Smooth Muscle Actin (1:1000) from Sigma-Aldrich Co. (MO, USA). Chemiluminescent HRP Substrate was the product of Millipore (MA, USA).

Animal CKD model

This experimental protocol was approved by the China Medical University Ethic Committee of Experimental Animals (Taichung, Taiwan). Principles of laboratory animal care (NIH publication) were followed. Thirty-six four-week old Sprague-Dawley adult male rats (BioLASCO Taiwan Co., Ltd. Resources) weighing 225-250 g were used in the study. These rats were acclimated and fed ordinary laboratory chow during the first week. The rats were housed in an animal room maintained at a relative humidity (RH) 50-60% within 23°C±1°C with a 12-h/12-h light/dark cycle. The animals were allowed free access to water and ordinary laboratory pellet chow containing 1.8-2.2% of calcium, 1.1% of phosphorus and 2650 kcal/kg energy. These rats were randomly assigned

to six groups: the normal sedentary, the normal 30-min exercise, the normal 60-min exercise, the doxorubicin induced CKD (DR-CKD), the DRCKD+30 min-exercise, and the DRCKD+60 min-exercise groups. These six groups were separately housed in twelve colony cages, 3 rats in each. CKD was induced by a single s.c. injection of 8.5 mg/kg of doxorubicin (20).

Treadmill exercise protocol

Initially, a pre-exercise training was tried by increasing gradually the running exercise from 5 to 10 min, and then to 20 min. and administered with doxorubicin 8.5 mg/kg s.c. after a 2 week-pre-exercise training. From the third week on, the rats were subjected to formal running exercise 30 m/min, 30 or 60 min/day, 3 times per week for a total period of 13 weeks. During the whole course, the sedentary group remained in the cages under the same environmental condition and inspected daily.

Blood, urine and tissue sample collection

Urine Collection. On finishing the treatment at week 13, rats were moved to the metabolic cage two days before the end of week 13. The urine was collected from 8:00 am to 8:00 am the following day. The total volume of urine per day for each rat was taken. The urine samples were freshly analyzed for urinary protein, creatinine and BUN or immediately stored in the freezer at 0-4^{o}C when not in use. Urine BUN and creatinine were measured by reagent (Siemens, Bakersfield, CA, USA) and automatic analyzer (Ciba-Corning Express Plus) (Ciba-Corning, USA). The urinary protein concentration was measured using ELISA reader.

Blood Collection. After urine collection, the blood samples were immediately withdrawn from the abdominal aorta under ether intraperitoneal ketamine and xylasine anesthesia. The sample blood was centrifuged at 3000×g to separate the serum. The serum obtained were used for measurement of parameters including cell count, serum calcium, phosphate, albumin, uric acid, cholesterol, triglyceride, BUN and creatinine, which were measured by reagent (Siemens, Bakersfield, CA, USA) and automatic analyzer (Ciba-Corning Express Plus) (Ciba-Corning, USA).

Tissue Collection. After euthanization, the organs were inspected visually for their external morphological changes. The kidneys were exsiccated and immediately frozen with liquid nitrogen and stored in -80^{o}C.

Glomerular volume

The glomerular volume was determined by the formula (21).

$GV = (\beta/k)\,(G_A)^{3/2}$ ……1

Where GV = glomerular volume

G_A =cross-sectional tuft area

β is the shape coefficient (1.38 for this case, for a sphere =1.38)

k is the size distribution coefficient (=1.1 for this case)

Histochemical examinations

Kidneys were fixed by immersion with 10% formalin in PBS (pH 7.4) at 4°C for 24 h and processed for paraffin embedding. Paraffin sections were dewaxed in xylene and rehydrated in a series of ethanol washes. The nuclei of these specimens were subjected to Weigert's Haematoxylin-Eosin stain. Otherwise, the collagen content was stained with Sirius Red. The area stained by Sirius Red were counted with the software Image-Pro Plus (MediaCybernetics, Bethesda, MD, USA).

ELISA of IL-6, TNF-α, SOD, TBARs and PDGF-BB

Serum levels of IL-6, TNF-α and PDGF-BB were measured by the Rat IL-6 EIA Kit from PeproTech Inc. (NJ, USA), Rat TNF-α Kit and PDGF-BB Kit (R&D Systems Inc., MN, USA), respectively. The SOD and the thiobarbituric acid reactive substance (TBARs) were assayed with the commercial ELISA kits provided by Cayman Chemical Co. (MI, USA). All ELISA protocols were performed by following the manufacturer's instructions. The SYSMEX K-1000 Reader used was a product of San-Tong Instrument Co. (Taipei, Taiwan).

Gelantinolytic zymography

The expression of MMP-2 and MMP-9, were assayed according to Leber and Balkwill (22). Briefly, the serum blood centrifuged at 10000×g. The supernatant serum (10 μL) was loaded onto a 7.5 % sodium dodecyl sulfate (SDS)-polyacrylamide gel copolymerized with 0.1% gelatin and subjected to electrophoresis under 100 V for 1.5 h. In order to remove SDS, the gel was washed twice, each time with 2.5% TritonX-100 solution for 30 min, and then rinsed with incubation buffer (0.05 M Tris-HCl buffer, pH 8.0, 5 mM $CaCl_2$ plus 5 mM $ZnCl_2$). The mixture was incubated at 37°C overnight. The gel was stained with Coomasie Blue at room temperature for 2 h as described (22). Gelatinases in the serum can be detected as unstained gelatin degraded zones on the gel. Its amount expressed was quantified with a densitometer (ImagePro Plus 5.0 Medica Cybernetics).

Western blotting

Frozen renal cortex tissue samples (approximately 100 mg) were homogenized with the homogenizer (T10 basic, The IKA Company, Germany) in 1 mL of Pro-PREP lysis buffer (pH 7.2). The homogenate was centrifuged at 12000×g for 20 min at 4°C, and the supernatant was

collected as tissue sample lysate. The sample protein lysates were heated at 100°C for 10 min before loading and separated on precasted 7.5% SDS-PAGE. The proteins were electrotransferred onto the PVDF membrane in transfer buffer for 1 h. The nonspecific binding to the membrane was blocked for 1 h at room temperature with 5% nonfat milk in TBS buffer. The membranes were then incubated for 16 h at 4°C with various primary antibodies. After extensive washing in TBS buffer, the membranes were the incubated with secondary antibody in blocking buffer containing 5% nonfat milk for 1 h at room temperature. Membranes were then washed with TBS buffer and the signals were visualized using the Luminescent Image Analyzer LAS-4000 (Fujifilm, Tokyo, Japan). Levels of TGF-β, p-PDGFR, p-PI3K, p-Akt, and α-SMA were analyzed by each immunoassay according to the instructions given by the manufacturers as mentioned in the above section "Chemicals And Kits". β-Actin was used as the reference protein.

Statistical analysis

Data obtained in the same group were analyzed by Student's *t* test with computer statistical software SPSS 10.0 (SPSS, Chicago, IL). ANOVA software statistical system was used with the Tukey's testing to analyze the variances and significances of difference between paired means. Significance of difference was judged by a confidence level of $p < 0.05$.

RESULTS

Change in physiological parameters

The body weight of the three normal controls was rather comparable. However, DR severely suppressed the body weight, which was recovered by exercise in an intensity-dependant fashion (Table I). The normal ratio of kidney to body weight resided in range 0.63 to 0.65 among all the three normal groups. DR induction caused edema and swelling of kidney and raised the ratio to 0.90%. Exercise with 30-min and 60-min programs respectively recovered it to 0.72% and 0.69% (Table I).

DR-induced rats showed swollen kidneys with edema, hence the glomerular volume (GV) increased about +21%. On receiving training, the GV reduced to +19% and +12%, respectively by 30-min and 60-min exercise (Table I). The normal values of rat blood cells were $(1.3\sim1.6)\times10^4/\mu L$, $(7.7\sim8.3)\times10^6/\mu L$, and $(8.40\sim8.97)\times10^5/\mu L$, respectively for WBC, RBC, and platelet. DR caused reduction of

Table I. *Changes of physiological parameters by exercise training.*

Parameter	Normal			DR-CKD		
	Control	30-min	60-min	Control	30-min	60-min
Body weight (g)	461 ± 60^{a}	422 ± 54^{a}	413 ± 52^{a}	274 ± 7^{b}	287 ± 14^{b}	303 ± 16^{c}
Ratio%, (Kw/Bw)	0.63 ± 0.1^{c}	0.63 ± 0.1^{c}	0.65 ± 0.1^{c}	0.90 ± 0.1^{a}	0.72 ± 0.1^{b}	0.69 ± 0.1^{b}
Glomerular volume (mm^3)	1.00 ± 0.2^{ab}	1.00 ± 0.1^{b}	0.9 ± 0.1^{c}	1.21 ± 0.1^{a}	1.19 ± 0.2^{ab}	1.12 ± 0.1^{ab}
WBC, $\times10^4/\mu L$	1.6 ± 0.03^{a}	1.5 ± 0.05^{a}	1.3 ± 0.08^{a}	1.4 ± 0.02^{a}	1.1 ± 0.02^{a}	1.3 ± 0.02^{a}
RBC, $\times10^6/\mu L$	8.3 ± 0.4^{a}	8.4 ± 0.1^{a}	7.7 ± 0.6^{a}	5.7 ± 0.4^{b}	6.1 ± 0.6^{b}	6.1 ± 0.6^{b}
Platelet, $\times10^5/\mu L$	6.8 ± 2.0^{c}	9.0 ± 1.0^{c}	8.6 ± 0.4^{c}	15.8 ± 2.9^{a}	13.0 ± 1.3^{ab}	11.7 ± 1.8^{bc}

**The values are indicated in mean±SD (n=6).*
Different superscripts in each row indicate significantly different.
Data obtained in the same group were analyzed by Student's t test with computer statistical software SPSS 10.0 (SPSS, Chicago, IL). ANOVA software statistical system was used with the Tukey's testing to analyze the variances and significances of difference between paired means. Significance level p<0.05.

Table II. *The serum and urinary biochemical parameters.*

Parameter (normal range, mg/dL)	Normal			DR-CKD		
	Control	30-min	60-min	Control	30-min	60-min
SERUM						
Calcium (5.3-13.0)	8.9±0.5^{a}	9.1±0.6^{a}	9.0±0.4^{a}	9.3±0.6^{a}	8.6±0.2^{a}	8.8±0.1^{a}
Phosphate (5.3-8.3)	7.1±0.3^{a}	7.4±1.0^{a}	8.5±1.1^{a}	8.9±0.4^{a}	7.2±0.3^{a}	8.1±1.0^{a}
Albumin (3.8-4.8)	4.2±0.1^{a}	4.6±0.3^{a}	4.4±0.2^{a}	2.8±0.0^{b}	3.0±0.1^{b}	3.1±0.4^{b}
Uric acid (2.0-13.0)	2.1±1.0^{b}	2.1±0.7^{b}	2.5±0.9^{b}	3.9±0.7^{a}	8.9±0.5^{a}	3.2±1.1^{b}
Cholesterol (40-130)	68±11^{c}	58±6^{c}	53±14^{c}	681±675^{a}	364±25^{ab}	72±8^{b}
Triglyceride (26-145)	47±11^{d}	46±13^{d}	45±10^{d}	532±82^{a}	266±41^{b}	207±28^{c}
BUN (15-21)	16±2^{b}	20±1^{b}	17±1^{b}	35±2^{a}	26±1^{a}	21±1^{b}
Creatinine (0.2-0.8)	0.6±0.1^{b}	0.6±0.1^{b}	0.5±0.1^{b}	0.9±0.3^{a}	0.8±0.1^{b}	0.7±0.1^{b}
URINE (mg/dL)						
Protein	21±14^{c}	23±11^{c}	21±5^{c}	163±16^{a}	158±7^{a}	138±10^{b}
Creatinine	172±15^{ab}	177±11^{b}	177±8^{a}	9±3^{c}	54±3^{c}	73±11^{b}
BUN	61±6^{c}	65±9^{c}	50±4^{d}	247±15^{a}	227±45^{a}	180±6^{b}

**Values are indicated in mean±SD (n=6).*
Different superscripts in each row indicate significantly different.
Data obtained in the same group were analyzed by Student's t test with computer statistical software SPSS 10.0 (SPSS, Chicago, IL). ANOVA software statistical system was used with the Tukey's testing to analyze the variances and significances of difference between paired means. Significance level $p<0.05$.

WBC and RBC, but increased the platelet count to 1.58×10^{6}/μL (Table I). Exercise caused only slight elevation of RBC, but significant suppression of platelets (Table I). Strangely, the WBC count was significantly reduced by exercise. Exercise only showed only slight amelioration on RBC and platelet counts (Table I).

Change of serum and urinary biochemical parameters

The serum calcium was totally unaffected by DR, although the phosphate level was slightly elevated by DR. No apparent difference was found among all other groups (Table II). The serum albumin level was severely decreased on DR treatment. Exercise was able to secure only a slight difference. The serum uric acid level slightly increased in all DR-treated groups, however still remaining within normal concentration range 2.0 to 13.0 mg/dL (Table II). DR triggered the elevation of serum levels of cholesterol, triglycerides, BUN and creatinine, which was seen

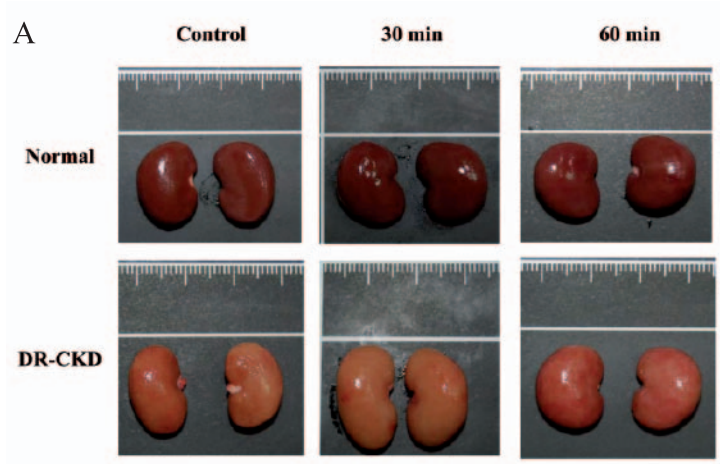

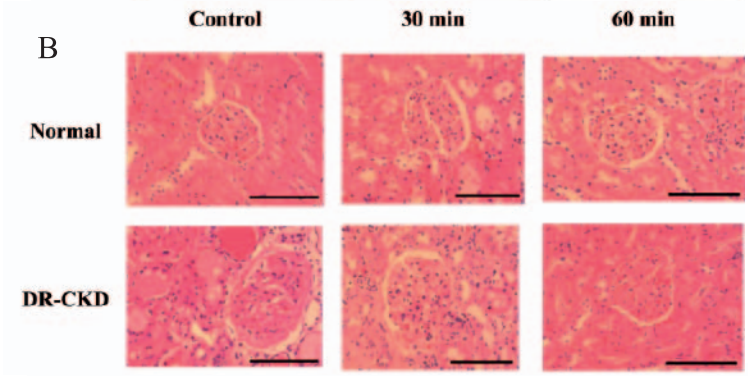

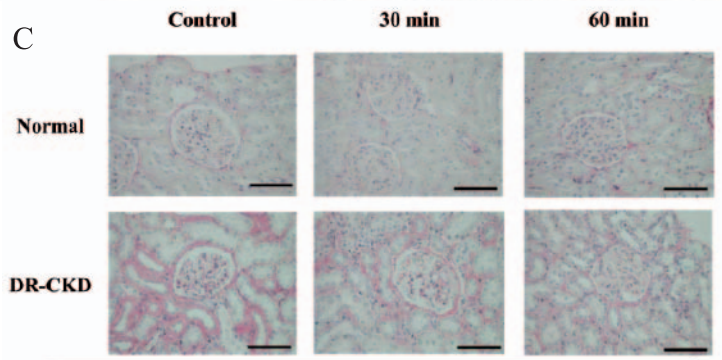

Group	Relative area stained by Sirius Red, ppm		
	Control	30 min	60 min
Normal	18.3±0.9[a]	18.4±0.3[a]	20.5±3.3[a]
DR-CKD	67.2±26.3[c]	30.0±4.9[b]	23.4±0.8[a]

*The areas stained by Sirius Red were counted with the software Image-Pro Plus (MediaCybernetics, Bethesda, MD, USA). (n = 6)
ppm: parts per million
= (the area stained by Sirius Red in the field×10^6)/entire area of the field

Fig. 1. ***A)*** *The renal morphology of rats affected by exercise intensity.* ***B)*** *The hematoxylin-eosin staining on glomeruli of rats trained with/and without different exercise intensity (400x).* ***C)*** *The Sirius Red staining on renal mesangiums of rats trained with/and without different exercise intensity. The table shown below indicates the quantification of the Sirius Red staining (No. of each group=6). Different superscripts in each row indicate significantly different. Data obtained in the same group were analyzed by Student's t test with computer statistical software SPSS 10.0 (SPSS, Chicago, IL). ANOVA software statistical system was used with the Tukey's testing to analyze the variances and significances of difference between paired means. Significance level $p<0.05$.*

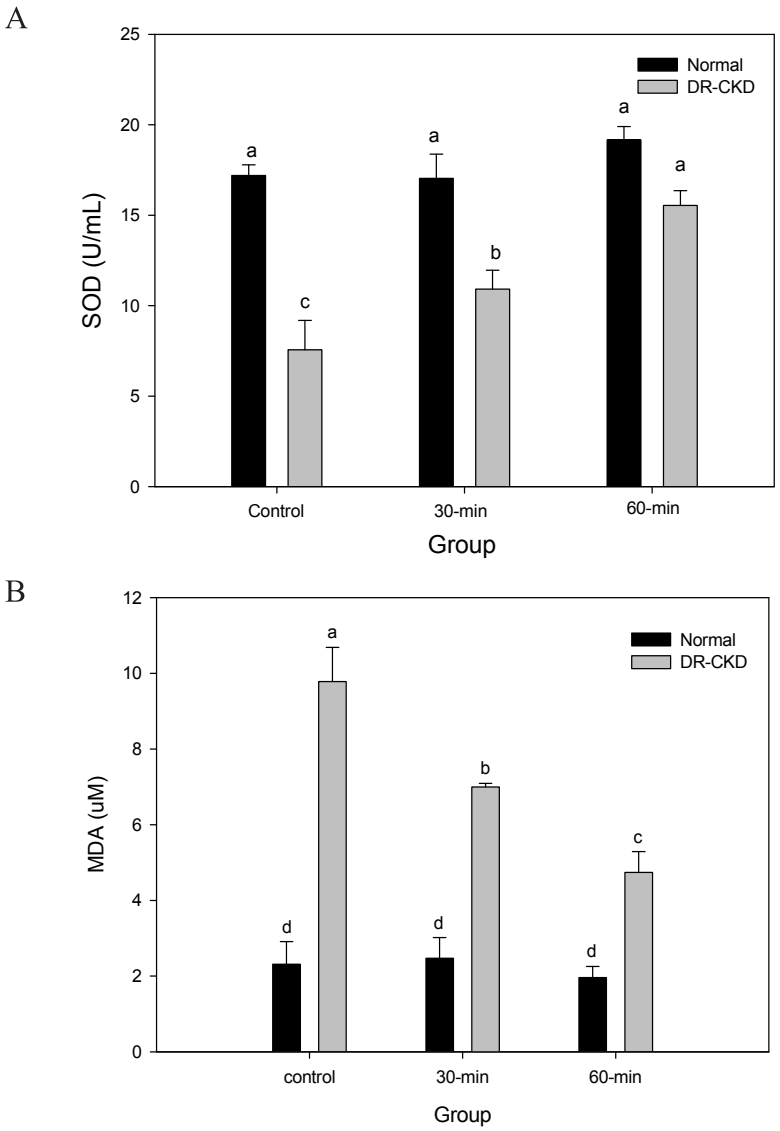

Fig. 2. ***A****) Serum levels of superoxide dismutase affected by exercise training.* ***B****) Serum levels of malondialdehyde affected by exercise training. Different superscripts indicate significantly different. Data obtained in the same group were analyzed by Student's t test with computer statistical software SPSS 10.0 (SPSS, Chicago, IL). ANOVA software statistical system was used with the Tukey's testing to analyze the variances and significances of difference between paired means. Significance level p<0.05 (No. of each group=6).*

significantly ameliorated by exercise, particularly by the 60-min training program (Table II). The urinary creatinine level was significantly suppressed, but the urinary BUN and protein levels were all elevated by DR treatment. By 60 min-exercise, the creatinine levels raised slightly, but not to the normal level; BUN was only suppressed slightly, although significantly comparing to the DR control, yet not recovering to the normal level (Table II).

Appearance of kidneys

The kidneys of DR-CKD rats looked pale and light in color compared to the controls (Fig. 1A). After exercise training, the kidneys of the DR-CKD

60-min exercise rats recovered slightly but not returning to normal color and size (Fig. 1A).

Exercise ameliorated glomerular swelling and the collagen deposition

The glomeruli in DR-CKD rats were swollen with edema (Fig. 1B). Exercise restored the glomerular size in an exercise-intensity-dependent fashion. The glomeruli recovered almost to normal size after a period of 11-week treadmill training with 60-min exercise protocol (Fig. 1B). In the renal interstitium and cortex of DR-CKD rats, a huge amount of collagen deposition occurred, which showed gradual attenuation resulting from exercise, the least amount was found in the DR-CKD with 60 min exercise program (Fig. 1C)

Exercise alleviated SOD but suppressed MDA levels in a strength-dependent manner

A similar situation was found for serum SOD. DR suppressed SOD to 7.5U/mL comparing with 17U/mL of the control. Exercise recovered most SOD levels in a strength dependent manner (Fig. 2A). On the contrary, the serum MDA level in all controls remained almost constantly in range of 1.9 to 2.5 μM (Fig. 2B). On induction with DR, the serum level of MDA in the DR-CKD rats was rapidly raised to 9.75 μM, which was effectively suppressed after exercise training in an intensity dependent manner to 7.0 μM (for the 30-min exercise) and 4.6 μM (for the 60-min exercise rats) (Fig. 2B).

Effect of exercise on expression of interleukin-6 and TNF-α

DR upregulated the expression of IL-6 to 18.7 ng/mL comparing to the control (14.9 ng/mL) (Fig. 3A). Moderate exercise (30-min) further raised the level to 21ng/mL (for the 30-min exercise control) and 23ng/mL, but 60-min strenuous exercise recovered its level respectively to 16.5ng/mL in the 60-min control and 17.5ng/mL in the 60-min exercise group (Fig. 3A). In the three normal groups, moderate exercise suppressed slightly, while the strenuous exercise upregulated significantly the level of TNF-α (Fig. 3B) compared to the normal control level 1080pg/mL. In contrast, DR downregulated TNF-α to below 200 pg/mL. Although both exercise trainings totally failed to recover the TNF-α level to normal levels, however, slight improvement was still seen with a strength-dependent manner (Fig. 3B).

Effect of exercise on the serum level of PDGF-BB

The level of PDGF-BB in the three control groups usually retained at below 500pg/mL. DR severely damaged kidney and upregulated PDGF-BB to a level of 3000pg/mL. Moderate exercise slightly suppressed it to 2500pg/mL. But more significant amelioration was furnished by more endurance exercise to 900pg/mL (Fig. 3C).

Effect of exercise on MMP-2 and MMP-9

MMP-2 was highly upregulated, but MMP-9 seemed to be totally unaffected, in the DR control group. The increase of MMP-2 was suppressed by exercise training in a strength-dependent manner. In contrast, levels of MMP-2 and MMP-9 in all three controls were rather comparable (Fig. 4).

Effect of exercise on TGF-β, p-PI3K, and p-Akt

DR upregulated TGF-β and simultaneously downregulated p-PI3K and p-Akt. No apparent changes were seen any of the normal groups (Fig. 5). Exercise upregulated TGF-β in an intensity–dependant fashion, and similar trend was found for both p-PI3K and p-Akt levels (Fig. 5).

DR upregulated p-PDGFR but did not affect level of α-SMA

The upregulation of p-PDGFR by DR was suppressed by exercise training in an intensity-dependant manner, moderately by the 30-min and entirely by the 60-min exercise. Instead, levels of α-SMA were unaffected in any of the groups (Fig. 6).

DISCUSSION

Body weight loss was slightly regained by 60-min treadmill exercise

CKD impairs muscle protein metabolism leading to muscle atrophy, as a consequence, body weight loss was apparently seen in the DRCKD groups (3). Both the resistance exercise (muscle overload) and endurance training (treadmill running) affect CKD-induced abnormalities in muscle protein metabolism and progenitor cell function. Exercise blunted the increase in disease-induced muscle proteolysis

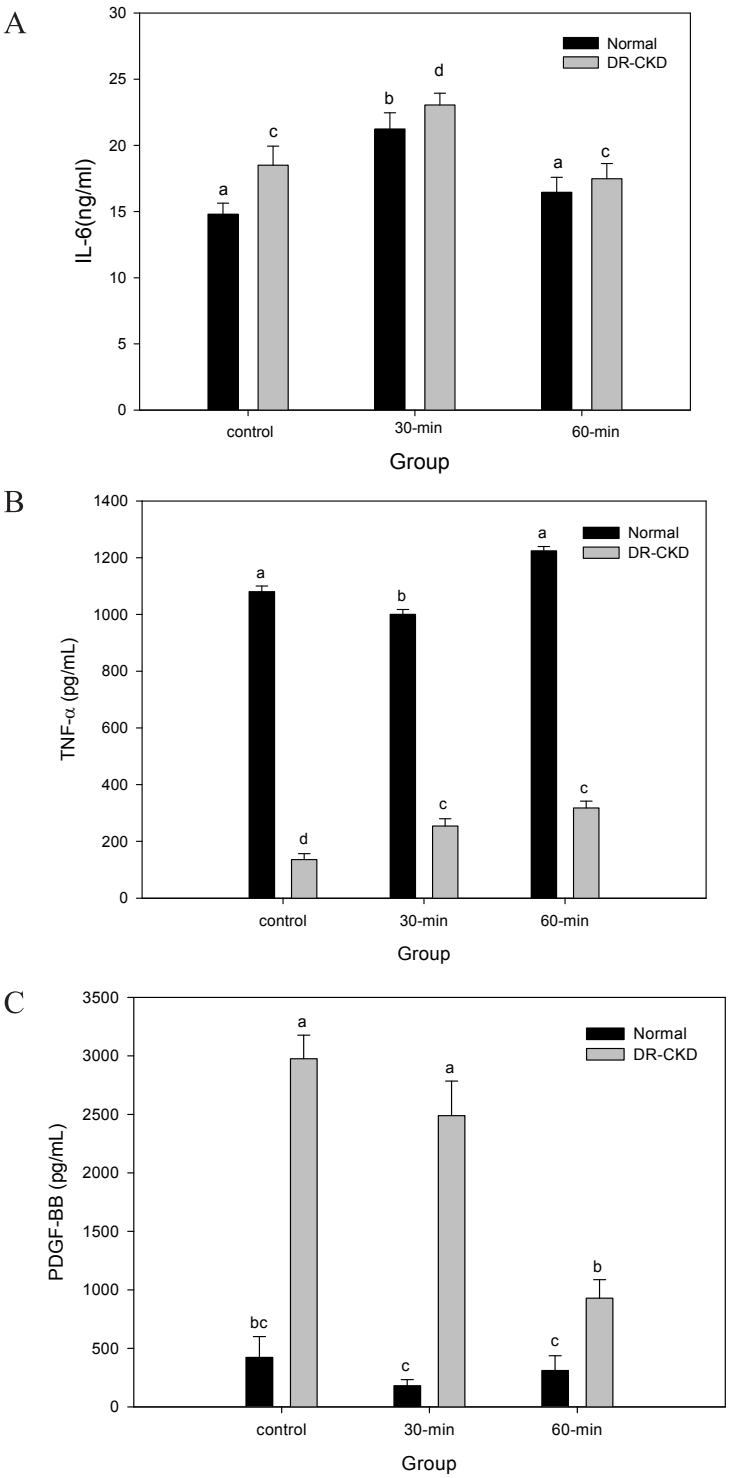

Fig. 3. ***A****) The cytokine IL-6 affected by exercise training.* ***B****) The cytokine TNF-α affected by exercise training.* ***C****) Cytokine PDGF-BB expression affected by exercise training. Different superscripts indicate significantly different. Data obtained in the same group were analyzed by Student's t test with computer statistical software SPSS 10.0 (SPSS, Chicago, IL). ANOVA software statistical system was used with the Tukey's testing to analyze the variances and significances of difference between paired means. Significance level p<0.05 (No. of each group=6).*

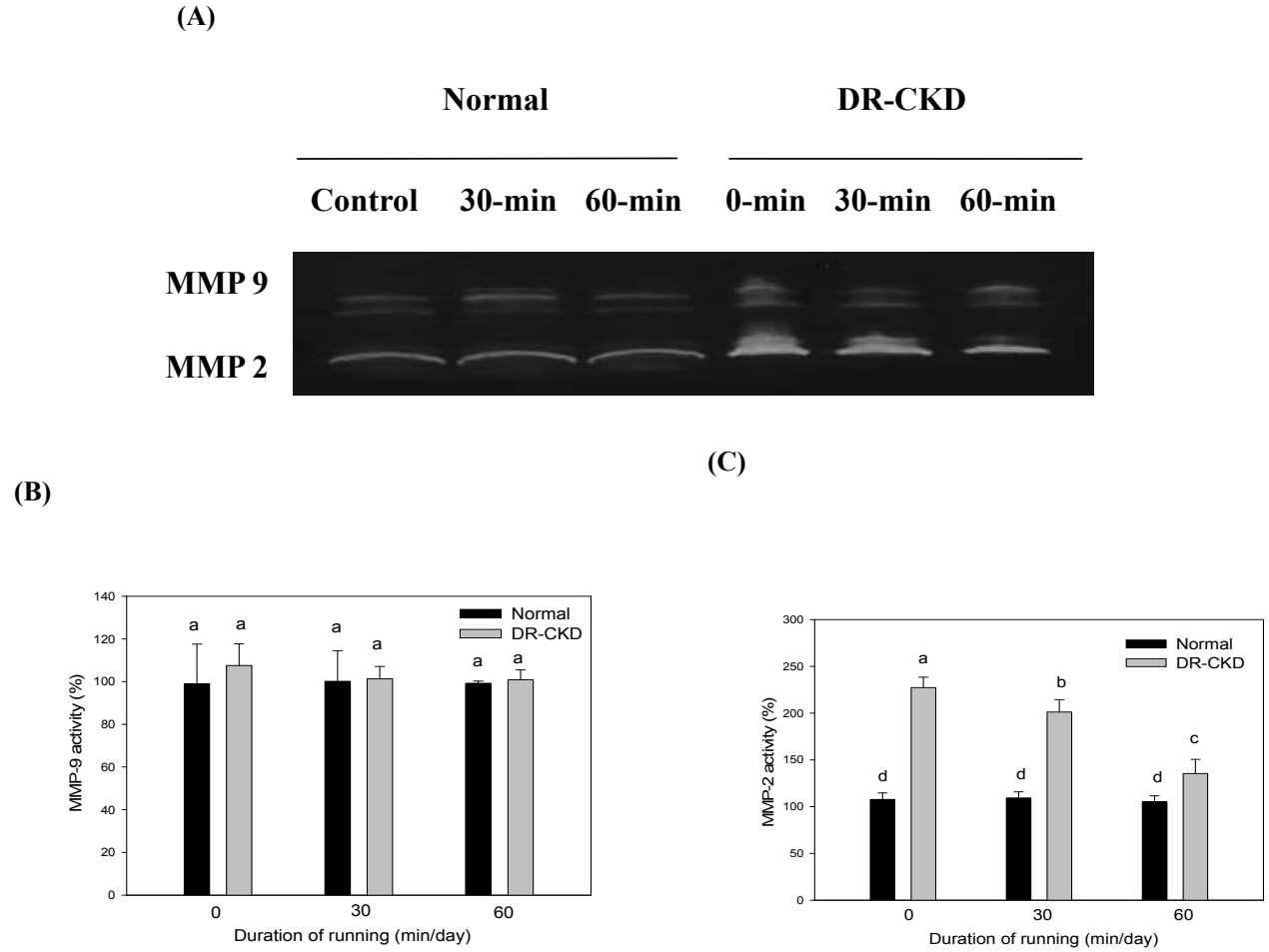

Fig. 4. *Zymography of serum levels of MMP's analyzed by Elisa Assay (**A**), and its quantified data for MMP-9 (**B**), and MMP-2 (**C**).*

(3). Treadmill exercise only showed a slight ameliorative effect in this regard (Table I). Wang et al. demonstrated muscle loading, but not treadmill running, corrected protein synthesis and progenitor cell (23).

Glomerular hypertrophy was recovered by exercise training

The type of structural and functional injury in AN is very similar to that of chronic proteinuric renal disease in humans (1). Mice with AN show glomerular hypertrophy and hyaline deposits with resorption droplets in tubule cells, mesangial expansion in glomeruli, tubular vacuolization, global glomerular sclerosis, tubular collapse and severe interstitial expansion (23). Numerous interventions including aerobic training, resistance exercise training, and combined training programs have reported beneficial to the end-stage renal disease (ESRD) (16).

Elevation of BUN, *urinary creatinine* and *protein was ameliorated by exercise*

Clinically, a level of BUN in human exceeding 20mg/dL can be considered as CKD. Elevated levels of serum and urinary BUN could mean CKD impaired muscle protein metabolism leading to muscle atrophy (3). Exercise has been known to improve insulin sensitivity in skeletal muscle, and help lipolisis and glycolysis (24), which explains the amerliorating effect of exercise on the urinary protein (Table II), being consistent with Wang et al.

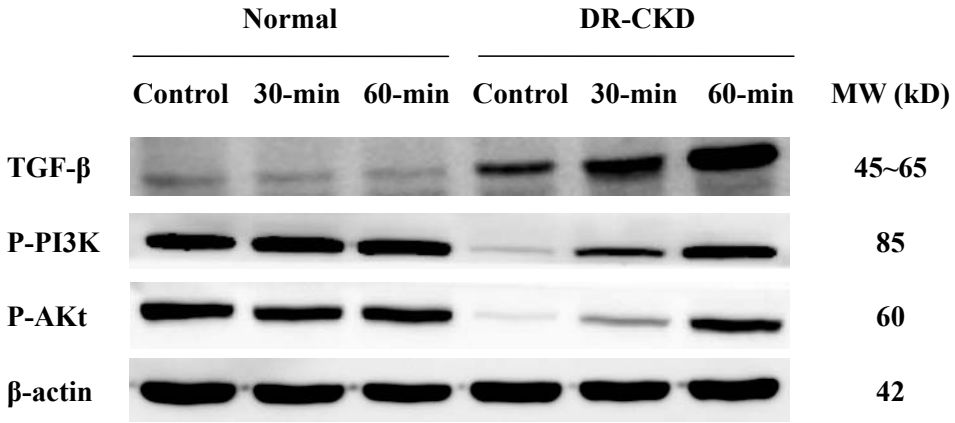

Fig. 5. *Effect of exercise training on the signals TGF-β, p-PI3K, and p-Akt associated with glomerulogenesis.*

(3).

Levels of serum calcium, phosphate, and albumin all remained normal in all groups. Only creatinine was slightly increased in the DRCKD group (Table II). In contrast, the corresponding serum biochemical parameters (mean±SD mg/dL) of human beings were: 9.16 (0.70) for calcium; 3.93 (0.84) for phosphate; 3.9 (0.5) for albumin; and 2.30 (0.84) for creatinine (25).

Cytokine expression intervened in carbohydrate and protein metabolism

Adriamycin-induced renal injury has been shown in numerous studies to be modulated by both non-immune and immune factors (4). IL-1, IL-2, and IL-6 can induce tissue proteolytic catabolism (24), which was highlighted in the increased levels of urinary BUN and protein (Table II). IL-6 is released from contracting muscles in large amounts and exerts its effect on adipose tissue, inducing lipolysis and gene transcription in abdominal subcutaneous fat (24).

A high level of IL-6 mediates protein breakdown in muscle (24). Hence the significantly lowered IL-6 in the 60 min-exercise group exhibited more significant body weight recovery compared to that of the 30-min exercise group (Table I). Pedersen and Fischer pointed out that muscle-derived IL-6 is likely to inhibit low-grade TNF-α production and, TNF-α-induced insulin resistance and could therefore, be important for mediating the beneficial health effects of exercise (24), a result consistent with our finding (Fig. 3A, 3B).

TGF-β1 inhibited the pre-fibrotic status in DR-CKD rats through downregulation of PDGF

DN is characterized by podocyte injury followed by glomerulosclerosis, tubulointerstitial inflammation and fibrosis. TGF-β1 induces the autophagy through TAK1 and Akt activation (14). The autophagic process constitutes an adaptative mechanism to glomerular injury by inhibiting apoptosis and promoting mesangial cell survival (14). DR upregulated, but exercise dowregulated PDGF-BB (Fig. 3C). Although DR also upregulated TGF-β, exercise further upregulated its level to higher levels in an intensity-dependant manner, depending on the strenuosity of exercise. In this regards, TGF-β1 is more likely an anti-apoptotic rather than an apoptotic (14). Evidence in our experiment showed the endurance exercise (60-min treadmill training) simultaneously upregulated TGF-β1, Akt, and PI3K, implicated in the improvement of the CKD status (14, 15).

PDGF has a role in growth-promoting activity for fibroblasts and smooth muscle cells, and in stimulating tissue repair processes (26). In chronic inflammatory conditions, the stimulatory effect of PDGF on connective tissue cells may lead to tissue fibrosis (27), consistent with our data (Figs. 1C and 3C). Accumulating evidence has supported that

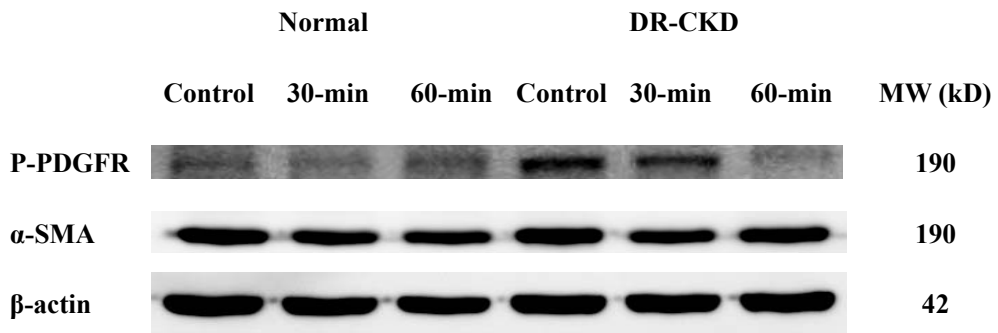

Fig. 6. *Fibrotic agents P-PDGFR and α-SMA affected by exercise training.*

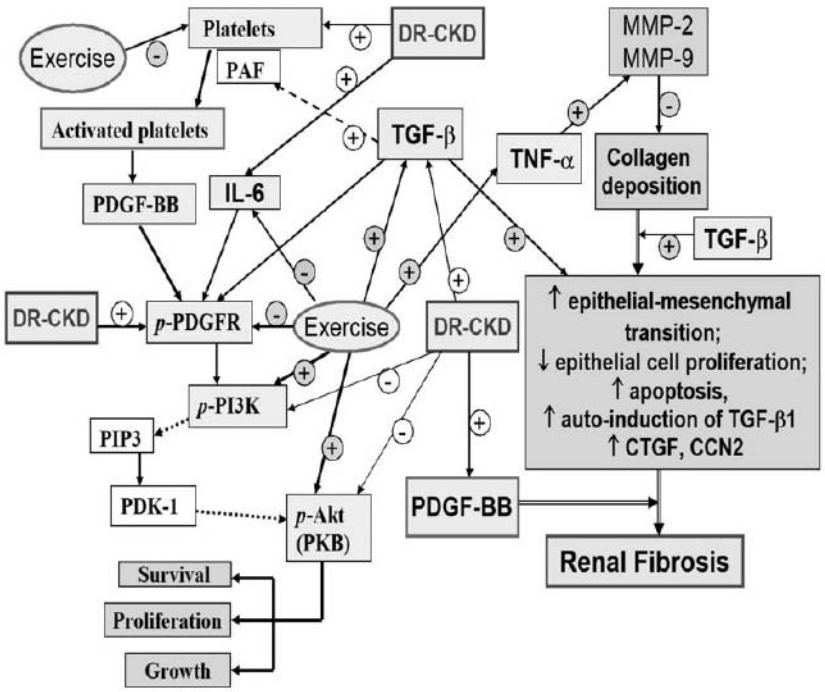

Fig. 7. *The action mechanism of exercise training to recover DR-CKD. CTGF, CCN2: connective tissue growth factor. PAF: platelet activation factor. The symbol '+' means upregulation or activation. The symbol '-' indicates downregulation or suppression.*

PDGF produced by mesangial cells or inflammatory cells may contribute to the development of glomerulonephritis through autocrine or paracrine mechanisms (26).

Antioxidative nature of exercise potentially implicated the protective effect on cardiovascular diseases

Exercise was capable of upregulating the SOD (Fig. 2A) and suppressing MDA levels (Fig. 2B), which may lead to the suppression of oxidative damage on serum LDL, an implication in the protective effect on the cardiovascular system. MDA level reached a peak on day 8 after treatment of DR. When these rats received SOD, they showed significant suppression of urinary protein excretion, serum and renal MDA compared to the DR control group (28). Alternatively, Zhu & Lu reported that nephrin plays an important role in maintaining glomerular filtration barrier. DR induced MDA

and suppressed SOD, resulting in reduced level of nephrin, contributing at least part of, if not entirely, the cause of reducing glomerular filtration rate (29).

Suppressed levels of MMPs regulated the collagen deposition and limited the severity of interstitial fibrosis

DR upregulated levels of MMP-2 and MMP-9, conversely, exercise suppressed these levels (Fig. 4A, 4B). Tubular cell epithelia-mesenchymal transition (EMT) is a fundamental contributor to renal fibrosis. In moderate and severe tubulo-interstitial damage, increased expression of MMP-2 was noted (30). The basement membrane containing type-IV collagen as its major collagen component, was attacked specifically by MMP-2. Kinetically, the huge substrate collagen deposition should have appeared before the expression of MMP-2. Thus, even exercise was shown to have effectively suppressed the expression of MMP-2 (Fig. 4), the huge amount of collagen previously already deposited in the interstitial compartment might not be degraded as immediately as expected. As a consequence, Siruis stain revealed much collagen deposition (Fig. 1C). Speculatively, only adequately efficient exercise is able to secure renal interstitial fibrosis. The results obtained are summarized in Fig. 7.

Conclusively, 60-min treadmill exercise training program may be more feasible in view of CKD recovery by rehabilitation. As rehabilitation is a personalized medicine, an appropriate design regarding the individual variation, the intensity, the duration and the frequency of exercise per week has to be well figured out. Our data also revealed that the endurance exercise is more associated with the normalization of signaling expressions involving TGF-β, PDGF-BB, *p*-PDGFR, *p*-PI3K, and *p*-Akt, which may help CKD patients to restore cell survival, proliferation, and growth.

ACKNOWLEDGEMENTS

The authors are grateful for financial support from the National Science Council NSC 97-2320-B-039-049-MY3, 99-2320-B-039-034, 99-2320-B-038-011-MY3. The authors also acknowledge financial support of CMU99-N1-09 and CMU100-TS-07 from China Medical University.

REFERENCES

1. Jeansson M, Bjorck K, Tenstad O, Haraldsson B. Adriamycin alters glomerular endothelium to induce proteinuria. J Am Soc Nephrol 2009; 20(1):114-22.
2. Vlassara H, Torreggiani M, Post JB, Zheng F, Uribarri J, Striker GE. Role of oxidants/inflammation in declining renal function in chronic kidney disease and normal aging. Kidney Int Suppl 2009; 114:S3-11.
3. Wang XH, Du J, Klein JD, Bailey JL, Mitch W. Exercise ameliorates chronic kidney disease-induced defects in muscle protein metabolism and progenitor cell function. Intl Soc Nephrol 2009; 76:751-9.
4. Lee VW, Haris DC. Adriamycin nephropathy: A model of focal segmental glomerulosclerosis. Nephrology 2011; 16:30-8.
5. Wynn TA. Cellular and molecular mechanisms of fibrosis. J Pathol 2008; 214:199-210.
6. Strutz F, Zeisberg M. Renal fibroblasts and myofibroblasts in chronic kidney disease. J Am Soc Nephrol 2006; 17:2992-8.
7. Zeisberg EM, Potenta SE, Sugimoto H, Zeisberg M, Kalluri R. Fibroblasts in kidney fibrosis emerge via endothelial-to-mesenchymal transition. J Am Soc Nephrol 2008; 19(12):2282-7.
8. Chen A, Sheu LF, Ho YS. et al. Experimental focal segmental glomerulosclerosis in mice. Nephron 1998; 78:440-52.
9. Border WA, Noble NA. Transforming growth factor beta in tissue fibrosis. N Engl J Med 1994; 331:1286-92.
10. Floege J, Eitner F, Alpers CE. A new look at platelet-derived growth factor in renal disease. J Am Soc Nephrol 2008; 19(1):12-23.
11. Bonner JC. Regulation of PDGF and its receptors in fibrotic diseases. Cytokine Growth Factor Rev 2004; 15(4):255-73.
12. Rankin CA, Itoh Y, Tian C, Ziemer DM, Calvet JP, Gattone VH 2nd. Matrix metalloproteinase-2 in a murine model of infantile-type polycystic kidney disease. J Am Soc Nephrol 1999; 10(2):210-7.
13. Dockrell ME, Phanish MK, Hendry BM. TGF-beta auto-induction and connective tissue growth factor expression in human renal tubule epithelial cells requires N-ras. Nephron Exp Nephrol 2009;

112(3):e71-9.
14. DingY, Kim JK, Kim SI, Na HJ, Jun SY, Lee SJ, Choi ME. TGF-β1 protects against mesangial cell apoptosis via induction of autophagy. J Biol Chem 2010; 285(48):37909-19.
15. Kwon DS, Kwon CH, Kim JH, Woo JS, Jung JS, Kim YK. Signal transduction of MEK/ERK and PI3K/Akt activation by hypoxia/reoxygenation in renal epithelial cells. Eur J Cell Biol 2006; 85(11): 1189-99.
16. Johansen KL. Exercise in the end-stage renal disease population. J Am Soc Nephrol 2007; 18:1845-54.
17. Carrero JJ, Yilmaz MI, Lindholm B, Stenvinkel P. Cytokine dysregulation in chronic kidney disease: How can we treat it? Blood Purif 2008; 26:291-9.
18. Teixeira de Lemos E, Reis F, Baptista S, et al. Exercise training decreases proinflammatory profile in Zucker diabetic (type 2) fatty rats. Nutrition 2009; 25(3):330-9.
19. Højbjerre L, Rosenzweig M, Dela F, Bruun JM, Stallknecht B. Acute exercise increases adipose tissue interstitial adiponectin concentration in healthy overweight and lean subjects. Euro J Endocrinol 2007; 157(5):613-23.
20. Bertani T, Poggi A, Pozzoni R, et al. Adriamycin-induced nephrotic syndrome in rats: sequence of pathologic events. Lab Invest 1982; 46(1):16-23.
21. Weibel ER. Stereological methods. In: Practical Methods for Biological Morphometry. London: Academic, 1979; p. 51-57.
22. Leber TM, Balkwill FR. Zymography: a single-step staining method for quantitation of proteolytic activity on substrate gels. Anal Biochem 1997; 249:24-8.
23. Wang Y, Wang YP, Tay YC, Harris DC. Progressive adriamycin nephropathy in mice: Sequence of histologic and immunohistochemical events. Kidney Int 2000; 58(4):1797-804.
24. Pedersen BK, Fischer CP. Beneficial health effects of exercise – the role of IL-6 as a myokine. Trends Pharmacol Sci 2007; 28:152-5.
25. Tangri N, Stevens LA, Griffith J, Tighiouart H, Djurdjev O, Naimark D, Levin A, Levey AS. A predictive model for progression of chronic kidney disease to kidney failure. JAMA 2011; 305(15):1553-9.
26. Heldin CH, Westermark B. Platelet-derived growth factor: Mechanism of action and possible *in vivo* function. Cell Regal 1990; 1:555-66.
27. Rubin K, Tingdtrom A, Hansson G.K, et al. Induction of B-type receptors for platelet-derived growth factor in vascular inflammation: Possible implications for development of vascular proliferative lesions. Lancet 1988; i:1353-6.
28. Wu SH, Yang YC, Wang ZM. Role of oxygen radicals in adriamycin-induced nephrosis. Chin Med J (Engl) 1990; 103(4):283-9.
29. Zhu Y, Lu L. Relationship between glomerular nephrin expression and oxidative stress reaction in rats with adriamycin-induced nephrosis. Zhongguo Dang Dai Er Ke Za Zhi 2009; 11:56-60.
30. Aresu L, Benali S, Garbisa S, Gallo E, Castagnaro M. Matrix metalloproteinases and their role in the renal epithelial mesenchymal transition. Histol Histopathol 2011; 26:307-13.

EARLY ANGIOGENIC RESPONSE TO SHOCK WAVES IN A THREE-DIMENSIONAL MODEL OF HUMAN MICROVASCULAR ENDOTHELIAL CELL CULTURE (HMEC-1)

V. SANSONE[1], M.C. D'AGOSTINO[2], C. BONORA[1], F. SIZZANO[3], L. DE GIROLAMO[4] and P. ROMEO[4]

[1]Orthopaedic Department, University of Milan, IRCCS Orthopedic Institute Galeazzi, Milan, Italy; [2]Orthopaedic Department, University of Milan, Clinical Institute Humanitas, Rozzano (MI), Italy; [3]Transplantation Immunology, Department of Genetics, Biology and Biochemistry, University of Turin, Turin, Italy; [4]IRCCS Istituto Ortopedico Galeazzi, Milan, Italy

Received July 11, 2011 - Accepted November 9, 2011

The exact nature of shock wave (SW) action is not, as yet, fully understood, although a possible hypothesis may be that shock waves induce neoangiogenesis. To test this hypothesis, a three-dimensional (3D) culture model on Matrigel was developed employing a human microvascular endothelial cell line (HMEC-1) which was stimulated with low energy soft- focused SW generated by an SW lithotripter. After 12 hours we observed a statistically significant increase in capillary connections subsequent to shock-wave treatment in respect to the control group and a marked 3-hour down-regulation in genes involved in the apoptotic processes (BAX, BCL2LI, GADD45A, PRKCA), in cell cycle (CDKN2C, CEBPB, HK2, IRF1, PRKCA), oncogenes (JUN, WNT1), cell adhesion (ICAM-1), and proteolytic systems (CTSD, KLK2, MMP10). Our preliminary results indicate that microvascular endothelial cells *in vitro* quickly respond to SW, proliferating and forming vessel-like structures, depending on the energy level employed and the number of shocks released. The early decreased expression in the analysed genes could be interpreted as the "first reactive response" of the endothelial cells to the external stimuli and the prelude to the events characterizing the neo-angiogenic sequence.

Over the last few decades the clinical use of shock waves (SW) has widened from its urological application of lithotripsy for gallstones to the treatment of both inflammatory and degenerative orthopaedic diseases in tendons, ligaments and soft tissues. In bone pathology, building on the early experience of Valchanou and Michailov (1), SW have been successfully employed in the treatment of non-union and in bone vascular diseases (2, 3). More recently, they have been proposed for wound care management, owing to the tissue trophic effect generated by the largest distribution of the high pressure focused acoustic waves into low energy soft focused or unfocused shock waves (uSW) (4).

Although the physical principles and the effects of SW on tissues have been broadly investigated, some cellular and biochemical aspects have not yet been completely clarified. *In vivo* studies have demonstrated the angiogenic activity of SW (5, 6). Experimental data suggest that one of their main biological effects is the production of nitric oxide (7), which has been shown to be effective in promoting

Key words: shock waves, endothelial cells, neo-angiogenesis, three dimensional cultures

Mailing address: Valerio Sansone, MD
Orthopaedic Department of the Università degli Studi di Milano, IRCCS Istituto Ortopedico Galeazzi,
Via R Galeazzi 4,
20161 Milano, Italy
Tel: +39 02 66214735 Fax: +39 02 66214736
e-mail: valerio.sansone@unimi.it.

0393-974X (2012)

DISCLOSURE: ALL AUTHORS REPORT NO CONFLICTS OF INTEREST RELEVANT TO THIS ARTICLE.

angiogenesis (8). Angiogenesis, the formation of new blood vessels from pre-existing capillaries, is indeed essential for tissue healing and is regulated by a variety of growth and angiogenic factors.

Current opinion suggests also that mechanical stimulation induced by SW produces a direct effect on the extracellular matrix (ECM) which then triggers cytoplasmatic and nuclear reactions that vary with the experimental model, the energy level, the number of impulses and the cell type (9). As has been demonstrated for specific bio-mechanical stimuli, SW could induce a biochemical reaction in responsive cells that affects growth, development, differentiation, apoptosis regulation and gene expression via signal transduction pathways (10)

The aim of this study is to verify the ability of uSW to induce new vessel proliferation (neoangiogenesis) and, at the same time, to investigate the initial response of endothelial cells to acoustic stimulation. For this purpose we employed an *in vitro* system consisting of a matrix support seeded with microvascular endothelial cells which resembles, as closely as possible, the structure of the natural tissues.

MATERIALS AND METHODS

3D cell culture

A human microvascular endothelial cell line (HMEC-1, Invitrogen) was used in this experiment. Cell cultures were established in the central well of 24-multiwell plates containing BD Matrigel™. BD Matrigel™ is derived from a protein mixture containing structural elements which are analogous to the components of ECM. It provides an excellent environment *in vitro* for the promotion, differentiation and proliferation of endothelial cells (11). Cultures were established at different cell densities (2500, 5000, and 10,000 cells/well respectively), for both untreated and uSW treated cells, with 5 wells prepared for each different density. Cells were cultured in MCDB 131 Medium (Invitrogen) without endothelial growth factors supplemented with 2% fetal bovine serum (FBS, Invitrogen). A control culture for each cell density was left untreated, whilst the other cultures, when they had reached 70-80% of confluence, were treated with a Dermagold™ 100 shock-wave electro-hydraulic SW-device (MTS Europe GmbH, Konstanz, Germany), designed to be applied cutaneously.

Device description and shock wave stimulation

In brief, in an electro hydraulic device, the discharged high voltage produced by two submerged opposite electrodes, emits a surrounding spherical SW which expands in the watery medium from the original first focal point (F1) to the walls of an ellipsoid reflector. Because of the geometric shape of the reflector, SW are conveyed to a second focal point (F2) which corresponds to the target tissue. In Dermagold™ 100 the paraboloid reflector generates soft focused (un-focused) SW.

Two different energy levels were used for treating the cells: level E1, with an Energy Flux Density (EFD) value of 0.01 mJ/mm^2 and Focus Total Energy (FTE) of 0.12 mJ at -6 dB, corresponding respectively to 83.5 mm of focal length and 8 mm of focal diameter; level E2, with an EFD value of 0.02 mJ/mm^2 and FTE of 0.40 mJ at -6 dB, corresponding to 83 mm of focal length and 8.7 mm of focal diameter. EFD conventionally represents the amount of acoustic energy delivered to, and flowing through, a distinct square area of the focus, perpendicular to the plane of wave propagation, and is defined in mJ/mm^2. The -6dB focus corresponds to the focus area where pressure is greater or equal to half the value of the maximum energy. Moreover, for each energy level (E1-E2), 200 and 800 impulses were applied at a frequency of 3 Hz (Table I).

The SW-device membrane was spread with ultrasound conduction gel, and then multiwells were placed on the membrane using a coupling device. Only the five central wells were seeded with cells, whereas the outer wells contained only the culture medium, to avoid acoustic interference. The plate was positioned on the coupling SW-device membrane, ensuring that all the wells containing cells lay on the membrane. Moreover, in order to avoid the creation of air interface and the risk of cavitation and stirring, a cylinder filled with water was positioned over the plate.

Angiogenic evaluation

After the treatment, plates were incubated at 37°C (in the presence of 5% of CO_2) for 12 h. Then all the samples were observed under an inverted microscope (Leica Microsystems) connected to a charged coupled device camera. The capillary density was evaluated by counting the number of connections formed by the endothelial cells in each microscopy field at 40X of magnification (10 fields were counted for each sample) with the aid of a specific software program (ImageJ, Wayne Rasband, NIH, USA, http://rsb.info.nih.gov/ij/download.html)

Gene expression analysis

The most responsive group in terms of numbers of capillary connections underwent gene expression analysis using the Super Array kit-Signal Transduction Pathway Finder (SABiosciences, Qiagen), able to profile 84 key

genes representative of 18 different signal transduction pathways.

The cells were harvested, and RNA was extracted using an Array Grade Total RNA Isolation kit (Super Array Bioscience Corp.). RNA purity was evaluated by spectrophotometer, measuring the absorbance rate at 260 and 280 nm. DNA copies (cDNA) were synthesized from the RNA by inverse transcriptase reaction, incubating the mixture at 42°C for 50 mins and at 75°C for 5 mins. Subsequently, biotinylated cDNA was obtained through subsequent reactions and incubation at 37°C for 4 h. The cDNA was then diluted in a suitable buffer and distributed on membranes inside an overnight hybridization oven. Then, after a series of washing cycles, the incubation with avidine-phosphatase alkaline complex and the chromogen produced a chemioluminescent reaction. The resulting patterns were scanned and the images were analysed using densitometry software. The variation in gene expression of the treated cells versus the untreated ones was evaluated normalizing the obtained values on a housekeeping gene expression (glyceraldehyde-phosphate dehydrogenase, GAPDH).

Statistical analysis

One-way-ANOVA was performed in order to evaluate the differences in the number of capillary connections between the treated cells and the controls during the *in vitro* angiogenesis, the Dunnett Test was used as a post-hoc test. The results were expressed as mean±SD. Prism 3.0 software (Graph Pad Software) was used for all statistical analyses. p value <0.05 was considered statistically significant.

RESULTS

Microscopic findings

The *in vitro* model was developed using a human microvascular endothelial cell line (HMEC-1) cultured in a three-dimensional matrix (BD Matrigel™). HMEC-1 is the first immortalized human microvascular endothelial cell line that retains the morphologic, phenotypic and functional features of normal human microvascular endothelial cells, secreting Von Willebrand factor and forming tubular structures when cultured on solid supports. In particular, when plated on Matrigel, these cells are able to form a three-dimensional network of capillary vessels which is comparable to the structure formed in the final stage of the angiogenic cascade (Kubota et al. 1988).

The cylinder of water placed above the plate ensured that no SW-induced stirring or cavitations were observed that could have affected our results. After 12 hours, the treated cells showed a substantial increase in the number of new vessel-like structures if compared to untreated cells. This morphological differentiation was more remarkable in the samples that were exposed to low energies and limited numbers of shots (Figs. 1 and 2). There was a statistically significant increase in the number of capillary connections (bifurcations) in the cells treated under the E1 condition of lower shock-wave energy (EDF of 0.01 mJ/mm2). Under E1 condition the behaviour of EC was also related to the number of shots applied; indeed, when HMEC-1, plated at a density of 2500 cells/well, received 200 shots, the number of bifurcations was 7.4±1.5 and 2.0±0.4 for treated and untreated cells respectively ($p<0.05$), whereas, when they received 800 shots the number was not significantly different from the untreated cells (4.1±0.8, $p>0.05$). Under the same conditions (E1 200 shots) HMEC-1, plated at a density of 5000 cells/well showed 19.1±5, and 10.6±2.1 respectively for treated and untreated cells ($p<0.05$) and 8.2±5.3 when they received 800 shots. When plated at 10000 cells/well, the cells showed 39.0±1.8 and 22.0±4.4 bifurcations respectively ($p<0.05$) when they were treated with 200 shots and were left untreated. When cells received 800 shots we observed 37.20±4.0 bifurcations ($p<0.05$) (Fig. 3).

As reported by other authors (12), we observed a disaggregation of the Matrigel scaffold and a negative effect on the formation of capillary connections at higher energies (data not shown).

Gene Expression

In samples showing the most marked increase in number of capillary connections (energy level E1 and 200 shots), we observed a decreased gene expression 3 hours after uSW treatment (Fig. 4). Indeed, cells showed a strong down-regulation of genes involved in the apoptotic process (BAX, anti-apoptotic BCL2LI, GADD45A, PRKCA), also in the cell cycle (CDKN2C, CEBPB, HK2, IRF1, PRKCA), oncogenes (JUN, WNT1), cell adhesion (ICAM-1), and proteolytic systems (CTSD, KLK2, MMP10). Table II illustrates the modulation of the gene expression (fold change) of six genes strongly implicated in the phenomena described. However,

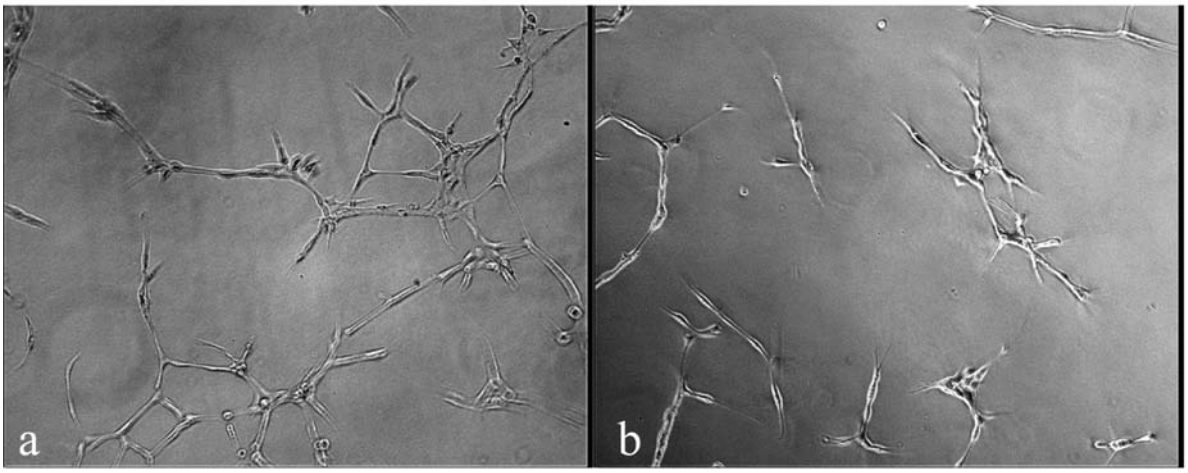

Fig. 1. *Microphotographs of uSW treated (**a**) and untreated (**b**) HMEC-1, seeded on Matrigel at 2500 cells/well and cultured for 12 hours. Picture in (a) shows cells treated at lower shock-wave energy level (E1, 0.01 mJ/mm^2) with a low number of impulses (200 shots). Under this condition the number of bifurcations in HMEC-1 cells was significantly higher than in untreated cells ($p<0.05$). Original magnification: 40X.*

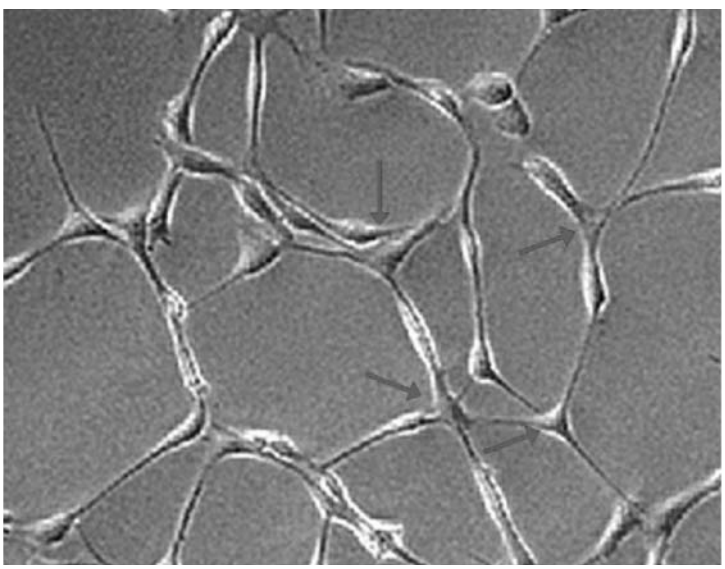

Fig. 2. *Detail of strict capillary connections and cellular organization in HMEC-1 culture treated with uSW (E1, 0.01 mJ/mm^2, 200 shots) (**a**). Capillary connections and bifurcations are not present in untreated cells (**b**). Original magnification: 100X.*

we did not observe any increased expression of receptors for angiogenic agents like endothelial nitric oxide synthase (eNOS) or vascular endothelial growth factor (VEGF).

DISCUSSION

Endothelial cells (ECs) are mechano-sensitive cells which physiologically react to flow shear stress. Particular regions of the cell membrane seem to be involved in the recognition of the different features of the laminar flow (13-15) which are subsequently transferred to the cytoskeleton (16, 17). Those cellular compartments engaged with selective sites of eNOS are thought to mediate the angiogenic (18) and anti-apoptotic effect (19) of the shear stress.

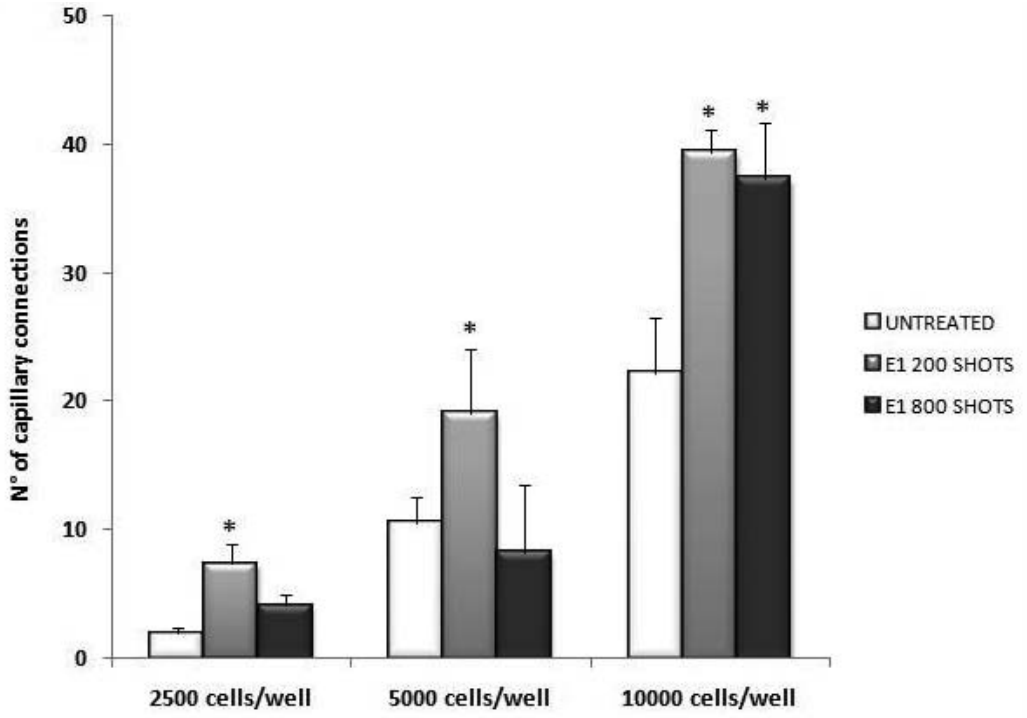

Fig. 3. *Count of capillary connections (bifurcations) in HMEC-1 seeded at different cell concentrations, 12 h after low energy uSW treatment (E1, 0.01 mJ/mm²) with different number of shots (200 shots, light grey bars; 800 shots, dark grey bars). Untreated HMEC-1 are shown as negative control (white bars). Data are expressed as mean ± SD. Under E1 condition the behaviour of EC was related to the number of shots applied; indeed at all densities, cells receiving 200 shots showed a significant increase in the number of bifurcations in comparison to untreated cells (7.4±1.5 vs 2.0±0.4 at 2500 cells/well; 19.1±5 vs 10.6±2.1 at 5000 cells/well; 39.0±1.8 vs 10000 cells/well; all p<0.05). On the other hand, E1 uSW treatment with 800 shots was able to induce a significant increase in the number of bifurcations just in HMEC-1 cells plated at high density (10000 cells/well) in comparison to untreated cells (37.20±4,0 vs 22.0±4.4 at, p<0.05).*

In clinical practice, several vascular pathologies are characterized by an intrinsic EC dysfunction and a diminished production of growth factors (GF) (20). Hence, new therapeutic options attempt to correct this sort of "biologic imbalance" by inducing neovascularisation, a process which can be achieved by supplementing the VEGF either via gene therapy or transplanting endothelial progenitor cells (20, 21).

On the other hand, SW stimulation represents an alternative, and innovative, therapeutic approach in those conditions where a strong angiogenic impulse is required – for example in severe skin wounds (4) or in myocardial ischemic lesions (6). Moreover, recent experimental studies suggest that the treatment of ischemic tissue with low energy SWs improves the recruitment of circulating endothelial progenitor cells (EPCs) due to enhanced expression of specific chemo-attractant factors (22).

Although the late neo-angiogenic response has been documented adequately, much less attention has been given to the very early changes induced by mechanical stimulus. Our study was established to investigate the early effects of unfocused shock waves on HMEC-1 cultured in a three-dimensional Matrigel model, where cells were stimulated using a source of low energy unfocused shock waves (soft–focussed) with a pulsation frequency of 3 Hz per second. The experimental Matrigel model, as with any *in vitro* model, is obviously not a perfect replica of the biological tissues. However, by reproducing the architecture of a mechano-sensitive structure such as the capillary network, it is possible to provide a valid model for analyzing the behaviour of ECs when submitted to an acoustic signal characterized

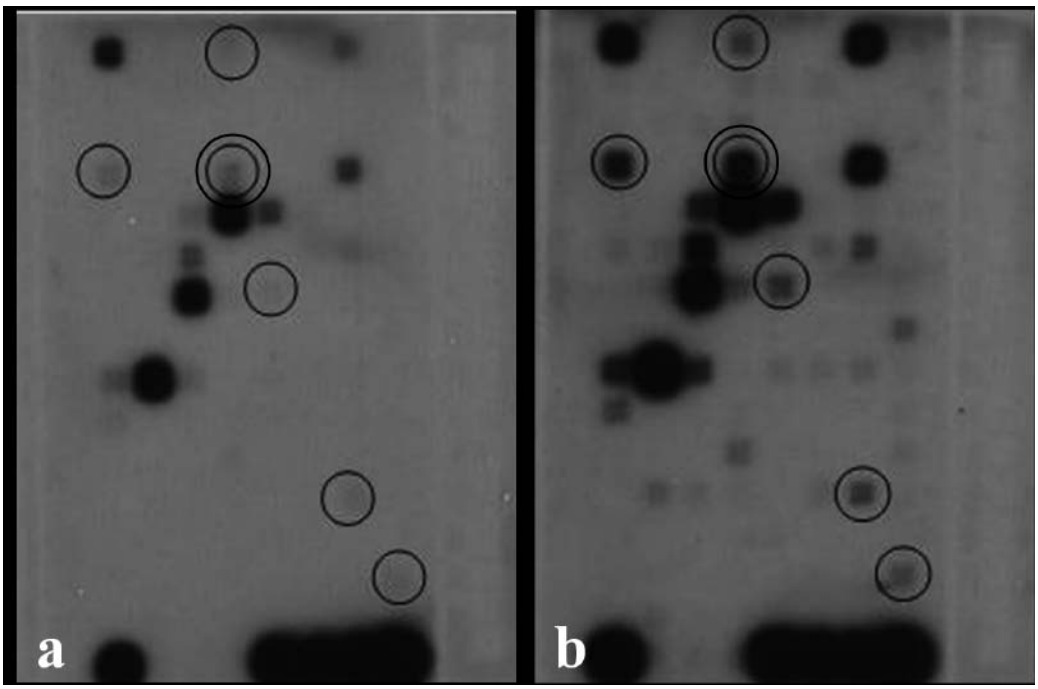

Fig. 4. *Gene expression analysis of HMEC-1 treated at lower energy level (E1, 0.01 mJ/mm²) with 200 shots after 3 h from treatment (a) and of untreated HMEC-1 (b). Downregulated genes are circled (from the top WNT1, CDKN2C, ICAM-1 (double circled), TANK, CEBPB and BAX).*

by regular impulse and larger focal extension. The employed multiwaves device generates shock waves in which the larger energy distribution area corresponds to a lower depth of penetration, due to the geometric properties of the paraboloid reflector, which causes the transmission of the acoustic wave front in a large area, nearly parallel (4) and almost laminar.

HMEC–1 are different from the lining EC of large vessels, and are thought to be involved in angiogenesis and in wound healing. We demonstrated that unfocused shock waves induced a quick morphological response (12 hours), characterized by a significant increase of vessel-like structures formation. The difference between treated and not-treated cells was statistically significant at lower shock-wave energy levels (E1, 0.01 mJ/mm² EDF) with a limited number of shots (200), thus demonstrating that the number of shots and cell concentration seem to affect the cell response to uSW.

Although derived from a different experimental model, analogous morphological results have been reported in an *in vivo* study by Zimpfer et al. (23). They described an increased microvascular density assessed by quantitative histology at 6 and 14 weeks, following a single uSW epicardial stimulation in myocardial infarction in a rat model. Stojadinovic et al. (24) reported an enhanced vascularisation after 4 and 7 days from treatment in a murine model of ischemic skin, and an up-regulation of pro-angiogenic genes after 6 hours. Additionally, Keji et al. (25) reported an increased capillary density in ischemic skeletal muscle 28 days after SW stimulation.

As described above, the pro-angiogenic effects of SW are most likely mediated by VEGF and NO. In our study, we did not observe either VEGF or eNOS modulation 3 hours after SW stimulation, whereas other authors demonstrated the production of VEGF and the increased expression of the specific angiogenesis pathway after 6 hours (24, 26). Instead, we observed a significant down-regulation of genes

Table I. *Experimental setting: each condition was tested in a well of 24-multiwell (n=5).*

	5000 cells/well	10000 cells/well
E1 200 shots	E1 200 shots	E1 200 shots
E1 800 shots	E1 800 shots	E1 800 shots
E2 200 shots	E2 200 shots	E2 200 shots
E2 800 shots	E2 800 shots	E2 800 shots

E1 = 0.01 mJ/mm2; E2 = 0.02 mJ/mm2

Table II. *Most relevant gene expression down-regulation (fold change) induced by uSW treatment (energy level E1 and 200 shots) and revealed 3 hours after treatment by gene array.*

Gene Symbol	Gene Bank	Function	Fold change	p-value
BAX	NM_004324	Apoptosis regulation	-8.0	0.042
CDKN2C	NM_0078626	Cell cycle regulation	-10.0	0.030
CEBPB	NM_0078626	Transcription regulation	-8.0	0.046
ICAM-1	NM_000201	Adhesion molecule	-10.0	0.009
WNT1	NM_005430	Signal transduction	-8.0	0.034
TANK	NM_004180	Signal transduction	-7.0	0.008

The gene expression was normalized on the expression of glyceraldehyde-phosphate dehydrogenase (GAPDH).

involved in the apoptotic process (BAX, anti-apoptotic BCL2LI, GADD45A, PRKCA), in cell cycle (CDKN2C, CEBPB, HK2, IRF1, PRKCA), in cell adhesion (ICAM-1), and in proteolytic systems (CTSD, KLK2, MMP10), even if some genes (like PRKCA, IRF-1and the proteolytic genes) are involved in many other processes and so their specific role in endothelial cells cannot be determined by gene-expression analysis alone. However, this SW-induced modulation, which is more significant for the antiapoptotic genes, could represent the "early reactive response" of HMEC-1 to the physical impulse induced by the uSW. These observations compare favorably with Kim and Von Recum (27) who remarked that mechanical stimulus induced by shear stress could improve the differentiation EPCs in ECs, regulating the expression of several genes involved in apoptosis and inducing EPCs to form capillary-like networks in 3D cultures.

A possible limitation of this study could be the presence of air between the cylindric holes of the well plates which could have partially affected the wave propagation. Another limitation lies in the fact that the central cell-seeded well received the maximum energy whilst the four peripheral ones received a slightly lower energy. What we observed is a sort of 'average' effect of the shock waves. However, this replicates the action of shock waves

in vivo, where the areas nearer the focal point receive a higher energy dose than those surrounding them.

In conclusion, our results seem to confirm that some aspects of the early gene response of ECs to uSW stimulation are comparable to those of the laminar shear stress flow, mainly characterized by an anti-apoptotic effect. We observed that, under specific experimental conditions, uSW were able to induce neovascularisation after 12 hours from a single stimulation. After 3 hours, the EC did not show specific pro-angiogenic activity, but just preparatory signals, such as the downregulation of the genes involved in cell cycle and cell adhesion, probably correlated to an upcoming detachment of endothelial junctions.

Further experimental studies are necessary to validate these hypotheses and to investigate whether the biological response of EC to SW stimulation involves the same intercellular pathways and regulatory mechanisms that characterise other types of biophysical stimuli. At the same time, new research into the gene expression could shed light on the triggering of the angiogenic process when acoustic stimulation is applied.

REFERENCES

1. Valchanou VD, Michailov P. High energy shock waves in the treatment of delayed and non-union of fractures. Int Orthop 1991; 15:181-4.
2. Schaden W, Fischer A, Seiler A. Extracorporeal shock wave therapy of non-union or delayed osseous union. Clin Orthop 2001; 387:90-4.
3. Wang CJ, Wang FS, Huang CC, Yang KD, Weng LH, Huang HY. Treatment for osteonecrosis of the femoral head: comparison of extracorporeal shock waves with core decompression and bone-grafting. J Bone Joint Surg Am 2005; 87:2380-7.
4. Schaden W, Thiele R, Kölpl C, et al. Shock wave therapy for acute and chronic soft tissue wounds: a feasibility study. J Surg Res 2007; 143:1-12.
5. Wang CJ, Wang FS, Yang, KD, Weng LH, Hsu CC, Huang CS, Yang LC. Shock wave therapy induces neovascularisation at the tendon-bone junction. A study in rabbits. J Orthop Res 2003; 6:984-9.
6. Fukumoto Y, Ito A, Uwatoku T, Matoba T, Kishi T, Tanaka H, Takeshita A, Sunagawa K, Shimokawa H. Extracorporeal cardiac shock wave therapy ameliorates myocardial ischemia in patients with severe coronary artery disease. Coron. Artery Dis 2006; 17:63-70.
7. Mariotto S, Cavalieri E, Amelio E, Ciampa AR, De Prati AC, Marlinghaus E, Russo S, Suzuki H. Extracorporeal Shock Waves: from lithotripsy to anti-inflammatory action by NO production. Nitric Oxide 2005; 12:89-96.
8. Cooke JP, Losordo DW. Nitric oxide and angiogenesis. Circulation 2002; 105:2133-5.
9. Speed CA. Extracorporeal shock wave therapy in management of chronic soft-tissue conditions. J Bone Joint Surg Br 2004; 86B:165-71.
10. Tarbell JM, Weinbaum S, Kamm RD. Cellular fluid mechanics and mechanotransduction. Ann Biomed Eng 2005; 12:1719-23.
11. Kubota Y, Kleinman HK, Martin GR, Lawley TJ. Role of laminin and basement membrane in the morphological differentiation of human endothelial cells into capillary-like structures. J Cell Biol 1988; 107:1589-98.
12. Steinbach P, Hofstaedter F, Nicolai H, Roessler W, Wieland W. Determination of the energy-dependent extent of vascular damage caused by high-energy shock waves in an umbilical cord model. Urol Res 1993; 21:279-82.
13. Fleming I, Busse R. Signal transduction of eNOS activation. Cardiovasc Res 1999; 43:532-41.
14. Ziegler T, Silacci P, Harrison VJ, Hayoz D. Nitric oxide synthase expression in endothelial cells exposed to mechanical forces. Hypertension 1998; 32:351-5.
15. Barakat AI, Lieu DK, Gojova A. Secrets of the code: do vascular endothelial cells use ion channels to decipher complex flow signals? Biomaterials 2006; 27:671-8.
16. Corson MA, James NL, Latta SE, Nerem RM, Berck BC, Harrison DG. Phosforylation of Endothelial Nitric Oxide Syntetase in response to fluid shear stress. Circ Res 1996; 79:984-91.
17. Davies PF, Barbee KA, Volin MV, et al. Spatial relationships in early signals events of flow mediated endothelial mechanotransduction. Annu Rev Physiol 1997; 59:527-49.
18. Baum O, Da Silva-Azevedo L, Willerding G, Wockel A, Planitzer G, Gossrau R, Pries AR, Zakrzewicz A.

Endothelial NOS is main mediator for shear stress–dependent angiogenesis in skeletal muscle after prazosin administration. Am J Physiol Heart Circ Physiol 2004; 287:H2300-8.

19. Dimmeler S, Hermann C, Galle J, Zehier AM. Upregulation of superoxide dismutase and nitric oxide synthase mediates the apoptosis suppressive effect of shear stress on endothelial cells. Arterioscler Thromb Vasc Biol 1999; 19:656-64.
20. Madeddu P. Therapeutic angiogenesis and vasculogenesis for tissue regeneration. Exp Physiol 2005; 90:315-26.
21. Chenggang Y, Wei X, Yan Z, Lingxi Z, Maoguo S, Jie L, Yan H, Shuzhong G. Transplantation of endothelial progenitors cells transferred by vascular endothelial growth factor gene for vascular regeneration of ischemic flaps. J Surg Res 2006; 135:100-6.
22. Aicher A, Heeshen C, Sasaki K, Urbich C, Zehier A, Dimmeler S. Low energy shock waves for enhancing recruitment of endothelial progenitor cells. A new modality to increase efficiency of cell therapy in chronic hind limb ischemia. Circulation 2006; 114:2823-30.
23. Zimpfer D, Seyedhossein A, Holfeld J, et al. Direct epicardial Shock Wave Therapy improves ventricular function and induces angiogenesis in ischemic heart failure. J Thorac Cardiovasc Surg 2009; 137:963-70.
24. Stojadinovic A, Elster AE, Khairul A, Douglas T, Mihret A, Zins S, Thomas AD. Angiogenic response to extracorporeal shock wave treatment in murine skin isografts. Angiogenesis 2008; 11:369-80.
25. Keiji O, Yoshihiro F, Kenta I, Toyokazu U, Kohtaro A, Takatoshi H, Hiroaki S. Extracorporeal Shock Wave Therapy Ameliorates Hindlimb Ischemia in Rabbits. Tohoku J Exp Med 2008; 214:151-8.
26. Wang FS, Wang CJ, Huang HJ. RAS induction of superoxide activates ERK-dependent angiogenic transcription factor HIF-1 α and VEGF-A expressions in shock wave-stimulated osteoblasts. J Biol Chem 2004; 279:10331-7.
27. Kim S, Von Recum H. Endothelial stem cells and precursors for tissue engineering: cell source, differentiation, selection, and application. Tissue Eng Part B Rev 2008; 14:133-47.

IN VITRO EXPOSURE OF HUMAN OSTEOARTHRITIC CHONDROCYTES TO ELF FIELDS AND NEW THERAPEUTIC APPLICATION OF MUSICALLY MODULATED ELECTROMAGNETIC FIELDS: BIOLOGICAL EVIDENCE

D. VANNONI[1], A. ALBANESE[2], E. BATTISTI[2], E. ACETO[1], S. GIGLIONI[1], C. CORALLO[1,2], S. CARTA[3], P. FERRATA[3], A. FIORAVANTI[4] and N. GIORDANO[1,2]

[1]Department of Internal Medicine, Endocrine-Metabolic Sciences and Biochemistry, University of Siena, Siena, Italy; [2]TAMMEF Centre, University of Siena, Siena, Italy; [3]Department of Human Pathology and Oncology, University of Siena, Siena, Italy; [4]COU of Rheumatology, Policlinico Le Scotte, Siena, Italy

Received May 4, 2011 – Accepted November 9, 2011

Osteoarthritis (OA) is the most frequently occurring rheumatic disease, caused by metabolic changes in chondrocytes, the cells that maintain cartilage. Treatment with electromagnetic fields (MF) produces benefits in patients affected by this pathology. Isolated human osteoarthritic (OA) chondrocytes were cultured *in vitro* under standard conditions or stimulated with IL-1ß or IGF-1, to mimic the imbalance between chondroformation and chondroresorption processes observed in OA cartilage *in vivo*. The cells were exposed for a specific time to extremely low frequency (ELF; 100-Hz) electromagnetic fields and to the Therapeutic Application of Musically Modulated Electromagnetic Fields (TAMMEF), which are characterized by variable frequencies, intensities, and waveforms. Using flow cytometry, we tested the effects of the different types of exposure on chondrocyte metabolism. The exposure of the cells to both systems enhances cell proliferation, does not generate reactive oxygen species, does not cause glutathione depletion or changes in mitochondrial transmembrane potential and does not induce apoptosis. This study presents scientific support to the fact that MF could influence OA chondrocytes from different points of view (viability, ROS production and apoptosis). We can conclude that both ELF and TAMMEF systems could be recommended for OA therapy and represent a valid non-pharmacological approach to the treatment of this pathology.

Osteoarthritis (OA) is a debilitating joint disease, affecting 60-70% of people over the age of 70 years, in which the surface of articular cartilage degrades and is unable to repair itself through natural processes. It causes considerable pain and loss of mobility, thus reducing the quality of life of millions of elderly people and resulting in substantial direct and indirect socioeconomic costs. Treatment of OA is often difficult and unsatisfactory and only a few methods are available. These include surgical treatment, consisting in the replacement of affected joints (although this has limited indications and is sometimes not sufficient); non-surgical treatment, which mostly involves medication with NSAIDs

Key words: electromagnetic fields, flow cytometry, biological interactions

Mailing address: Dr Daniela Vannoni,
Dip. Di Medicina Interna,
Sc. Endocrino metaboliche e Biochimica,
Sez. di Biochimica,
Via A. Moro, 2 53100 Siena, Italia
Tel: +39 577 234292 Fax: +39 577 234285
e-mail: Vannoni@unisi.it

0393-974X (2012)

DISCLOSURE: ALL AUTHORS REPORT NO CONFLICTS OF INTEREST RELEVANT TO THIS ARTICLE.

(non-steroidal anti-inflammatory drugs); or adjuvant therapies, such as physical therapy. Autologus chondrocyte transplantation is often used in the treatment of joint lesions to avoid a secondary OA.

The hypothesis of stimulating bone and cartilage regeneration through the application of specific electric and magnetic fields that affect growth and repair mechanisms has recently been proposed and investigated by many authors (1-3). The effects of electromagnetic fields (MF) on human cells seem to depend on their respective codes (frequency, intensity, waveform), as described in numerous *in vitro* and *in vivo* studies (4-8). For example, many papers have reported that bone and cartilage can be stimulated by MF to increase the synthesis of extracellular matrix molecules (9, 10). It has also been shown that the extracellular matrix of the hyaline cartilage is piezoelectric, meaning that it is capable of converting electromagnetic oscillations to mechanical vibrations and vice versa (11). The analgesic-therapeutic efficacy and tolerability of an extremely low frequency (ELF) electromagnetic field, modulated at a frequency of 100 Hz with a sinusoidal waveform and a mean induction of a few gauss, has been demonstrated in various hyperalgic pathologies - especially those of the locomotor apparatus, such as osteoporosis (12, 13), rheumatoid arthritis (12) and osteoarthritis (14, 15).

In order to verify the usefulness of applying as broad a magnetic field as possible, we introduce, in contrast with the traditional ELF-MF, the new TAMMEF system (Therapeutic Application of Musically Modulated Electromagnetic Field), whose parameters (frequency, intensity, waveform) are modified in time and vary randomly within the respective ranges, so that all the possible codes can occur during a single application (usually 30 minutes).

The aim of our study is to analyze the *in vitro* effects of MF on human chondrocytes from OA patients, comparing the ELF and the TAMMEF systems and focusing our attention on cell proliferation, the induction of apoptosis and oxidative stress. The treatment was performed in the absence or presence of factors known to interfere with OA chondrocyte metabolism, such as inflammatory cytokine interleukin-1ß (IL-1ß) or the stimulatory insulin-like growth factor 1 (IGF-1). This model mimics, *in vitro*, the imbalance between chondroformation and chondroresorption processes observed in OA cartilage *in vivo*. During the pathology this delicate equilibrium is progressively altered, leading to excessive tissue degradation and, finally, tissue disruption

The selection of articular osteoarthritis chondrocytes as the model for our study was based on previous research into the autologous transplantation of *in vitro* cultivated chondrocytes, which is used in the treatment of articular lesions (16, 17).

The research protocol was approved by our local ethics committee, and each femoral head donor provided informed written consent.

MATERIALS AND METHODS

Reagents

Dulbecco's modified Eagle's medium (DMEM), fetal bovine serum (FBS), L-glutamine, penicillin, streptomycin, amphotericin B, hyaluronidase, Pronase E from Streptomyces griseus, collagenase type II, trypsin/EDTA, urea, CHAPS, Tris-HCl, dithioerythritol, 2',7'-dichlorofluorescein diacetate (DCFH-DA), propidium iodide (PI), rhodamine 123 (Rhod123) and *o*-phthaldialdehyde (OPT) were all obtained from Sigma-Aldrich. (St. Louis, MO, USA). A cell strainer was purchased from BD Biosciences (Franklin Lakes, NJ, USA) and flasks from Costar (Cambridge, MA, USA). The AlamarBlue® Assay was obtained from Invitrogen, (Carlsbad, CA, USA) and ERK1/2 antibodies and goat polyclonal to rabbit IgG were acquired from Abcam (Cambridge Science Park, Cambridge, UK).

Cell culture

Human chondrocytes were obtained from twenty adult patients (12 males and 8 females, aged 56-78 years) suffering from severe osteoarthritis and undergoing femoral head replacement.

Articular cartilage slices isolated from the femoral condyles were dissected under aseptic conditions. The separation of chondrocytes was started not later than 24 hours after procurement.

Visually intact cartilage was sampled from the femoral condyles, diced into small fragments and digested in a spinner bottle. All enzymatic solutions were made in DMEM with antibiotics and antimycotics (2 mM L-glutamine, penicillin (100 U/mL), streptomycin (100 µg/mL) and 0.25 µg/ml amphotericin B) and 10% FBS.

The articular cartilage was treated with 0.25% sheep testes hyaluronidase in DMEM for 90 min at 37°C.

The hyaluronidase solution was then replaced by 0.25% Pronase E from Streptomyces griseus in DMEM for 60 min at 37°C. The cartilage was subsequently washed twice with DMEM containing 10% FBS and digested with collagenase type II (1 mg/mL) in DMEM at 37°C for 1-2 h. The cell suspension was filtered on a 70 µm cell strainer, rinsed in the medium and centrifuged at 100 x g for 10 min. The viability and number of isolated cells were estimated by vital staining using trypan blue. Usually, $1x10^6$ chondrocytes can be obtained from the femoral condyles of one individual. The chondrocytes were then cultured in DMEM supplemented with 100 U penicillin, 100 µg/mL streptomycin, 2 mM glutamine, and 10% FBS in 75 cm^2 flasks, and incubated at 37°C in an atmosphere of 5% CO_2, 95% air, until confluence (2-3 weeks); the FBS was then reduced to 5% (standard conditions).

When confluence was reached, the chondrocytes were isolated from the culture flasks by adding 0.1% trypsin/EDTA, then centrifuged and put into fresh flasks at a density of $2x10^6$ cells. The DMEM medium was changed every 2-3 days.

During cell stimulation, consisting in the addition to the culture medium of IL-1ß or IGF-1 to a final concentration of 5 ng/ml, FBS was further reduced to 2%.

Magnetic fields

We used two different kinds of MFs: 1) ELF MF (Extremely Low Frequency Magnetic Fields) modulated at a frequency of 100 Hz with a sinusoidal waveform and a mean induction of a few gauss; 2) the new TAMMEF system (Therapeutic Application of Musically Modulated Electromagnetic Fields), whose parameters (frequency, intensity and waveform) vary in time because they are generated by a piece of music (Rachmaninov's Piano Concerto number 2 in C minor, Op.18 for piano and orchestra) (14). Further details have been described previously (18). To conduct the experiments, the flasks containing the biological samples (about 70×10^6 cells) were positioned between the magnetic poles in order to be directly within the generated EMF. The resulting functional modifications in the cellular microenvironment depended not only on the particular microenvironment or the MF, but also on changes in the field due to the responses of the cells themselves (18).

Cell treatment

Cells from all the patients were pooled and randomly divided into three groups: group A, termed Sham Exposed (SE), served as the reference control. During the treatments, these cells were removed from the incubator and maintained far from the MF, so they could not be influenced by the magnetic fields; group B was exposed to ELFs; group C was exposed to TAMMEFs.

The treatments consisted of 30 min exposure to MF, once per day for 15 days, for the cells that were cultured in standard conditions, that is without the addition of factors to the medium. Cell proliferation and cytotoxicity under these conditions were evaluated. ROS production, glutathione (GSH) content and transmembrane potential (Dy_m), on the other hand, were assayed both under standard conditions and under stimulation with IL-1ß or IGF-1. In the latter case the stimulated cells were immediately treated with magnetic fields (groups B and C) or incubated far from the MF (group A) for 12 h.

Cell survival and proliferation

Cell survival and proliferation were monitored during treatment with MF (at 3, 7 and 15 days of exposure), using the alamarBlue® Assay (Invitrogen S.R.L, DAL1025, MI, Italy). Cells were seeded in micro-well plates ($2x10^4$ cells/0.33 cm^2); the culture medium was removed and replaced with 10% (v/v) alamarBlue® in DMEM without FBS and incubated for 4 h at 37°C in 5% CO_2 atmosphere. The system incorporates the fluorometric/colorimetric redox indicator, which changes from the oxidized form (non-fluorescent, blue) to the reduced form (fluorescent, red) in response to chemical reduction of the growth medium due to cell growth; continuous growth maintains a reduced environment while the inhibition of growth maintains an oxidized environment.

OD was read using a Multiskan EX microplate spectrofluorometer 200-240 V (Thermo Fisher Scientific, 81 Waltham MA 02454 USA) at excitation 530 nm and emission 590 nm. The change of colour from the initial blue to the final red was directly proportional to the reduced amount of the reagent and provided an estimation of the number of viable cells submitted to the test.

Growth curves were constructed by counting cells after exposure to MF, for 10 minutes each day, at 3, 7, and 15 days, and plotting OD versus time. The controls were sham-exposed and treated in exactly the same way as exposed cells, except magnetic fields were not applied to the control flasks. Each experiment was repeated three times (total of four) with similar results. The variation within each experiment was <5% in most cases, while the variation between experiments was usually no more than 10%.

Western blotting

To assess the expression of ERK1/2 following MF exposure, 10 µg of proteins from groups A, B and C were boiled for 5 min and submitted to 12% SDS-PAGE according to Laemmli (19). The bands were transferred from the gel to a nitrocellulose membrane (0.45 µ), 100V was applied for 1 h at 4°C and then they were stained with Ponceau-S. The membrane was blocked with 0.3%

non-fat powdered milk in 1x PBS containing 0.1% Tween 20, washed twice for 10 min with the same solution and incubated overnight at 37°C with antibodies against ERK1/2 (1:2000) (Abcam, Cambridge Science Park, Cambridge, UK).

The membrane was then washed in 1x PBS containing 0.1% (v/v) Tween 20. The bound primary antibodies were detected using goat polyclonal to rabbit IgG peroxidase-conjugate (1:3000) (Abcam, Cambridge Science Park, Cambridge, UK) and visualized using a Chemidoc™ XRS 170-870 molecular imager (Bio-Rad, Hercules, CA, USA) with Quantity One software (© 2006, Bio-Rad Laboratories, Inc). Western blots were quantified by densitometry using TotalLab 1.0 (Nonlinear dynamics, Newcastle upon Tyne, UK).

Flow Cytometric Analysis

Cell cycle

DNA content was analysed using PI, as previously described (20). The percentages of cells in the G1, S and G2 phases were determined using the MODFIT program (Verity Software, Topsham, ME, USA). At least 20,000 events were collected for each sample using Cell Quest software(© Becton Dickinson and Company, 1997); debris was excluded from the analysis by an appropriate morphological gate of forward scatter *versus* side scatter.

The cell cycle was evaluated in chondrocytes cultured in standard conditions, that is without the addition of external factors (IGF-1 or IL-1ß). This analysis was performed at the 4th, 7th and 15th day of treatment.

ROS production

ROS production was measured by the conversion of nonfluorescent 2',7'-dichlorofluorescein diacetate (DCFH-DA) to fluorescent 2',7'-dichlorofluorescein (DCF), corresponding to the amount of H_2O_2 generated by increased oxidative metabolism; so cytofluorimetric measurement of the DCF produced can provide an index of intracellular oxidation (20). Therefore, to monitor ROS production over time, we incubated the cells with DCFH-DA (10 µM final concentration) for 30 min. To measure the intensity of the DCF fluorescence, the cells were kept in ice until analysis using a fluorescence-activated cell sorting (FACS) Calibur flow cytometer (Becton Dickinson, Mountain View, CA, USA) equipped with an excitation laser line at 488 nm and CellQuest software (Becton Dickinson). The DCF (green fluorescence) was collected in a log scale through a 530±20 band pass filter. Monoparametric histograms of the fluorescence distribution were plotted to estimate ROS production. ROS generation, GSH depletion and mitochondrial changes (Dy_m) were monitored over time to demonstrate the presence or absence of oxidative stress in the cultures, resulting from the treatment with MF. Since mitochondrial functionality is a crucial factor in cytotoxic processes, we evaluated the Dy_m value using rhodamine 123, a cationic lipophilic vital marker specific for mitochondria, which is incorporated in mitochondria in a manner dependent on Dy_m.

We performed three series of experiments. In the first series, the cells were cultured in standard conditions, treated for 15 days (30 min/die) with ELF or TAMMEF fields and assayed after 4, 7 and 15 days from the beginning of treatment. In the second series, the cells were cultured in the presence of the insulin-like growth factor IGF-1, which favours chondroformation and in the third series the cells were cultured in the presence of IL-1ß, which is abundant in OA and a potent stimulator of chondroresorption. In both second and third series the cells were treated for 12 h with ELF or TAMMEF fields and immediately assayed.

Glutathione content assay

GSH content was evaluated using *o*-phthaldialdehyde (OPT) (Sigma-Aldrich, Milan, Italy), as described by Treumer (21). Briefly, the OPT method is based on reaction with both glutathione amino- and sulfhydryl groups, which yields a cyclic highly fluorescent product. The OPT-GSH fluorescent product appears in the green fluorescence channel. For staining, 1×10^6 cells were resuspended in 500 µl HEPES N-[2-hydroxyethyl] piperazine-*N*'-[2-ethanesulfonic acid]-buffered saline pH 7.4 and 1 mM OPT in dimethylformamide was added. After 5 min of incubation at room temperature, the suspension was immediately washed and the cells analysed using a FACSCalibur flow cytometer as above. The OPT-GSH (green fluorescence) was collected in a log scale through a 530±20 band pass filter. Monoparametric histograms of the fluorescence distribution were plotted to estimate GSH content.

Mitochondrial transmembrane potential

Dy_m was assessed by flow cytometry uptake of the cationic lipophilic dye Rhod 123 and PI using a commercial product (Sigma-Aldrich, Milan, Italy) according to the method described previously (20). Briefly, at different times of incubation, approximately 5×10^5 cells for each sample were treated with Rhod 123 and incubated for 30 min at 37°C in the dark. The cells were then washed twice in phosphate-buffered saline (PBS) and the pellet was resuspended in 200 µl of binding buffer plus 10 µl of the PI stock solution (10 µg/ml final concentration). The cells, kept in ice, were analysed using a FACSCalibur flow cytometer. The Rhod123 (green fluorescence) and the PI (red fluorescence) were both collected in a log scale, through a 530±20 and a 575±152.8.nm band pass

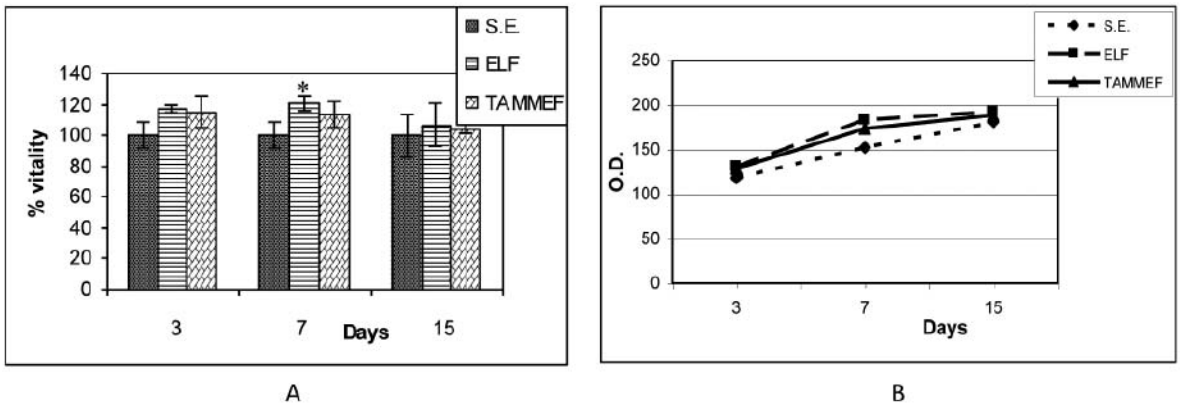

Fig. 1. *Chondrocyte vitality after 3, 5, 7 days of treatment with magnetic fields (ELF and TAMMEF).* ***A)*** *The values are calculated as mean of O.D. and are reported as %± SD respect to the control (S.E.).*P<0.05.* ***B)*** *Growth curves resulting from mean of O.D. at 530 nm excitation and 590 nm emission.*

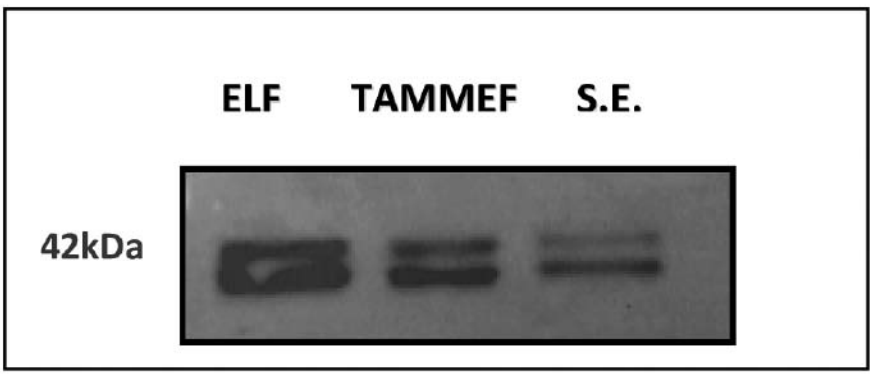

Fig. 2. *Differential expression of ERK1/2 proteins, evaluated by Western blot analysis in osteoarthritic chondrocytes, treated with ELF and TAMMEF fields.*

filter, respectively.

RESULTS

Growth curves

The cells submitted to treatment with electromagnetic fields were visibly more vital and proliferative than the untreated cells. The difference was statistically significant after 7 days of ELF treatment (+20% with respect to SE). Fig. 1, A and B report the growth curves.

Western blot

The results of the Western blot analysis (Fig. 2) supported previous findings, showing an increase in ERK1/2 expression, with respect to SE, of 76.7% after ELF and of 61.1% after TAMMEF treatment. Therefore ELF treatment produces an increase in expression of 40.4% with respect to TAMMEF treatment.

Cell cycle

In Fig. 3 the time course is reported of the DNA content during exposure to ELF or TAMMEF. It can be observed that after 4 days the number of cells in the G0/G1 phase decreased in both treatments, while cells in the G2/M phase increased, demonstrating that both MF treatments induced more divisions. The same occurred after 7 days of treatment, while after 15 days the G0/G1 peak increased, meaning

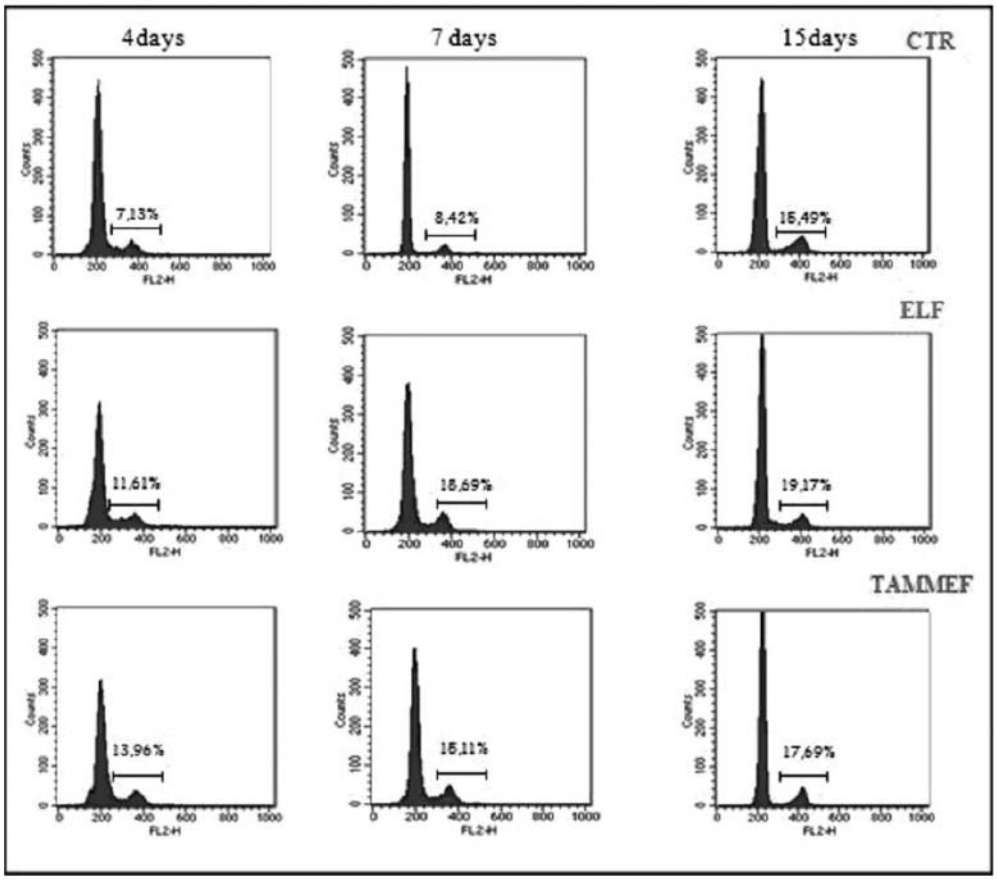

Fig. 3. *Flow cytometric analysis reporting the distribution of the cells during the cell cycle, analyzed after 4, 7 and 15 days of exposure to ELF and TAMMEF MFs. The logarithm of fluorescence intensity in the FL1-H channel (X axis) is an indicator of DNA content; the number of cells is indicated on the Y-axis.*

that most of the cells had completed their mitosis. An important result is that no hypodiploid peak was detectable after ELF or TAMMEF treatment, meaning that no apoptosis or stress was induced by the exposure.

In standard conditions, ROS production increased slightly at the beginning of the treatment, then returned to levels comparable to the controls; likewise, the production of reduced GSH increased in the early stages of treatment to deal with the production of ROS, and decreased during treatment until it stabilized at the lower baseline. In the case of mitochondrial transmembrane potential, there was no significant difference between controls and treated cells at any stage of the treatment.

The figures related to these experiments are not reported because of their non-statistical relevance. In the cells cultured under stimulation, on the other hand, the cytofluorimetric analysis highlighted significant differences.

Regarding the production of ROS, we can see from the histograms in Fig. 4 that the level decreased slightly in the presence of growth factor IGF-1, although there were no significant differences between the control and treated cells. In the case of administration of IL-1β (Fig. 4), on the other hand, there was a significant decrease of about 50% following TAMMEF treatment, while no significant decreasing was observed after ELF treatment.

The production of intracellular GSH increased significantly after MF, both in the case of stimulation with IGF-1 and with IL-1β (Fig. 5). In particular, the

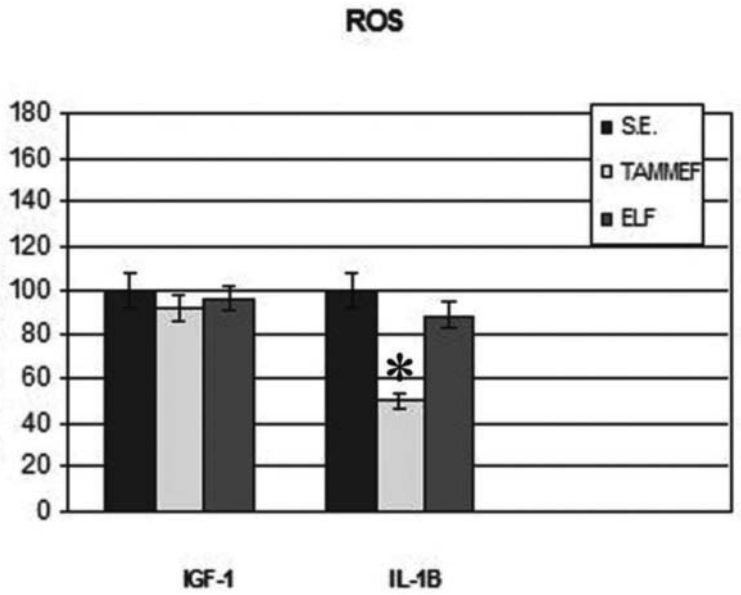

Fig. 4. *Fluorescence intensity recorded after ROS production by chondrocytes treated with IGF-1 (5 ng/ml) (left) and IL-1β (5 ng/ml) (right) and 12 hours of magnetic stimulation. The values are reported as %± SD respect to the control (S.E.).*P<0.05.*

increase was highly significant ($p<0.01$) in the cells stimulated with IGF-1, in line with the decrease of ROS (Fig. 4), especially after TAMMEF: this explains an increase in antioxidant power, represented by the increase in GSH, to counteract reactive oxygen species.

Fig. 6 shows that both stimulations in both treatments induced a decrease in fluorescence, resulting in hyperpolarization of the mitochondrial membrane. This leads to closure of megapores and failure to release cytochrome c (proapoptotic factor) from mitochondria to the cytosol. In the control cells, however, the fluorescence was much higher, indicating that the membranes were depolarizing, with the consequent opening of megapores, allowing entry of the fluorescent probe and the release of proapoptotic substances.

DISCUSSION

Both ELF and TAMMEF treatments can provide benefits in terms of the growth and proliferation of human osteoarthritic chondrocytes (15, 22, 23). Cultures treated with ELF and TAMMEF systems received greater stimuli to proliferate in the first days of treatment in comparison to the controls. However, after two weeks the growth rate in the cultures treated with ELF and TAMMEF was similar to that of the untreated cultures, excluding tumoural cell evolution caused by uncontrolled proliferation.

Differences in the growth rate between treated and untreated cultures can be interpreted as a possible influence that magnetic fields may have on the state of cells' electric charge, in terms of the ability of chondrocytes to restore the correct intracellular energetic equilibrium (24).

As mentioned above, our study demonstrates that magnetic fields do not affect cell viability and proliferation even after long-term exposure, which could therefore hypothetically be applied in *in vivo* studies. The molecular mechanisms through which low frequency electromagnetic fields could interfere with chondrocyte proliferation and differentiation have been partially clarified. Fabbri et al. (25) reported that this effect appears to be mediated by the rapid phosphorylation and activation of ERK1/2 (extracellular signal-regulated kinases) through a Ras-independent pathway.

Furthermore, other investigators have demonstrated that exposure to ELF stimulates ROS

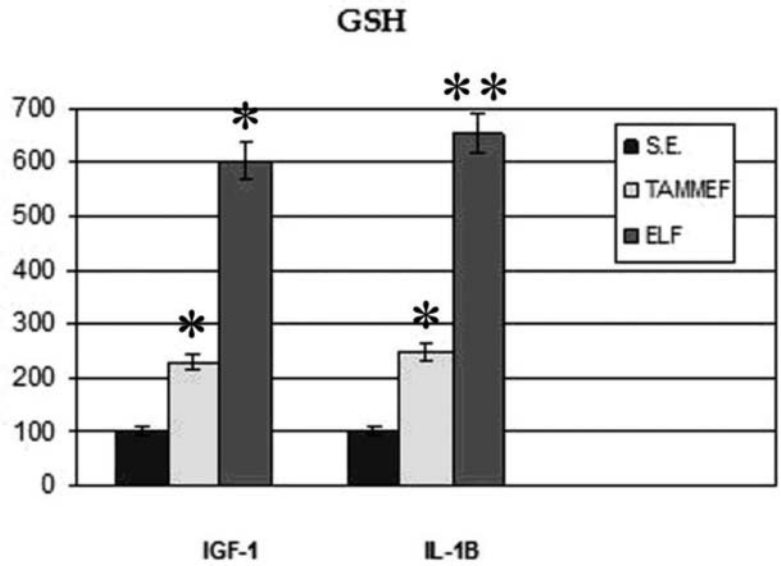

Fig. 5. *Fluorescence intensity recorded after GSH production by chondrocytes treated with IGF-1 (5 ng/ml) (left) and IL-1β (5 ng/ml) (right) and 12 hours of magnetic stimulation. The values are reported as %± SD respect to the control (S.E.).*P<0.05. **P<0.01.*

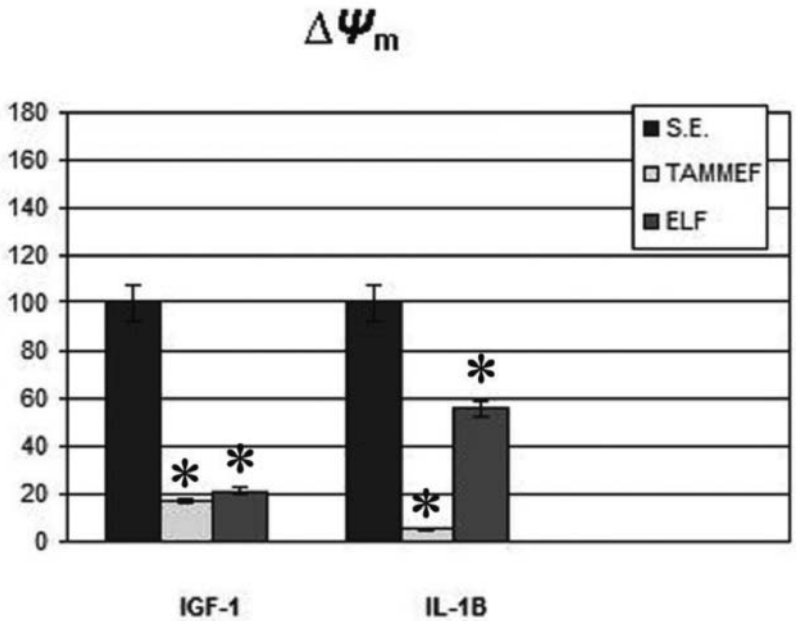

Fig. 6. *Transmembrane potential Fluorescence intensity recorded by chondrocytes (marked with Rho123) treated with IGF-1 (5 ng/ml) (left) and IL-1β (5 ng/ml) (right) and 12 hours of magnetic stimulation. The values are reported as %± SD in respect to the control (S.E.).*P<0.05. **P<0.01.*

production (26). In this study the effects of ELF and TAMMEF on ROS and GSH production was evaluated. In particular the use of a DCF probe, which is sensitive to variations in cell redox state, revealed a decrease in intracellular ROS, while the use of an OPT probe revealed an increase in

intracellular GSH. This equilibrium was observed after TAMMEF treatment in particular.

In the study of the inflammatory activity involved in osteoarthritis, it has been shown that some cytokines may be responsible for the catabolic process that takes place in osteoarthritic cartilage (27, 28). IL-1β, TNF-α and IL-6 seem to be particularly relevant for OA. On the other hand, Shi et al. (29) found that insulin-like growth factors (IGF) act in contraposition to cytokines, as mentioned above. Osborn et al. (30) demonstrated that IGF-1 stimulates mitotic activity and differentiation in chondrocyte cultures. ELF and TAMMEF treatment of osteoarthritic chondrocytes stimulated by IGF-1 or IL-1β revealed beneficial effects in comparison to untreated chondrocytes. In particular, in the presence of IL-1β, ROS production decreased by 50% in TAMMEF-treated chondrocytes. In the presence of IGF-1 this effect was evident in both ELF and TAMMEF treatments and in controls. GSH intracellular release increased simultaneously.

Blanco et al. (31) found that mitochondrial dysfunction seems to interfere with the cartilage degradation process. For this reason, mitochondrial transmembrane potential was evaluated in basal condition and under IL-1β and IGF-1. In particular, Rhodamine 123, a lipophilic cationic probe, penetrates the plasma membrane, which is converted into a green fluorescent molecule after ROS production (32). Our study shows that a decrease in fluorescence signal indicates the restoration of transmembrane potential. This important change in mitochondrial membrane permeability seems to be induced by both ELF and TAMMEF treatments, but in a higher percentage in the latter.

In conclusion, the results shown in this work favour the use of magnetotherapy in rheumatic diseases and in particular the use of the innovative TAMMEF system in OA applications. In fact, the aim of this work was to investigate the non-dangerous aspects of ELF and TAMMEF systems and magnetotherapy itself in terms of cells viability, proliferation, ROS production, apoptosis etc. Futhermore, we want to focus our attention on the fact that both ELF and TAMMEF systems are not only safe for cells, but they also have little benefits. In future studies we will better investigate the molecular mechanisms of the benefits due to magnetotherapy (such as cytokines and chemokines) involved in the anti-inflammatory pathways in the treatments of OA.

ACKNOWLEDGEMENTS

Our thanks to Prof. Anna Di Stefano, Dr. Simona Frosali and Dr. Cristina Ulivieri for their technical support and suggestions. We thank the University Language Centre for the assistance with the proofreading.

This work was supported by contribution of the Fondazione Monte dei Paschi di Siena, Siena-Italy and contribution of TAMMEF centre.

REFERENCES

1. Bassett C. Review: Biological significance of piezoelectricity. Calc Tiss Res 1968; 1:252-72.
2. Bassett C. Biophysical principles affecting bone structure. In Biochemistry and Physiology of Bone (Ed. Bourne G.H.). Academic Press, New York , 1971 vol. 3, pp. 1-68.
3. Bassett C, Pawluk RJ, Pilla AA. Acceleration of fracture repair by electromagnetic fields: a surgically noninvasive method. Ann NY Acad Sci 1974; 238-42.
4. Ciombor DM, Lester G, Aaron RK, Neame P, Caterson B. Low frequency EMF regulates chondrocyte differentiation and expression of matrix proteins. J Orthop Res 2002; 20:40-50.
5. Wilmot JJ, Chiego JR, Carlson DS, Hanks CT, Moskwa JJ. Autoradiographic study of the effects of pulsed electromagnetic fields on bone and cartilage growth in juvenile rats. Arch Oral Biol 1993; 38:67-74.
6. Dini L, Abbro L. Bioeffects of moderate-intensity static fields on cell cultures. Micron 2005; 36:195-217.
7. Yoshizawa H, Tsuchiya T, Mizoe H, et al. No effect of extremely low-frequency magnetic field observed on cell growth or initial response of cell proliferation in human cancer cell lines. Bioelectromagnetics 2002; 23:355-68.
8. Gál P, Kilík R, Špaková T, Pataki Š, Sabo J Pomfy M, Longauer F, Hudká R. He-Ne laser irradiation accelerates inflammatory phase and epithelization of skin wound healing in rats. Biologia 2005; 60:691-6.

9. Aaron RK, Ciombor DM. Electrical stimulation of bone induction and grafting. In: Habal M, Reddi AH, editors. Bone grafts and bone substitutes. Philadelphia: W.B. Saunders 1992; p. 192-205.
10. Rosen AD. Mechanism of action of moderate-intensity static magnetic fields on biological systems. Cell Biochem Biophys 2003; 39:163-73.
11. Jacobson JI, Gorman R, Yamanashi WS, Saxena BJ, Clayton L. Lowamplitude extremely low frequency magnetic fields for the treatment of osteoarthritic knees: a double-blind clinical study. Altern Ther Health Med 200; 7:54-67.
12. Giordano N, Battisti E, Geraci S, Santacroce C, Lucani B, Fortunato M, Matii G, Gennari C. Analgesic-antiinflammatory effect of 100 Hz variable magnetic field in R.A. Clin Exp Rheum 2000; 18:263.
13. Giordano N, Battisti E, Santacroce C, Geraci S, Tanganelli V, Matii G, Gennari C, Gennari L, Rigato M. Evaluation of early biomarkers of cartilage degeneration in the diagnosis and clinic-therapeutic monitoring of primary osteoarthrosis. Clin Ther 2001; 152(3):179-82.
14. Rigato M, Battisti E, Fortunato M, Giordano N. Comparison between the analgesic and therapeutic effects of a musically modulated electromagnetic field (TAMMEF) and those of a 100 Hz electromagnetic field: blind experiment on patients suffering from cervical spodylosis or shoulder periarthritis. J Med Eng Technol 2002; 26:253-8.
15. Battisti E, Piazza E, Rigato M, Nuti R, Bianciardi L, Scribano A, Giordano N. Efficacy and safety of a musically modulated electromagnetic field (TAMMEF) in patients affected by knee osteoarthritis. Clinic Exp Rheum 2004; 22:568-72.
16. Bačenková D, Rosochs J, Švihla R, Vaško G, Bodnár J. Repair of knee chondral defect by a combination of autologus chondrocytes and osteochondral allografts – an animal model (in Slovak). Acta Chir Orthop Traum Cechoslov 2001; 68:363-8.
17. Rosocha J, Vaško G, Bačenková D, et al. Preliminary clinical experience with the preparation and therapeutic use of autologus osteoblasts chondrocytes. Cell Tissue Banking 2002; 3:127-32.
18. Albanese A, Battisti B, Vannoni D, Aceto E, Galassi G, Giglioni S, Tommassini V, Giordano N. Alterations in adenylate kinase activity in human PBMCs after in vitro exposure to electromagnetic field: comparison between Extremely Low Frequency electromagnetic field (ELF) and Therapeutic Application of Musically Modulated Electromagnetic Field (TAMMEF). J Biomed Biotec 2009; art. No. 717941 Epub
19. Laemmli UK. Cleavage of structural proteins during the assembly of the head of bacteriophage T4. Nature 1970; 5259:680-5.
20. Ettorre A, Andreassi M, Anselmi C, Neri P, Andreassi L, Di Stefano A. Involvement of oxidative stress in apoptosis induced by a mixture of isothiazolinones in normal human keratinocytes. J Invest Dermatol 2003; 121:328-36.
21. Treumer J, Valet G. Flow-cytometric determination of glutathione alterations in vital cells by o-phthaldialdehyde (OPT) staining. Exp Cell Res 1986; 163:518-24.
22. Fioravanti A, Nerucci F, Collodel G. Biochemical and morphological study of human articular chondrocytes cultivated in the presence of pulsed signal therapy. Ann Rheum Dis 2002; 61(11):1032-3.
23. Pezzetti F, De Mattei M, Caruso A. Effects of pulsed electromagnetic fields on human chondrocytes:an in vitro study. Calcif Tissue Int 1999; 65(5):396-401.
24. Hofbauer LC. The roles of osteoprotegerin and osteoprotegerin ligand in the paracrine regulation of bone resorption. J Bone Miner Res 2000; 15:2-12.
25. Fabbri E, Barbin L, Capuzzo A, Biondi C. Adenyl cyclase activity and glucose release from the liver of the European eel, Anguilla anguilla. Am J Physiol 1998; 275:1563-70.
26. Wolf FI, Torsello A, Tedesco B, Fasanella S, Boninsegna A, D'Ascenzo M, Grassi C, Azzenga GB, Cittadini A. 50-Hz extremely low frequency electromagnetic fields enhance cell proliferation and DNA damage: Possible involvment of a redox mechanism. Biochim Biophys Acta 2005; 1743(1-2):120-9.
27. Loeser RF. Molecular mechanism of cartilage destruction: mechanics, inflammatory mediator, and aging collide. Arthritis Rheum 2006; 54:1357-60.
28. Tetlow LC, Adlam DJ, Wooley DE. Matrix metalloproteinase and proinflammatory cytokine production by chondrocytes of human osteoarthritic cartilage. Arthritis Rheum 2001; 44:585-94.
29. Shi J, Wang DM, Wang CM, Hu Y, Liu AH, Zhang

YL, Sun B, Song JG. Insulin receptor substrate-1 suppresses transforming growth factor-β1-mediated epithelial-mesenchymal transition. Cancer Res 2009; 69:7180-7.

30. Osborn KD, Trippel SB, Mankin HJ. Growth factor stimulation of adult articular cartilage. J Orthop Res 2005; 7:35-42.
31. Blanco F, Lopez-Armada M, Rego I. Mitochondria and Chondrocytes: Role in Osteoarthritis. In: Buckwalter JA, Stoltz JF, eds. Osteoarthritis; Inflammatory and Degradation: A Continuum 2007; 192-205, IOS Press, Amsterdam.
32. Petrat F, Pindiur S, Kirsch M, Groot H. Mitochondrial photochemical drugs do not release toxic amounts of 10(2) within the mitochondrial matrix space. Arch Biochem Biophys 2003; 412(2):207-15.

TISSUE DISTRIBUTION AND METABOLISM OF GUANOSINE IN RATS FOLLOWING INTRAPERITONEAL INJECTION

P. GIULIANI[1], P. BALLERINI[2], R. CICCARELLI[2], S. BUCCELLA[2], S. ROMANO[1], I. D'ALIMONTE[2], A. POLI[3], A. BERAUDI[3], E. PEÑA[3], S. JIANG[4], M.P. RATHBONE[5], F. CACIAGLI[2] and P. DI IORIO[1]

[1]Department of Human Movement Sciences, University of Chieti-Pescara, Chieti, Italy; [2]Department of Biomedical Sciences, University of Chieti-Pescara, Chieti, Italy; [3]Department of Evolutionist and Experimental Biology, University of Bologna, Italy; [4]Department of Surgery, McMaster University, Canada; [5]Department of Medicine, McMaster University, Canada

Received July 15, 2011 – Accepted November 10, 2011

The first two authors contributed equally to the paper

Guanosine has long been known as an endogenous purine nucleoside deeply involved in the modulation of several intracellular processes, especially G-protein activity. More recently, it has been reported to act as an extracellular signaling molecule released from neurons and, more markedly, from astrocytes either in basal conditions or after different kinds of stimulation including hypoxia. Moreover, *in vivo* studies have shown that guanosine plays an important role as both a neuroprotective and neurotrophic agent in the central nervous system. Specific high-affinity binding sites for this nucleoside have been found on membrane preparations from rat brain. The present study was undertaken to investigate the distribution and metabolic profiles of guanosine after administering the nucleoside to gain a better understanding of the biological effects of this potential drug candidate. Rats were given an intraperitonal (i.p.) injection of 2, 4, 8 or 16 mg/kg of guanosine combined with 0.05% of [^{3}H]guanosine. Plasma samples were collected 7.5, 15, 30, 60 and 90 min after the guanosine-mixture administration and analyzed by either a liquid scintillation counter or by HPLC connected to a UV and to an on-line radiochemical detector to measure the levels of guanosine and its metabolic products guanine, xanthine and uric acid. The levels of guanosine, guanine and xanthine were also measured in brain, lung, heart, kidney and liver tissue homogenates at the defined time points after the injection of 8 mg/kg of the guanosine-mixture. We found that the levels of radioactivity in plasma increased linearly in a dose- and time-dependent manner. Guanosine was widely distributed in all tissues examined in the present study, at almost twice its usual levels. In addition, guanine levels dramatically increased in all the organs. Interestingly, enzymatic analysis of the plasma samples showed the presence of a soluble purine nucleoside phosphorylase, a key enzyme in the purine salvage pathway and nucleoside catabolism. Since guanosine has been shown to be neuroprotective and astrocytes have been reported to play critical roles in mediating neuronal survival and functions in different neurodegenerative disorders, we also performed uptake and release

Key words: guanosine, guanine, distribution, metabolism, guanosine/guanine uptake, guanine-based purine release

Mailing address: Prof. P. Ballerini,
Department of Biomedical Sciences,
University of Chieti-Pescara
Via dei Vestini n. 29, Pal B NPD
66013 Chieti Scalo, Italy
Tel: +39 871 3554014 Fax: +39 871 3554011
e-mail: p.ballerini@unich.it

0393-974X (2012)

experiments using primary cultures of rat brain astrocytes. Astrocytes actively and specifically take up both guanosine and guanine and release the respective nucleotides which, in turn, undergo breakdown extracellularly. The high levels of guanine found in the culture medium following astrocyte preloading with guanosine indicates that guanine should also be considered as a potential signaling molecule able to mediate, at least in part, the biological effects that, until now, have been ascribed to guanosine. These findings indicate that newly synthesized guanosine/guanine-based analogues could represent a novel therapeutic approach to neurodegenerative disorders and support the evidence that astrocytes could represent novel, promising therapeutic targets in brain diseases.

Extracellular adenine-based purines, mainly adenosine (ADO) and ATP have long been accepted as important molecules in intercellular communication. They are released from almost all cell types including neurons and glial cells (1, 2) and are able to mediate several diverse biological effects.

Like ADO and ATP, extracellular guanine-based purines (GBPs), mainly GTP, GMP and their metabolic nucleoside product guanosine (GUO) have been shown to act as signaling molecules. Indeed GTP, like ATP, has been reported to be taken up and stored in synaptic vesicles (3), thus suggesting a GBP vescicular co-release with other neurotransmitters. Moreover, astrocytes, one of the most numerous type of cells in the central nervous system (CNS), have been shown to release GBPs and it is interesting to note that, under the hypoxic/hypoglycemic insult, these cells released GBPs to a greater extent than their adenine-based counterparts (4).

In the CNS, GMP and GUO have been reported to have a similar neuroprotective profile (5, 6). GUO has been shown to control glutamate release from astrocytes and to enhance glutamate uptake in these cells (3). Interestingly, even though GTP and GMP are able to mimic these effects, the increase of glutamate uptake was not enhanced in an additive manner by the combination of GMP, GTP and GUO nor was it modified by astrocyte treatment with GMP-PNP, the poorly hydrolysable analogue of GTP, raising the possibility that GUO was the active compound (7).

GUO has been shown to exert a number of neuroprotective effects also in *in vivo* experimental models. The oral (p.o.) or intraperitoneal (i.p.) administration of this nucleoside has been reported to induce: a) enhanced locomotor recovery of rats submitted to moderate spinal crush (8); b) reduced neuronal death and amelioration of symptoms in a rat model of Parkinson's Disease (9); c) prevention of quinolinic acid (QA)-induced seizures (10); d) modulation of the EEG changes occurring following QA infusion (11). Moreover GUO: a) produced antinociceptive effects in the hot plate, glutamate, capsaicin, formalin and acetic acid models (12); b) reduced thermal hyperalgesia and prevented locomotor deficits and body weight loss in a rat model of peripheral mononeuropathy (13); c) protected mice against leucopenia and thrombocytopenia and decreased the frequency of micronucleated polychromatic erythrocytes induced by X-ray irradiation (14), and its levels have been shown to increase after nucleoside p.o. or i.p. administration in either the cerebral spinal fluid (15, 16) or in the spinal tissue (17) in rats.

GUO levels, and consequently their biological effects, can also be influenced by the activity of purine nucleoside phosphorylase (PNP), the enzyme that reversibly catalyzes the phosphorolysis of inosine, GUO (Fig. 1) to hypoxanthine and guanine (GUA) (18).

In the present study, we report the distribution of GUO and of its metabolites -namely GUA, xanthine (XAN) and uric acid- after i.p. injection of this nucleoside in rats.

The extracellular concentration of GUO, GUA and their metabolic products, similar to their adenine-based counterparts, can be also partially attributed to the activity of cell membrane nucleoside/nucleobase transporters, namely the concentrative nucleoside transporters (CNTs), which are active transport systems, and the equilibrative nucleoside/nucleobase transporters (ENTs) which are involved in the bidirectional passive transport (19, 20). Their uptake/release activity, beyond their role in retrieval of nucleosides for nucleotide biosynthesis, is also a recognized and crucial cell strategy for the modulation of the extracellular signaling effects mediated by both adenine and guanine-based

purines.

Taking into account this further relevant regulatory mechanism, the interesting neuroprotective effects exerted by exogenous GUO and the potential beneficial role played by glial cells in several brain diseases, we also evaluated the uptake of GUO and GUA and the release of GBPs in primary cultures of rat brain astrocytes, the main neural cell type responsible for the maintenance of brain homeostasis (21).

MATERIALS AND METHODS

Chemicals

[^{3}H]GUO (15 Ci/mmol) and [^{3}H]GUA (15 Ci/mmol) were purchased from American Radiolabeled Chemicals, Inc. (St. Louis, MO, USA). The scintillation cocktail, Ultima Gold and Ultima FloM, were purchased from PerkinElmer Inc (Monza, Italy). Dulbecco's modified Eagle's medium, fetal calf serum, penicillin/streptomycin and trypsin were from Gibco-BRL (San Giuliano Milanese, Italy). Tetrabutylammonium phosphate was purchased from Waters SpA (Vimodrone, Italy). Unless indicated otherwise, all the other chemicals were purchased from Sigma-Aldrich (Milano, Italy) and were of the highest purity analytical grade. HPLC analysis was performed using HPLC grade solvents that were always filtered immediately prior to use.

Animals

Male Sprague-Dawley rats weighing 200-250 g (Charles River Laboratories, Milano, Italy) were used in this study. The animals were housed individually and kept on a 12 h light/dark cycle. Food and water were allowed *ad libitum*.

The rats were randomly divided into different groups (5 rats/group), and three sets of experiments were run: I) rats were treated with an i.p. injection of 1 ml of saline solution (control group) to evaluate the endogenous amount of GUO and its derivatives in plasma and tissues; II) rats were treated with an i.p. injection of 1 ml of 2, 4, 8 or 16 mg/kg GUO combined with 0.05% of [^{3}H]GUO (15 Ci/mmol) to evaluate the plasma concentration of GUO and its metabolites at 7.5, 15, 30, 60 and 90 min after i.p. injection (5 rats/dose); III) rats were treated with i.p. injection of 1 ml of 8 mg/kg of the GUO/[^{3}H]GUO mixture and were then sacrificed to evaluate levels of GUO and its metabolites in the tissues at the same time periods reported above (5 rats/time point).

Animal studies were conducted in accordance with the European Animal Care Guidelines, and the experimental procedures were approved by the Animal Research Ethics Board of the University of Chieti-Pescara.

Determination of plasma concentration of guanosine and its derivatives

Blood (0.5 ml) was collected from the lateral tail vein into heparinized tubes in either control (set I) or treated rats (set II). Each treated animal of set II underwent sequential blood sampling at 7.5, 15, 30, 60 and 90 min after injection. Plasma was separated by centrifugation at 1,700 g for 10 min at 4°C and divided into two aliquots. The liquid scintillation cocktail (Ultima Gold) was added to the first aliquot, and the total radioactivity was counted by liquid scintillation counter (Tri-Carb 2100TR, PerkinElmer, Monza, Italy).

The second aliquot was used for HPLC analysis. $HClO_4$ was added to plasma samples (final concentration of 0.4 M) to precipitate plasma proteins. The mixture was vortex-mixed and then centrifuged (10,000 g for 10 min at 4°C); the supernates containing the soluble molecules were neutralized with KOH solution, centrifuged (10,000 g for 10 min at 4°C), filtered (0.2 μm filters, Millipore, Vimodrone, Italy), immediately frozen at –80°C and stored until HPLC analysis.

Determination of tissue concentration of guanosine and its metabolites

After the injection of the 8 mg/kg of GUO/[^{3}H] GUO mixture, rats (set III) were sacrificed at the times indicated and the brain, heart, lung, liver and kidney were immediately removed, washed with saline solution, blotted with filter paper and weighed. In addition, rats from the control group (set I) were also sacrificed and the same organs were removed for comparison purposes. Tissues (200 mg) were then minced and homogenized into 1 ml of ice cold 0.4 M $HClO_4$ using an Ultra-Turrax homogenizer (Ika Labortechnik, Staufen, Germany), and centrifuged (10,000 g for 10 min at 4°C). Each supernate fraction was adjusted to pH 7 with KOH and centrifuged to remove $KClO_4$. Samples were then filtered with 0.2 μm filters (Millipore, Vimodrone, Italy) immediately frozen at –80°C and stored until HPLC analysis.

HPLC analysis

GUO and its metabolites, GUA, XAN and uric acid were assayed by Agilent 1100 series HPLC (Agilent Technologies, Waldbronn, Germany). Separation was carried out as previously reported (4) with a reverse-phase analytical column (LiChroCART 125-4 LiChrospher 100 RP-18 5 μm, Merck, Darmstadt, Germany) and a flow rate of 1.5 ml/min. A 15-min linear gradient was applied from 100% buffer A (60 mM KH_2PO_4 and 5 mM tetrabutylammonium phosphate, pH 6) to 100% buffer B (30% methanol plus 70% buffer A). The amounts of the unlabeled compounds were measured with a diode array detector (DAD) (Agilent Technologies, Waldbronn, Germany) on the basis of the absorption at 254

nm (290 nm for uric acid); the compounds were identified by their migration times and UV spectrum, comparing them with the relative standards.

The labeled compounds were simultaneously assayed by an on-line radiochemical detector (FLO-ONE 500 TR, Packard Instrument, Meriden, CT, USA). The liquid scintillation cocktail (Ultima-FloM) was pumped at 3 ml/min and mixed continuously with the HPLC eluate. The mixture was passed through a 500 µl detector flow cell. After background radioactivity subtraction, radio-chromatograms were integrated and the cpm under each peak were obtained. Radioactivity associated with each HPLC-identified substance was measured and reported as microgram equivalents of administered GUO per gram of tissue and/or ml of plasma.

Plasma purine nucleoside phosphorylase activity

Enzyme activity was determined by HPLC, measuring the conversion of inosine to hypoxanthine. The reaction mixture was composed of 50 mM HEPES pH 7.0 containing 1 mM inosine and 10 mM phosphate used as substrate and co-substrate, respectively. The final reaction volume was 1 ml. The reaction was started by the addition of 100 µl of plasma, and the mixture was incubated by shaking at 37°C. After 15 min, the reaction was stopped by the addition of $HClO_4$ (final concentration of 0.4 M), and the samples were centrifuged at 10,000 g for 5 min at 4°C. The supernate was neutralized with KOH and centrifuged again. Samples were then filtered with 0.2 µm filters (Millipore, Vimodrone, Italy) and analyzed by HPLC coupled with a UV-DAD detector using the conditions described in the previous section to calculate the amount of inosine and hypoxanthine. Samples, to which no substrate was added, were run and served as blanks. Data were the mean ± S.E.M. of at least 3 experiments.

Cell culture

Primary cultures of astrocytes were prepared from neonatal rats 2 to 4 days after birth as described previously (22). Briefly, cerebral cortices were collected in a growth medium of high-glucose Dulbecco's modified Eagle's medium supplemented with 10% fetal calf serum and 1% penicillin/streptomycin (10,000 U/ml penicillin G sodium and 10,000 µg/ml streptomycin sulfate in 0.85% saline). The tissue was then washed in phosphate-buffered saline (PBS), cut in small fragments, and digested with 0.025% trypsin/0.04% EDTA solution in PBS for 20 min at 37°C. The cells were then dissociated in 0.01% DNase solution in growth medium for 10 min at 37°C and centrifuged at 1000 rpm for 10 min. The pellet was resuspended in a growth medium containing 5 mM L-leucine methyl ester to constrain microglia contamination. Cells, seeded on poly(D-lysine)-coated T75 flasks, were grown in this medium for the first 24 h and were then maintained in an identical medium without leucine methyl ester. The medium was replaced every 3 to 4 days. At the 7th and 13th days *in vitro*, cells were shaken for 3 h at 80 rpm on a plate shaker to minimize attachment and thus microglial contamination of the cultures. Astrocytes were detached from the culture flasks by treatment (5–10 min at 37°C) with 0.025% trypsin/0.04% EDTA. Astrocytes were replated onto poly(D-lysine)-coated 35-mm dishes at a concentration of $5x10^5$ cells/dish. The cells were used for experimental procedures 48 h after seeding.

[^{3}H]guanosine and [^{3}H]guanine incorporation into primary cultures of rat brain astrocytes

Astrocyte cultures were rinsed twice with a modified Krebs-HEPES buffer (KHB) containing 15 mM HEPES, pH 7.4, 120 mM NaCl, 4 mM KCl, 1.2 mM $MgSO_4$, 1.2 mM KH_2PO_4, 1 mM $CaCl_2$, and 10 mM D-glucose and then pre-incubated with fresh modified KHB on a rocking platform in a humidified incubator at 37°C for 5 min. The incubation was initiated by adding different concentrations (ranging from 0.001 to 10 µM) of [^{3}H]GUO or [^{3}H]GUA (15 Ci/mmol each) to the cells. After designated time intervals, the incorporation of GBPs was terminated by two ice-cold washes with unlabeled medium to remove extracellular substrates. Finally, astrocytes were scraped, lysed and then briefly sonicated in ice. An aliquot (100 µl) of lysates was taken for measurement of the total radioactivity using the liquid scintillation counter. Protein concentration was measured by the Bradford method with bovine serum albumin as the standard. Data were the mean ± S.E.M. of at least 3 experiments.

Determination of efflux of guanine-base purines from primary cultures of rat brain astrocytes

Astrocyte cultures were incubated for 15 min on a rocking platform in a humidified incubator at 37°C with modified KHB containing 100 nM [^{3}H]GUO (15 Ci/mmol). At the end of the period of incubation, cultures were quickly washed twice with ice-cold unlabeled medium. Cells then were maintained in unlabeled modified KHB for 15 min in an humidified incubator at 37°C. At the end of this time period, the medium was collected, centrifuged, filtered and analyzed by HPLC connected to the on-line radiochemical detector, using the conditions described in the "HPLC analysis" section. When used, the inhibitor of ecto-5'-nucleotidase, α-β methylenadenosine 5'-diphosphate (AOPCP), was added to the unlabeled modified KHB to a final concentration of 100 µM until the end of the experiment. Finally, cells were scraped, lysed, and sonicated and an aliquot of lysates was taken for the measurement of protein concentration as previously described. The amount of GBPs was expressed as pmol/

ml/15 min/mg protein. Data were the mean ± S.E.M. of at least 3 experiments.

Statistical analysis

The unpaired Student's *t*-test was used to compare two groups. One-way analysis of variance was used to test for significant differences between multiple groups. Statistical significance was defined as $P < 0.05$.

RESULTS

Levels of radioactivity in plasma

Rats were given i.p. injections of GUO at doses of 2, 4, 8 or 16 mg/kg combined with 0.05% of [^{3}H] GUO, referred to henceforth as GUO-mixture. The level of total radioactivity over time in rat plasma following the administration is shown in Fig. 2. Plasma levels of radioactivity increased in a time-dependent and dose-dependent manner, reaching a plateau phase after 60 min.

Concentration of guanosine and of its metabolic products in plasma

Following i.p. administration of the GUO-mixture (2, 4, 8 or 16 mg/kg), HPLC coupled with both a UV-DAD detector and an on-line radiochemical detector allowed the identification and quantification of GUO (Fig. 3A) and of its metabolic products GUA (Fig. 3B), XAN (Fig. 3C) and uric acid (Fig. 5).

Interestingly, as shown in Fig. 3, A-C, following the i.p. administration at all the different doses used, the amounts of unchanged GUO (Fig. 3A) in the different plasma samples resulted always significantly lower than those of its metabolic derivatives 7.5 min after the injection, indicating that a rapid and marked metabolic breakdown occurs.

The concentration profiles of GUO, GUA, and XAN in plasma were very similar over time at all assayed doses of the administered mixture (Fig. 3, A-C). Indeed, following the injection, the plasma levels of each compound rapidly increased reaching a maximum at 15 min and then decreased with time (Fig. 3, A-C).

After the i.p. injection of the GUO-mixture at doses of 2 mg/kg and 4 mg/kg, the peak plasma concentrations were respectively 0.019±0.003 and 0.069±0.017 µg equivalents/ml for GUO, 0.230±0.060 and 0.490±0.083 µg equivalents/ml for GUA, and 0.110±0.028 and 0.390±0.085

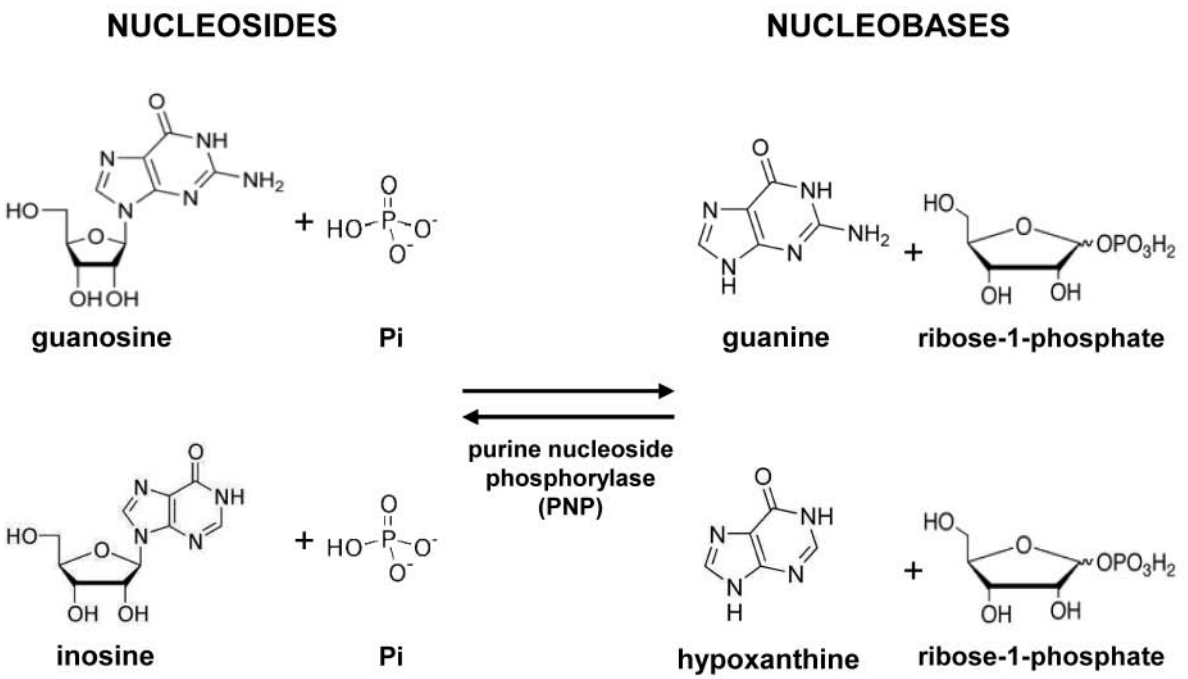

Fig. 1. *Purine nucleoside phosphorylase (PNP) catalyses the reversible phosphorolysis of purine nucleosides (guanosine or inosine) resulting in the formation of ribose-1-phosphate and purine bases (guanine or hypoxanthine).*

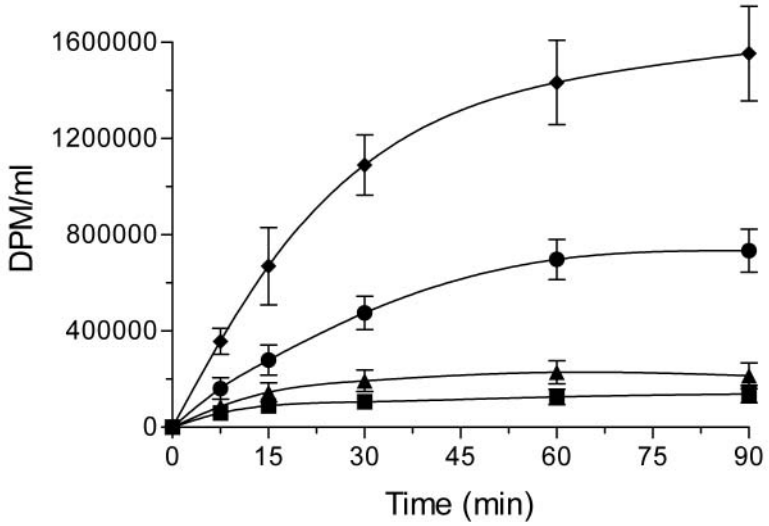

Fig. 2. *Plasma concentration - time profiles of total radioactivity after i.p. injection of the guanosine mixture at doses of 2 mg/kg (■), 4 mg/kg (▲), 8 mg/kg (●) or 16 mg/kg (♦). Each point represents the mean ± S.E.M. of five rats. If the S.E.M. is not shown, it is smaller than the symbols.*

µg equivalents/ml for XAN. The corresponding values for the doses of 8 mg/kg and 16 mg/kg of the GUO-mixture were respectively 0.124±0.020 and 0.244±0.028 µg equivalents/ml for GUO, 0.880±0.150 and 1.350±0.210 µg equivalents/ml for GUA, and 0.660±0.090 and 1.150±0.180 µg equivalents/ml for XAN The calculated AUC_{0-90}, reported in Fig. 4 shows that the concentration of each compound increased linearly in a dose-dependent manner with the following rank order: GUA > XAN > GUO.

When XAN is converted to uric acid by the xanthine dehydrogenase/oxidase enzyme complex, tritium on carbon atom number 8 present in the molecule of [^{3}H]GUO is cleaved resulting in the presentation of uric acid as an unlabeled compound. In this case, the amount of uric acid in the different plasma samples was measured using HPLC coupled with UV-DAD detector. Similar to the labeled compounds, the concentration of uric acid reached a maximum at 15 min after the i.p. injection of the GUO-mixture at all the concentrations used and decreased within the following 75 min (Fig. 5). The area under the plasma concentration-time curve calculated in the time interval 0-90 min (AUC_{0-90}) increased in a dose-dependent manner as shown in the inset of Fig. 5.

Enzymatic activity of purine nucleoside phosphorylase (PNP) in plasma

To verify whether the presence of GUA in rat plasma samples could derive from the catalytic activity of PNP, an enzyme which, using inorganic phosphate, is known to cleave GUO to GUA and inosine to hypoxanthine yielding ribose-1-phosphate (Fig. 1), the plasma PNP activity was measured. Since in plasma the spectrophotometric method might not be optimal due to turbidity and to the low activity (23), the HPLC method has been preferred for this measurement. The addition of 1 mM inosine, currently used as substrate, to the plasma samples resulted in a PNP activity of 11.19±2.75 nmol/ml/min. These findings support the hypothesis that GUO can be rapidly converted into GUA once it reaches the blood after any route of administration.

Tissue distribution of guanosine and of its labeled metabolic products

It is well known that the introduction of radiotracers provides a powerful analytical tool when either biodistribution or pharmacokinetic observations have to be made with new molecules. In

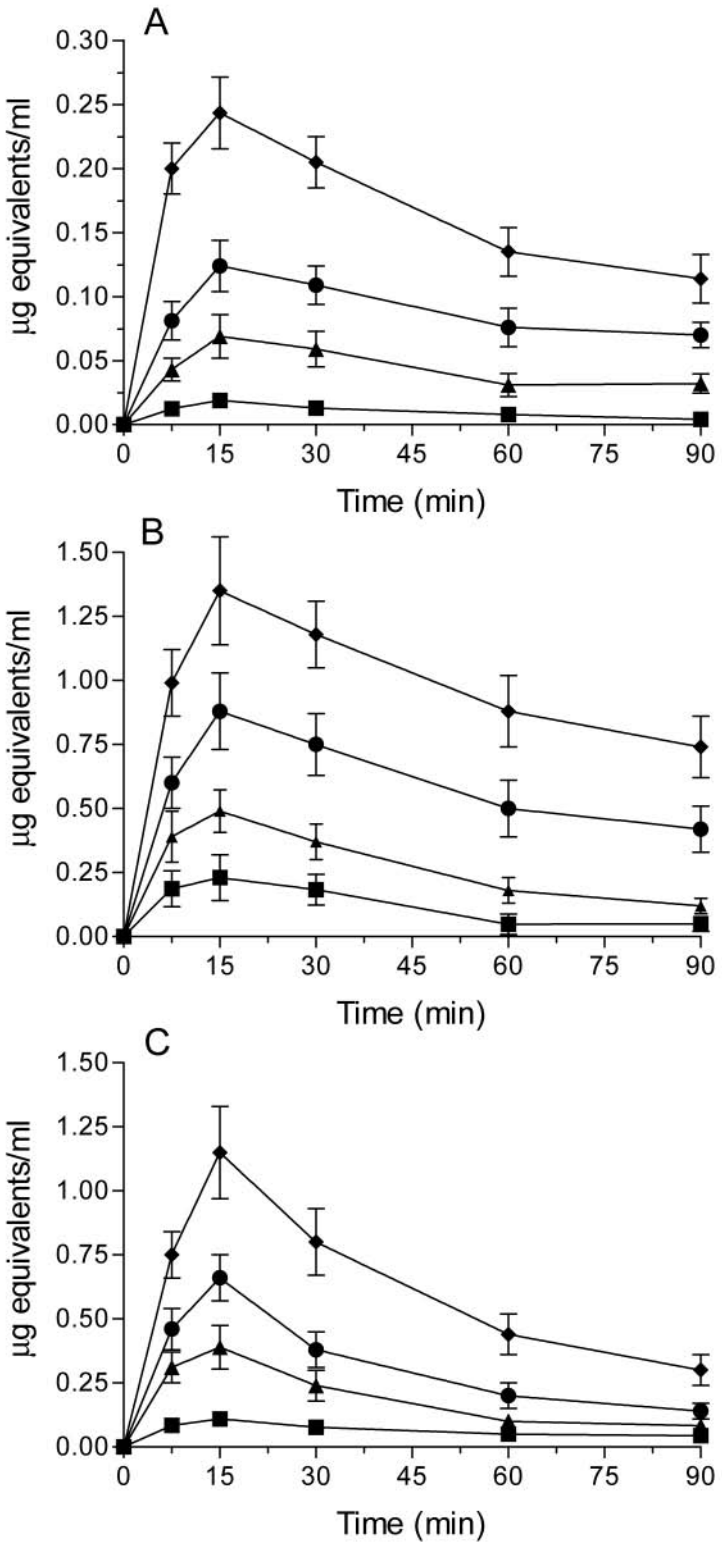

Fig. 3. *Plasma concentration - time profiles of guanosine (**A**), guanine (**B**) and xanthine (**C**) after i.p. injection of the guanosine mixture at doses of 2 mg/kg (■), 4 mg/kg (▲), 8 mg/kg (●) or 16 mg/kg (♦). Plasma purine levels were determined by HPLC coupled with an on-line radiochemical detector as detailed in Materials and Methods. Each point represents the mean ± S.E.M. of five rats. If the S.E.M. is not shown, it is smaller than the symbols.*

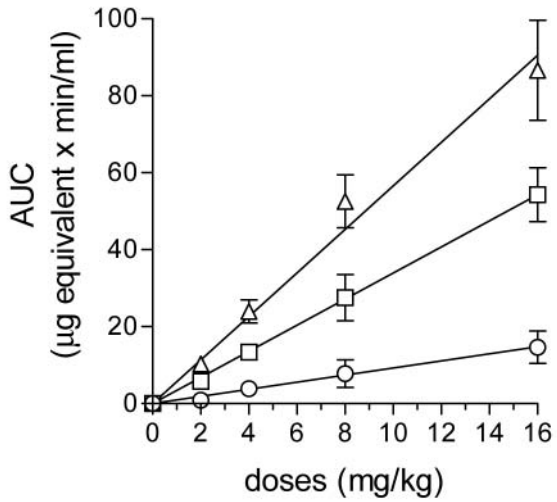

Fig. 4. *The AUC_{0-90} of guanosine (○), guanine (Δ) and xanthine (□) after the i.p. injection of the four different doses of guanosine mixture. Each point represents the mean ± S.E.M. of five rats. If the S.E.M. is not shown, it is smaller than the symbols.*

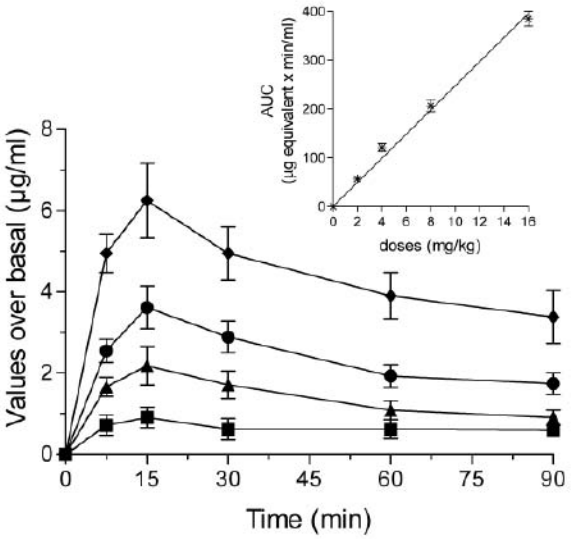

Fig. 5. *Plasma concentration - time profiles of uric acid after i.p. injection of the guanosine mixture at doses of 2 mg/kg (■), 4 mg/kg (▲), 8 mg/kg (●) or 16 mg/kg (♦). Plasma uric acid levels were determined by HPLC coupled with a UV-DAD detector as detailed in Materials and Methods. The AUC_{0-90} of uric acid after the i.p. injection of the different doses of guanosine mixture is shown in the inset. Each point represents the mean ± S.E.M. of five rats.*

fact, it allows the detection of very low concentrations of the labeled compound in the different chosen biological samples.

The values for the presence of GUO, GUA and XAN in different tissues were extrapolated using their respective radiolabeled compounds formed after the i.p injection of the GUO-mixture and are expressed as µg equivalents of the GUO-mixture injected per g of tissue. The values obtained from liver, kidney, heart, lung and brain at the different time points (7.5, 15, 30, 60 and 90 min after the administration of 8 mg /kg of the GUO-mixture) are reported in Fig. 6**.**

Significant concentrations of GUO and, its metabolites were found in all the tissues examined. The concentration profiles of GUO, GUA, and XAN were similar to those reported for the plasma samples (Fig. 3A-C), the maximal concentrations being reached 15-30 min after the injection. In all the tissues analyzed, the maximal amounts of GUO and GUA were significantly higher than those measured in plasma. XAN was highly concentrated in liver and kidney indicating that these organs actively metabolize GUO.

Plasma and tissue concentrations of endogenous guanosine and of its metabolic products

The endogenous levels of GUO, GUA and XAN were analyzed in control animals and are shown in Fig. 7.

At peak levels after the 8 mg/kg i.p. injection of the GUO-mixture, the amounts of GUO and its derivatives, have been reported as folds of increase relative to the respective concentrations evaluated in control animals (Fig. 7). All tissues showed a 2-fold increase in GUO levels compared to controls with the exception of the liver in which GUO levels were about 3.6-fold greater than control values (Fig. 7). GUA levels dramatically increased by at least 9-10-fold except for plasma in which the increase was about 2-fold the controls.

XAN levels also increased after the administration of the GUO-mixture. XAN concentrations were approximately 2-fold the basal levels in plasma,

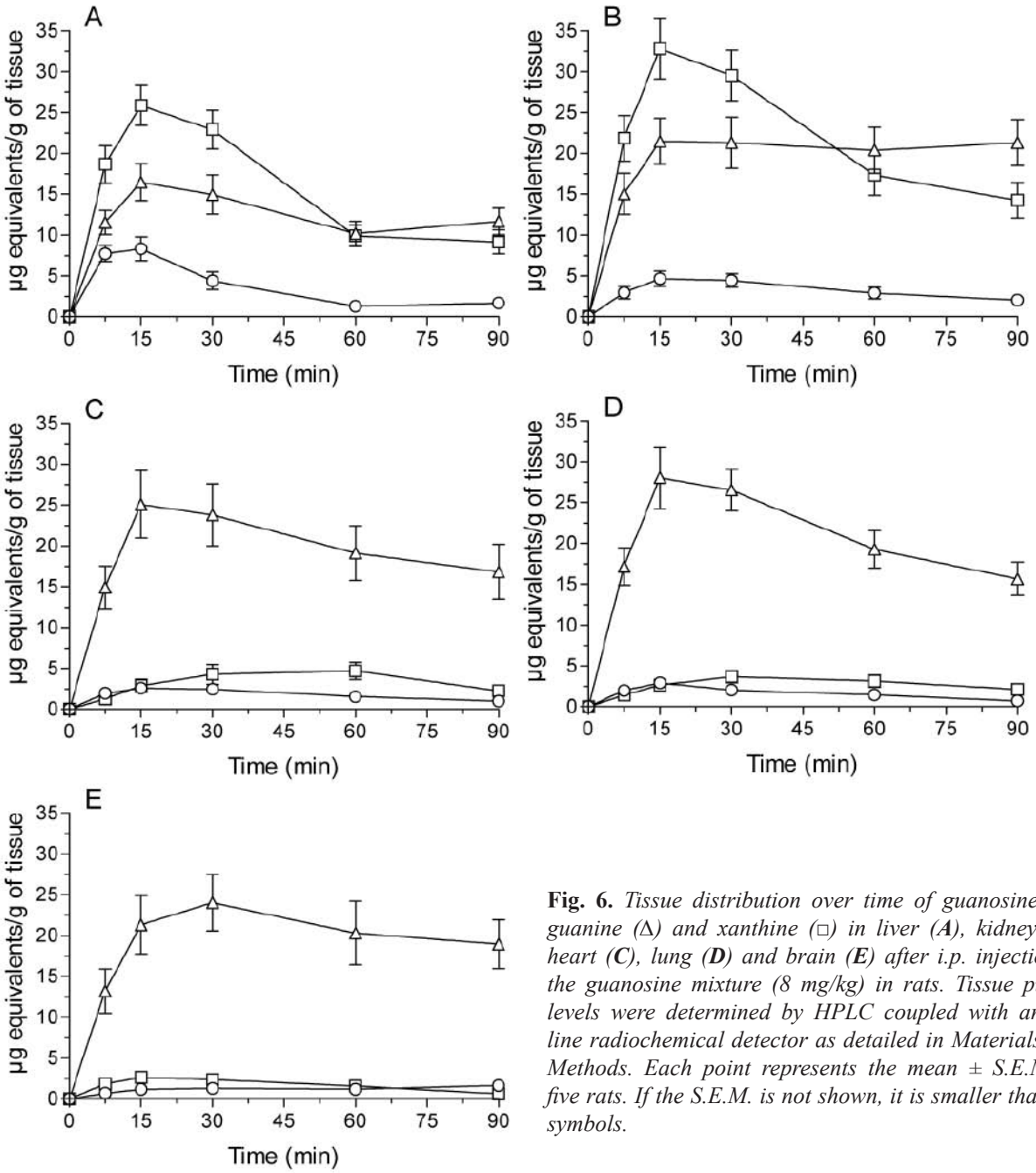

Fig. 6. *Tissue distribution over time of guanosine (○), guanine (Δ) and xanthine (□) in liver (**A**), kidney (**B**), heart (**C**), lung (**D**) and brain (**E**) after i.p. injection of the guanosine mixture (8 mg/kg) in rats. Tissue purine levels were determined by HPLC coupled with an on-line radiochemical detector as detailed in Materials and Methods. Each point represents the mean ± S.E.M. of five rats. If the S.E.M. is not shown, it is smaller than the symbols.*

heart, lung and brain (Fig. 7) and about 3- and 5-fold the controls in liver and kidney, respectively. This agrees with the findings of Shin et al. (24) who reported that, after intramuscular administration of [^{3}H]GUO, the total radioactivity was most highly concentrated in the kidney.

Guanosine and guanine accumulation in primary cultures of rat brain astrocytes

To measure the accumulation of [^{3}H]GUO and [^{3}H]GUA by primary cultures of rat brain astrocytes, 0.1 mM of either the nucleoside or the nucleobase were used. As shown in Figs. 8A and 8C, at 37°C

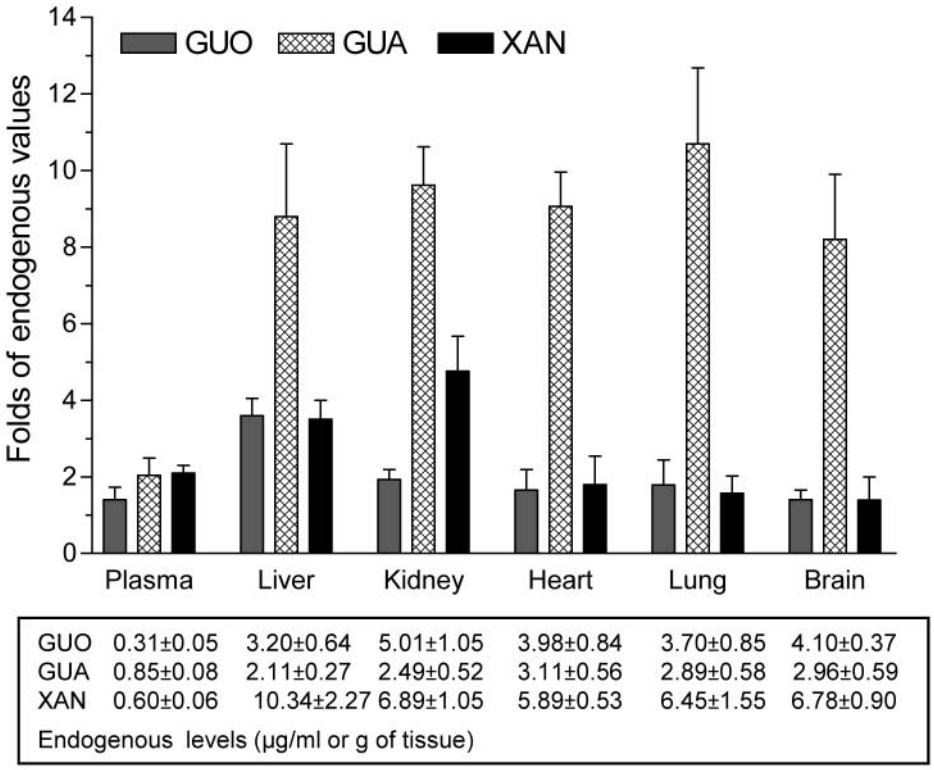

Fig. 7. *Effect of the administration of the guanosine (GUO) mixture (8 mg/kg) expressed as increase over basal values of GUO and its metabolic derivatives. The endogenous levels of GUO, guanine (GUA) and xanthine (XAN) have been measured in control animals and reported in the inset below. Each column represents the mean ± S.E.M. of five rats.*

[^{3}H]GUO and [^{3}H]GUA were linearly taken up by the cells in a time-dependent manner.

With increasing concentrations (Fig. 8, B and D), the accumulation of tritium in the cells, after 15 min of incubation, reached saturation at the higher concentration used. This is consistent with previously reported results indicating that these uptakes occur, at least in part, by facilitated rather than simple diffusion (25). Similar results were obtained when the experiments were carried out in Na^+-free medium (data not reported) thus excluding a significant Na^+-dependent uptake for these compounds in physiological conditions.

Efflux of guanine-based purines in primary cultures of rat brain astrocytes

To evaluate the efflux of GBPs, cells were pre-incubated with 0.1 mM [^{3}H]GUO for 15 min. After an adequate wash, astrocytes were maintained for a further 15 min in a fresh unlabeled medium. At the end of this period, significant amounts of GUO, GUA and XAN, were found (Fig. 9).

To assess whether GUO and its metabolites were released *per se* or were the result of the extracellular breakdown of guanine-based nucleotides, the cells were pre-treated with 100 mM AOPCP a specific inhibitor of ecto-5'-nucleotidase (7, 16) the enzyme that acts as the final step in converting extracellular nucleoside-5'-monophosphates, including GMP, into their respective nucleosides. As shown in Fig. 9, this compound dramatically reduced the extracellular amounts of GUO and of its metabolic products. The levels of GMP in the cell medium were 0.090±0.016 and 0.782±0.124 pmol/15min/mg protein in the absence and in the presence of AOPCP, respectively.

DISCUSSION

GUO exerts neuroprotective actions which have been related to inhibition of apoptosis,

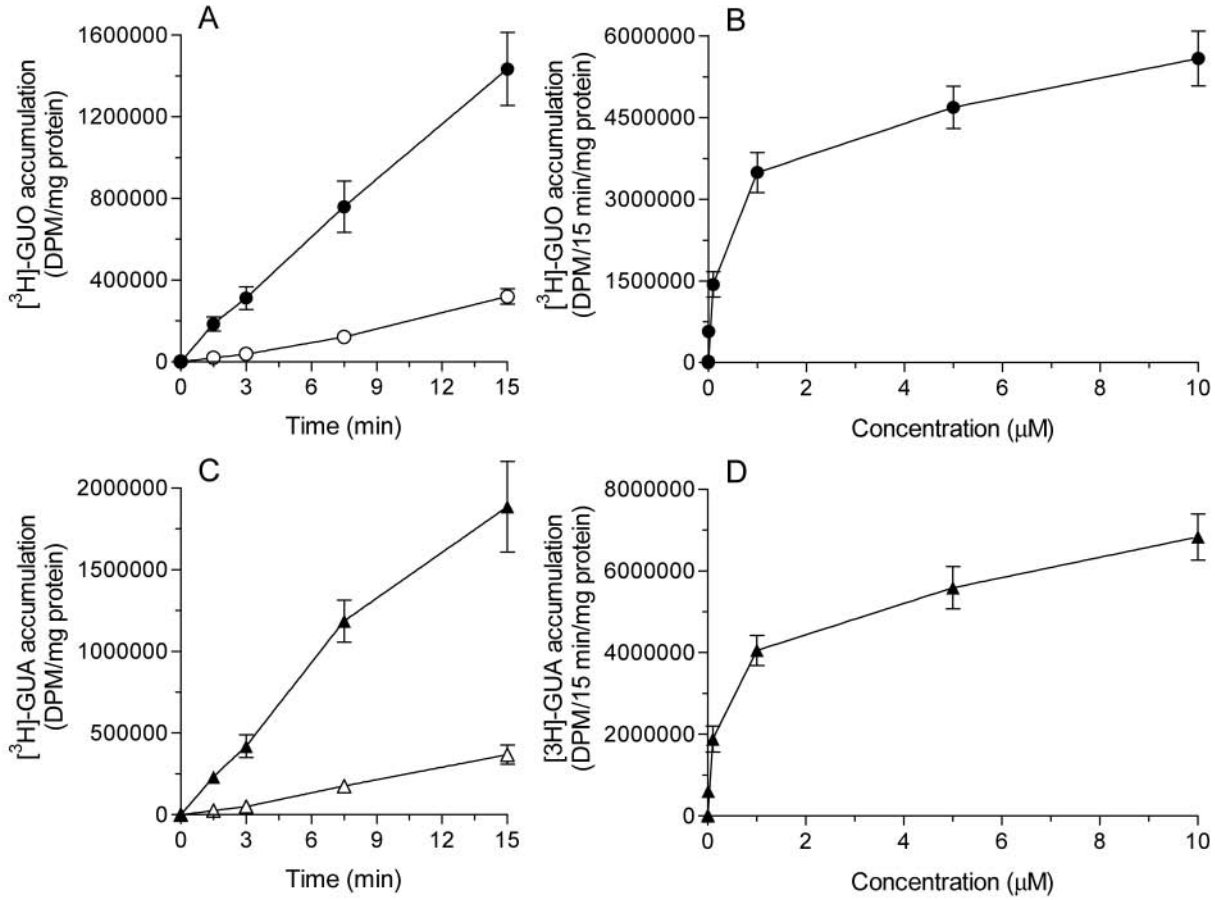

Fig. 8. *Time course (**A**, **C**) and concentration dependence (**B**, **D**) of [³H]guanosine ([³H]-GUO) (●) and [³H]guanine ([³H]-GUA) (▲) accumulation by primary cultures of rat brain astrocytes. The time courses (A, C) were carried out at 37°C (closed) or 0°C (opened). Each point represents the mean ± S.E.M. of at least three experiments. If the S.E.M. is not shown, it is smaller than the symbols.*

cytotoxicity, glutamatergic neurotransmission, and protein aggregate formation (9, 26, 27) as well as to stimulation of glutamate uptake (3), synaptogenesis (28) and tissue repair (8, 29, 17). Moreover, this nucleoside has neurotrophic effects by enhancing the production of several trophic factors (30).We also previously reported a specific high-affinity binding site for GUO on membrane preparations from rat brain (31), thus, GUO or its analogs could be studied as a potential new approach in the treatment of neurodegenerative disorders.

In addition, it has been recently reported that GUO and its metabolic product GUA exert antiproliferative effects (32) and that GUO enhances the antitumor activity of other agents including acriflavine (24) and cytosine-beta-D-arabinofuranoside (33).

Nevertheless, to our knowledge, only one study has reported a pharmacokinetic analysis of GUO following administration of this nucleoside (each dose containing a percentage of [³H]GUO) in rats (24). However, in this study, the authors did not take into account that GUO, like ADO and inosine, undergoes extracellular metabolism. PNP catalyses the reversible conversion of GUO into GUA and of inosine into hypoxanthine, reactions occurring in mammalian metabolism during the well-known "purine salvage pathway" aimed at the formation of the corresponding mononucleotides (18). PNP is

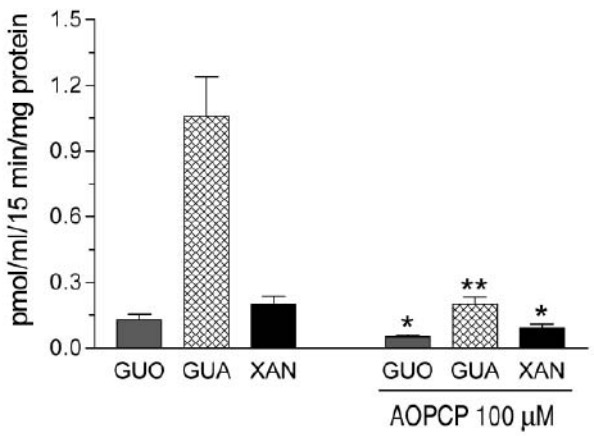

Fig. 9. *Guanine-based purine release from primary cultures of rat brain astrocytes incubated for 15 min with modified KHB containing 100 nM [³H]guanosine (15 Ci/mmol). The cells were then maintained in unlabeled modified KHB, in the presence or in the absence of 100 µM AOPCP, for 15 min and guanosine (GUO), guanine (GUA) and xanthine (XAN) levels were determined by HPLC coupled with an on-line radiochemical detector as detailed in Materials and Methods. Each column represents the mean ± S.E.M. of at least three experiments (* P < 0.05 and ** P < 0.01 vs. untreated cells).*

widely expressed in human tissue and its activity is detectable in plasma of normal subjects.

We therefore investigated the distribution of not only GUO but also of its metabolic products following i.p. administration of a mixture containing GUO and [³H]GUO (the radiotracer being the 0.05% of the total) in rats. The levels of radioactivity in rat plasma increased over time in a dose-dependent manner, this finding being consistent with data reported by Shin et al. (24).

As early as 7.5 min following the i.p injection, GUO was detectable in the plasma at a level of 0.035% of the administered nucleoside mixture and, more interestingly, GUO metabolites, GUA and XAN, were also present with their amounts being much higher (about 10- and 5-fold, respectively) than of GUO itself. This findings fits well with our results showing the presence of PNP activity in plasma samples.

In plasma samples, uric acid was also detectable at levels significantly higher than those of GUO by 7.5 min following the mixture administration. It is known that the urate oxidase gene is inactivated in hominoids (34) and human blood uric acid concentration is much higher (up to 100-fold) than in other animal species including rodents (35) where urate oxidase rapidly metabolizes uric acid into allantoin. Thus, the effects of urate in this species, deriving from a modification of blood or tissue levels of uric acid to which they might be particularly sensitive, may not be really predictive for human pathophysiology. In our opinion, these kinds of metabolic mismatches should also be considered when determining the clinical relevance of animal models. In the present study, we therefore decided to measure only GUA and XAN, along with GUO in the chosen tissue samples.

The tissue distribution of GUO and of its metabolic products was tested after a single i.p. administration of 8 mg/kg GUO-mixture. This dosage was chosen on the basis of previous *in vivo* studies in which GUO, given to rats via i.p. injection at the same concentration (7.5-8 mg/kg), was reported to exert relevant neuroprotective effects (36, 13). Similar to the findings in plasma, a significant and early increase in GUO, GUA and XAN levels was observed in the tissues analyzed. Interestingly, the concentrations in each tissue were higher than those measured in plasma, indicating rapid distribution and accumulation of these compounds in the different organs. High amounts of XAN were detected in liver and kidney as early as 7.5 min following the injection; the levels of this metabolite were about 40- and 50-fold those reported for plasma and about 10-fold higher than those reported for the other tissues examined, suggesting an important role for liver and kidney in GUO metabolism and likely in its excretion.

GUO and its derivatives are endogenous compounds and they are present both outside and inside the cells of all mammalians (including humans). We found that the amounts of the endogenous GUO, GUA and XAN measured in the different tissues are in agreement with those reported by others (37, 38), and, based on the significant increase of each compound following the injection

of GUO, it is reasonable to conclude that the contribution of endogenous GUO, GUA and XAN is almost negligible.

It is interesting to note that the GUO/GUA ratio, which was about 1.5-2 in the different organs for the endogenous compounds, was inverted following the i.p. injection. This was true except for plasma where the amount of GUA was always higher than that of GUO. These results may be explained by the presence and activity of a plasma PNP rapidly metabolizing GUO into GUA which, in its turn, is widely distributed. Moreover, GUA distribution is supported by the evidence that endothelial cells, which in particular districts (e.g. brain) represent key elements in the blood-tissue interface, can actively take up nucleosides, synthetic nucleoside analogues, and nucleobases via either ENTs or CNTs. These mechanisms, working together, deeply influence nucleoside and nucleobase levels in the vascular system.

Given that: a) rapid plasma metabolism of GUO into GUA occurs, b) several well-documented neuroprotective effects for GUO have been reported, c) astrocytes have been shown to be the main sources of both adenine or guanine-based purines within the CNS (3, 4), we also evaluated whether primary cultures of rat brain astrocytes were able to take up and to release GUO and GUA in resting conditions. Following loading the cells with either [^{3}H]GUO or [^{3}H]GUA, the cultured astrocytes were able to accumulate these compounds in a time- and dose-dependent manner. The accumulation was similar in a Na^+-free medium confirming that, in physiological conditions, ENTs mediate the transport of these GBPs. Nagasawa et al. (25) using similar culture conditions also found that astrocytes were able to take up either the nucleoside or the nucleobase, with GUA being more avidly transported than GUO.

We have also shown that after cell loading with [^{3}H]GUO, labeled GUO, GUA and XAN were found in the extracellular medium. GUA levels were higher than GUO ones, suggesting the presence and the activity of an extracellular form of PNP which we are exploring further. However, when astrocytes were pretreated with AOPCP to inhibit the extracellular conversion of GMP into GUO, the amounts of GUO, GUA and XAN were markedly reduced, indicating that GUO and its metabolic products found in the astrocyte culture medium mainly derive from the extracellular breakdown of the released nucleotides. This is similar to the findings with ADO which, in the extracellular space, is largely derived from ATP breakdown (39) and is consistent with the findings of Souza and co-workers who reported that antinociceptive, anticonvulsant or amnesic effects of GMP administration are due to its conversion to GUO (40, 16).

In conclusion, it is clear from this study that following i.p. administration to rats, GUO is absorbed and extensively converted to GUA by either intracellular or extracellular PNP. The nucleoside, along with its direct metabolite, is widely distributed, able to cross the blood brain barrier and is therefore capable of exerting neuroprotective effects. In the brain, astrocytes actively participate in the complex trafficking of not only GUO, but also of GUA between the intracellular and extracellular compartments. This indicates that this nucleobase could mediate some of the biological activities exerted by GUO and should be considered a new, interesting signaling molecule for further studies. Based on these considerations, newly synthesized guanosine/guanine-based analogues are being tested in our laboratories.

Even though recent progress has unveiled new, interesting aspects of the physiology of ecto-enzymes involved in the complex pathways of the purinergic system, including that of an indirect but crucial control of subtype receptor activation, they remain still poorly known. Nevertheless from a long-term perspective, molecular and functional studies on these enzymes, both at intracellular and extracellular levels, including PNP, the altered expression/activity of which is known to cause a severe immunodeficiency associated with neurological disorders, should eventually contribute to a better understanding of the processes involved in neurodegeneration, inflammation and vascular alterations and potentially to the development of new therapeutic interventions.

ACKNOWLEDGEMENTS

The authors thank Dr. Cosmo Rossi for technical assistance. This research was supported by grants from the Italian Ministero dell'Istruzione, dell'Università e della Ricerca (MIUR): PRIN 20085HBSWS.

REFERENCES

1. Parpura V, Zorec R. Gliotransmission: Exocytotic release from astrocytes. Brain Res Rev 2010; 63(1-2):83-92.
2. Fields RD. Nonsynaptic and nonvesicular ATP release from neurons and relevance to neuron-glia signaling. Semin Cell Dev Biol 2011; 22:214-19.
3. Schmidt AP, Lara DR, Souza DO. Proposal of a guanine-based purinergic system in the mammalian central nervous system. Pharmacol Ther 2007; 116(3):401-16.
4. Ciccarelli R, Di Iorio P, Giuliani P, D'Alimonte I, Ballerini P, Caciagli F, Rathbone MP. Rat cultured astrocytes release guanine-based purines in basal conditions and after hypoxia/hypoglycemia. Glia 1999; 25(1):93-8.
5. Caciagli F, Di Iorio P, Giuliani P, Middlemiss MP, Rathbone MP. The neuroprotective activity of guanosine involves the production of trophic factors and the outflow of purines from astrocytes. Drug Dev Res 2000; 50:32.
6. Frizzo ME, Lara DR, Prokopiuk Ade S, Vargas CR, Salbego CG, Wajner M, Souza DO. Guanosine enhances glutamate uptake in brain cortical slices at normal and excitotoxic conditions. Cell Mol Neurobiol 2002; 22(3):353-63.
7. Frizzo ME, Antunes Soares FA, Dall'Onder LP, Lara DR, Swanson RA, Souza DO. Extracellular conversion of guanine-based purines to guanosine specifically enhances astrocyte glutamate uptake. Brain Res 2003; 972(1-2):84-9.
8. Jiang S, Khan MI, Lu Y, Wang J, Buttigieg J, Werstiuk ES, Ciccarelli R, Caciagli F, Rathbone MP. Guanosine promotes myelination and functional recovery in chronic spinal injury. Neuroreport 2003; 14(18):2463-7.
9. Su C, Elfeki N, Ballerini P, D'Alimonte I, Bau C, Ciccarelli R, Caciagli F, Gabriele J, Jiang S. Guanosine improves motor behavior, reduces apoptosis, and stimulates neurogenesis in rats with parkinsonism. J Neurosci Res 2009; 87(3):617-25.
10. de Oliveira DL, Horn JF, Rodrigues JM, Frizzo ME, Moriguchi E, Souza DO, Wofchuk S. Quinolinic acid promotes seizures and decreases glutamate uptake in young rats: reversal by orally administered guanosine. Brain Res 2004; 1018(1):48-54.
11. Torres FV, da Silva Filho M, Antunes C, Kalinine E, Antoniolli E, Portela LV, Souza DO, Tort AB. Electrophysiological effects of guanosine and MK-801 in a quinolinic acid-induced seizure model. Exp Neurol 2010; 221(2):296-306.
12. Schmidt AP, Böhmer AE, Schallenberger C, Antunes C, Tavares RG, Wofchuk ST, Elisabetsky E, Souza DO. Mechanisms involved in the antinociception induced by systemic administration of guanosine in mice. Br J Pharmacol 2010; 159(6):1247-63.
13. Schmidt AP, Paniz L, Schallenberger C, Böhmer AE, Wofchuk ST, Elisabetsky E, Portela LV, Souza DO. Guanosine prevents thermal hyperalgesia in a rat model of peripheral mononeuropathy. J Pain 2010; 11(2):131-41.
14. Gudkov SV, Gudkova OIu, Shtarkman IN, Gapeev AB, Chemeris NK, Bruskov VI. Guanosine and inosine as natural geneprotectors for mice blood cells exposed to X-rays. Radiats Biol Radioecol 2006; 46(6):713-8.
15. Soares FA, Schmidt AP, Farina M, Frizzo ME, Tavares RG, Portela LV, Lara DR, Souza DO. Anticonvulsant effect of GMP depends on its conversion to guanosine. Brain Res 2004; 1005(1-2):182-6.
16. Vinadé ER, Schmidt AP, Frizzo ME, Portela LV, Soares FA, Schwalm FD, Elisabetsky E, Izquierdo I, Souza DO. Effects of chronic administered guanosine on behavioral parameters and brain glutamate uptake in rats. J Neurosci Res 2005; 79(1-2):248-53.
17. Jiang S, Ballerini P, Buccella S, Giuliani P, Jiang C, Huang X, Rathbone MP. Remyelination after chronic spinal cord injury is associated with proliferation of endogenous adult progenitor cells after systemic administration of guanosine. Purinergic Signal 2008; 4(1):61-71.
18. Bzowska A, Kulikowska E, Shugar D. Purine nucleoside phosphorylases: properties, functions, and clinical aspects. Pharmacol Therapeut 2000; 88:349-425.
19. Gray JH, Owen RP, Giacomini KM. The concentrative nucleoside transporter family, SLC28. Pflugers Arch 2004; 447(5):728-34.
20. Robillard KR, Bone DB, Hammond JR. Hypoxanthine uptake and release by equilibrative

nucleoside transporter 2 (ENT2) of rat microvascular endothelial cells. Microvasc Res 2008; 75(3):351-7.
21. De Keyser J, Mostert JP, Koch MW. Dysfunctional astrocytes as key players in the pathogenesis of central nervous system disorders. J Neurol Sci 2008; 267(1-2):3-16.
22. Di Iorio P, Ballerini P, Traversa U, et al. The antiapoptotic effect of guanosine is mediated by the activation of the PI 3-kinase/AKT/PKB pathway in cultured rat astrocytes. Glia 2004; 46(4):356-68.
23. Yamamoto T, Moriwaki Y, Takahashi S, Nasako Y, Yamakita J, Hiroishi K, Higashino K. Determination of plasma purine nucleoside phosphorylase activity by high-performance liquid chromatography. Anal Biochem 1995; 227(1):135-9.
24. Shin DH, Choi KS, Cho BS, Song S, Moon DC, Hong JT, Lee CK, Chung YB. Pharmacokinetics of guanosine in rats following intravenous or intramuscular administration of a 1:1 mixture of guanosine and acriflavine, a potential antitumor agent. Arch Pharm Res 2008; 31(10):1347-53.
25. Nagasawa K, Kawasaki F, Tanaka A, Nagai K, Fujimoto S. Characterization of guanine and guanosine transport in primary cultured rat cortical astrocytes and neurons. Glia 2007; 55(14):1397-404.
26. Pettifer KM, Jiang S, Bau C, Ballerini P, D'Alimonte I, Werstiuk ES, Rathbone MP. MPP(+)-induced cytotoxicity in neuroblastoma cells: Antagonism and reversalby guanosine. Purinergic Signal 2007; 3(4):399-409.
27. Tarozzi A, Merlicco A, Morroni F, et al. Guanosine protects human neuroblastoma cells from oxidative stress and toxicity induced by Amyloid-beta peptide oligomers. J Biol Regul Homeost Agents 2010; 24(3):297-306.
28. Gerrikagoitia I, Martínez-Millán L. Guanosine-induced synaptogenesis in the adult brain in vivo. Anat Rec (Hoboken) 2009; 292(12):1968-75.
29. Jiang S, Zavitz CC, Wang J, et al. Non-adenine based purines accelerate wound healing. Purinergic Signal 2006; 2(4):651-61.
30. Di Iorio P, Caciagli F, Giuliani P, et al. Purine nucleosides protect injured neurons and stimulate neuronal regeneration by intracellular and membrane receptor-mediated mechanisms. Drug Dev Res 2001; 52(1-2): 303-15.
31. Traversa U, Bombi G, Di Iorio P, Ciccarelli R, Werstiuk ES, Rathbone MP. Specific [(3)H]-guanosine binding sites in rat brain membranes. Br J Pharmacol 2002; 135(4):969-76.
32. Garozzo R, Sortino MA, Vancheri C, Condorelli DF. Antiproliferative effects induced by guanine-based purines require hypoxanthine-guanine phosphoribosyltransferase activity. Biol Chem 2010; 391(9):1079-89.
33. Sidi Y, Panet C, Cyjon A, Fenig E, Beery E, Nordenberg J. Guanosine potentiates the antiproliferative effect of cytosine-beta-D-arabinofuranoside in melanoma cell lines. Cancer Invest 1993; 11(5):523-9.
34. Keilin J. The biological significance of uric acid and guanine excretion. Biol Rev Camb Philos Soc 1959; 34:265-96.
35. Khalpey Z, Yuen AH, Lavitrano M, McGregor CG, Kalsi KK, Yacoub MH, Smolenski RT. Mammalian mismatches in nucleotide metabolism: implications for xenotransplantation. Mol Cell Biochem 2007; 304(1-2):109-17.
36. Su C, Elfeki N, Ballerini P, D'Alimonte I, Bau C, Ciccarelli R, Caciagli F, Gabriele J, Jiang S. Guanosine improves motor behavior, reduces apoptosis, and stimulates neurogenesis in rats with parkinsonism. J Neurosci Res 2009; 87(3):617-25.
37. Kelly KJ, Plotkin Z, Dagher PC. Guanosine supplementation reduces apoptosis and protects renal function in the setting of ischemic injury. J Clin Invest 2001; 108(9):1291-8.
38. Kovács Z, Kékesi KA, Bobest M, et al. Post mortem degradation of nucleosides in the brain: comparison of human and rat brains for estimation of *in vivo* concentration of nucleosides. J Neurosci Methods 2005; 148(1):88-93.
39. Zamzow CR, Xiong W, Parkinson FE. Astrocytes affect the profile of purines released from cultured cortical neurons. J Neurosci Res 2008; 86(12):2641-9.
40. Schmidt AP, Böhmer AE, Leke R, et al. Antinociceptive effects of intracerebroventricular administration of guanine-based purines in mice: evidences for the mechanism of action. Brain Res 2008; 1234:50-8.

CIRCULATING CYTOKINES PRESENT IN THE SERUM OF PERIPHERAL ARTERIAL DISEASE PATIENTS INDUCE ENDOTHELIAL DYSFUNCTION

C. BOTTI[1], C. MAIONE[1], G. DOGLIOTTI[2], P. RUSSO[1], G. SIGNORIELLO[3], A.M. MOLINARI[1], M.M. CORSI[2,4], V. SICA[1] and G. COBELLIS[1]

[1]Department of General Pathology, Second University of Naples, Naples, Italy; [2]Department of Human Morphology and Biomedical Sciences 'Città Studi', University of Milan, Milan, Italy; [3]Department of Public Health, Second University of Naples, Naples, Italy; [4]Clinical Pathology, Policlinico San Donato IRCCS, San Donato, Milan, Italy

Received September 7, 2011 – Accepted November 21, 2011

The first two authors contributed equally to this work

Peripheral arterial disease (PAD) is a chronic condition caused by atherosclerosis and is a severe complication of type 2 diabetes (T2D). We hypothesised that chronic condition of arterial disease engenders inflammation and endothelial damage in response to circulating cytokines released in the blood stream of PAD patients. We explored the levels of circulating cytokines in PAD patients with and without diabetes by multiplex cytokine array compared with non-PAD controls. Serum from PAD patients with or without diabetes showed high levels of VEGF, IFN-γ, TNF-α, MCP-1, and EGF. VEGF levels correlated with TNF-α and IFN-γ, significantly. Endothelial cells (ECs) were exposed to the different altered cytokines to evaluate changes in cell growth, migration and tubule-like formation, displaying impairment on proliferation, migration and tubule formation. Our findings demonstrate that a set of cytokines is significantly increased in the serum of PAD patients. These cytokines act to induce endothelial dysfunction synergistically. VEGF strongly correlated with TNF-α and IFN-γ, opening new therapeutic perspectives.

Peripheral Arterial Disease (PAD) is a chronic condition caused by atherosclerosis and the most severe manifestation of PAD is Critical Limb Ischemia (CLI). Approximately 12% of the adult population suffers from PAD, and the prevalence is equal in men and women (1). The most common risk factors associated with PAD are increasing age, smoking and diabetes.

Diabetes increases the risk of developing symptomatic and asymptomatic PAD by 1.5- to 4-fold and leads to an increased risk of cardiovascular events and early mortality (2, 3). In a NHANES study (4), 26% of participants with PAD had diabetes; in the Edinburgh Artery Study, the prevalence of PAD was greater in participants with diabetes or impaired glucose tolerance (20.6%) than in those with normal glucose tolerance (12.5%-(5)).

In diabetes, an impaired vascular collateralization has been extensively shown, but the causes leading to its pathogenesis are not fully understood.

Key words: peripheral arterial disease, cytokines, diabetes, inflammation

Mailing address: Dr Gilda Cobellis,
Dipartimento di Patologia Generale,
Seconda Università di Napoli,
Via L. De Crecchio, 7,
80138 Napoli, Italy
Tel: +39 0815665681 Fax: +39 081292399;
e-mail: g.cobellis@unina2.it

0393-974X (2012)

DISCLOSURE: ALL AUTHORS REPORT NO CONFLICTS OF INTEREST RELEVANT TO THIS ARTICLE.

Poor collateral development is associated to reduced number of circulating endothelial progenitor cells (EPC) (6). Thus, depletion of circulating EPCs may contribute to endothelial dysfunction, as an early event in the atherogenetic process and poor collateralization as a late event, leading to clinical manifestations of atherosclerosis and cardiovascular disease progression (7).

Advances made in understanding the mechanisms that are involved in the pathophysiology of atherosclerosis indicate that normal homeostasis of the arterial wall is essential to prevent development of atherosclerosis, identifying the inflammation as an important element for the pathogenesis of vascular disease, in its early and late clinical manifestations.

Many molecular aspects of vascular inflammation present in atherosclerosis are common to acute inflammation and immune phenomena. All these have at their basis a condition of endothelial dysfunction (8).

Recent studies suggested that components of the immune system are altered in type 2 diabetes (T2D), suggesting that inflammation participates in the pathogenesis of T2D (9). Therefore, we hypothesised that in PAD patients, with or without diabetes, elevated circulating levels of cytokines may induce alterations in endothelial function, specifically inhibiting proliferation, migration and tubule-like formation.

Our data indicate that the vascular disease, alone and in combination with diabetes, produced such an impressive up-regulation of different inflammatory (IFN-γ, MCP-1 and TNF-α) and arteriogenic cytokines (VEGF and EGF). VEGF levels correlated significantly with TNF-α and IFN-γ. These cytokines act synergistically, exerting a negative effect on endothelial cell activation, indicating that the combination of these factors may be involved in the pathogenesis of endothelial dysfunction. Pharmacological modulation of these factors can help the development of new therapeutic strategies.

MATERIALS AND METHODS

Patient's inclusion criteria

Fifteen patients were enrolled in this study and classified into two groups: PAD (n=9) and PAD + type 2 diabetes (n=6). Thirteen healthy control subjects were recruited from the local community. Lower extremity vascular disease was diagnosed by a history of claudication or rest pain, ankle-brachial index (ABI), Laser Doppler analysis. All patients were treated with autologous bone marrow cell transplantation between February 2008 and July 2010. The protocol was approved by the Ethics Committee of the Seconda Universita' of Naples and was registered at the Trial Registration, NCT00306085. All subjects gave written informed consent before evaluation for inclusion. Routine laboratory screening was performed for all patients.

Bone marrow harvest

Bone marrow was extracted from the iliac crest under anaesthesia in a sterile manner, anti-coagulated with heparin (1:50), and passed through filtering devices to remove large particulate matter such as fat, bone chips and/or clots (Fenwal Bone Marrow kit collection 4R2104, Fenwal Inc Blood Technologies, Lake Zurich, IL, USA). A fraction of 10 ml of bone marrow aspirates were collected in tubes with Na Citrate (129 mM) and serum collected after centrifugation. Peripheral blood was obtained by venepuncture and collected, as previously described.

Serum cytokines

Serum cytokine concentrations were quantified using a biochip array analyzer (Evidence, Randox Laboratories Ltd, Crumlin, UK). Using this procedure, all molecule assays are performed simultaneously using just 100 µL of sample, assay diluent, 1 panel-specific conjugate solution and 1 signal reagent (luminol and peroxide 1:1). The biochip used consists of a 9.9-mm solid substrate (silica) on which discrete test regions have been constructed. The binding ligands (antibodies) are attached to predefined sites (DDR) on the chemically modified surface of the biochip. After a simple enzyme-linked immunosorbent assay procedure, each spot is imaged to capture the chemiluminescent signals generated at each spot on the array. The light signal is captured by a charge-coupled device camera (CCD-camera) as part of an imaging station and converted by image-processing software to provide results compared with calibration curves for each location on the biochip.

The concentrations of SDF-1 levels in peripheral blood were measured using commercial ELISA kits (R&D Systems, Minneapolis, MN, USA), according to the manufacturer's instructions. This assay employs the quantitative sandwich enzyme immunoassay technique. Standards and samples were pipetted into the wells, pre-coated with an antibody against SDF-1, to allow the link of specific molecules to immobilized antibody. After washing any unbound substance, an enzyme-linked monoclonal antibody specific for SDF-1 was added to the wells and colour developed in proportion to the amount

of SDF-1 using a colorimetric assay. Quantification was obtained at 450 nm using an ELISA reader (TECAN, Infinite 2000).

Endothelial Cell (EC) culture

Human Umbilical Vein Endothelial Cells (HUVEC) were purchased from Provitro (Stemcells) and cultured in sterile endothelial growth medium (EGM-2, Clonetics, San Diego, CA, USA). The cells were grown at 37°C in a humidified 95% air/5% CO_2 environment. For all experiments HUVEC were used at passage 4.

Hypoxic culture conditions were achieved in a BD GasPak EZ Anaerobe Gas Generating Pouch System (BD Biosciences, San Diego, CA, USA). As certified by the manufacturer, the Anaerobe Gas Generating Pouch System produces an atmosphere containing 10% carbon dioxide and 1% oxygen.

EC proliferation

HUVEC were plated ($40x10^4$ cells/well in 96-well plates) and incubated at 37°C in hypoxic conditions for 24 h in presence of endothelial basal medium (EBM), endothelial growth medium (EGM-2) and 25 mM glucose alone or in combination with the following cytokines: VEGF (62.32 pg/ml), IFN-γ (1.65 pg/ml), TNF-α (3.6 pg/ml), MCP-1 (153.9 pg/ml), EGF (34.17 pg/ml), purchased from Provitro. After 24 hours, the number of living cells was measured by determination of ATP cellular levels using ViaLight ®Plus Kit (Lonza). All experiments were performed in triplicate.

EC migration

A total of $4 x10^4$ cells were resuspended in 250 µl of EBM and pipetted into the upper chamber of a modified Boyden chamber (Costar Transwell assay, 8 µm pore size, Corning, NY). The chamber was placed in a 24-well culture dish in presence of EGM-2 alone, EGM-2 with VEGF (62.32 pg/ml), IFN-γ (1.65 pg/ml), TNF-α (3.6 pg/ml), MCP-1(153.9 pg/ml) and EGF (34.17 pg/ml) (Provitro), EGM-2 + 25 mM glucose, EGM-2 + the combination of all cytokines and 25 mM glucose. After 24-h incubation at 37°C in hypoxic conditions, transmigrated cells were counted by independent investigators with an inverted microscope (Leica) using a 63x oil immersion objective.

EC tube formation in Matrigel

For analysis of capillary tube formation, 150 µl Matrigel (Becton Dickinson) was laid into a 96-well plate (Falcon, Germany) and incubated at 37°C for 30 minutes. HUVEC were trypsinized and $4x10^4$ cells were suspended in 150 µl of complete endothelial growth medium (EGM-2), EGM-2 with VEGF (62.32pg/ml), IFN-γ (1.65pg/ml), TNF-α (3.6pg/ml), MCP-1(153.9pg/ml) and EGF (34.17pg/ml) (Provitro), EGM-2 + 25 mM glucose, EGM-2 + the combination of all cytokines + 25 mM glucose and plated onto Matrigel. Cells were incubated at 37°C in hypoxic conditions and capillary tube formation in Matrigel was observed under an inverted microscope (Leica) after 24 hours of incubation.

Statistical analysis

All data are represented as mean ± S.D. Statistical analyses of the cytokine array were performed by the analysis of variance (ANOVA) and by multiple comparisons. To quantify correlations between cytokine levels and disease, the Spearman ranked correlation coefficient (r) was determined, using SPSS 17.0 version software.

RESULTS

Patient baseline characteristics

Between February 2008 and July 2010, we enrolled 15 patients (12 men/ 3 women) with severe PAD classified as stage III and IV, according to the Leriche-Fontaine classification with a median age of 75±14. Six patients showed type II diabetes. The characteristics of the patients are shown in Table Ia. Due to the severity of the disease, all patients (n=15) underwent autologous transplantation of bone marrow cells as ultimate therapeutic option. Thirteen healthy subjects (7 men, 6 women) with a median age of 67±10 were considered as control and their characteristics shown in Table Ib.

Cytokine levels in PAD and in PAD + T2D sera

A key role in the pathogenesis of inflammatory disorders is played by cytokines. We decided to measure the levels of 12 different cytokines, implicated in inflammation, using high sensitivity cytokine arrays. We included also SDF-1, due to its possible role in the migration of stem cells (11).

Serum cytokine levels were measured in patients presenting symptomatic PAD, PAD+T2D and healthy subjects of similar age, gender and race (Table II). Applying the analysis of variance (ANOVA) between the two different groups (Controls and (PAD and PAD+D)), we found a significant increase in the levels of VEGF, IFN-γ, TNF-α, MCP-1 and EGF in the serum of patients with PAD with or without diabetes (Fig. 1). Furthermore, by multiple comparison analysis, VEGF, TNF-α and MCP-1

Table I. *Patients' (**a**) and healthy controls' (**b**) characteristics.*

a)

	Patient	Age	Sex	Diabetes	Dyslipidemia	Hypertension	Ulcers	Smoker	Leriche-Fontaine stages	ABI index	Heart failure
PAD	Pt4	47	m	no	yes	no	no	yes	IV	n.d.	no
	Pt7	83	f	no	yes	yes	no	no	III	n.d.	no
	Pt8	78	m	no	yes	no	no	no	IV	sx:0.42 dx:0.35	yes
	Pt10	52	m	no	no	yes	yes	no	IV	dx: n.d. sx:0.60	no
	Pt11	80	m	no	no	no	yes	no	IV	sx:0.64	yes
	Pt12	85	f	no	no	yes	yes	no	IV	sx: 0.40 dx:0.30	no
	Pt15	71	m	no	no	no	no	no	III	sx:0.70	no
	Pt16	87	m	no	no	no	yes	no	IV	sx:n.d. dx:n.d.	no
	Pt18	39	m	no	no	no	no	yes	III	sx:0.91 dx:0.64	yes
PAD+D	Pt1	80	m	yes	no	yes	no	ex smoker	IV	sx:0.46 dx:0.56	no
	Pt3	75	m	yes	no	no	yes	no	III	sx:0.86 dx:0.61	no
	Pt6	60	m	yes	no	no	no	yes	IV	n.d.	no
	Pt9	74	m	yes	no	yes	yes	no	IV	sx:0.30 dx:0.38	no
	Pt13	72	m	yes	no	no	yes	no	IV	sx:0.53	no
	Pt17	83	f	yes	no	no	yes	no	III	sx:0.86 dx:0.92	no

b)

	Patient	Age	Sex	Diabetes	Dyslipidemia	Hypertension	Smoker	Heart failure
CONTROLS	Ctr6	55	m	no	no	no	yes	no
	Ctr15	43	m	no	no	no	no	no
	Ctr16	67	f	no	no	yes	no	no
	Ctr17	58	m	no	no	no	yes	no
	Ctr18	76	m	no	no	yes	ex smoker	no
	Ctr20	64	f	no	no	yes	no	no
	Ctr24	75	f	no	no	yes	no	no
	Ctr25	81	m	no	no	yes	no	no
	Ctr27	68	f	no	no	no	yes	no
	Ctr28	57	m	no	no	yes	no	no
	Ctr30	73	f	no	no	no	no	no
	Ctr31	66	f	no	no	no	no	no
	Ctr32	68	m	no	no	no	ex smoker	no

Table II. *High sensitivity array. The cytokine array was performed both on peripheral blood (PB) of the group of patients (PAD and PAD+D) and healthy controls.*

	SAMPLE	IL2 (pg/ml)	IL4 (pg/ml)	IL6 (pg/ml)	IL8 (pg/ml)	IL10 (pg/ml)	VEGF (pg/ml)	IFN-γ (pg/ml)	TNF-α (pg/ml)	IL1A (pg/ml)	IL1B (pg/ml)	MCP1 (pg/ml)	EGF (pg/ml)	SDF1 (pg/ml)
PAD	PB 4	1.24	1.89	2.14	2.48	0.57	31.79	1.19	2.01	0.13	0.95	117.48	7.49	144.22
	PB 7	2.84	2.68	3.4	56.32	1.16	161	2.79	5.05	1.65	0.72	215.26	38.92	3926.29
	PB 8	1.11	1.81	1.67	5.14	0.66	67.81	0.8	3.2	0.15	0.59	159.41	2.69	2409.61
	PB 10	1.02	2.64	0.75	4.78	0.52	34.7	0.92	2.65	0.14	0.83	103	59.15	2313
	PB 11	3.69	1.73	46.67	19.44	0.69	279.69	5.94	8.7	0.17	0.51	187.11	91.47	3554.45
	PB 12	1.11	2.56	6.69	8.44	0.59	23.9	1.47	2.92	0.13	0.56	256.42	43.45	2426.91
	PB 15	1.46	2.13	2.11	2.33	0.52	2.84	0.32	1.91	0.12	0.75	86.56	0.66	3102.26
	PB 16	1.11	2.48	5.99	3.05	0.53	45.78	0.6	4.81	0.19	1.42	5.67	3.29	2636.96
	PB 18	1.33	2.76	0.66	5.63	0.49	23.22	1.96	2.33	0.11	1	13.964	43.9	nd
	AVERAGE	**1.6**	**2.3**	**7.8**	**12**	**0.63**	**74**	**1.8**	**3.7**	**0.3**	**0.8**	**127**	**32**	**2564**
PAD+D	PB 1	1.62	2.36	2.95	8.68	0.75	37.35	0.59	2.45	0.15	1.53	142.51	60.7	2448.95
	PB 3	1.75	2.01	3.57	9.57	9.62	70.16	2.68	3.42	0.38	0.69	223.57	62.05	2542.12
	PB 6	4.41	3.03	2.28	16.61	1.31	62.31	1.8	3.98	0.26	1	151.94	84.86	2496.37
	PB 9	1.54	2.32	5.59	9.06	0.64	42.83	2.22	4.66	0.24	1.05	270.48	12.2	4406.94
	PB 13	1.02	2.52	1.31	2.58	0.35	7.42	0.33	1.16	0.2	0.36	33.4	8.34	530.57
	PB 17	1.33	2.32	3.98	8.21	0.43	4.95	1.58	3.38	0.17	0.48	201.25	3.11	4100.64
	AVERAGE	**1.9**	**2.4**	**3.3**	**9.2**	**2.2**	**37**	**1.5**	**3.2**	**0.2**	**0.8**	**170**	**38**	**2754**
CONTROLS	PB 6	1.33	2.36	0.73	1.87	0.66	4.87	0.4	1.7	0.14	0.69	54.63	2.65	nd
	PB 15	1.41	2.48	2.08	11.51	0.67	8.78	1.43	2.05	0.37	1.02	89.38	1.96	nd
	PB 16	3.77	4.25	0.57	2.33	0.57	7.23	0.36	1.32	0.09	0.89	63.4	3.26	nd
	PB 17	1.33	2.95	0.97	2.46	0.64	9.55	0.26	1.97	0.14	0.74	81.26	3.75	nd
	PB 18	1.46	2.2	0.65	2.23	1.1	15.03	0.31	1.97	0.1	0.53	65.13	23.12	nd
	PB 20	1.58	3.11	0.61	3.64	0.86	7.82	0.28	1.59	0.38	2.04	43.89	6	nd
	PB 24	2.68	1.85	0.81	2.01	0.55	1.91	0.38	1.24	0.13	1.82	35.59	1.79	nd
	PB 25	1.46	2.6	1.4	3.07	0.5	28.77	0.65	1.61	0.18	0.59	71.05	13.11	nd
	PB 27	1.37	2.44	0.67	2.28	0.72	11.7	0.87	1.59	0.15	0.85	81.71	27.91	nd
	PB 28	2.72	1.93	0.58	1.82	0.64	3.75	0.62	1.61	0.1	0.85	19.06	4.27	nd
	PB 30	2.48	2.36	1.34	2.74	0.73	10.88	1.7	2.8	0.12	5.61	138.3	5.02	nd
	PB 31	1.5	2.72	0.71	3.75	0.57	14.78	0.56	1.97	0.19	0.55	91.49	23.03	nd
	PB 32	1.33	3.19	0.96	3.08	1.29	11.05	0.44	2.99	0.14	0.99	66	9.38	nd
	AVERAGE	**1.9**	**2.6**	**0.9**	**3.3**	**0.7**	**10**	**0.6**	**1.9**	**0.2**	**1.3**	**69**	**9.6**	**2320***

*(31)

Each value is expressed in pg/ml and the average of each cytokine is reported.

discriminated between patients and healthy subjects, whereas IFN-γ and EGF did not (VEGF p=0.028; TNF-α p=0.016; MCP-1 p=0.011). These results provide evidence of adaptive immune responses in patients affected by chronic arterial disease, in terms of increased production of inflammatory and arteriogenic cytokines in the blood. This may reveal a relationship of cytokine levels with the clinical manifestations of PAD, with or without the diabetes, although in a relatively small number of subjects. We also measured the levels of different cytokines in bone marrow blood (BM), collected at the moment of the transplantation procedure undergone by PAD patients and we found that the average levels of the cytokines were comparable, indicating a homogenous distribution of cytokines in the two compartments, i.e. peripheral blood and bone marrow (data not shown).

We examined for an association in circulating cytokines. We found that there was a strong correlation between VEGF and IFN-γ (r=0.59, p= 0.021) and between VEGF and TNF-α (r= 0.78, p= 0.001) in patients with PAD, with or w/o the diabetes, whereas VEGF did not correlate with the inflammatory marker MCP-1 (r= 0.38, p= 0.156) nor with levels of EGF (r=0.50, p= 0.058) (Fig. 2).

Increasing evidence suggests that cytokines act as signal transducing molecules into the cells and are involved in a variety of immunological, inflammatory and infectious diseases. Our results indicate that

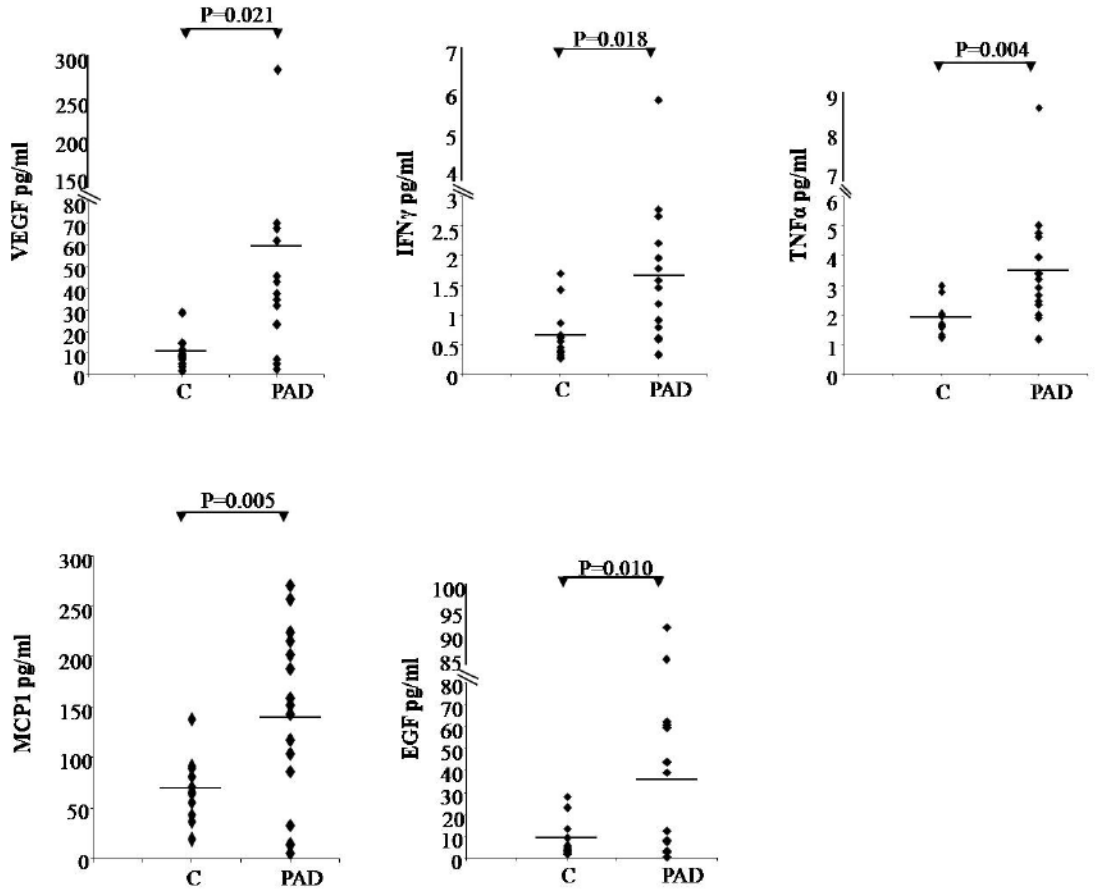

Fig. 1. *Scatter plots of the cytokines significantly increased (VEGF, IFN-γ, TNF-α, MCP-1 and EGF) in the bloodstream of peripheral arterial disease patients (PAD) and healthy controls (C). The average value of each concentration has been depicted in each scatter plot. The p value refers to a repeated ANOVA measures comparing patients and controls.*

in patients with vascular disease a significant up-regulation of different inflammatory (IFN-γ, MCP-1 and TNF-α) and arteriogenic cytokines (VEGF and EGF) is shown. Therefore, by using the cytokine array, we identified a set of cytokines present in patients suffering from severe vascular disease, which may be involved in the pathogenesis of the disease. Furthermore, the close correlation between VEGF, IFN-γ and TNF-α suggest at least a partially-shared, common trigger for production of these cytokines in vascular disease.

Effects of combination of cytokines on proliferation of HUVEC cells

A translational approach was then applied to investigate endothelial activation occurring in response to these cytokines. Endothelial cells were exposed to the different cytokines to evaluate changes in cell growth, migration and tube-like formation. In order to mimic ischemic conditions associated to the arterial disease and therefore present in the legs of our patients, we evaluated the combined effect of the hypoxia and the combination of cytokines (VEGF, IFN-γ, TNF-α, MCP-1 and EGF) on proliferation of HUVEC cells. Hypoxia is one of the most potent stimuli to restore adequate oxygen (O_2) delivery to ischemic tissues *in vivo* and represents a strong stimulus to increase proliferation of endothelial cells *in vitro* (10). To this end, we exposed cells to low O_2 (1%) and measured the HUVEC cell growth, in combination with the different cytokines found altered in our patients, both individually

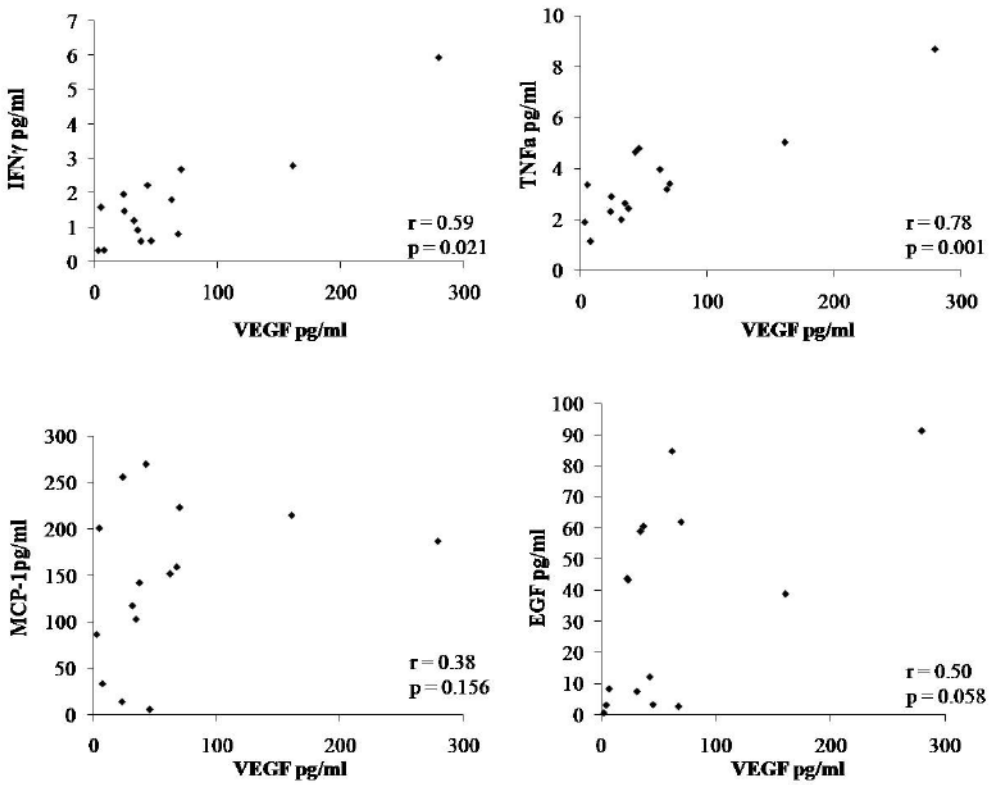

Fig. 2. *Correlations between VEGF and IFN-γ, TNF-α, MCP-1 and EGF in the total cohort of PAD patients (n=15) measured using the Spearman method. R coefficients and p values are reported.*

and collectively. We also measured the effect of hyperglycemic condition associated to hypoxia.

Cells were exposed to hypoxic conditions in presence of a single cytokine at the average concentration found in PAD patients. As depicted in Fig. 3a, the treatment of cells for 24 h with a single cytokine, at the average concentration found in PAD patients, did not reduce the proliferation compared to hypoxic condition alone. When HUVEC cells were exposed to the cocktail of all cytokines, their growth was significantly inhibited, suggesting that simultaneous presence of different cytokines affected negatively the proliferation of endothelial cells (Fig. 3a).

In addition, we evaluated the effect of the high glucose condition, mimicking the hyperglycemic environment present in diabetes. The exposure to high glucose (25 mM) affected endothelial cells proliferation under hypoxic condition (Fig. 3a).

Taken together, these results suggested that under low oxygen conditions (1%) the endothelial cells growth was not influenced by the exposure to a single cytokine. However, when combined, the cytokines negatively affected the growth.

We then evaluated whether the effects of the combination of cytokines can be rescued under optimal (10%) serum condition. As shown in Fig. 3b, the capability of HUVEC cells to proliferate was negatively affected also in the presence of serum (p value ≤ 0.05), whereas the hyperglycemic condition did not have a detrimental effect when used alone, but a negative addictive effect was observed when

a

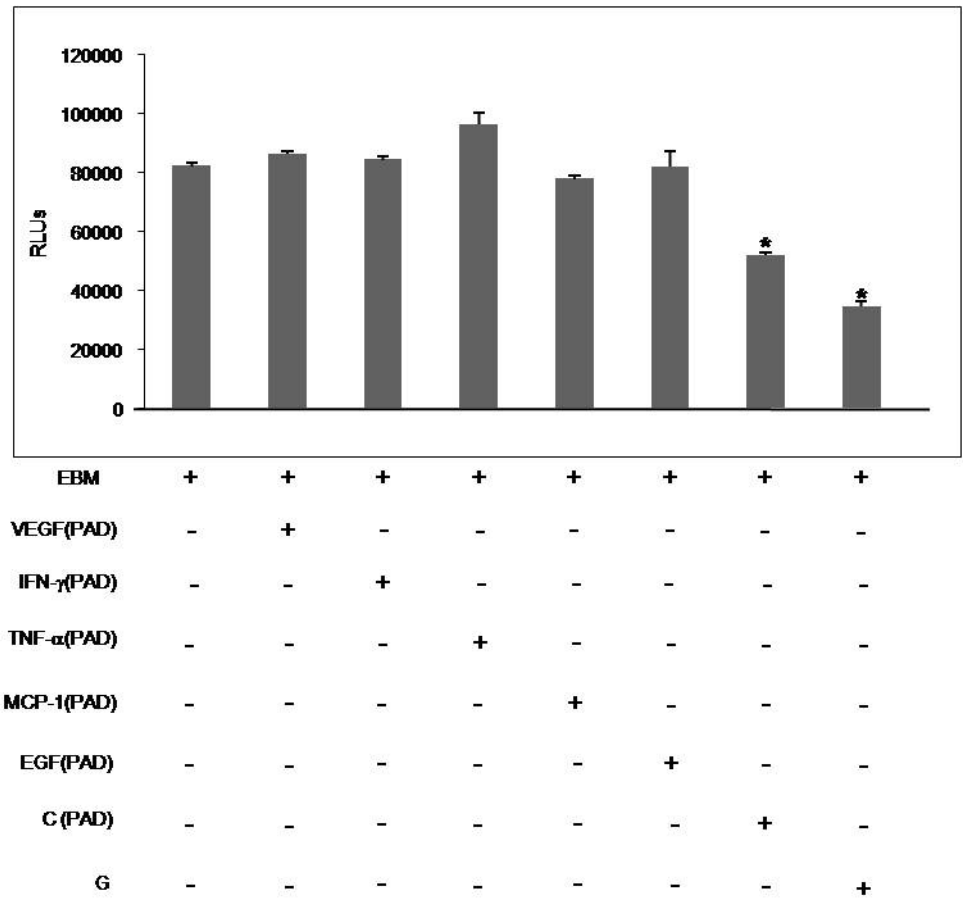

b

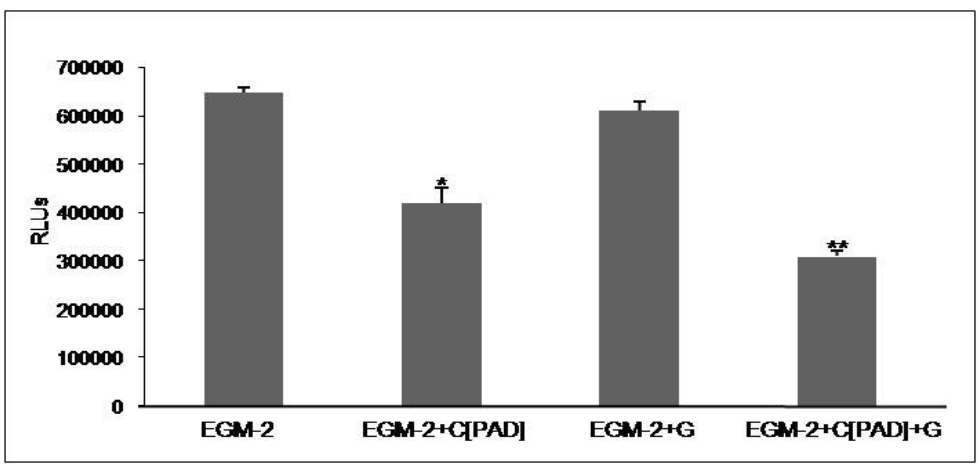

Fig. 3. ***a)*** *Proliferation of HUVEC cells. Cells were incubated in serum-free medium for 24 h in hypoxic conditions in the presence of different cytokines, both individually and collectively, used at the average concentration found in PAD patients (C PAD) and under hyperglycemic conditions (G).* ***b)*** *Cells were incubated in 10% serum for 24 h in hypoxic conditions in the presence of the cocktail of different cytokines (C PAD) and under hyperglycemic conditions (G), alone or in combination with cytokines. Each histogram indicates the RLUs related to cell growth measured under hypoxic conditions. Error bars represent SD of n = 3. * denotes statistical differences when p ≤ 0.05 compared to control and ** when p ≤0.01 compared to control.*

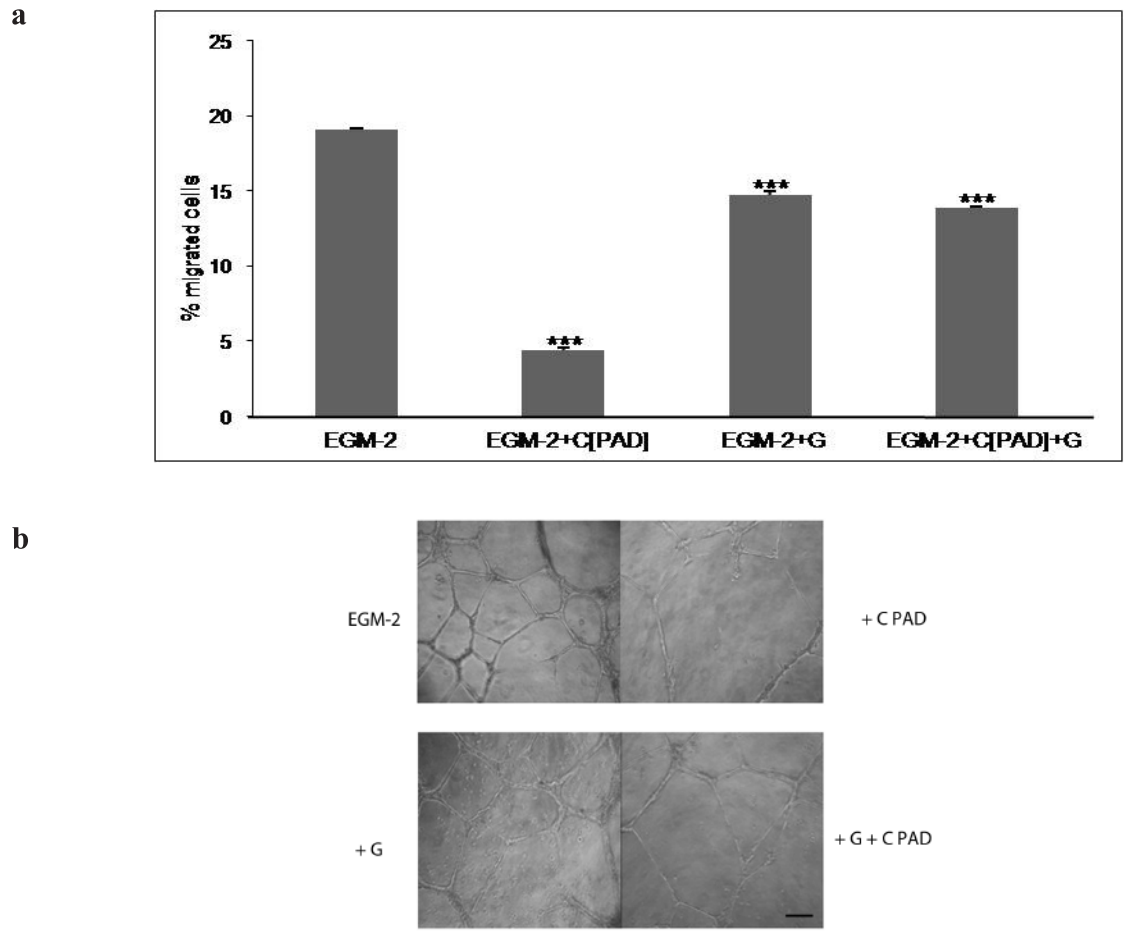

Fig. 4. ***a****) HUVEC cell migration assay. Cells were placed in presence of serum (EGM-2) under hypoxic conditions using cytokines collectively at the average concentration found in PAD patients (C PAD) and under hyperglycemic conditions (G), alone or in combination with cytokines. Statistical differences were denoted by *** when p ≤ 0.0001 compared to control.* ***b****) Tube formation of HUVEC cells in hypoxic conditions in presence of proangiogenic culture medium (EGM-2), in response to cytokines used collectively at the average concentration found in PAD patients (C PAD) and under hyperglycemic conditions (G), alone or in combination with cytokines. Magnification 10X. Scale bar 100 µm.*

combined with the cocktail of all cytokines.

Taken together, our findings indicate that cytokines exert a marked synergistic effect on endothelial proliferation.

Effects of combination of cytokines on migration of HUVEC cells

Endothelial cell migration is a prerequisite for angiogenesis, which involves the formation of new blood vessels. The angiogenic and migratory properties of endothelial cells are coordinated by a range of factors, receptors, cell-adhesion molecules, inflammatory cytokines and chemokines (11).

We then evaluated the effect of cytokines on migratory capacity of endothelial cells under optimal (10%) serum condition, since the starvation abolished the migratory ability (data not shown). When cells were exposed to the cytokines at average concentration found in our patients, the migration capability of endothelial cells was significantly repressed under hypoxic conditions (Fig. 4a).

When incubated with 25 mM glucose, the migration ability of HUVEC cells was slightly reduced compared to EGM-2. Of note, the presence

of high glucose condition in combination with cytokines at concentration found in PAD patients inhibited the migration of HUVEC cells (Fig. 4a), suggesting that inflammatory and arteriogenic cytokines have an inhibitory effect on endothelial cell proliferation and migration, when used in combination.

Effects of combination of cytokines on tubule formation

The final event during angiogenesis is the organisation of endothelial cells in a three-dimensional network of tubes. We then investigated whether the presence of cytokines in hypoxic environment can influence the formation of vessel-like structures.

When seeded into extracellular matrix composites in the presence of proangiogenic growth factors, HUVEC cells were able to form three-dimensional networks of vessel-like structures (Fig. 4b), suggesting that these cells had an intrinsic capacity to form tubule-like structures. The addition of cytokines at average concentration found in our patients under hypoxia led to a less organised tubule formation, suggesting that also the network formation *in vitro* is influenced by the combination of these cytokines. A less severe phenotype was observed when cells were exposed to hyperglycemia, corroborating the idea that the hyperglycemia alone allowed the endothelial cells to form vessel-like structures, although the association with cytokines had an inhibitory effect.

These observations may be particularly relevant to PAD pathogenesis, as it may indicate that tissue ischemia *per se* is sufficient to promote proliferation and migration of endothelial cells for recovery of ischemia through angiogenesis (12). However, the circulating cytokines lead to the inability of endothelial cells to proliferate, migrate and form tubule-like structures in ischemic conditions, suggesting that: I) chronic condition led to an abnormal production of cytokines; II) the pharmacological modulation of these circulating factors can help the development of new therapeutic strategies to induce neoangiogenesis processes.

DISCUSSION

Vascular disease is a prerequisite for many human diseases and is associated with generalised endothelial dysfunction. Several mechanisms have been described to explain impaired endothelial activation and seem to be linked to tissue inflammation. Inflammation plays a central role in atherosclerotic lesion development and progression, accompanied by other vascular incidents (8).

Accumulating data suggested that vascular repair mechanisms are important to maintain normal homeostasis of the arterial wall and to prevent development of pathologic processes, such as atherosclerosis. Therefore, defective repair of endothelial injury seems to be altered in vascular disorders.

Components of the immune system, namely, altered levels of specific cytokines and chemokines, participate in the pathogenesis of type 2 diabetes. Chronic hyperglycemia, together with enhanced inflammatory markers, seems to impair insulin secretion and induces b-cells death (9). According to this study, the onset of arterial diseases and its progression are largely determined by the progressive failure of endothelial cells to restore blood flow determined by chronic inflammation.

To understand the biochemical and cellular mechanisms that account for reduced or impaired vascular cell function, in patients suffering from severe vascular disease, with and without the diabetes, we investigated the role played by circulating cytokines on endothelial cells. In this study, for the first time, a positive correlation was observed between circulating cytokines present in PAD patients' serum and impaired endothelial functions.

We found high concentrations of inflammatory (IFN-γ, TNF-α and MCP-1) and arteriogenic cytokines (VEGF and EGF). Vascular endothelial growth factor (VEGF) is one of the most important inducers of angiogenesis (13). Nevertheless, VEGF is also the major pathogenic factor for diabetic retinopathy (DR) and represent the major therapeutic target. In fact, VEGF plays an essential and causative role in retinal inflammation, vascular lesions, and vascular leakage in DR (14).

Epidermal growth factor (EGF) plays an important role in the regulation of cell growth, proliferation, and differentiation in many cell types, by binding to its receptor EGFR. Recently, it has

been demonstrated that this factor is essential for endothelial progenitor cells (EPCs), at least *in vitro* with VEGF, to preserve the endothelial function (15).

Tumour necrosis factor-alpha (TNF-α) is a pleiotropic inflammatory cytokine, which serves a variety of functions, many of which are not yet fully understood. The cytokine possesses both growth stimulating properties and growth inhibitory processes, and it appears also to have self-regulatory properties (16). Lastly, it acts as a key player in the local inflammatory immune response, initiating a cascade of cytokines to increase vascular permeability, recruiting macrophages and neutrophils to a site of infection (17).

Monocyte chemotactic protein-1 (MCP-1), member of the small inducible gene (SIG) family, plays a role in the recruitment of monocytes to sites of injury and infection (18) across endo- and epithelial barriers, both *in vitro* and *in vivo*. The contribution of endothelial MCP-1 signaling via its CCR2 receptor results in monocyte adhesion to inflamed endothelium (19).

IFN-γ, or type II interferon, has important immunoregulatory functions along with its antiviral activity. It is a potent activator of macrophages, it has anti-proliferative effects on transformed cells and it can potentiate the antiviral and antitumoral effects of the type I interferon (20).

It has already been demonstrated that circulating levels of VEGF are increased in patients with PAD (21-24). In addition, we found a strong correlation between circulating VEGF and TNF-α levels in patients with PAD or PAD+D, as well as VEGF and IFN-γ. These findings are consistent with a recent study (25) that identifies TNF-α as an immediate proangiogenic gene in macrophages in response to the injury process. Up-regulated expression of TNF-α precedes VEGF expression in isolated rat aortic macrophages. On the other hand, overexpresssion of TNF-α is required for optimal VEGF production and angiogenesis. TNF-α has been shown to stimulate VEGF production by isolated cells (26), but there is a gap in understanding how this cytokine regulates the angiogenic response to injury in complex multicellular network.

Recently, in mouse models of psoriasis and retinopathy, simultaneous blocking of VEGF and TNF-α was obtained using a chimeric decoy receptor resulting in effective therapeutic strategy (27). Considering this information, this approach can be an effective therapeutic strategy for treatment of PAD.

A promising therapeutic option for patients with peripheral arterial disease (PAD) is based on cell-based therapy through autologous bone marrow transplantation (28-29). The efficacy of bone marrow transplantation to augment neoangiogenesis seems to involve multiple mechanisms. All of them may actively contribute to the angiogenic process, either by engrafting endothelial progenitor cells within the vessel wall and by providing soluble factors, which promote the recruitment, proliferation and differentiation of progenitor endothelial cells, as well as reducing inflammation. In fact, a growing body of evidence suggests that the multi-potential stem cells present in bone marrow possess immunomodulatory and reparative properties (30). Therefore, bone marrow transplantation can down-regulate many inflammatory effectors, making the engraftment or the activation of progenitor endothelial cells easier.

Our study has a limitation in the number of patients recruited with the result of an insufficient statistical power to reach definite conclusions. Additional randomized trials are required to determine whether the "paracrine hypothesis" is efficient in the modulation of reparative processes.

However, our data may offer a new physiopathological hypothesis for endothelial dysfunction in patients with vascular disease and the pharmacological modulation of these factors can help to develop new therapeutic strategies to improve regenerative processes.

ACKNOWLEDGEMENTS

The authors want to thank Fondazione Banco Napoli, Ministero della Università e Ricerca (PRIN), Fondazione Luigi Califano for funding the study. In addition, we are grateful to Dr Paola Mantovano, Dr Stefano Lillo and Dr Andrea Silvestroni for assistance.

REFERENCES

1. Olin JW, Sealove BA. Peripheral artery disease: current insight into the disease and its diagnosis and

management. Mayo Clin Proc 2010; 85(7):678-92.
2. Norgren L, Hiatt WR, Dormandy JA, Nehler MR, Harris KA, Fowkes FG, Rutherford RB; TASC II Working Group. Inter-society consensus for the management of peripheral arterial disease. Int Angiol 2007; 26:81-157.
3. Criqui MH, Fronek A, Barrett-Connor E, Klauber MR, Gabriel S, Goodman D. The prevalence of peripheral arterial disease in a defined population. Circulation 1985; 71(3):510-15.
4. Selvin E, Hirsch AT. Contemporary risk factor control and walking dysfunction in individuals with peripheral arterial disease: NHANES 1999-2004. Atherosclerosis 2008; 201(2):425-33.
5. MacGregor AS, Price JF, Hau CM, Lee AJ, Carson MN, Fowkes FG. Role of systolic blood pressure and plasma triglycerides in diabetic peripheral arterial disease: The Edinburgh Artery Study. Diabetes Care 1999; 22(3):453-8.
6. Lambiase PD, Edwards RJ, Anthopoulos P, Rahman S, Meng YG, Bucknall CA, Redwood SR, Pearson JD, Marber MS. Circulating humoral factors and endothelial progenitor cells in patients with differing coronary collateral support. Circulation 2004; 109:2993-9.
7. Fadini GP, Miorin M, Facco M, et al. Circulating endothelial progenitor cells are reduced in peripheral vascular complications of type 2 diabetes mellitus. J Am Coll Cardiol 2005; 45(9):1449-57.
8. Pate M, Damarla V, Chi DS, Negi S, Krishnaswamy G. Endothelial cell biology: role in the inflammatory response. Adv Clin Chem 2010; 52:109-30.
9. Donath MY, Shoelson SE. Type 2 diabetes as an inflammatory disease. Nat Rev Immunol 2011; 11(2):98-107.
10. Isner JM. Tissue responses to ischemia: local and remote responses for preserving perfusion of ischemic muscle. J Clin Invest 2000; 106(5):615-9.
11. Lamalice L, Le Boeuf F, Huot JL. Endothelial cell migration during angiogenesis. Circ Res 2007; 100(6):782-94.
12. Cobellis G, Silvestroni A, Lillo S, et al. Long-term effects of repeated autologous transplantation of bone marrow cells in patients affected by peripheral arterial disease. Bone Marrow Transplant 2008; 42(10):667-72.
13. Grunstein J, Roberts WG, Mathieu-Costello O, Hanahan D, Johnson RS. Tumor-derived expression of vascular endothelial growth factor is a critical factor in tumor expansion and vascular function. Cancer Res 1999; 59(7):1592-8.
14. Jeganathan VS. Anti-angiogenesis drugs in diabetic retinopathy. Curr Pharm Biotechnol 2011; 12(3):369-72.
15. Bouchentouf M, Forner K, Cuerquis J, et al. A novel and simplified method of culture of human blood derived early endothelial progenitor cells for the treatment of ischemic vascular disease. Cell Transplant 2011; 20(9):1431-43.
16. Ferguson LR, Huebner C, Petermann I, Gearry RB, Barclay ML, Demmers P, McCulloch A, Han DY. Single nucleotide polymorphism in the tumor necrosis factor-alpha gene affects inflammatory bowel diseases risk. World J Gastroenterol 2008; 14(29):4652-61.
17. Wajant H, Pfizenmaier K, Scheurich P. Tumor necrosis factor signalling. Cell Death Differ 2003; 10(1):45-65.
18. Codullo V, Baldwin HM, Singh MD, et al. An investigation of the inflammatory cytokine and chemokine network in systemic sclerosis. Ann Rheum Dis 2011; 70(6):1115-21.
19. Maus U, Henning S, Wenschuh H, Mayer K, Seeger W, Lohmeyer J. Role of endothelial MCP-1 in monocyte adhesion to inflamed human endothelium under physiological flow. Am J Physiol Heart Circ Physiol 2002; 283(6):2584-91.
20. Schoenborn JR, Wilson CB. Regulation of Interferon-γ during innate and adaptive immune responses. Adv Immunol 2007; 96:41-101.
21. Roller RE, Renner W, Dorr A, Pilger E, Schnedl WJ. Oxidative stress and increase of vascular endothelial growth factor in plasma of patients with peripheral arterial occlusive disease. Thromb Haemost 2001; 85(2):368.
22. Blann AD, Belgore FM, McCollum CN, Silverman S, Lip PL, Lip GY. Vascular endothelial growth factor and its receptor, Flt-1, in the plasma of patients with coronary or peripheral atherosclerosis, or Type II diabetes. Clin Sci 2002; 102(2):187-94.

23. Sandri M, Beck EB, Adams V, et al. Maximal exercise, limb ischemia, and endothelial progenitor cells. Eur J Cardiovasc Prev Rehabil 2011; 18(1):55-64.
24. Wu FT, Stefanini MO, Mac Gabhann F, Kontos CD, Annex BH, Popel AS. VEGF and soluble VEGF receptor-1 (sFlt-1) distributions in peripheral arterial disease: an in silico model. Am J Physiol Heart Circ Physiol 2010; 298(6):2174-91.
25. Ligresti G, Aplin AC, Zorzi P, Morishita A, Nicosia RF. Macrophage-derived tumor necrosis factor-alpha is an early component of the molecular cascade leading to angiogenesis in response to aortic injury. Arterioscler Thromb Vasc Biol 2011; 31(5):1151-9.
26. Alagappan VK, McKay S, Widyastuti A, Garrelds IM, Bogers AJ, Hoogsteden HC, Hirst SJ, Sharma HS. Proinflammatory cytokines upregulate mRNA expression and secretion of vascular endothelial growth factor in cultured human airway smooth muscle cells. Cell Biochem Biophys 2005; 43(1):119-29.
27. Jung K, Lee D, Lim HS, Lee SI, Kim YJ, Lee GM, Kim SC, Koh GY. Double anti-angiogenic and anti-inflammatory protein Valpha targeting VEGF-A and TNF-alpha in retinopathy and psoriasis. J Biol Chem 2011; 286(16):14410-8.
28. Menasché P. Cell therapy for peripheral arterial disease. Curr Opin Mol Ther 2010; 12(5):538-45.
29. Lawall H, Bramlage P, Amann B. Treatment of peripheral arterial disease using stem and progenitor cell therapy. J Vasc Surg 2011; 53(2):445-53.
30. English K, French A, Wood KJ. Mesenchymal stromal cells: facilitators of successful transplantation? Cell Stem Cell 2010; 7(4):431-42.
31. Kodama K, Nishigami K, Sakamoto T, Sawamura T, Hirayama T, Misumi H, Nakao K. Tight heart rate control reduces secondary adverse events in patients with type B acute aortic dissection. Circulation 2008; 118(14):167-70.

CONCOMITANT EVALUATION OF FLOW-MEDIATED VASODILATION AND EPICARDIAL FAT THICKNESS IN IDIOPATHIC DEEP VENOUS THROMBOSIS

G. MAZZOCCOLI[1], M.P. DAGOSTINO[1], A. FONTANA[2], M. COPETTI[2], F. PELLEGRINI[2,3], M. GRILLI[1] and A. GRECO[4]

[1]Department of Medical Sciences, Division of Internal Medicine, IRCCS Scientific Institute and Regional General Hospital "Casa Sollievo della Sofferenza" San Giovanni Rotondo, Italy; [2]Unit of Biostatistics, Scientific Institute and Regional General Hospital "Casa Sollievo della Sofferenza", S.Giovanni Rotondo, Italy; [3]Department of Clinical Pharmacology and Epidemiology, Consorzio Mario Negri Sud, Chieti, Italy; [4]Unit of Geriatrics, Scientific Institute and Regional General Hospital "Casa Sollievo della Sofferenza", S.Giovanni Rotondo, Italy

Received July 7, 2011 – Accepted December 12, 2011

Flow mediated vasodilation (FMD) evaluates the endothelium-dependent vasodilation, is a reliable marker of arterial endothelial dysfunction and is related to coronary artery disease. Visceral fat predicts an unfavorable cardiovascular and metabolic risk profile in humans and echocardiographic assessment of epicardial fat (EF) is a reliable marker of visceral adiposity. We measured the FMD and EF thickness in 77 subjects, 38 without idiopathic deep vein thrombosis (DVT) (mean age 65.95±16.29 years) and 39 with idiopathic DVT (mean age 65.49±17.22 years). The purpose of this work is to investigate the presence of statistical association between FMD and DVT and between EF thickness and DVT. Furthermore, to account for possible atherosclerosis risk factor unbalances, comparison between FMD and DVT (and between EF and DVT) was assessed using a multivariate logistic regression model which included the following covariates: FMD, EF, age, sex, smoking and the presence of obesity. Subjects without DVT showed significant lower values of EF thickness (9.07±1.89 mm *vs* 12.32±1.73 mm, p=0.005) and borderline-significant greater values of FMD (9.01±2.77% *vs* 7.47±5.37%, p=0.058) as compared to those with DVT. In conclusion, the data presented indicate that subjects affected by spontaneous deep vein thrombosis may have an impaired endothelium-dependent vasodilation, a marker of arterial endothelial dysfunction related to coronary artery disease, and an increased epicardial adipose tissue, a marker of cardiometabolic risk.

Atherosclerosis and venous thrombosis have been found associated in recent epidemiological studies, and venous thromboembolism is related to indicators of atherosclerosis and/or arterial thromboembolic events and may be considered as a long-term risk factor for arterial cardiovascular events (1-6). A linking alteration may be represented by impaired endothelial function (7). Endothelial dysfunction results from functional changes characterized by vasospasm, coagulation abnormalities and increased vascular proliferation and has been reported to be the initial step in atherosclerosis (8). Peripheral endothelial function can be non-invasively evaluated by the measurement of the flow-mediated dilation

Key words: endothelial dysfunction, venous thrombosis, atherosclerosis, flow-mediated dilation, epicardial fat thickness

Mailing address: Gianluigi Mazzoccoli, MD,
Unit of Internal Medicine,
Department of Medical Sciences,
Scientific Institute and Regional General Hospital
"Casa Sollievo della Sofferenza" San Giovanni Rotondo, Italy
Tel: +39 0882 835228; Fax: +39 0882 410563
e-mail: g.mazzoccoli@operapadrepio.it

0393-974X (2012)

DISCLOSURE: ALL AUTHORS REPORT NO CONFLICTS OF INTEREST RELEVANT TO THIS ARTICLE.

(FMD) of the brachial artery by using high-resolution ultrasound methods (9, 10).

Increased visceral adipose tissue, the fat that surrounds the internal organs (e.g., heart, intestines) in the cavities of the body, predicts an unfavorable cardiovascular and metabolic risk profile and is strongly correlated with atherogenic and diabetogenic features and with increased levels of prothrombotic factors and proinflammatory cytokines (11-13). The direct measurement of epicardial fat (EF) thickness via transthoracic echocardiography is considered an affordable and reliable marker for visceral adiposity and is strongly correlated to the results obtained with whole body magnetic resonance imaging scan (14, 15).

In this study we have evaluated the FMD and EF thickness in subjects with and without idiopathic deep venous thrombosis (DVT).

MATERIALS AND METHODS

Subjects

The study was approved by the local Scientific and EthicasCommittee and was conducted on consecutive subjects hospitalized in the Department of Internal Medicine. We enrolled 77 inpatients, 38 without DVT and 39 with idiopathic DVT. Subjects gave written informed consent and the investigation conformed to the principles outlined in the Declaration of Helsinki. Exclusion criteria included pregnancy, cancer, concomitant infection, leg trauma or bone fracture, cast therapy, surgical procedures in the last 90 days, condition of being chronically ill, bedridden or non-ambulatory and treatment with prothrombotic agents (steroids, estrogens). Subjects were chosen to obtain two matched groups, homogeneous in respect to the common risk factors for atherosclerosis (age, male gender, obesity, current cigarette smoking, dyslipidemia, diabetes mellitus, arterial hypertension), in respect to cardiovascular diseases (stable and unstable angina, myocardial infarction, cerebrovascular accident such as non-hemorrhagic stroke, peripheral vascular disease) and in respect to medication history (use of statins, anti-hypertensive agents, anti-platelet drugs) and biochemical parameters (total, LDL and HDL cholesterol, triglycerides, plasma glucose and erythrocyte sedimentation rate, ESR). Heparin was administered to the subjects with venous thrombosis after ultrasonographic evaluations in the form of low-molecular-weight heparin (enoxaparin, at a dosage of 1mg/kg twice a day).

Biochemical parameters

In all enrolled subjects, a venous blood sample was drawn after an overnight fast for the determination of plasma glucose, lipid parameters (total and HDL cholesterol, triglycerides) and erythrocyte sedimentation rate (ESR). Plasma glucose, lipids and ESR were measured by standard methods. The common risk factors for atherosclerosis (age, gender, obesity, smoking, dyslipidemia, diabetes mellitus, arterial hypertension) were considered and reported.

The screening for mutations and conditions associated with thrombophilia (antithrombin III, protein C or protein S deficiency, factor V Leiden, prothrombin G20210A mutation, hyperhomocysteinemia and lupus-like anticoagulants) was carried out on all the subjects and the subjects with alterations of these factors were excluded from the study.

Weight in kilograms (to the nearest 0.1 kg) and standing height in centimeters (to the nearest 0.5 cm) were measured at the clinical examination by standard protocols. Level of overweight was measured by body mass index (BMI, calculated as body weight divided by height squared). We asked questions on the number of cigarettes smoked per day and duration of smoking to provide the foundation for the definitions of smoking status and pack-years of smoking. Blood pressure was measured in both study groups using the same protocol. Three measurements were taken with a random-zero sphygmomanometer, and the mean of the last 2 of 3 measurements was used. Hypertension was defined as systolic blood pressure of 140 mm Hg or higher, or diastolic blood pressure of 90 mmHg or higher, or current treatment with blood pressure medications.

Plasma glucose was determined by the glucose oxidase method. Diabetes mellitus was defined at baseline as fasting glucose levels of 126mg/dL (7mmol/L) or higher, non-fasting glucose levels of 200 mg/dL (11.1mmol/L) or higher, or a history of or treatment for diabetes. Impaired fasting glucose level was defined as 110mg/dL (6.1mmol/L) or higher but lower than 126mg/dL (7mmol/L). Plasma total cholesterol (milligrams per deciliter) and triglyceride levels (milligrams per deciliter) were measured by enzymatic methods and low-density lipoprotein (LDL) cholesterol (milligrams per deciliter) was calculated indirectly using the Friedewald equation. High-density lipoprotein (HDL) cholesterol was measured

after precipitation of the other lipoprotein fractions by dextran sulfate. A total cholesterol level > 200mg/dl, a low-density lipoprotein (LDL) cholesterol level > 100mg/dl, a high-density lipoprotein (HDL) cholesterol level < 40mg/dl for male subjects or < 50mg/dl for female subjects and a triglyceride level ≥ 150mg/dl were considered for definition of dyslipidemia.

No statistically significant difference was found between the groups for plasma glucose, total, LDL and HDL cholesterol, triglycerides and ESR.

Echo-Doppler study

The presence of DVT was established by using CUS of lower limb veins, that combines real-time imaging of the deep veins with venous compression. Lower extremity venous imaging was performed with the subject supine and the head elevated (10-20 degrees), the leg positioned with the knee slightly elevated and the hips slightly rotated externally. DVT was classified as definite or absent. Definite DVT was defined by a positive duplex ultrasound finding. A clinical diagnosis in the absence of objective tests was not considered to be a DVT.

The ultrasonographic evaluations of the endothelial function and the flow-mediated endothelial dependent vasodilatation was effectuated by Flow-Mediated Dilatation (FMD) measurement in the brachial artery of the non-dominant arm. The validity of the method has been confirmed in previous studies (16, 17). The diameter of the brachial artery was measured by an expert sonographer on ultrasound images obtained in B-mode with a high resolution 5–10MHz multi-frequency linear probe connected to an ESAOTE Technos-MPX (Esaote, Genova, Italy). All the subjects had refrained from smoking, drinking alcohol or coffee or taking anti-oxidative agents for at least 12 hours. Subjects were examined in the morning (between 9 and 11 a.m.) and after 10 min of rest in a supine position in a quiet, temperature controlled room (21°C to 23°C) the brachial artery was explored at the antecubital fossa level on a longitudinal plane, optimizing the depth and the acoustic window pre-sets and keeping them in the same position during the study, by using a mechanical probe-holder arm. After the basal measurement of the diameter and of the speed of the brachial artery flow, a sphygmomanometer cuff was inflated around the forearm at a pressure of 50 mmHg higher than the basal systolic pressure and deflated after five minutes. The measurement of the vessel diameter and the speed of the flow were taken before and after the deflation every 30 seconds for 3 minutes, registered in telediastole, coinciding with R wave of the ECG, which was continuously monitored. The variations of the diameter during the reactive hyperemia were expressed as percentage increase of the diameter compared to the basal value. The measurement was registered at the media-adventitia interface of anterior (near) and posterior (far) vessel walls. For each scanning the diameters were measured in four heart cycles and the average was calculated by dividing the difference between the maximum diameter and the basal one by the maximum diameter. The intraobserver variability for the repeated measurements of resting arterial diameter was 0.021±0.005%. When this study was performed on 2 separate days on 16 subjects, the within-subject difference for the measurement of the percent increase in the arterial diameter during reactive hyperemia was 1.3±0.5%.

Echocardiographic study

Each subject underwent transthoracic two-dimensional (2D) guided M-mode echocardiogram performed with an Esaote MyLab TM Gold Cardiovascular instrument (Esaote, Genova, Italy) by standard techniques with subjects in the left lateral decubitus position. Echocardiograms were recorded on videotape. The echocardiographic study required the recording of 10 or more cycles of 2D parasternal long- and short-axis views and 10 or more cycles of M-mode with optimal cursor beam orientation in each view. Echocardiograms were performed by the same expert sonographer who was blinded to the subjects' clinical data and anthropometric features. The ultrasonographic evaluations were carried out on enrollment. When the measurements were performed on 2 separate days on 10 subjects, the within-subject difference for the measurement of the EF was 1.4±0.7%, indicating good reproducibility of the echocardiographic measurements. We measured epicardial fat thickness on the free wall of right ventricle from both parasternal long- and short-axis views. We used imaging constraints to make sure that the epicardial fat thickness was not measured obliquely. Measurements on M-mode strips obtained from both 2D views with longitudinal cursor beam orientation in each view were also performed. The maximum values at any site were measured, and the average value was considered.

Statistical analysis

Subjects' baseline characteristics were reported as mean ± standard deviation (SD) or frequencies and

percentages for continuous and categorical variables, respectively (Table I). Normal distribution of continuous variables was verified using Shapiro-Wilk normality test. Comparisons of baseline characteristics between subjects with DVT and subjects without DVT were made using the *Chi*-square test for categorical variables and the Student's two-sample *t*-test for continuous variables. The linear correlation between two variables was assessed by Pearson correlation coefficient. Adjusted comparisons between EF and FMD in subjects with DVT and subjects without DVT were assessed by a multivariate logistic regression model. A parsimonious set of variables, other than EF and FMD, were chosen to assess the multivariate logistic regression model, with the use of stepwise selection (retention threshold $p<0.10$).

P-values <0.05 were considered for statistical significance. All analyses were performed using SAS Release 9.1 (SAS Institute, Cary, NC, USA).

RESULTS

The final study population included 77 subjects, 38 without idiopathic DVT (mean age 65.95±16.29 years) and 39 with idiopathic DVT (mean age 65.49±17.22 years). The main anthropometric and baseline clinical characteristics of the subjects studied are reported in Table I. Group sample sizes of 38 and 39 achieved 94% power to detect a large Cohen effect size of 0.8 with a significance level (alpha) of 0.05, using a two-sided two-sample *t*-test. Subjects without DVT showed significantly lower values of EF thickness (9.07±1.89 mm *vs* 12.32±1.73 mm, $p<0.001$) and non-significant greater values of FMD (9.01±2.77% *vs* 7.47±5.37%, p= 0.129) than those with DVT. Furthermore, the number of smokers were significatively greater in patients without DVT than those with DVT (37.8% *vs* 12.8%, p=0.012). Comparison between FMD and DVT (and between EF and DVT) was further adjusted by: age, sex, smoking and the presence of obesity. Therefore, the adjusted association between the EF and the presence of DVT still remained statistically significant (p=0.005) whereas the adjusted association between the FMD and the presence of DVT became more pronounced, although not statistically significant (p=0.058). Box plots of FMD and EF in subjects with and without DVT are shown in Fig. 2 along with adjusted p-values derived from multivariate logistic regression model.

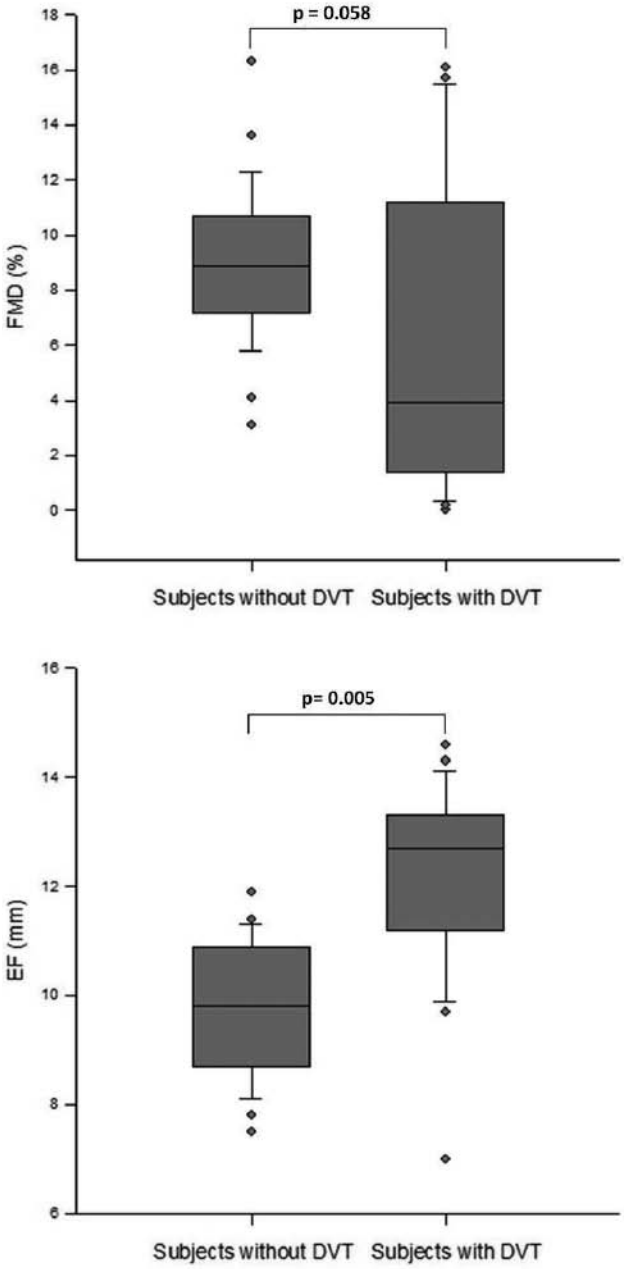

Fig. 1. *Box plots of flow mediated vasodilation (FMD) and epicardial fat thickness (EF) in subjects with and without idiopathic deep venous thrombosis (DVT). Adjusted p-values from multivariate logistic regression model were reported.*

No significant correlation was found between continuous EF and FMD in the whole sample (r=-0.07, p=0.564), in patients without DVT (r=-

Table I. *Subjects' baseline characteristics reported as mean ± standard deviation (SD)*

Variable	Without DVT	With DVT	p-value
Number of subjects nr(%)	38	39	-
Age (years)	65.95±16.29	65.49±17.22	0.905
Male gender nr(%)	23 (62.16)	21 (53.85)	0.463
Obesity nr(%)	9 (23.68)	14 (35.90)	0.242
Smoke nr(%)	14 (37.84)	5 (12.82)	0.012
Dyslipidemia nr(%)	10 (27.03)	13 (33.33)	0.550
Diabetes mellitus nr(%)	4 (10.81)	6 (15.38)	0.555
Arterial hypertension nr(%)	16 (43.24)	19 (48.72)	0.632
Cardiovascular events nr (%)	4 (10.81)	1 (2.56)	0.147
Statins nr(%)	10 (27.03)	8 (20.51)	0.504
Anti-platelet drugs nr(%)	14 (37.84)	12 (30.77)	0.516
Flow mediated dilation (%)	9.01±2.77	7.47±5.37	0.129
Epicardial fat thickness (mm)	9.07±1.89	12.32±1.73	<0.001

***DVT**: Deep Venous Thrombosis*

0.15, p=0.420) and in patients with DVT (r=0.109, p=0.509).

DISCUSSION

A high proportion of subjects with venous thrombosis demonstrate preclinical atherosclerotic changes and higher risk of subsequent development of atherosclerotic disease (18-22). An early alteration in the course of arteriosclerotic disease is represented by endothelial dysfunction. Endothelium maintains blood fluidity through its ability to express anticoagulant and vasodilatory molecules in health conditions. Inflammation, infection and trauma alter the endothelial function and transform the endothelium into a prothrombotic and proinflammatory surface, favouring platelet and leukocyte deposition, followed by blood clotting activation, expression of adhesive molecules, procoagulant activities and mitogenic factors, leading to the development of thrombosis, smooth muscle cell migration/proliferation and atherosclerosis (23-25). FMD measurement in the brachial artery is a reliable method to evaluate endothelial function and its impairment is related to coronary sclerosis and is considered predictive of cardiovascular events (26-29).

Another marker of cardiovascular and metabolic risk is represented by EF thickness. Epicardial adipose tissue may act as a local energy supply for the myocardium or buffer against toxic levels of free fatty acids and is a very active endocrine organ, expressing various inflammatory factors and hormones, such as IL-1β, IL-6, monocyte chemotactic protein-1 (MCP-1), TNF-alpha, visfatin, leptin. EF may have an effect on local coronary artery health secreting adiponectin, a serum

protein with anti-inflammatory and anti-atherogenic properties, but its secretion is markedly decreased in subjects with coronary artery disease. (30). The aim of this study is to investigate whether two markers of cardiovascular risk (i.e. the endothelium dependent vasodilatation and the epicardial adipose tissue), are associated by idiopathic deep vein thrombosis. Endothelial dysfunction and epicardial adipose tissue contribute to risk assessment, but maybe with different specificities, reflecting respectively the risk associated to peripheral vascular disease, coronary artery disease and metabolic derangement (38-40). The data obtained show that subjects with DVT have a statistically significant decrease of FMD, indicating a severe impairment of endothelium dependent vasodilation and consequently a severe endothelial dysfunction. On the other hand, our subjects with DVT have a statistically significant increase of epicardial adipose tissue thickness, a recognized marker of cardiometabolic risk. Previous scientific papers reported that FMD decreases in subjects with deep vein thrombosis (31). Our data confirm this evidence, and in addition suggest that transthoracic echocardiographic assessment of the epicardial adipose mass, reflecting intra-abdominal visceral fat, may serve as a valuable marker of visceral adiposity and consequently of cardiometabolic risk, probably more reliable than anthropometric techniques requiring measurement of the waist (e.g., waist-circumference, waist-to-hip ratio) or weight and height, especially in the presence of idiopathic deep vein thrombosis and with advancing age (32-37).

Our study presents some limitations, as we enrolled subjects meeting stringent criteria of inclusion. This allowed us to compare well-matched groups, but the results obtained may not apply to a more general population of subjects and further studies are needed to evaluate the utility of FMD and EF measurement for cardiovascular risk assessment in subjects affected by idiopathic DVT.

In conclusion, atherothrombosis and deep vein thrombosis are considered different disease entities, but epidemiological data suggest the possibility of an association, and endothelial dysfunction may represent a shared alteration. Increased epicardial fat thickness and altered endothelium-dependent vasodilation are markers of increased cardiovascular risk The data obtained in our study show that subjects with idiopathic DVT have impairment of FMD and increase of EF thickness and these alteration might predict increased risk of cardiovascular events. The possible interactions between cardiovascular disease and unprovoked deep vein thrombosis may have important consequences for the prognosis of the subjects and for the choice of therapeutic strategies. Visceral, and in particular epicardial, adipose tissue is related to metabolic syndrome and cardiovascular risk and endothelial dysfunction has been shown to predict cardiovascular events. The evaluation of endothelial function and epicardial adipose tissue amount might represent valuable, affordable and reliable tools to refine clinical risk stratification, to plan risk profile modification and to evaluate the effectiveness of pharmacotherapy and the results of medical treatment in subjects with idiopathic deep vein thrombosis.

REFERENCES

1. Prandoni P, Bilora F, Marchiori A, Bernardi E, Petrobelli F, Lensing A, Prins MH, Girolami A. An association between atherosclerosis and venous thrombosis. N Engl J Med 2003; 349(4):1435-41.
2. Jerjes-Sanchez C. Venous and arterial thrombosis: a continuous spectrum of the same disease? Eur Heart J 2005; 26(1):3-4.
3. Van der Hagen PB, Folsom AR, Jenny NS, Heckbert SR, O'Meara ES, Reich LM, Rosendaal FR, Cyshman M. Subclinical atherosclerosis and the risk of future venous thrombosis in the Cardiovascular Health Study. J Thromb Haemost 2006; 4(9):1903-8
4. Reich LM, Folsom AR, Key NS, Boland LL, Heckbert SR, Rosamond WD, Cushman MJ. Prospective study of subclinical atherosclerosis as a risk factor for venous thromboembolism. J Thromb Haemost 2006; 4(9):1886-90.
5. Prandoni P. Venous thromboembolism and atherosclerosis: is there a link? J Thromb Haemost 2007; 5(1):270-275.
6. Ageno W, Becattini C, Selby R, Kamphuisen PW. Cardiovascular risk factors and venous thromboembolism: a meta-analysis. Circulation 2008; 117(1):93-102.
7. Migliacci R, Becattini C, Pesavento R, et al.

Endothelial dysfunction in subjects with spontaneous venous thromboembolism. Haematologica 2007; 92(6):812-8.
8. Lahera V, Goicoechea M, de Vinuesa SG, Miana M, de las Heras N, Cachofeiro V, Luño J. Endothelial dysfunction, oxidative stress and inflammation in atherosclerosis: beneficial effects of statins. Curr Med Chem 2007; 14(2):243-8.
9. Bots ML, Westerink J, Rabelink TJ, de Koning EJ. Assessment of flow-mediated vasodilatation (FMD) of the brachial artery: effects of technical aspects of the FMD measurement on the FMD response. Eur Heart J 2005; 26(4):363-8.
10. Peretz A, Leotta DF, Sullivan JH, Trenga CA, Sands FN, Aulet MR, Paun M, Gill EA, Kaufman JD. Flow mediated dilation of the brachial artery: an investigation of methods requiring further standardization. BMC Cardiovasc Disord 2007; 7:11-19.
11. Sacks H, Fain JN. Human epicardial adipose tissue: A review. American Heart Journal 2007; 153 (6):907-17.
12. Rabkin SW. Epicardial fat: properties, function and relationship to obesity. Obes Rev 2007; 8(3):253-61.
13. Cheng KH, Chu CS, Lee KT, et al. Adipocytokines and proinflammatory mediators from abdominal and epicardial adipose tissue in subjects with coronary artery disease. Int J Obes (Lond) 2008; 32(2):268-74.
14. Iacobellis G, Leonetti F, Di Mario U. Images in cardiology: massive epicardial adipose tissue indicating severe visceral obesity. Clin Cardiol 2003; 26:237.
15. Iacobellis G, Willens HJ. Echocardiographic epicardial fat: a review of research and clinical applications. J Am Soc Echocardiogr 2009; 22(12):1311-9.
16. Corretti MC, Anderson TJ, Benjamin EJ,et al. Guidelines for the Ultrasound Assessment of Endothelial-Dependent Flow-Mediated Vasodilation of the Brachial Artery. A Report of the International Brachial Artery Reactivity Task Force. JACC 2002; 39(2):257-65.
17. Roman MJ, Naqvi TZ, Gardin JM, Gerhard-Herman M, Jaff M, Mohler E. Clinical application of noninvasive vascular ultrasound in cardiovascular risk stratification: a report from the American Society of Echocardiography and the Society of Vascular Medicine and Biology. J Am Soc Echocardiogr 2006; 19(8):943-54.
18. Tsai AW, Cushman M, Rosamond WD, Heckbert SR, Polak JF, Folsom AR. Cardiovascular risk factors and venous thromboembolism incidence: the longitudinal investigation of thromboembolism etiology. Arch Intern Med 2002; 162(10):1182-9.
19. Prandoni P, Ghirarduzzi A, Prins MH, et al. Venous thromboembolism and the risk of subsequent symptomatic atherosclerosis. J Thromb Haemost 2006; 4(9):1891-6.
20. Sørensen HT, Horvath-Puho E, Pedersen L, Baron JA, Prandoni P. Venous thromboembolism and subsequent hospitalisation due to acute arterial cardiovascular events: a 20-year cohort study. Lancet 2007; 370(9601):1773-9.
21. Heit JA. The epidemiology of venous thromboembolism in the community. Arterioscler Thromb Vasc Biol 2008; 28(3):370-2.
22. Isma N, Svensson PJ, Gottsäter A, Lindblad B. Prospective analysis of risk factors and distribution of venous thromboembolism in the population-based Malmö Thrombophilia Study (MATS). Thromb Res 2009; 124(6):663-6.
23. Eriksson EE, Karlof E, Lundmark K, Rotzius P, Hedin U, Xie X. Powerful inflammatory properties of large vein endothelium *in vivo*. Arterioscler Thromb Vasc Biol 2005; 25(4):723-8.
24. Chirinos JA, Heresi GA, Velasquez H, et al. Elevation of endothelial microparticles, platelets, and leukocyte activation in subjects with venous thromboembolism. J Am Coll Cardiol 2005; 45(9):1467-71.
25. Smeeth L, Cook C, Thomas S, Hall AJ, Hubbard R, Vallance P. Risk of deep vein thrombosis and pulmonary embolism after acute infection in a community setting. Lancet 2006; 367:1075-9.
26. Takase B, Uehata A, Akima T, Nagai T, Nishioka T, Hamabe A, Satomura K, Ohsuzu F, Kurita A. Endothelium-dependent flow mediated vasodilation in coronary and brachial arteries in suspected coronary artery disease. Am J Cardiol 1998; 82(12):1535-9.
27. Matsuo S, Matsumoto T, Takashima H, Ohira N, Yamane T, Yasuda Y, Tarutani Y, Horie M. The relationship between flow-mediated brachial artery vasodilation and coronary vasomotor responses to bradykinin: comparison with those to acetylcholine.

J Cardiovasc Pharmacol 2004; 44(2):164-70.
28. Thanyasiri P, Celermajer DS, Adams MR. Endothelial dysfunction occurs in peripheral circulation subjects with acute and stable coronary artery disease. Am J Physiol Heart Circ Physiol 2005; 289(2):513-7.
29. Gresele P, Momi S, Migliacci R. Endothelium, venous thromboembolism and ischaemic cardiovascular events. Thromb Haemost 2010; 103(1):56-61.
30. Iacobellis G, Corradi D, Sharma AM. Epicardial adipose tissue: anatomic, biomolecular and clinical relationships with the heart. Nat Clin Pract Cardiovasc Med 2005; 2:536-4.
31. Jezovnik MK, Poredos P, Stalc M. Impairment of the vasodilatation capability of the brachial artery in subjects with idiopathic venous thrombosis. J Atheroscler Thromb 2010; 17:1190-8.
32. Lind L, Johansson L, Hulthe J, von Belowb C, Ahlstrom H. Vasodilation and visceral fat in elderly subjects The Prospective Investigation of the Vasculature in Uppsala Seniors (PIVUS) study Atherosclerosis 2007; 194:e64–e71.
33. Corradi D, Maestri R, Callegari S, Pastori P, Goldoni M, Luong TV, Bordi C. The ventricular epicardial fat is related to the myocardial mass in normal, ischemic and hypertrophic hearts. Cardiovasc Pathol 2004; 13(6):313-6 .
34. Silaghi A, Piercecchi-Marti MD, Grino M, Leonetti G, Alessi MC, Clement K, Dadoun F, Dutour A. Epicardial Adipose Tissue Extent: Relationship With Age, Body Fat Distribution, and Coronaropathy. Obesity 2008; 16:2424-30.
35. Iacobellis G, Ribaudo MC, Assael F, Vecci E, Tiberti C, Zappaterreno A, Di Mario U, Leonetti F. Echocardiographic epicardial adipose tissue is related to anthropometric and clinical parameters of metabolic syndrome: a new indicator of cardiovascular risk. J Clin Endocrinol Metab 2003; 88(11):5163-8
36. Iacobellis G, Leonetti F. Epicardial adipose tissue and insulin resistance in obese subjects. J Clin Endocrinol Metab 2005; 90:6300-2.
37. Seo JA, Kim BG, Cho H, et al. The cutoff values of visceral fat area and waist circumference for identifying subjects at risk for metabolic syndrome in elderly Korean: Ansan Geriatric (AGE) cohort study. BMC Public Health 2009; 9:443.
38. Borch KH, Braekkan SK, Mathiesen EB, Njølstad I, Wilsgaard T, Størmer J, Hansen JB. Abdominal obesity is essential for the risk of venous thromboembolism in the metabolic syndrome: the Tromso study. J Thromb Haemost 2009; 7:739-45.
39. Steffen LM, Cushman M, Peacock JM, Heckbert SR, Jacobs DR Jr, Rosamond WD, Folsom AR. Metabolic syndrome and risk of venous thromboembolism: longitudinal investigation of thromboembolism Etiology. J Thromb Haemost 2009; 7:746-51.
40. Holst AG, Jensen G, Prescott E. Risk factors for venous thromboembolism results from the Copenhagen City Heart Study. Circulation 2010; 121:1896-903.

COMPARISON OF THE PRIMARY STABILITIES OF CONICAL AND CYLINDRICAL ENDOSSEOUS DENTAL IMPLANTS: AN *IN-VITRO* STUDY

E. ALEO[1], G. VARVARA[2], A. SCARANO[2], B. SINJARI[2] and G. MURMURA[2]

[1]Research and Development Department, GEASS S.r.l., Pozzuolo del Friuli, Udine, Italy;
[2]Department of Oral, Nano and Biotechnological Sciences, Dental School, "G. d'Annunzio" University of Chieti–Pescara, Chieti, Italy

Received November 28, 2011 – Accepted January 27, 2012

The aim of this study is to determine the differences in primary stability between conical and cylindrical dental implants. The insertion and removal torques were the parameters used to measure the primary stability of the implants. Ten conical and cylindrical dental implants were positioned in polyurethane foam blocks to simulate bone density classes D1, D2, D3 and D4. The insertion and removal torques were quantified using a digital torque gauge. The maximum insertion torque and the maximum removal torque measured for the D1 and D4 synthetic bone were significantly higher for the conical implants than the cylindrical implants. In this *in-vitro* model, conical implants show significantly higher primary stability than cylindrical implants for the D1 and D4 synthetic bone classes.

The attainment of implant stability at the time of emplacement is an essential factor in the clinical outcome of osseointegration (1). Implant stability can be seen as a combination of mechanical stability, which is the result of compressed bone holding the implant tightly in place, and biological stability, which is the result of new bone cells at the site of the implant, and the consequent osseointegration. Dental implant geometry, bone quality, and surgical protocol are the main elements that influence the primary stability of an implant, with particular negative emphasis on poor bone quality (2-5). Unfortunately, the long-term success for implant therapy becomes less certain when fixtures are placed into bone of poor quality and limited quantity. Various shapes of dental implants are available and usually provide good primary stability in cases of favorable bone density. Indeed, manufacturers now produce dental implants that they guarantee to provide good primary stability even with poor bone quality.

The original endosseous implants were cylindrical in design, but this is not suitable for all applications. A conical shape was thus developed, especially for immediate implant placement after tooth extraction, with their use then extended to provide a degree of compression of the cortical bone in poor bone implant sites. Indeed, tapered implants provide tighter contacts between the implant and the tissue than cylindrical implants, due to the different diameters between the upper and lower sections of the implants (6, 7).

A number of devices and techniques have been developed to assess primary implant stability, including radiographic investigations, resonance frequency analysis, insertion torque, removal torque, and the Periotest® (8). However, one major problem

Key words: primary stability, conical implants, torque, polyurethane foam

Mailing address: Dr Giuseppe Varvara,
Department of Oral, Nano and Biotechnological Sciences,
"G. d'Annunzio" University of Chieti–Pescara,
Via dei Vestini, 31
66100 Chieti, Italy
Tel: +39 0871 3554125 Fax: +39 0871 3554148
e-mail: gvarvara@unich.it

0393-974X (2012)

DISCLOSURE: ALL AUTHORS REPORT NO CONFLICTS OF INTEREST RELEVANT TO THIS ARTICLE.

in measuring implant stability is the lack of a gold standard technique (9).

It has been suggested that measurement of the insertion torque that is required to properly seat an implant in its bone bed also represents a measure of the stability of an implant. High peak insertion torque has been considered advantageous towards improved primary stability (2, 3, 10, 11). Indeed, clinical studies have demonstrated a close relationship between initial stabilization and the success of an osseointegrated implant (12).

The removal torque test is a method based on the unscrewing of the implant from the bone, and this has been used extensively to quantify the torsional strength of bone–implant contact in experimental animal studies (13).

To study the primary stability of dental implants with different shapes, synthetic bone test specimens are often used in favor of cadaver samples, because of their low variance in material properties and their improved availability. Cadaver samples show high variability due to the mechanical properties of the substrate, which depend on the site selected, and the donor sex, age and metabolic condition (14). Solid rigid polyurethane foams are widely used as standard test materials for simulating human cancellous bone (2, 6, 15-17). These polyurethane foams are available in blocks, and they have been used to investigate the fixing of bone screws.

The aim of this study is to compare different shapes of dental implants, as conical and cylindrical, in respect to their initial stability as *in-vitro* implants in solid rigid polyurethane foam blocks, with the insertion and removal torques used to asses the primary implant stability.

MATERIALS AND METHODS

Synthetic bone specimens

Polyurethane foam cylinders (diameter, 25 mm; height, 40 mm; Sawbones, Pacific Research Laboratories, Washington, DC, USA) were used as the *in-vitro* bone substitute (Fig. 1). This material has been tested successfully with other types of implants, and has been validated by the American Society for Testing Materials (ASTM) as having mechanical properties that are similar to those of human cancellous bone (2, 3, 6, 17-20). To simulate the bone classification from dense cortical to fine trabecular bone, homogeneous blocks with densities of 0.64, 0.48, 0.32, 0.16 g/cm^3 were used (D1 to D4, respectively).

Implant installation

The conical dental implants were WAY® Venezia implants (GEASS S.r.l., Pozzuolo del Friuli, Udine, Italy), with a minimum diameter of 2.54 mm, a maximum diameter of 4.10 mm, and a length of 15 mm. The cylindrical dental implants were HEXA® implants (GEASS S.r.l., Pozzuolo del Friuli, Udine, Italy), with a minimum diameter of 2.77 mm, a cylinder diameter of 3.00 mm, a maximum diameter of 4.10 mm, and a length of 15 mm (Fig. 2). For the present study, a unique surface finishing was used (sandblasting). The threads of these two implant groups had the same pitch and height.

Ten dental implants were tested with each polyurethane foam 'bone' density. The procedure for the placements of the conical implants was initiated according to the manufacturer's instructions; 2.1 mm and 2.5 mm diameter twist drills were used first, which were then followed by the final drilling at 3.8 mm diameter, to the 15 mm length. For the undersized D4 bone preparation, the final placement length used was 9 mm. For the oversized D1 bone preparation, the final drill length used was 15 mm or 9 mm. The procedure for the placements for the cylindrical implants started with the 2 mm twist drill, followed by the pilot drill, the 3 mm twist drill, and finally the countersink. For the higher density polyurethane foam, the tapper was also used.

Insertion torque test

The implants were placed perpendicular to the synthetic bone sample, and were inserted by rotating the chuck rotational axis clockwise with a uniform speed of 10 revolutions per minute. During the installation, the insertion torques were measured for all of the implants every 0.2 s, using a digital torque gauge (Imada, HTG2 series, Northbrook, IL), until the peak torque was reached. A dial indicator depth gauge that was sensitive to 0.01 mm was used to accurately measure the insertion depth of the implants (Mitutoyo, Kawasaki, Kanagawa, Japan).

The relationship between the insertion torques and the lengths of the implants in the placements was determined according to the conical and cylindrical implant geometries.

Removal torque test

The removal torques were also measured every 0.2 s,

by counter-clockwise rotation of the chuck rotational axis, until the implants were removed. The relationship between the removal torques and the lengths of the implants in the placements was determined according to the conical and cylindrical implant geometries.

Statistical analysis

The mean insertion and removal torques (±standard deviations) were calculated. All of the measurements were evaluated statistically using an independent *t*-test, to determine whether there were any significant differences across the maximum insertion torques and the maximum removal torques. A $p < 0.01$ was considered significant.

RESULTS

Measurement of the insertion torque

The insertion torques were measured for the conical and the cylindrical implant and placement systems for the D1, D2, D3 and D4 foam 'bone' blocks, each according to the implant length, and hence implant diameter, in the placement (Fig. 3). Note that for the D1 and D4 synthetic bone types the conical implants were tested for oversized and undersized preparations, respectively.

Measurement of the maximum insertion torque

The maximum insertion torque is the torque that was measured at the end of the dental implant insertion into the placement. The maximum insertion torques of these implants into the placements in the different bone density classes are given in Table I. For the D1 and D4 'bone' blocks, the maximum insertion torques for the conical implants were significantly greater than those of the cylindrical implants ($p < 0.01$; Table I).

Measurement of the removal torque

The removal torques were measured for the conical and the cylindrical implant and placement systems for the D1, D2, D3 and D4 foam 'bone' blocks, each according to the implant length (Fig. 4). Note that for the D1 and D4 synthetic bone types the conical implants were tested for oversized and undersized preparations, respectively.

Measurement of the maximum removal torque

The removal torque is the torque that was needed to unscrew the dental implant from the placement. The maximum removal torques of these implants from the placements in the different bone density classes are given in Table I. For the D1 and D4 'bone' blocks, the maximum removal torques for the conical implants were significantly greater than those of the cylindrical implants ($p < 0.01$; Table I).

DISCUSSION

The aim of the present study is to investigate the effects of conical and cylindrical implant designs on the initial stability of implants positioned in polyurethane foam 'bone' blocks.

To eliminate the effects of the potential variability of the bone parameters on the primary stability of the implants, these were inserted into a homogeneous material. Indeed, an *in-vivo* bone model would increase the heterogeneity across the samples, as bone can present different density, hardness and mechanical properties even in the same segment, which will affect the primary stability of an implant. The ASTM has validated polyurethane blocks as having mechanical properties that simulate human cancellous bone (15). Polyurethane has been

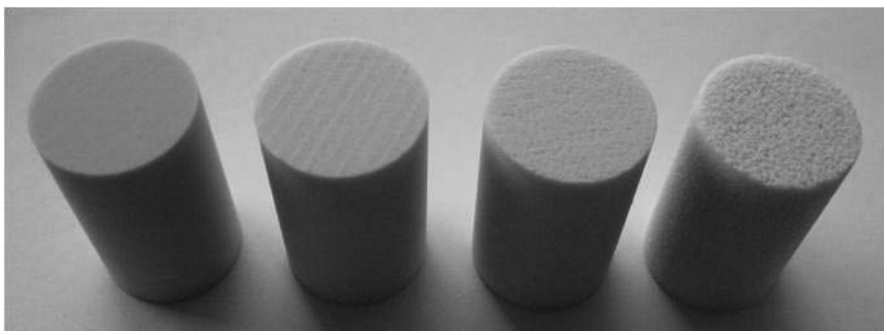

Fig. 1. *The synthetic bone blocks of four different densities, as the D1 D2, D3 and D4 bone classes (left to right).*

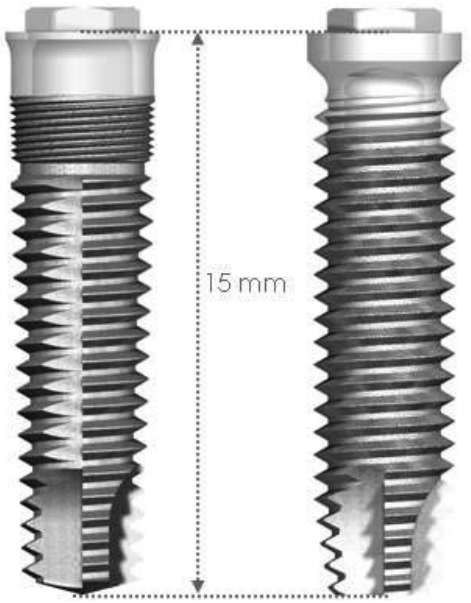

Fig. 2. *Conical (left) and cylindrical (right) implant designs used in this study.*

used as a standard material for mechanical tests for implantable devices in the oral and orthopedic implant fields. In the present study, polyurethane foam cylinders of different densities were used to resemble the human bone classes, according to the Misch classification of D1, D2, D3 and D4 bone (21).

In the past, a wide range of methods have been developed to test the stability of implants. Of these methods, which have included radiographic investigations, resonance frequency analysis, insertion torque, removal torque, and the Periotest® (8), measurement of insertion torque is widespread and it appears to be a more accurate method for estimating primary stability (2, 3, 10-12). In the present study, both the insertion torque and removal torque data were collected.

For the insertion torque, this was seen to increase with increasing screw length for both the conical and the cylindrical implants. The trends in the data show linear progression for the cylindrical implants, according to the diameter of the implant, which is fixed from 3 mm to 13 mm of the total implant length. In contrast, the conical implants show a more curvilinear shape to the insertion torque curves, which can be explained by the gradual increase in the outer implant diameter.

The removal torques showed trends in the data that are in agreement with the progression of the insertion torque curves, with a clear peak for the conical implants and a decreased peak for the cylindrical implants. Of note, the removal torque curves of the cylindrical implants show a pronounced cyclicity for all of the bone classes, which is probably due to eccentric rotation of the system. This was not as visible for the conical implants. At the same time, the order of magnitude of this cyclic behavior is not significant in terms of the removal torque measures in the present study.

Considering the maximum insertion torques, no differences in initial stabilities were seen between the conical and cylindrical dental implants for the D2 and D3 synthetic bone blocks; however, they do show significant differences for the D1 and D4 synthetic bone. Therefore, these findings indicate that conical implants have higher primary stability than cylindrical implants when the surgical conditions are complicated and clinically disadvantageous, as seen for these *in-vitro* D1 and D4 bone classes.

These data are essentially in agreement with histomorphometric results obtained by Trisi and Rao (22). These authors demonstrated that the large distribution of the histomorphometric data in each of these bone classes resulted in overlapping data for the adjacent classes, so that their statistical tests did not show significant differences between the adjacent D2 and D3 classes. Of note, the densities of actual bone cannot be separated clearly into four different types, as *in vivo* there is a continuous gradient of bone density, with all of the intermediate values seen. Thus, the surgeon can also have difficulty in distinguishing between these neighboring categories, although this is less of a problem between the D1 and D4 bone classes.

From the results of animal study there were no significant differences in the success rate and the histomorphometric analysis between the cylindrical and conical implants (23).

The continuous increase in the insertion torques for the conical implants was probably caused by the tighter contact with the surrounding synthetic bone than seen for the cylindrical implants, due to the different implant diameters from the lower to

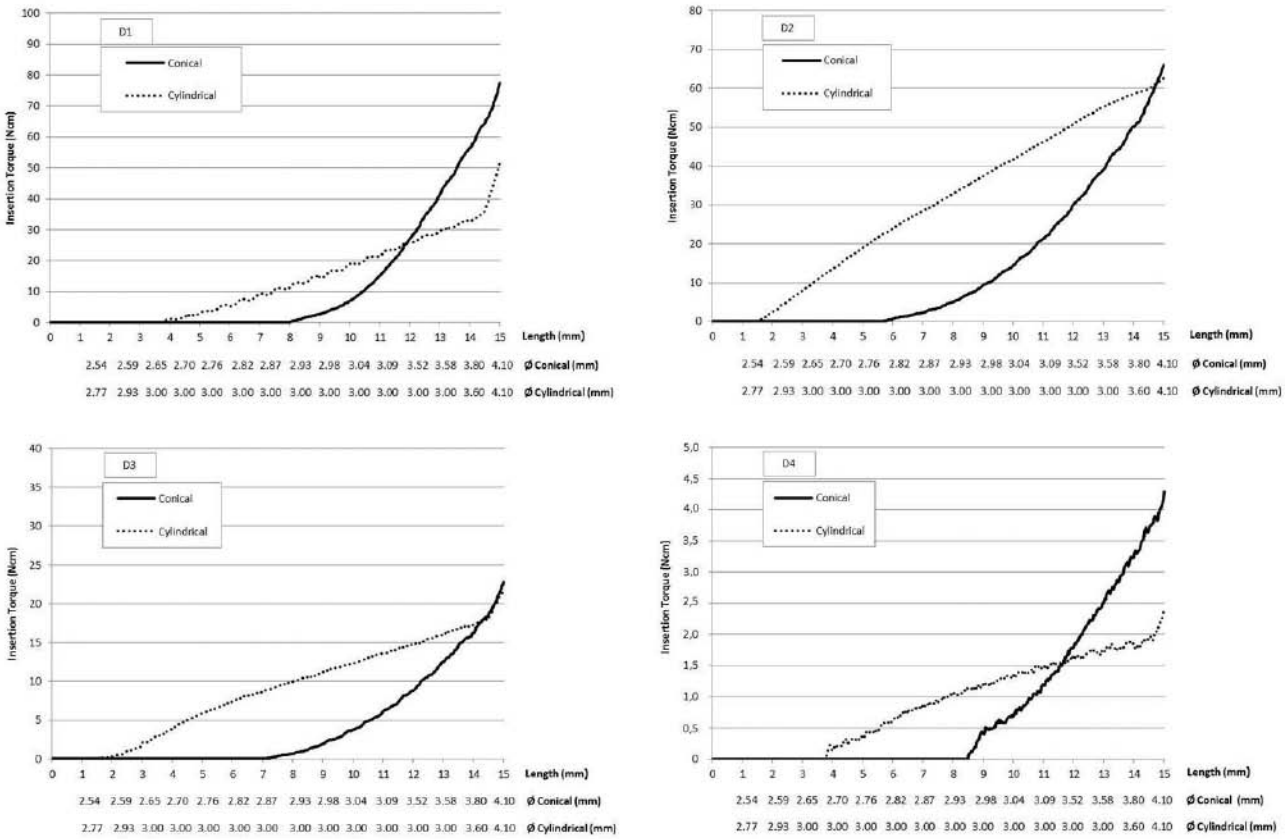

Fig. 3. *Insertion torques for the conical and cylindrical implants in the D1, D2, D3 and D4 synthetic bone blocks (as indicated).*

the upper parts of the conical implants. These data also confirm previous studies for endosseous dental implant and orthodontic miniscrews, which have indicated that conical implants have higher primary stability than cylindrical implants (10, 19). These data thus further support the use of a conical shape of the implant for poor bone quality, to decrease emplacement failure. They are in agreement with the concept that the tapered shape of these conical implants increases the primary stability by providing pressure on the cortical bone of regions of poor bone quality (6, 7).

Although the conical implants also show higher removal torques than the cylindrical implants, both types of implant show lower maximum removal torques than maximum insertion torques. These findings are in agreement with recently published data using the same standardized bone system (5). Other studies have indicated that even if the insertion process is completed when the rotational force and torque are at their highest, the interfacial strain decreases when the screw is in equilibrium, because of the changes in the surrounding bone when the rotational force is removed (20).

While such studies using insertion torque and synthetic bone provide a good method to study these mechanical relationships, it should be noted that the torque-in and torque-out values are different from those that would be measured *in vivo*. This arises because these *in-vitro* synthetic bone blocks do not have the same dampening effects as the *in-vivo* maxilla and mandible bone. Thus, in these studies, the data cannot be considered as absolute values, but need to be considered as comparisons between these two dental implant systems.

In conclusion, this study demonstrates that design

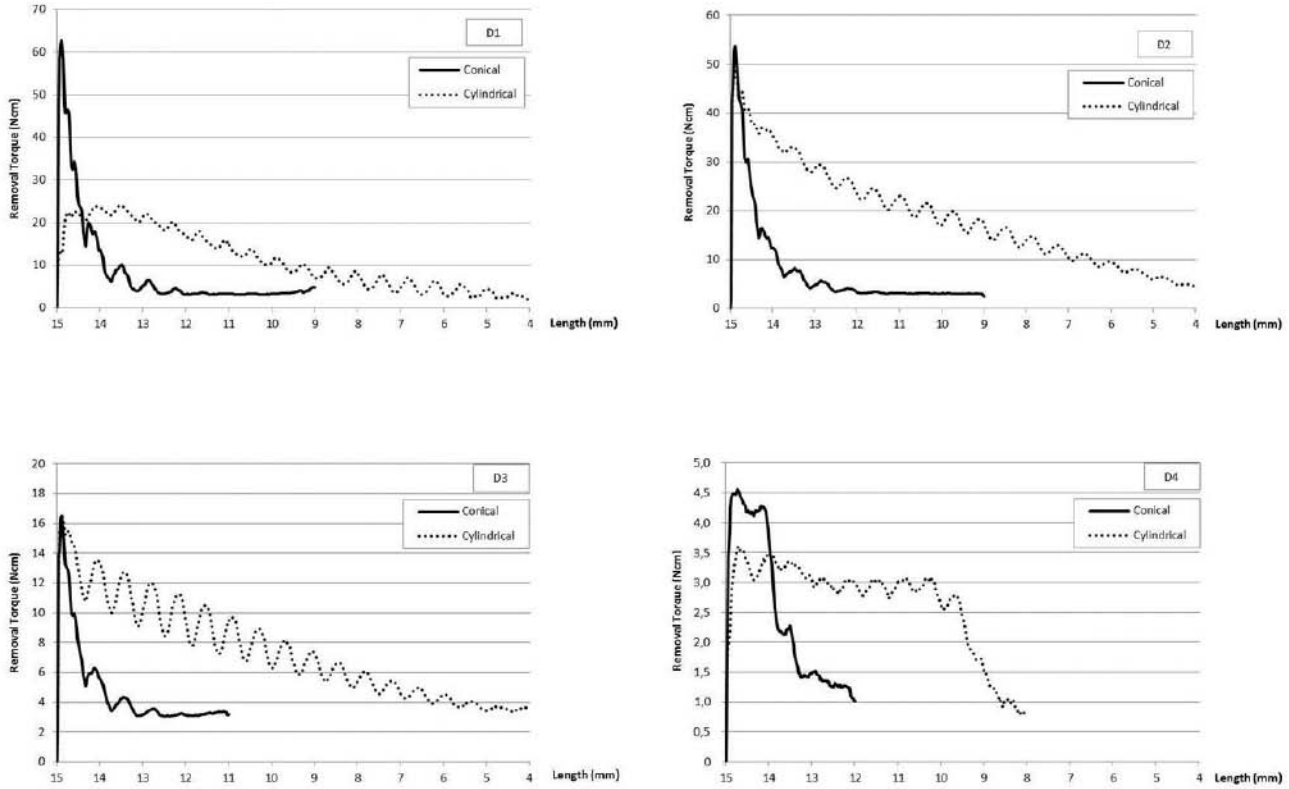

Fig. 4. *Removal torques for the conical and cylindrical implants in the D1, D2, D3 and D4 synthetic bone blocks (as indicated).*

Table I. *Maximum insertion and removal torques for the conical and cylindrical implants in the placements of the D1, D2, D3 and D4 synthetic bone types.*

Implant system	**Maximum torque (N.cm)**			
	D1 (0.64 g/cm^3)	**D2 (0.48 g/cm^3)**	**D3 (0.32 g/cm^3)**	**D4 (0.16 g/cm^3)**
Insertion				
Conical	77.52±3.64*	65.86±4.03	22.73±2.61	4.29±0.35*
Cylindrical	52.06±6.84*	62.79±9.13	21.90±3.96	2.43±0.88*
Removal				
Conical	63.13±1.44*	54.06±1.91	16.66±2.05	4.69±0.27*
Cylindrical	28.00±5.86*	49.13±6.49	16.80±3.39	3.79±0.68*

Data are means ±SD.
**Conical versus cylindrical, p <0.01.*

of the dental implant is important for initial implant stability, with the demonstration that a conical shape of the implant can show greater insertion and removal torques compared with a cylindrical design. This will be particularly evident when the surgical conditions are complicated and clinically disadvantageous, which thus ensures greater primary stability for the use of conical implants in such cases.

ACKNOWLEDGEMENTS

The authors would like to thank Luciano Prez (GEASS S.rl.) for his valued and irreplaceable contribution in the experiments carried out, and Marco Prosperi and Mirco Zanuttini (GEASS S.r.l.) for their support.

REFERENCES

1. Gapski R, Wang HL, Mascarenhas P, Lang NP. Critical review of immediate implant loading. Clin Oral Implants Res 2003; 14:515-27.
2. Tabassum A, Meijer GJ, Wolke JG, Jansen JA. Influence of the surgical technique and surface roughness on the primary stability of an implant in artificial bone with a density equivalent to maxillary bone: a laboratory study. Clin Oral Implants Res 2009; 20:327-32.
3. Tabassum A, Meijer GJ, Wolke JG, Jansen JA. Influence of surgical technique and surface roughness on the primary stability of an implant in artificial bone with different cortical thickness: a laboratory study. Clin Oral Implants Res 2010; 21:213-20.
4. Fanuscu MI, Chang TL. Three-dimensional morphometric analysis of human cadaver bone: microstructural data from maxilla and mandible. Clin Oral Implants Res 2004; 15:213-8.
5. Dos Santos MV, Elias CN, Cavalcanti Lima JH. The effects of superficial roughness and design on the primary stability of dental implants. Clin Implant Dent Relat Res 2011; 13:215-23.
6. Chong L, Khocht A, Suzuki JB, Gaughan J. Effect of implant design on initial stability of tapered implants. J Oral Implantol 2009; 35:130-5.
7. O'Sullivan D, Sennerby L, Meredith N. Influence of implant taper on the primary and secondary stability of osseointegrated titanium implants. Clin Oral Implants Res 2004; 15:474-80.
8. Atsumi M, Park SH, Wang HL. Methods used to assess implant stability: current status. Int J Oral Maxillofac Implants 2007; 22:743-54.
9. Ceherli MC, Karasoy D, Akca K, Eckert SE. Meta-analysis of methods used to assess implant stability. Int J Oral Maxillofac Implants 2009; 24:1015-32.
10. Sakoh J, Wahlmann U, Stender E, Nat R, Al-Nawas B, Wagner W. Primary stability of a conical implant and a hybrid, cylindric screw-type implant *in vitro*. Int J Oral Maxillofac Implants 2006; 21:560-6.
11. Trisi P, Perfetti G, Baldoni E, Berardi D, Colagiovanni M, Scogna G. Implant micromotion is related to peak insertion torque and bone density. Clin Oral Implants Res 2009; 20:467-71.
12. Akça K, Chang TL, Tekdemir I, Fanuscu MI. Biomechanical aspects of initial intraosseous stability and implant design: a quantitative micro-morphometric analysis. Clin Oral Implants Res 2006; 17:465-72.
13. Johansson C, Albrektsson T. Integration of screw implants in the rabbit: a 1-year follow-up of removal torque of titanium implants. Int J Oral Maxillofac Implants 1987; 2:69-75.
14. Szivek JA, Thompson JD, Benjamin JB. Characterization of three formulations of a synthetic foam as models for a range of human cancellous bone types. J Appl Biomater 1995; 6:125-8.
15. ASTM F1839-08. Standard specification for rigid polyurethane foam for use as a standard material for testing orthopedic devices and instruments. American Society for Testing and Materials.
16. Patel PS, Shepherd DE, Hukins DW. Compressive properties of commercially available polyurethane foams as mechanical models for osteoporotic human cancellous bone. BMC Musculoskelet Disord 2008; 9:137.
17. Kim JW, Baek SH, Kim TW, Chang YI. Comparison of stability between cylindrical and conical type mini-implants. Mechanical and histological properties. Angle Orthod 2008; 78:692-8.
18. Bardyn T, Gédet P, Hallermann W, Büchler P. Quantifying the influence of bone density and thickness on resonance frequency analysis: an *in-vitro* study of biomechanical test materials. Int J Oral Maxillofac Implants 2009; 24:1006-14.

19. Lim SA, Cha JY, Hwang CJ. Insertion torque of orthodontic miniscrews according to changes in shape, diameter and length. Angle Orthod 2008; 78:234-40.
20. Song YY, Cha JY, Hwang CJ. Mechanical characteristics of various orthodontic mini-screws in relation to artificial cortical bone thickness. Angle Orthod 2007; 77:979-85.
21. Misch CE, Qu Z, Bidez MW. Mechanical properties of trabecular bone in the human mandible: implications for dental implant treatment planning and surgical placement. J Oral Maxillofac Surg 1999; 57:700-6; discussion 706-8.
22. Trisi P, Rao W. Bone classification: clinical-histomorphometric comparison. Clin Oral Implants Res 1999; 10:1-7.
23. O'Sullivan D, Sennerby L, Meredith N. Influence of implant taper on the primary and secondary stability of osteointegrated titanium implants. Clin Oral Implants Res 2004; 15:474-80.

ENDOCYTOSIS AND INTRACELLULAR LOCALISATION OF TYPE 1 RIBOSOME-INACTIVATING PROTEIN SAPORIN-S6

A. BOLOGNESI[1], L. POLITO[1], V. SCICCHITANO[1], C. ORRICO[2], G. PASQUINELLI[2], S. MUSIANI[1], S. SANTI[3], M. RICCIO[4], M. BORTOLOTTI[1] and M.G. BATTELLI[1]

[1]Department of Experimental Pathology, [2]Department of Radiological and Histopathological Sciences, Alma Mater Studiorum - University of Bologna, Bologna, Italy; [3]IGM-CNR, Unit of Bologna, c/o IOR, Bologna, Italy; [4]Department of Anatomy and Histology, University of Modena and Reggio Emilia, Modena, Italy

Received May 25, 2011 – Accepted December 21, 2011

The first two authors contributed equally to this work

Saporin-S6 is a single-chain ribosome-inactivating protein (RIP) that has low toxicity in cells and animals. When the protein is bound to a carrier that facilitates cellular uptake, the protein becomes highly and selectively toxic to the cellular target of the carrier. Thus, saporin-S6 is one of the most widely used RIPs in the preparation of immunoconjugates for anti-cancer therapy. The endocytosis of saporin-S6 by the neoplastic HeLa cells and the subsequent intracellular trafficking were investigated by confocal microscopy that utilises indirect immunofluorescence analysis and transmission electron microscopy that utilises a direct assay with gold-conjugated saporin-S6 and an indirect immunoelectron microscopy assay. Our results indicate that saporin-S6 was taken up by cells mainly through receptor-independent endocytosis. Confocal microscopy analysis showed around 30% co-localisation of saporin-S6 with the endosomal compartment and less than 10% co-localisation with the Golgi apparatus. The pathway identified by the immunofluorescence assay and transmission electron microscopy displayed a progressive accumulation of saporin-S6 in perinuclear vesicular structures. The main findings of this work are the following: i) the nuclear localisation of saporin-S6 and ii) the presence of DNA gaps resulting from abasic sites in HeLa nuclei after intoxication with saporin-S6.

Ribosome-inactivating proteins (RIPs) (1) are depurinating enzymes that are expressed in a large number of plants. These proteins have *N*-glycosidase activity that removes a specific adenine residue (A_{4324} in rat liver rRNA) from rRNA and irreversibly damages ribosomes and causes the inhibition of protein synthesis. RIPs also depurinate DNA; thus, the denomination of polynucleotide adenine glycosylase (PNAG) was proposed. These proteins are divided into type 1 and type 2 RIPs depending on the type of polypeptide chains that constitute the structure. The majority of known RIPs are single-chain proteins (type 1 RIPs). Other RIPs are galactoside-specific lectins consisting of A chain(s)

Key words: anti-cancer drugs, endocytosis, intracellular trafficking, saporin-S6, type 1 ribosome-inactivating proteins

Mailing address:
Prof. Maria Giulia Battelli,
Via S. Giacomo 14,
40126 Bologna, Italy
Tel: +39 051 2094700
Fax: +39 051 2094746
email: mariagiulia.battelli@unibo.it

0393-974X (2012)

DISCLOSURE: ALL AUTHORS REPORT NO CONFLICTS OF INTEREST RELEVANT TO THIS ARTICLE.

with the same enzymatic activity as type 1 RIPs and are linked to cell binding B chain(s) with lectin properties (type 2 RIPs). Certain type 2 RIPs are potent toxins, the most well-known being ricin and abrin. Other type 2 RIPs have a similar structure and enzymatic properties but are less toxic (2-4).

The mechanism of the entry and intracellular routing of type 2 RIPs has been extensively studied, particularly the mechanism of ricin. Ricin, through the lectin chain, binds the terminal galactose or *N*-acetylgalactosamine residues of glycoproteins and glycolipids on the cell surface. After the endocytosis of ricin by clathrin-dependent and independent mechanisms, ricin is routed through the endosomal compartment to the multi-vesicular body and about 5% of the protein is sorted in the trans-Golgi network (TGN). Several lines of evidence indicate that this small amount of ricin is responsible for ricin targeting to the ribosome and cytotoxicity. Ricin reaches the endoplasmic reticulum (ER) through the retrograde transport system that mediates the routing of misfolded proteins from the TGN to the ER compartment (5). The translocation of type 2 RIPs from the ER to the cytosol has been proposed to occur in two steps: the reduction of the disulphide bridge between the A and B chains; and the cytosolic entry of the A chain using the quality control pathway that leads to ER-associated protein degradation (6, 7). The localisation of a recombinant ricin A chain fused to EGFP (enhanced green fluorescent protein) in the ER was shown by confocal microscopy and immunogold labelling electron microscopy (8).

The B chain facilitates the endocytosis of type 2 RIPs that justifies, at least in part, the higher toxicity of certain type 2 RIPs to cells and animals compared to type 1 RIPs. The toxicity of type 2 RIPs to the mouse is highly variable with a lethal dose at 50% (LD_{50}) ranging from 1µg/kg to 40µg/kg body wt, whereas the LD_{50} of type 1 RIPs ranges between 1 and 44 mg/kg (2). In particular, the type 1 RIP saporin-S6 (from *Saponaria officinalis*), hereinafter referred to as saporin, kills mice with a LD_{50} at 6 days of 4µg/kg body wt (9).

Saporin and other type 1 RIPs have been extensively used in generating immunotoxins (10, 11) to target the specific epitopes expressed on the surface of tumour or other unwanted cells. In these cases, the carrier largely mediates the binding and endocytosis of the conjugates that are responsible for selective cytotoxicity. Thus, the study of the intracellular localisation of saporin is essential for investigating a possible anti-cancer utilisation of saporin-containing immunotoxins (12).

Of note, saporin and other type 1 RIPs were shown to induce apoptotic cell death alone or as a toxic component of immunotoxins (13). Moreover, ricin and saporin were cytotoxic through more than one cell death mechanism (14). Recently, it has been shown that a saporin mutant that is unable to inhibit protein synthesis can induce apoptosis of intoxicated cells (15). Thus, RNA damage is not required to trigger apoptosis.

In previous studies, the mechanism of endocytosis and the intracellular fate of type 1 RIPs, gelonin (16-18), saporin (19-22), and trichosanthin (23, 24) were investigated. Although in some cell types a receptor-mediated endocytosis by the LDL receptor family was suggested, the interaction of type 1 RIPs with cells needs to be clarified.

In this study, we examined the endocytosis of saporin and the intracellular routing and subcellular localisation in HeLa cells by indirect immunofluorescence using a confocal microscope and direct and indirect gold staining using an electron microscope. In particular, we tried to establish whether saporin is able to enter the cell nucleus and induce DNA depurination.

MATERIALS AND METHODS

Saporin

Saporin was isolated as previously described (25) from the seeds of *Saponaria officinalis* kindly supplied by the Azienda Regionale delle Foreste della Regione Emilia Romagna, Casola Valsenio, RA, Italy. Protein purity was analysed by reverse-phase HPLC on a Vydac C4 column (Hesperia, CA, USA) as described previously (26) and was close to 99% of the total protein.

Antibodies

Rabbit anti-saporin polyclonal antibodies were prepared as previously described (27). The anti-GM130 monoclonal antibody was from BD Transduction Laboratories, Heidelberg, Germany. The anti-BiP/GRP78 monoclonal antibody was from Stressgen Biotechnology, San Diego, CA, USA. Fluorescein isothiocyanate (FITC)-

conjugated goat anti-rabbit IgG polyclonal antibodies were from Calbiochem, Darmstadt, Germany. Cy™5-conjugated donkey anti-mouse IgG polyclonal $F(ab')_2$ antibodies were from Jackson ImmunoResearch Lab. Inc., West Grove, PA, USA. Five nanometres gold-conjugated goat anti-rabbit IgG were from Nanoprobes, Yaphank, NY, USA. Gold-labelled goat anti-rabbit IgG 10 nm was from GE Healthcare, Buckinghamshire, UK.

Cells

HeLa cells were maintained in RPMI 1640 medium (Sigma-Aldrich, St. Louis, MO, USA) and supplemented with 10% heat-inactivated foetal bovine serum (FBS, Sigma-Aldrich), $2x10^{-3}$ M L-glutamine, 100 U/ml penicillin and 100 µg/ml streptomycin (Sigma-Aldrich) (hereinafter referred to as the complete medium) in humidified air with 5% CO_2 at 37°C. Cell viability was analysed before each experiment by Trypan blue dye exclusion.

Cell protein synthesis

The concentration of saporin inhibiting protein synthesis by 50% (IC_{50}) was assessed 24 h after seeding HeLa cells on 24-well plates (30,000 cells/well), as previously described (28) with minor modifications.

In the short-term experiments, the cultures were incubated in the absence or presence of 10^{-5} M saporin for 90 min at 37°C in complete medium and were pulsed for 30 min with 2 µCi/ml L-[4,5-^{3}H]leucine (85 Ci/mmol, GE Healthcare) in leucine- and serum-free RPMI 1640 containing the same saporin concentration. Cells were washed with $5x10^{-3}$ M sodium phosphate buffer, pH 7.5, containing $1.4x10^{-1}$ M NaCl (PBS) before the radiolabeled leucine incorporation was determined.

Immunofluorescence assay

HeLa cells were seeded on cover slips in 24-well plates (30,000 cells/well) in complete medium. After 24 h, cells were treated with saporin as detailed in the legend to Fig. 1.

At the end of each treatment, cells were washed three times with serum-free medium at 0°C and fixed with 1% p-formaldehyde in $1x10^{-1}$ M sodium phosphate buffer, pH 7.5, for 30 min at 30°C, washed twice with PBS and permeabilised with 1% saponin for 45 min at 30°C. After saturation with 1% bovine serum albumin (BSA, Sigma-Aldrich) in PBS (PBS/BSA) for 1 h at 30°C, cells were incubated with rabbit anti-saporin antibodies 1:8000 in PBS/BSA for 60 min at 30°C and washed and the FITC-conjugated anti-rabbit antibodies that were diluted 1:100 in PBS/BSA for 60 min at 30°C were added. Double-staining experiments were performed by incubating saporin-treated cells with rabbit anti-saporin antibodies and anti-GM130 monoclonal antibody (1:1000) or anti-BiP monoclonal antibody (1:100). The detection of primary antibodies was performed with FITC-conjugated anti-rabbit and Cy™5-conjugated anti-mouse antibodies (1:20). Finally, cover slips were mounted on glass slides using a Mowiol 4-88 (Sigma-Aldrich) solution (10% w/v) containing the anti-fade 1,4-diazobicyclo-[2.2.2]-octane (2.5% w/v, DABCO, Sigma-Aldrich) in $1x10^{-1}$ M Tris-HCl buffer, pH 8.5, and glycerol (20% v/v).

Fluorescence microscopy was performed with a Leitz Orthoplan microscope equipped with a 100 W epi-illumination and 40x and 100x objectives. Colour photomicrographs were obtained using a Kodak MDS 120 digital camera. The double immunofluorescence experiments were analysed by a Radiance 2000 confocal microscope, and the co-localisation was evaluated by using the LaserPix software (both from BioRad, Hercules, CA, USA) as already detailed (29).

Transmission electron microscopy

For electron microscopy experiments, $2x10^5$ cells were seeded in 6-well microtitre plates in 1 ml of complete medium. After 18 h, cells were treated with saporin at 37°C for the indicated time.

a) Morphological alteration of saporin-treated HeLa cells - To ascertain cell modifications induced by the RIP, HeLa cells were incubated with $1x10^{-6}$ M saporin for 20 h, washed three times with PBS, harvested with a cell scraper and centrifuged at 300x*g* for 5 min. Pelleted cells were washed twice with PBS, fixed with 4% p-formaldehyde in $1x10^{-1}$ M sodium phosphate buffer, pH 7.5, for 24 h at 4°C. The pellets were washed with $1.5x10^{-1}$ M sodium phosphate buffer, pH 7.5, postfixed in 1% buffered osmium tetroxide, dehydrated through a graded ethanol series (70-100%) and embedded in epoxy resin. Ultrathin sections were counterstained with uranyl acetate and lead citrate and observed on a transmission electron microscope (Philips 400T, Eindhoven, Netherland).

b) Saporin conjugation with colloidal gold - Saporin was conjugated to 5 nm colloidal gold particles (Nanoprobes) following the manufacturer's instructions. Briefly, $3x10^{-6}$ M saporin in $1x10^{-1}$ M carbonate/bicarbonate buffer, pH 10, was added at 1/10 v/v to colloidal gold that was previously adjusted to pH 10 with the same buffer. The mixture was gently stirred for 5 min at room temperature and after saturation with polyethylenglycol (PEG) 8000 (final concentration 1%) was ultracentrifuged at 49000x*g* for 2 h at 4°C. The loose pellet containing the conjugate was resuspended in $2x10^{-2}$ M Tris-HCl buffer, pH 7.5, containing 1% PEG 8000 and centrifuged as described above. The conjugate was stored at 4°C.

c) Pre-embedding experiments - HeLa cells were treated with $1x10^{-5}$ M saporin containing 1/10 of the 5

nm gold-saporin conjugate. After 20, 40, 60 and 120 min at 37°C, cells were harvested, fixed and processed for electron microscopy as described above.

d) Post-embedding experiments - An immunoelectron microscopy assay was performed on HeLa cells exposed to non-conjugated $1x10^{-5}$ M saporin in a continuous manner as described above. After fixing overnight with 4% p-formaldehyde and washing with $1.5x10^{-1}$ M sodium phosphate buffer, pH 7.5, the cells were dehydrated through a graded ethanol series (70-100%) and embedded in acrylic resin (Unicryl, BBInternational, England). Polymerisation was achieved by UV light at 4°C. Ultrathin sections were collected on gold grids, blocked in PBS/BSA for 15 min and incubated overnight at 4°C with a rabbit anti-saporin polyclonal antibody diluted 1:8000 in PBS/BSA. Grids were subsequently washed with PBS and incubated for 30 min at room temperature with 5 nm gold-conjugated anti-rabbit IgG diluted 1:10 in PBS/BSA. After washing with PBS and distilled water, grids were counterstained with uranyl acetate (3% in water) and lead citrate and observed in a transmission electron microscope. In a parallel experiment, rabbit anti-saporin polyclonal antibody was diluted 1:4000 in PBS/BSA followed by incubation with 10 nm gold-labelled anti-rabbit IgG diluted 1:5 in PBS/BSA.

Comet assay

HeLa cells were seeded in 6-well plates (100,000 cells/well) in complete medium 18 h before treatment with saporin 10^{-5} M for 2 h and incubated overnight at 37°C in the absence of RIP. The following day, cells were washed twice in PBS, harvested with a scraper, counted and resuspended in PBS at a concentration of 10^5 cells/ml. The cell suspension of 10 µl was quickly mixed with 100 µl of 1% LM agarose (Trevigen Gaithersburg, MD, USA) at 37°C, and 40 µl of this mixture was dropped onto a glass slide. Dried samples were lysed at 4°C for 2 h in the dark with a solution containing 2.5 M NaCl, 100 mM EDTA, 10 mM Tris-base, 1% sodium lauryl sarcosine and 1% Triton X-100. Afterwards, the samples were equilibrated for 30 min in freshly prepared FLARE™ buffer (Trevigen) containing 0.01 M HEPES-KOH, 0.1 M KCl and 0.01 M EDTA. Half of the samples were incubated for 1 h at 37°C with 40 µl *E. coli* endonuclease IV (Trevigen) that was diluted 1:75 with FLARE™ buffer containing BSA supplied by Trevigen. Subsequently, the slides were incubated for 30 min in the buffer containing 0.5 M EDTA and 0.2 M NaOH, pH 13, and subjected to electrophoresis (24 V, 300 mA) for 40 min at 4°C in the same buffer. The samples were washed twice with distilled water and fixed in 70% ethanol for 5 min. The slides were mounted as above using a Mowiol 4-88 solution (10% w/v) in $1x10^{-1}$ M Tris-HCl buffer, pH 8.5, containing glycerol (20% v/v) and DAPI (2.5% w/v).

RESULTS

Effect of saporin on protein synthesis by HeLa cells

Saporin cytotoxicity was verified by protein synthesis determination. Protein synthesis by HeLa cells was 83.8±9.2% after incubation with $1x10^{-5}$ M saporin for 120 min. The IC_{50} after 24 h incubation was $6.14x10^{-7}$ M.

Intracellular localisation of saporin by immunofluorescence analysis

The pulse-chase exposure of HeLa cells to saporin for different times at 37°C showed that the RIP was already intracellularly localised after 20 min (Fig. 1A). The FITC-conjugated anti-saporin antibody was in endocytic vesicles distributed in the cytosol. The fluorescence pattern reached and accumulated in a perinuclear vesicular structure. The small amount of staining visible in the nuclear spot could not confirm nor exclude the presence of saporin inside the nucleus.

The double immunofluorescence analysis performed by confocal microscopy showed an approximate 30% co-localisation of saporin with the endoplasmic reticulum (ER) marker BiP as demonstrated by the co-localisation binary map (Fig. 1B). After 20, 40 and 60 min of exposure to saporin, there was not a significant difference in the amount of protein that localised in the ER. A similar pattern was observed with the co-localisation analysis of saporin and the Golgi marker GM130 that showed around 7% (Fig. 1C) of the saporin localised in the Golgi apparatus. After 60 min of total incubation time, 4% of the endocytosed saporin was present in the nucleus (Fig. 1D).

Effect of saporin exposure to HeLa ultrastructure

HeLa cells exposed to $1x10^{-6}$ M saporin for 20 h were similar to untreated cells (Fig. 2A) and only a few apoptotic cells were found. However, in the vast majority of treated cells minimal organelle injury was seen; mitochondria had dilated cristae and a contracted appearance (Fig. 2B); autophagocytic vacuoles, often involving degenerated mitochondria, were a common finding as well as focal dilatation of rough ER cisternae (Fig. 2C). The Golgi apparatus

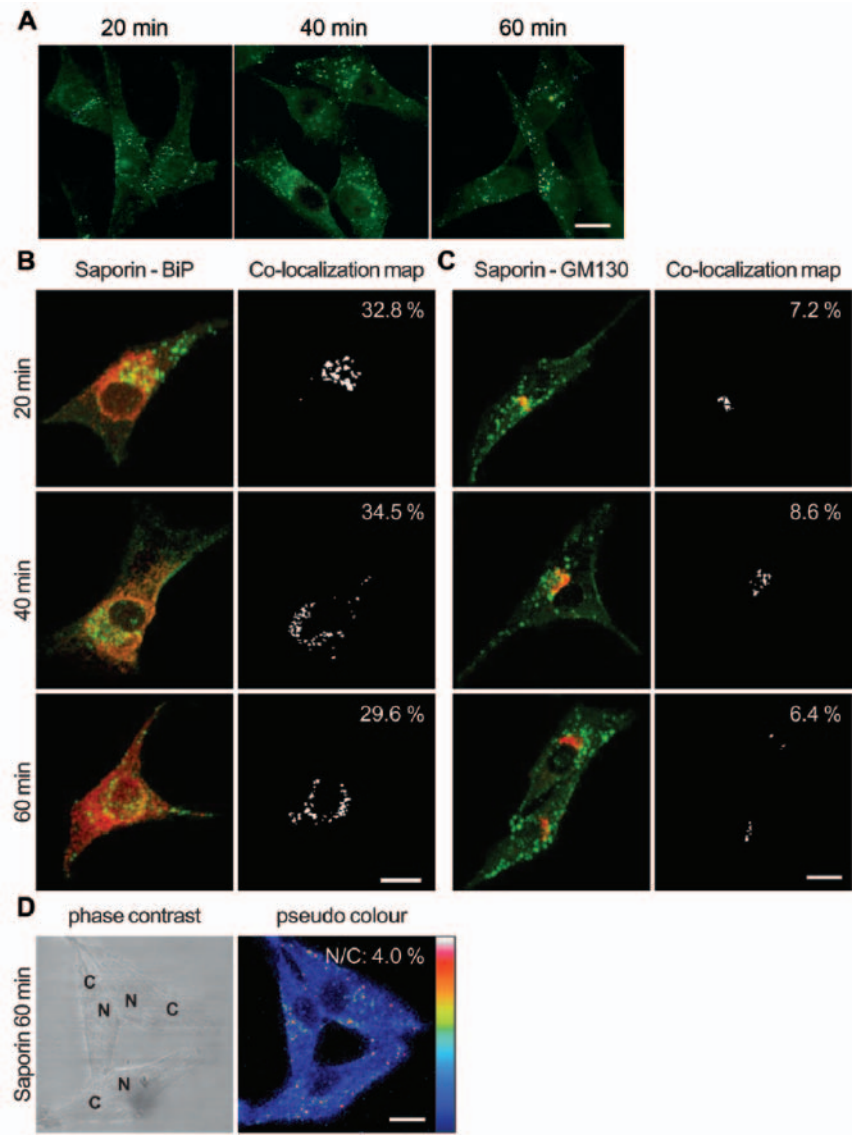

Fig. 1. *Detection of saporin by indirect immunofluorescence. HeLa cells were incubated with 10^{-5} M saporin for 20 min at 37°C, washed and incubated at 37°C up to the indicated time. Fluorescence microscopy (**A**): After fixation and permeabilisation, cells were treated with the anti-saporin polyclonal antibody and stained with the FITC-conjugated anti-rabbit antibody. Confocal microscopy and co-localisation (**B-D**): After fixation and permeabilisation, cells were treated with the anti-saporin polyclonal antibody and the anti-BiP (**B**) or anti-GM130 (**C**) antibodies. The secondary antibodies gave a green signal for saporin and a red signal for the ER (B) or Golgi apparatus (C). The percentage of co-localisation is reported together with the co-localisation binary map. **D**) The amount of saporin inside the nucleus was calculated as nuclear/cytoplasmic ratio (N/C) of grey levels and expressed as percentage. Scale bar, 10 µm.*

appeared to be well preserved.

Analysis of saporin internalisation pathway by transmission electron microscopy

The saporin internalisation pathway in the cytosolic compartment was assessed by transmission electron microscopy using pre-embedding and post-embedding procedures.

a) Experiments with gold-saporin conjugates - Time-lapse analysis of 5 nm gold-saporin complexes showed that, after 20 min of incubation, gold particles were mainly located on the plasma membrane and

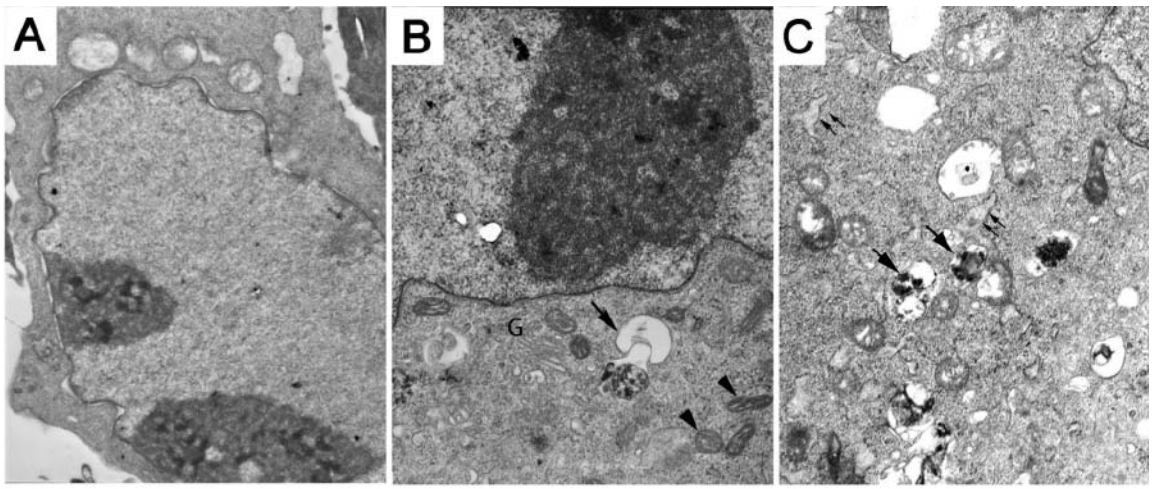

Fig. 2. *Effects of saporin on the ultrastructure of HeLa cells. Untreated HeLa cells showing normal ultrastructure (**A**). Following 20 h exposure to 10^{-6} M saporin HeLa cells show contracted mitochondria with dilated cristae (arrowheads) (**B**), numerous autophagocytic vacuoles (large arrows), often involving degenerated mitochondria, and focal dilatation of rER cisternae (small arrows) (**C**); the Golgi apparatus (G) is unaffected. Magnification: A: x9200; B: x8000; C: x11000.*

in clear vesicles and vacuoles (Fig. 3A); only in a few instances were the particles found within coated vesicles (Fig. 3B). After 40 min, gold particles were clustered in late endosomes and lysosomes in proximity to the nuclear area. Lack of gold particles in lipofuscin (Lp) suggests that gold-labelled saporin is not destined towards terminal autophagic compartment (Fig. 3C). Occasionally, clusters of gold particles were seen close to rER cisternae (Fig. 3D). The localisation of gold particles in the nuclear zone was particularly evident after 60 min (Fig. 3E) and 120 min (Fig. 3F). Interestingly, the Golgi complexes were well preserved. In control experiments, the gold-saporin complexes internalisation was inhibited by cold temperature (i.e., 4°C). Moreover, HeLa cell incubation with unconjugated-gold particles showed gold particles exclusively in the sub-plasmalemmal cytoplasmic compartment (data not shown).

b) Experiments with immunogold labelling - Comparative post-embedding analysis using a rabbit anti-saporin polyclonal antibody followed by incubation with 10 nm gold-labelled anti-rabbit IgG confirmed results from the pre-embedding procedure described above. However, after 20 min, single gold particles were observed in sub-plasmalemmal clear vacuoles and free in the cytoplasm (Fig. 4). Occasionally, after 60 min, gold particles were seen in hybrid structures formed by fusion of clear vacuoles with rER cisternae (Fig. 4E). Starting from 40 min of incubation, gold particles were seen in proximity to the nuclear envelope and within the nucleus of individual cells (Fig. 5). Nuclear localisation of saporin was present in approximately 10% of the cells; however, the gold labelling intensity varied greatly ranging from moderate (8% of HeLa cells containing less than 10 gold particles/individual nuclear area) to intense (2% of HeLa cells showing more than 10 gold particles/individual nuclear area).

Identification of DNA damage by endonuclease IV comet assay

This method relies on *E. coli* endonuclease IV that is able to detect and repair DNA gaps resulting from the recognition of abasic sites.

The chromatin of control cells was intact, which is a sign that the experimental procedure did not alter the nuclei (Fig. 6A). In more than 90% of the cases, the electrophoresis of nuclei from cells treated with saporin revealed the formation of tails, an index of DNA fragmentation (Fig. 6B). These damages are repaired in most cells by endonuclease IV, which

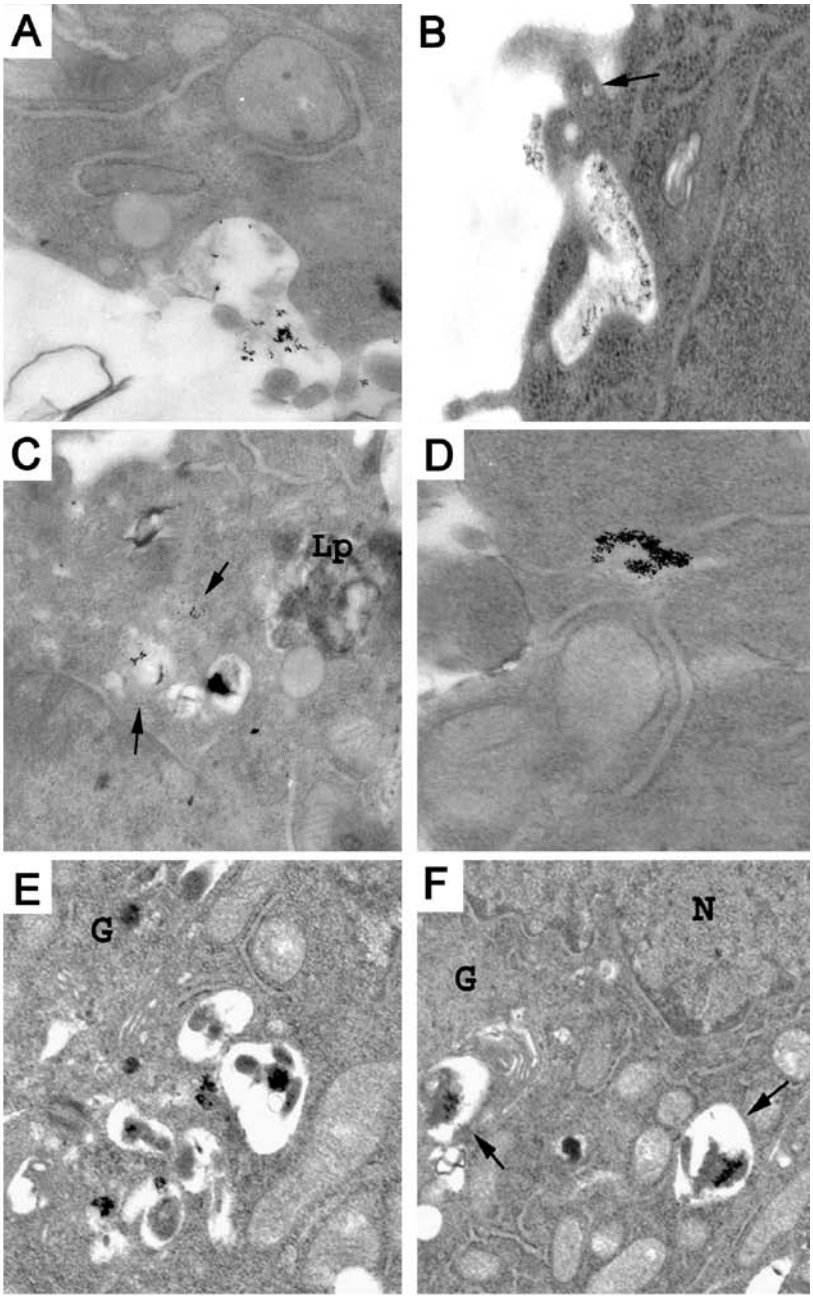

Fig. 3. *Ultrastructural analysis of saporin internalisation pathway by gold-labelled saporin.* ***A****) After 20 min of incubation with* 10^{-5} *M saporin, 5 nm gold particles are located in large invaginations of the plasma membrane; (****B****) collections of gold particles within a large pinocytotic vacuole; the arrow indicates a single gold particle in a coated vesicle; (****C****) after 40 min, clusters of gold particles (indicated by the arrows) are found in late endosomes in the Golgi zone close to the nuclear area; lipofuscin (Lp) do not contain gold particles; (****D****) occasionally clusters of gold particles are seen in close association with rER cisternae. Large collections of colloidal particles (arrows) are seen adjacent to the nuclear area after 60 (****E****) and 120 (****F****) min of incubation with 5 nm gold-saporin conjugate. The Golgi apparatus is normal-looking. Pre-embedding; 5 nm gold-saporin complexes. Magnification: x21500 (A); x36000 (B); x21500 (C); x27000 (D); x16500 (E); x13200 (F).*

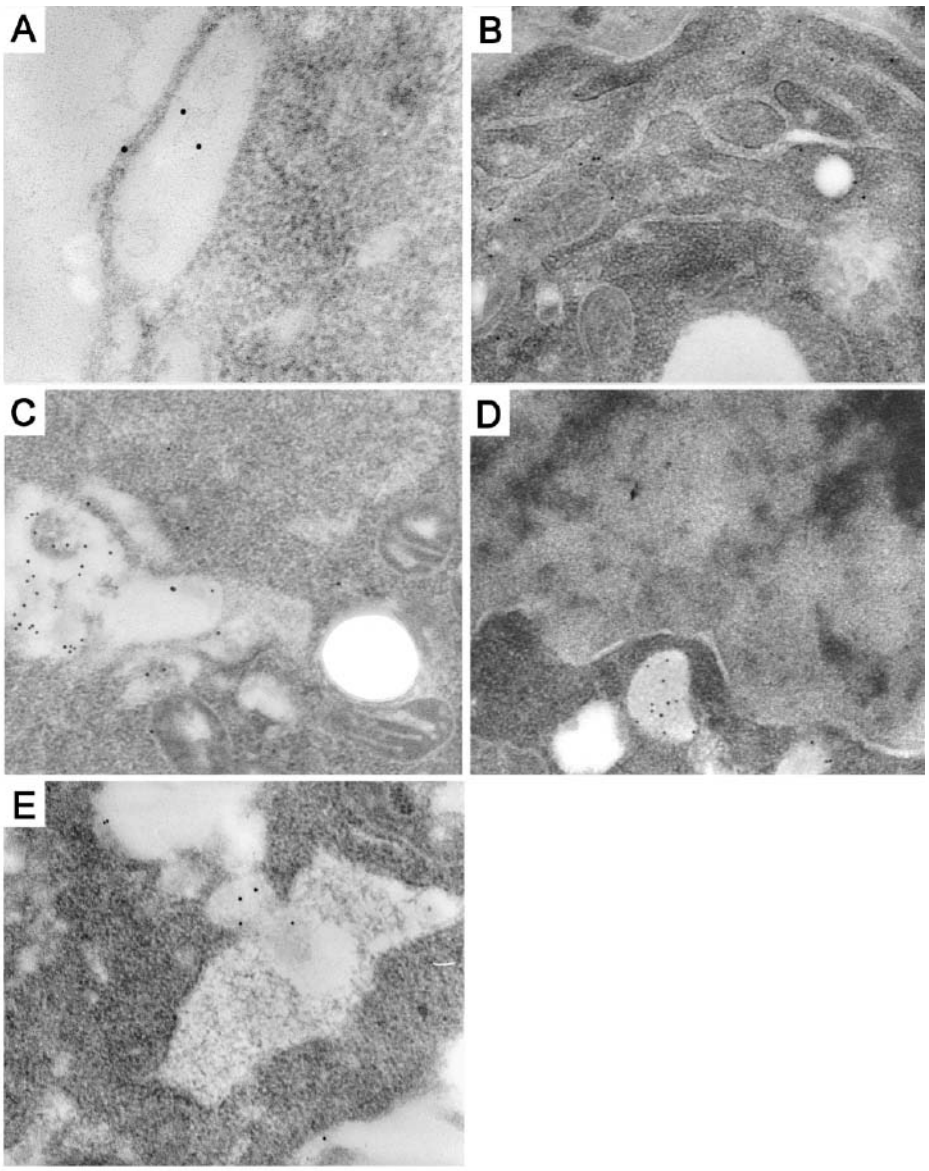

Fig. 4. *Ultrastructural analysis of saporin internalisation pathway by immunogold labelling.* ***A****) After 20 min of incubation with* 10^{-5} *M saporin, 10 nm gold particles were seen in sub-plasmalemmal clear vacuoles;* ***(B)*** *single gold particles were also observed free in the cytoplasm;* ***(C)*** *and* ***(D)*** *after 40 min, vacuoles containing gold particles were located in close proximity to the nuclear envelope;* ***(E)*** *gold particles in hybrid structures formed by fusion of clear vacuoles with rER cisternae (60 min of incubation). Post-embedding; anti-saporin polyclonal antibody followed by incubation with a 10 nm gold-labelled secondary antibody. Magnification: x46000 (A); x36000 (B, C, D); x46000 (E).*

is able to reassemble chromatin in nuclei. Less than 8% of the nuclei from saporin-treated cells appeared tailed after endonuclease IV treatment.

DISCUSSION

The present paper shows the endocytosis of saporin in HeLa cells and subsequent intracellular trafficking of saporin. This study gives detailed data for the first time regarding the full sequence of uptake and intracellular fate of type 1 RIPs. HeLa cell morphology was investigated by transmission electron microscopy. Reversible cell damage involving mitochondria, rough ER cisternae, and

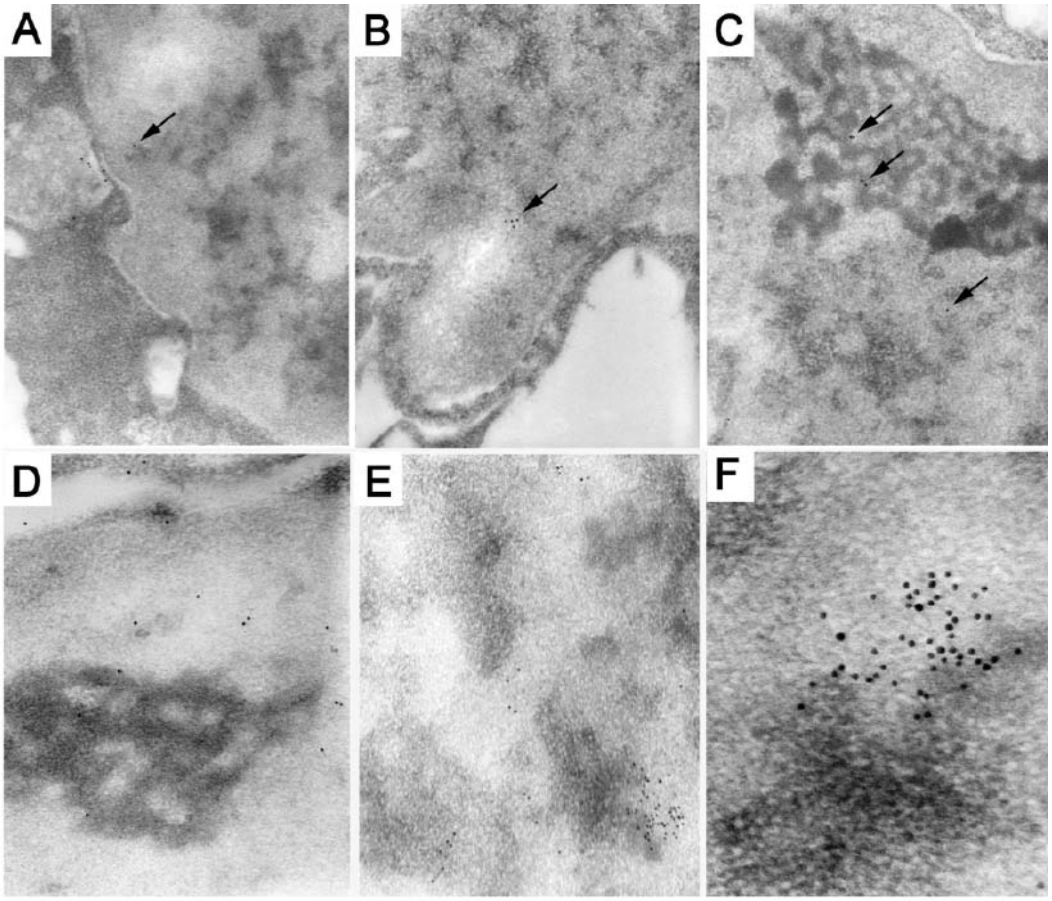

Fig. 5. *Nuclear localisation of saporin by immunogold labelling. After 40 min of saporin (10^{-5} M) treatment, individual HeLa cells showed: (**A**) isolated gold particles in a vacuole in proximity with the nucleus containing itself a single gold particle; (**B**) a few gold particles in the nucleolar zone; (**C**) some gold particles in a nucleus. In A-C the arrows indicate intranuclear gold particles. After 60 min of incubation, the number of gold particles seen in the nucleus of individual cells increased (**D-F**). Post-embedding; anti-saporin polyclonal antibody followed by incubation with a 10 nm gold labelled secondary antibody. Magnification: x16500 (A-C), x57000 (D); x38000 (E); x120000 (F).*

formation of vacuoles was observed after 20 h exposure to 10^{-6} M saporin. To study the cellular interactions of saporin and follow the progressive intracellular localisation, we used experimental conditions (10^{-5} M saporin up to 2 h) that did not result in strong inhibition of protein synthesis and visible cell alterations.

Both direct and indirect methods were utilised. Using an indirect immunofluorescence assay, the presence of saporin inside the cell was detected in the vesicular structure after only 20 min of cell exposure to the RIP. Moreover, the pulse-chase method allowed us to see saporin in vesicles that were progressively close to the nucleus. The confocal microscopy analysis confirmed the suggested intracellular routing of saporin and evaluated the co-localisation of saporin within the ER, Golgi apparatus and nucleus. However, the results of confocal microscopy did not allow us to draw a definitive intracellular pathway for saporin. For this reason, a transmission electron microscopic study was performed. To overcome any doubt about a different localisation of free and gold-conjugated saporin, direct and indirect methods were used. In the direct method, saporin was conjugated with very small gold particles (5 nm) to increase the test definition. The indirect immunoelectron microscopy assay was set up to obtain a good preservation of

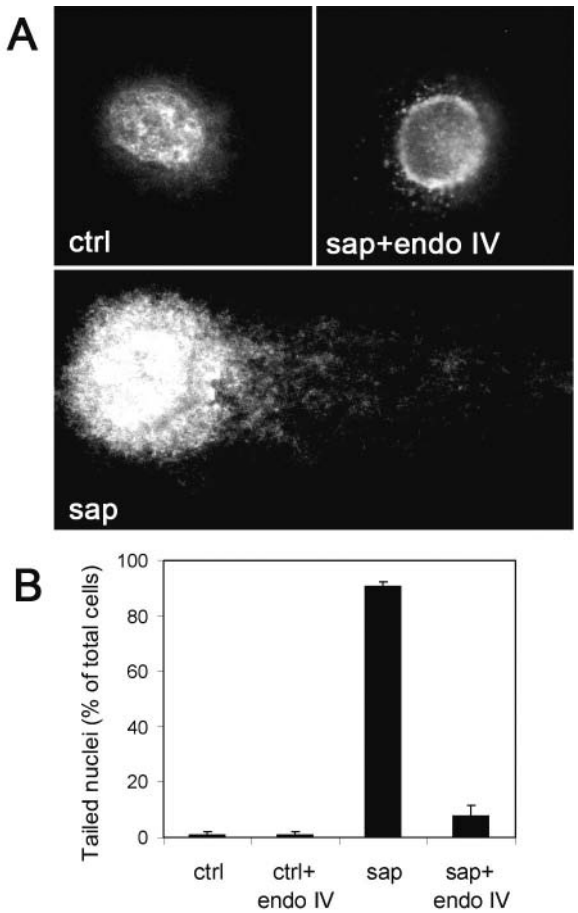

Fig. 6. *Detection of saporin enzymatic activity on cellular DNA by comet assay. HeLa cells were incubated in the absence (control cells or ctrl) or presence of saporin 10^{-5} M for 2 h and in medium without RIP overnight at 37°C (sap). Cells were prepared for the Comet assay as described in Materials and Methods. Half of the samples were incubated with endonuclease IV (ctrl+ endo IV, sap + endo IV). The slides were observed on an Eclypse E600 fluorescence microscope with a 100x immersion objective using a filter specific for DAPI (358 nm excitation λ, 461 nm emission λ).* ***A)*** *Morphology of representative nuclei.* ***B)*** *Percentage of tailed nuclei with respect to the total. Results are the means of three independent experiments with more than 100 cells counted for each slide. Standard deviations did not exceed 10%.*

cell morphology and ensure antibody recognition of saporin, i.e., the immunolabelling localisation. Finally, the evidence of a sporadic nuclear localisation of saporin prompted us to ascertain by endonuclease IV/comet assay the presence of DNA damage in intoxicated cells, possibly related to saporin depurinating activity.

Previous studies that analysed the cellular interactions of type 1 RIPs examined a single step of the sequence of events leading to cell death and could not reach conclusive indications. The first aspect examined by this study was the mechanism of saporin endocytosis. The type 1 RIP gelonin was reported to be internalised by a non-specific fluid phase pinocytosis (17, 18). Consistently, saporin uptake by HeLa cells was not due to specific binding sites (30). However, receptor-mediated endocytosis through the LDL-receptor family was concluded as a mechanism for saporin (19, 21) and another type 1 RIP, trichosanthin (23). The very low binding capacity and entry into the cell exhibited by saporin as compared to type 2 RIPs suggests a low number of receptors on the cell surface or a low binding affinity. These data confirm that this step is the foremost cause of low cytotoxicity. A discrepancy was reported between the level of α_2-macroglobulin receptor, an LDL receptor-related protein, and saporin cytotoxicity, i.e. receptor positive and negative cell lines have similar sensitivities towards saporin toxicity (31), suggesting a receptor-independent endocytosis of the RIP. The present results clearly indicate that saporin endocytosis is performed by HeLa cells mainly through non-coated vesicles.

The identification of the pathway that followed saporin entry into the endosomal compartment also needed to be clarified. Ammonium chloride, chloroquine and monensin have been utilised to study the intracellular routing of gelonin in HeLa cells (16) and saporin in haematological blasts (20). These substances had no effect on the inhibition of cell protein synthesis induced by type 1 RIPs, suggesting a lack of involvement of lysosomes and Golgi cisternae in the intracellular transport of these proteins to the cytosol. Consistent with these data, the confocal microscopy analysis showed around 30% co-localisation of saporin with the endosomal compartment and less than 10% with the Golgi apparatus. An immunofluorescence assay showed a progressive accumulation of saporin in a perinuclear vesicular structure. The pathway marked out by pre-embedding and post-embedding experiments confirmed the progression of saporin through an

endosomal vesicle to the perinuclear area. Single gold particles were observed free in the cytoplasm after only 20 min of cellular exposure to saporin and in hybrid structures formed by fusion of clear vacuoles with rER cisternae after 60 min of incubation. These data suggest that saporin reaches the cytoplasmic target by more than one mechanism. These results are in agreement with a report demonstrating that saporin, in contrast to the ricin A chain, enters the cytosol through a Golgi-independent pathway (22).

The main finding of this work is the demonstration of the nuclear localisation of saporin. Of note, this observation was obtained only with the post-embedding technique, demonstrating that the direct labelling of proteins may alter their intracellular trafficking. In addition, the nuclear localisation of saporin was observed in a limited percentage of intoxicated cells. This result is in agreement with the low percentage of nuclear localisation calculated from the confocal microscopy data. The fact that saporin may reach the nucleus raises questions about the biological meaning of the depurinating activity of RIPs on DNA, i.e., the role of this enzymatic activity on RIP cytotoxicity. The presence of saporin in the nucleus suggests that the DNA damage could be one of the mechanisms used by this protein and possibly other RIPs to kill the cell, specifically by inducing the DNA-dependent apoptotic death. The low percentage of gold-labelled nuclei also suggests that saporin utilises more than one mechanism of cell killing.

A specific comet assay was developed to further investigate the possibility that saporin, albeit in small amounts, could reach the nucleus and exert its activity on DNA. This assay was able to detect DNA gaps resulting from the detachment of purinic/pyrimidinic bases by showing DNA degradation. The addition of endonuclease IV allowed the shape recovery of the nuclei, highlighting the repair of the DNA damage due to base cleavage that could be induced by the deadenylation activity of RIP. Afterwards, a low percentage of tailed nuclei were still observed due to the incomplete action of the DNA repair system or the presence of non-recoverable breaks.

The results obtained with the comet assay indicate that saporin might be able to enter the nucleus of HeLa cells and induce DNA damage through its enzymatic PNAG activity, suggesting that the nuclear injury could be one of the mechanisms used by RIP to trigger cell death, e.g., activating DNA-dependent apoptosis (14). In this case, the action of saporin can be compared to ricin, which induced damage to nuclear DNA preceding apoptosis of endothelial cells (32).

In conclusion, our results, by showing the localisation of saporin within the ER, Golgi apparatus and nucleus, indicate that saporin reaches different subcellular compartments of HeLa cells by more than one pathway, in agreement with previous reports (20, 22). Moreover, the DNA damage apparently related to saporin depurinating activity could be one of the mechanisms of cell killing by saporin, in addition to the well-known ribosomal injury. According to previous reports (14, 15), our results suggest that saporin, and possibly other RIPs, utilises more than one mechanism to trigger cell death.

ACKNOWLEDGEMENTS

This study was supported by the University of Bologna and the Pallotti's Legacies for Cancer Research.

REFERENCES

1. Stirpe F, Battelli MG. Ribosome-inactivating Proteins: progresses and problems. Cell Mol Life Sci 2006; 63:1850-66.
2. Battelli MG. Cytotoxicity and toxicity to animals and humans of ribosome-inactivating proteins. Mini-Rev Med Chem 2004; 4:513-21.
3. Girbes T, Ferreras JM, Arias FJ, et al. Non-toxic type 2 ribosome-inactivating proteins (RIPs) from Sambucus: occurrence, cellular and molecular activities and potential uses. Cell Mol Biol (Noisy-le-grand) 2003; 49:537-45.
4. Ferreras JM, Citores L, Iglesias R, Jiménez P, Girbés T. Sambucus Ribosome-Inactivating Proteins and Lectins. Toxic Plant Proteins, Plant cell Monographs; Lord JM, Hartley MR; Eds.; Springer-Verlag: Berlin, Germany, 2010; 18:107-31.
5. Sandvig K, Grimmer S, Lauvrak SU, Torgersen ML, Skretting G, van Deurs B, Iversen TG. Pathways followed by ricin and Shiga toxin into cells. Histochem Cell Biol 2002; 117:131-41.

6. Roberts LM, Lord JM. Ribosome-inactivating proteins: entry into mammalian cells and intracellular routing. Mini-Rev Med Chem 2004; 4:505-12.
7. Lord JM, Spooner RA. Ricin trafficking in plant and Mammalian cells. Toxins 2011; 3:787-801.
8. Liu Q, Zhan J, Chen X, Zheng S. Ricin A chain reaches the endoplasmic reticulum after endocytosis. Biochem Biophys Res Commun 2006; 343:857-63.
9. Stirpe F, Gasperi-Campani A, Barbieri L, Falasca A, Abbondanza A, Stevens WA. Ribosome-inactivating proteins from the seeds of *Saponaria officinalis* L. (soapwort), of *Agrostemma githago* L. (corn cockle) and of *Asparagus officinalis* L. (asparagus), and from the latex of *Hura crepitans* L. (sandbox tree). Biochem J 1983; 216:617-25.
10. Bolognesi A, Polito L. Immunotoxins and other conjugates: pre-clinical studies. Mini-Rev Med Chem 2004; 4:563-83.
11. Kreitman RJ. Immunotoxins for targeted cancer therapy. AAPS J 2006; 8:E532-51.
12. Polito L, Bortolotti M, Pedrazzi M, Bolognesi A. Immunotoxins and other conjugates containing saporin-S6 for cancer therapy. Toxins. 2011; 3:697-720.
13. Bolognesi A, Tazzari PL, Olivieri F, Polito L, Falini B, Stirpe F. Induction of apoptosis by ribosome-inactivating proteins and related immunotoxins. Int J Cancer 1996; 68:349-55.
14. Polito L, Bortolotti M, Farini V, Battelli MG, Barbieri L, Bolognesi A. Saporin induces multiple death pathways in lymphoma cells with different intensity and timing as compared to ricin. Int J Biochem Cell Biol 2009; 41:1055-61.
15. Sikriwal D, Ghosh P, Batra JK. Ribosome inactivating protein saporin induces apoptosis through mitochondrial cascade, independent of translation inhibition. Int J Biochem Cell Biol 2008; 40:2880-8.
16. Goldmacher VS, Blattler WA, Lambert JM, McIntyre G, Stewart J. Cytotoxicity of gelonin conjugated to targeting molecules: effects of weak amines, monensin, adenovirus, and adenoviral capsid proteins penton, hexon, and fiber. Mol Pharmacol 1989; 36:818-22.
17. Madan S, Ghosh PC. Interaction of gelonin with macrophages: effect of lysosomotropic amines. Exp Cell Res 1992; 198:52-8.
18. Colaço M, Bapat MM, Misquith S, Jadot M, Wattiaux-De Coninck S, Wattiaux R. Uptake and intracellular fate of gelonin, a ribosome-inactivating protein, in rat liver. Biochem Biophys Res Commun 2002; 296:1180-5.
19. Cavallaro U, Nykjaer A, Nielsen M, Soria MR. Alpha 2-macroglobulin receptor mediates binding and cytotoxicity of plant ribosome-inactivating proteins. Eur J Biochem 1995; 232:165-71.
20. Battelli MG, Bolognesi A, Olivieri F, Polito L, Stirpe F. Different sensitivity of CD30+ cell lines to Ber-H2/saporin-S6 immunotoxin. J Drug Target 1998; 5:181-91.
21. Ippoliti R, Lendaro E, Benedetti PA, Torrisi MR, Belleudi F, Carpani D, Soria MR, Fabbrini MS. Endocytosis of a chimera between human pro-urokinase and the plant toxin saporin: an unusual internalization mechanism. FASEB J 2000; 14:1335-44.
22. Vago R, Marsden CJ, Lord JM, Ippoliti R, Flavell DJ, Flavell SU, Ceriotti A, Fabbrini MS. Saporin and ricin A chain follow different intracellular routes to enter the cytosol of intoxicated cells. FEBS J 2005; 272:4983-95.
23. Shaw PC, Lee KM, Wong KB. Recent advances in trichosanthin, a ribosome-inactivating protein with multiple pharmacological properties. Toxicon 2005; 45:683-9.
24. Zhang F, Sun S, Feng D, Zhao WL, Sui SF. A novel strategy for the invasive toxin: hijacking exosome-mediated intercellular trafficking. Traffic 2009; 10:411-24.
25. Barbieri L, Stoppa C, Bolognesi A. Large scale chromatographic purification of ribosome-inactivating proteins. J Chromatogr 1987; 408:235-43.
26. Bolognesi A, Polito L, Lubelli C, Barbieri L, Parente A, Stirpe F. Ribosome-inactivating and adenine polynucleotide glycosylase activities in *Mirabilis jalapa* L. tissues. J Biol Chem 2002; 277:13709-16.
27. Strocchi P, Barbieri L, Stirpe F. Immunological properties of ribosome-inactivating proteins and a saporin immunotoxin. J Immunol Methods 1992; 155:57-63.
28. Bolognesi A, Polito L, Farini V, et al. CD38 as a target of IB4 mAb carrying saporin-S6: design of an immunotoxin for ex vivo depletion of hematological CD38+ neoplasia. J Biol Regul Homeost Agents

2005; 19:145-52.

29. Battelli MG, Musiani S, Buonamici L, Santi S, Riccio M, Maraldi NM, Girbes T, Stirpe F. Interaction of volkensin with HeLa cells: binding, uptake, intracellular localization, degradation and exocytosis. Cell Mol Life Sci 2004; 61:1975-84.
30. Battelli MG, Montacuti V, Stirpe F. High sensitivity of cultured human trophoblasts to ribosome-inactivating proteins. Exp Cell Res 1992; 201:109-12.
31. Bagga S, Hosur MV, Batra JK. Cytotoxicity of ribosome-inactivating protein saporin is not mediated through alpha2-macroglobulin receptor. FEBS Lett 2003; 541:16-20.
32. Brigotti M, Alfieri R, Sestili P, et al. Damage to nuclear DNA induced by Shiga toxin 1 and ricin in human endothelial cells. FASEB J 2002; 16:365-72.

THE GASEOUS MESSENGER CARBON MONOXIDE IS RELEASED FROM THE EYE INTO THE OPHTHALMIC VENOUS BLOOD DEPENDING ON THE INTENSITY OF SUNLIGHT

M. KOZIOROWSKI[1], S. STEFAŃCZYK-KRZYMOWSKA[2], A. TABĘCKA-ŁONCZYŃSKA[1], P. GILUN[2] and M. KAMIŃSKI[3]

[1]Department of Animal Physiology and Reproduction, University of Rzeszow, Rzeszów, Poland;
[2]Department of Local Physiological Regulation, Institute of Animal Reproduction and Food Research of the Polish Academy of Sciences, Olsztyn, Poland;
[3]Chemical Faculty, Gdańsk University of Technology, Gdańsk, Poland

Received April 18, 2011 – Accepted January 16, 2012

Circadian and seasonal rhythms in daylight affect many physiological processes. In the eye, energy of intense visible light not only initiates a well-studied neural reaction in the retina that modulates the secretory function of the hypothalamus and pineal gland, but also activates the heme oxygenase (HO) to produce carbon monoxide (CO). This study was designed to determine whether the concentration of carbon monoxide (CO) in the ophthalmic venous blood changes depending on the phase of the day and differing extremely light intensity seasons: summer and winter. The concentration of CO in the venous blood flowing out from the nasal cavity, where heme oxygenase (HO) is expressed, but no photoreceptors, was used as a control. Sixteen mature males of a wild boar and pig crossbreed were used for this study. Samples of ophthalmic and nasal venous blood and systemic arterial and venous blood were collected repeatedly for two consecutive days during the longest days of the summer and the shortest days of the winter. The concentrations of CO in blood samples was measured using a standard addition method. During the longest days of the summer the concentration of CO in ophthalmic venous blood averaged 3.32±0.71 and 3.43±0.8 nmol/ml in the morning and afternoon, respectively, and was significantly higher than in the night averaging 0.89±0.12 nmol/ml ($p<0.001$). During the shortest day of the winter CO concentration in ophthalmic venous blood was 1.11±0.10 and 1.13±0.14 nmol/ml during the light and nocturnal phase, respectively, and did not differ between phases, but was lower than in the light phase of the summer ($p<0.01$). The CO concentration in the control nasal venous blood did not differ between seasons and day phases and was lower than in ophthalmic venous blood during the summer ($p<0.01$) and winter ($p<0.05$). The results indicate that the gaseous messenger carbon monoxide is released from the eye into the ophthalmic venous blood depending on the intensity of sunlight.

The role of gaseous messengers, such as nitric oxide (NO) carbon monoxide (CO) and hydrogen sulfide (H_2S), in the physiological regulations was recently the subject of numerous studies, but their functions were still not fully explained. There is much evidence demonstrating that they do not participate

Key words: carbon monoxide, eye physiology, gaseous messenger

Mailing address:
Marek Koziorowski,
ul. Rejtana 16C,
Rzeszów 35-959, Poland
Tel: +48 17 872 32 57
Fax: +48 17 872 32 61
e-mail: mkozioro@univ.rzeszow.pl

0393-974X (2012)

DISCLOSURE: ALL AUTHORS REPORT NO CONFLICTS OF INTEREST RELEVANT TO THIS ARTICLE.

solely in the local regulations (1-3). In 1996, Dan A. Oren published an inspirational hypothesis on humoral phototransduction that assumed that the information of light intensity might be transmitted from the retina to the brain not only by a neural pathway as generally accepted but also by CO and NO using a humoral pathway (1).

Circadian and seasonal rhythms in the daylight affect many physiological processes. In the eye, energy of intense visible light not only initiates a well-studied neural reaction in the retina that modulates the secretory function of the hypothalamus and pineal gland (4), but also activates the heme oxygenase (HO) to produce CO (5). In the tissue of both human and other animals, there are two isoforms of HO: inducible (HO-1), and constitutive (HO-2) which act to break the rings of the heme to produce CO, ferrous iron and biliverdin/bilirubin (6-8). The vascularisation of the retina, the biconcave shape of red blood cells and the approximately one billion heme rings per erythrocyte create a special environment for the absorbtion of photons of light energy; the photons activate HO to break heme rings resulting in the production of CO (1, 5). Therefore, the question arises whether the CO is produced in structures of the eye exclusively for local use, or whether it is released into the venous blood flowing out from the eye from which it could reach the venous ophthalmic sinus and venous cavernous sinus to take part in the systemic regulation by the humoral pathway.

The local role of CO in the eye physiology is not well established. However, it has been demonstrated that CO generated in the retina can be locally involved in dark adaptation and light sensitivity (9). Induction of HO-1 in the retina by intense visible light was demonstrated earlier (5). High levels of HO-1 mRNA and HO-2 protein inducting syntheses of CO and modulating soluble guanylate cyclase to cGMP were found in all photoreceptors in turtle amacrine cells and bipolar and ganglion cells of the inner retina in rats (10). Incubation of the turtle retina with CO stimulated cGMP production (11). Treatment of the retina in combination with CO and nitric oxide (NO) dramatically increased cGMP synthesis in the retina compared to NO or CO treatment alone (10, 11). Moreover, HO-1 appears to be involved in the regulation of intraocular pressure via CO production (12). HO-1 was also upregulated in central retinal artery occlusion (13). CO has been found to be a very important vasodilator (14-16). When endogenous or exogenous CO diffuses into the vascular smooth muscle cells, it elicits vasodilatation by increasing cGMP production, and consequently it hyperpolarizes the muscle cells by opening potassium channels and modulate intracellular cGMP concentration (17-20). Direct modulation of large-conductance calcium-activated potassium (BK_{Ca}) channels in vascular smooth muscle cells by CO was also shown (21). It has been demonstrated that inhalation of CO for 60 min increases significantly the diameter of the human retinal arteries and veins, as measured by retinal vessel analyzer and enhanced retinal blood flow by 12% (22).

The present study was designed to determine whether the concentration of CO in the ophthalmic venous blood changed depending on the phase of day and differing extremely light intensity seasons: summer and winter. As a control, the concentration of CO in the venous blood flowing out from the nasal cavity, where HO is expressed (23, 24) but photoreceptors are not present, was also determined.

To study the neuro-hormonal response to the intensity of sunlight a good animal model was needed. We decided to use a crossbreed resulting from the mating of domestic swine and a wild boar (maintained behavioural reactions and seasonal reproduction). The size of their blood vessels allows for the implantation of the polyethylene catheter into the angularis oculi vein (25). This catheter allows for repeated collection of ophthalmic venous blood from the ophthalmic sinus of conscious animals while maintaining a normal physiological condition over two consecutive days.

MATERIALS AND METHODS

Basic statements

All the procedures were carried out in compliance with Polish legal regulations (Act of January 21, 2005), which determine the terms and conditions for performing experiments on animals, and were in accordance with the protocol of the Local Ethics Commission for Animal Experiments in Lublin No. 8/2007. Mature males of a wild boar and pig crossbreed (12 months of age, body mass ~100-120 kg, n=16) were used for the study. The animals were housed in an experimental farm in Kolbuszowa

(50°N) near Rzeszów (Physiology and Reproduction of Animals Department, Rzeszów University). They were kept under natural illumination and had *ad libitum* access to water and food.

The experiments were performed during two seasons: during the days with the longest periods of light in the summer (second half of June) and during the days with the shortest periods of light in the winter (second half of December). During the summer, the animals were maintained in an open-sided shed and exposed to approximately 30,000 lx of natural illumination during the day. The mean ambient temperature was 24°C during the light phase and 12°C during the nocturnal phase. During the winter, the animals were housed in a room with windows and were exposed to between 40 and 50 lx of natural illumination at the eye level of the animals during the day. The mean temperature during the day and night was 12°C. A dim, red spotlight was used to assist in the collection of blood samples during the nocturnal phase.

Surgical procedures and blood sample collection

Five hours before the collection of blood samples, the animals were premedicated with atropine (0.05 mg/kg I.M.; Biowet, Gorzów Wielkopolski, Poland) and azaperone (Stresnil 2 mg/kg I.M.; Janssen Pharmaceutica, Beerse, Belgium). General anesthesia was induced with thiopental sodium (Thiopental, Sandoz GmbH, Austria). Two silastic catheters (o.d., 2.4 mm; i.d., 1.8 mm) were inserted into the dorsal nasal vein. The first catheter was directed into the proximal part of the nasal vein to collect nasal venous blood. The second catheter was inserted in the opposite direction such that it passed through the angularis oculi vein and ended near the venous ophthalmic sinus. This catheter placement allowed for the collection of venous blood flowing out of the eye (Fig. 1). Two additional catheters (o.d., 2.4 mm; i.d., 1.8 mm) were inserted into the carotid artery and jugular vein to collect systemic arterial and venous blood. For two consecutive days, blood samples (10 ml) were collected from the nasal vein and the venous ophthalmic sinus every four hours during the day (4:00, 8:00 and 12:00 a.m. and 4:00, 8:00 and 10:00 p.m.) and every two hours during the night (12:00 p.m., 2:00 a.m.). Systemic arterial blood samples were simultaneously collected every eight hours during the day, and systemic venous blood samples were collected every eight hours during the day and night from each animal.

The analysis of trace levels of CO in blood samples

The determination of CO concentrations in blood samples was performed at the Chemical Faculty, Gdansk University of Technology, using a standard addition

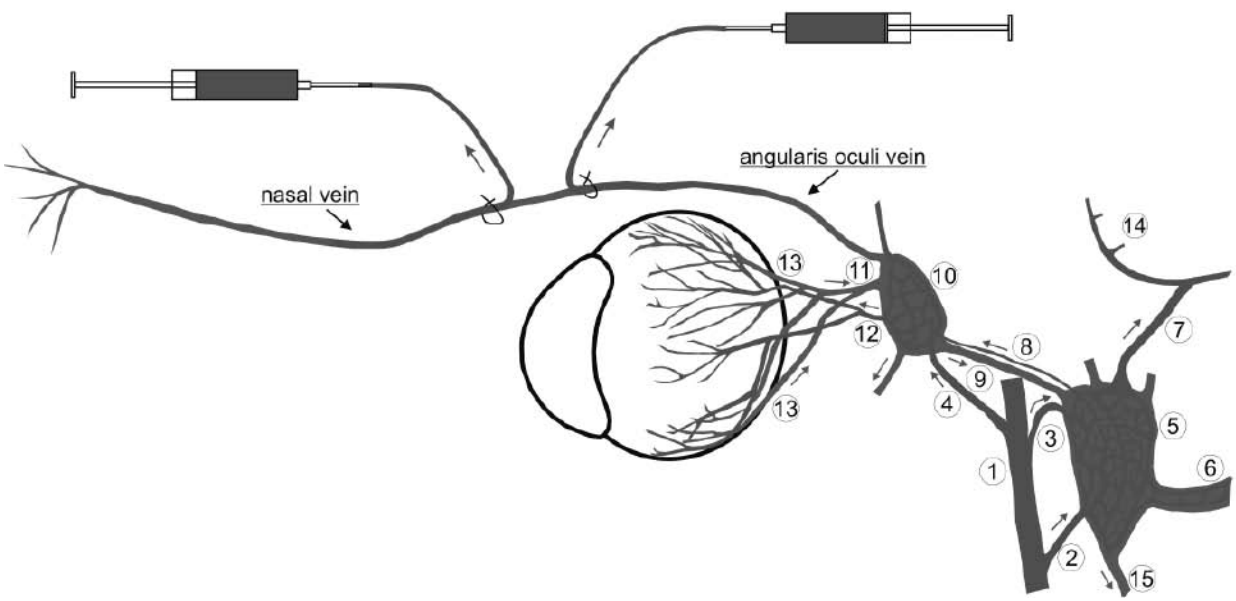

Fig. 1. *A simplified scheme of the experiment with ophthalmic and nasal venous blood collection points and the depiction of the arterial blood supply of the eye and the effluent venous blood. 1, maxillary artery; 2-3, branches of the epidural rete mirabile; 4, external ophthalmic artery; 5, epidural rete mirabile in the cavernous sinus; 6, intercavernous sinus; 7, internal carotid artery; 8, anastomotic branch with epidural rete mirabile; 9, emissary vein of the foramen orbitorotundum; 10, ophthalmic venous sinus and the rete mirabile of the external ophthalmic artery; 11, ophthalmic vein; 12, ophthalmic external artery; 13, ciliary vein; 14, circle of Willis; 15, to jugular vein.*

method. The analytical procedure is based on combining the Headspace (HS) analytical technique (extraction of CO from the blood sample via its gaseous phase) with the column gas chromatography technique, which uses a packed column for the separation of the gaseous sample components (molecular sieve 5A, 80-100 mesh, activated at 350°C). Trace concentrations of CO were determined as concentrations of methane (CH_4) using a flame ionization detector (FID) after stoichiometric catalytic conversion of CO to CH_4 in a Raney nickel-packed microreactor that was located between the outlet of the column and the inlet of the FID detector (Col-/5A/-GC-/CO-CH4/-FID). The application of the 5A molecular sieve column ensured the separation of CO and oxygen (O_2) and thus, eliminated the possible influence of O_2 on the determination of trace amounts of CO.

Chromatographic conditions used for the determination of trace amounts of CO in blood samples: Gas chromatograph - Agilent 6890; Column: 2 m x 2.1 mm i. d. - GC column packed with molecular sieve 5A (80-100 mesh); Detector: FID (280°C) with Raney Ni – methanizer; Carrier: helium; 10 cm^3 min^{-1}; Oven temperature: 130°C; Injection port: splitless; 100°C – injection using gas-tight syringe; sample volume: 0.5 cm^3; limit of detection (LOD): 0.5 ppm (v/v) CO.

The concentration of CO (nmol/ml) in the blood samples was calculated using the formula:

$$C_X = \frac{C_W V_W \cdot (A_W - A_2) \cdot A_1}{V_L \cdot A_W \cdot (A_2 - A_1)}$$

where C_x is the concentration of CO in the blood sample, C_w is the concentration of CO in the standard mixture added to the HS vial containing the sample, V_L is the volume of the liquid sample (blood) put into the HS vial, V_w is the volume of the standard gas mixture introduced into the HS vial, A_1 is the CO peak area for the blood sample, A_2 is the CO peak area for the blood sample with the standard addition and A_w is the CO peak area for the standard mixture.

A more detailed description of the procedure for CO/CO_2/CH_4/O_2 separation, as well as the determination of trace amounts of CO in gas samples, was previously described (26).

Statistical analysis

All data are presented as the mean ± SEM. The concentrations of CO in venous blood flowing out from the eye and from the nasal area obtained during the morning, afternoon and night (Fig. 2 and Fig. 4) were compared between the vessels and between experimental periods using a nonparametric Mann-Whitney *t*-test. The venous outflows of CO from the eye and nasal area during the light phase of the summer (Fig. 3) were analyzed by determining the total area under the respective curves, and these data were also compared by nonparametric Mann-Whitney *t*-test. All analyses were performed with the use of Prism GraphPad Software (San Diego, CA).

RESULTS

During summer days, when animals were exposed to approximately 30,000 lx of natural illumination, the concentration of CO in ophthalmic venous blood flowing out from the eye and collected from ophthalmic sinus was the highest in the morning ($P<0.001$) and the afternoon ($p<0.05$) compared to samples collected in parallel from control nasal venous blood (Fig. 2A). CO concentration in ophthalmic venous blood did not differ between samples that were collected in the morning and afternoon of summer days (Fig. 2 A, B). During the nocturnal phase, CO concentration in ophthalmic venous blood was approximately three times lower ($P<0.001$) than during the light phase of the day (Fig. 2 A, B) and did not differ from the CO concentrations in systemic arterial or venous blood or from nasal venous blood. The average concentration of CO was 1.30±0.4 nm/ml in the systemic arterial blood supplying the eye and 1.24±0.7 nm/ml in systemic venous blood. The CO concentration in the nasal venous blood was low (Fig. 2 A, B) and did not differ from that in the systemic venous blood. The mean areas under the curve for CO concentrations measured over the entire light phase (Fig. 3) for ophthalmic venous blood flowing out from the eye and for nasal venous blood were significantly different ($p<0.01$).

In the winter, when animals were maintained in rooms where the sunlight intensity during the day was between 40 and 50 lx, the CO concentrations of ophthalmic venous blood collected during the light and nocturnal phases were both higher than in nasal venous blood ($p<0.05$), but they were almost three times lower ($p<0.01$) than the CO concentration of ophthalmic venous blood collected during the light phase of the summer (Fig. 2 A, B and Fig. 4A, B). The CO concentration in ophthalmic venous blood did not differ between the samples collected during the light and nocturnal phases in the winter season (Fig. 4 A, B). In addition, the concentration of CO in the control nasal venous blood did not change

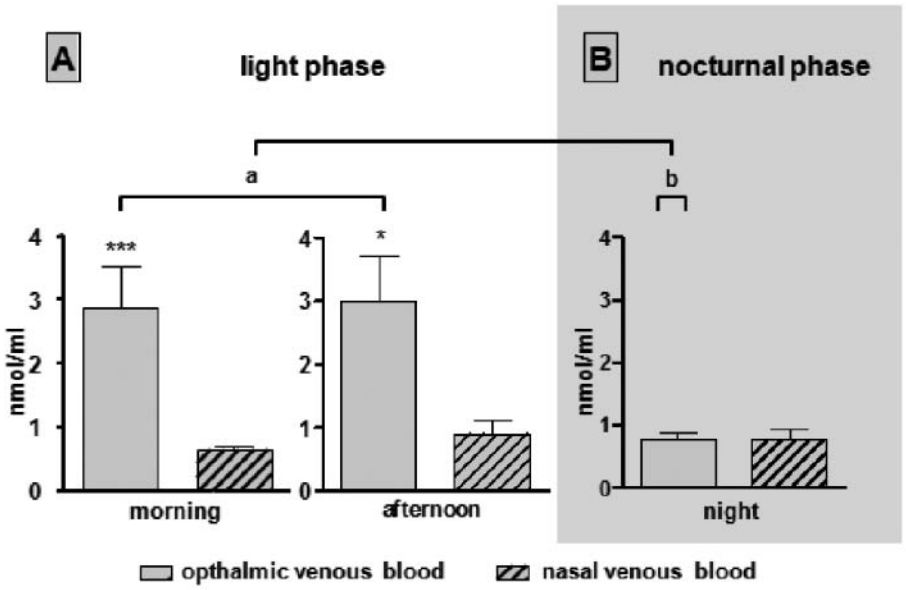

Fig. 2. *Concentration of CO (mean ± SEM) in the venous blood outflow from the eye and nasal areas during the summer. **A**) Light phase of the long days. **B**) Nocturnal phase of the long days. *P<0.05; ***P<0.001; (a/b) P<0.001.*

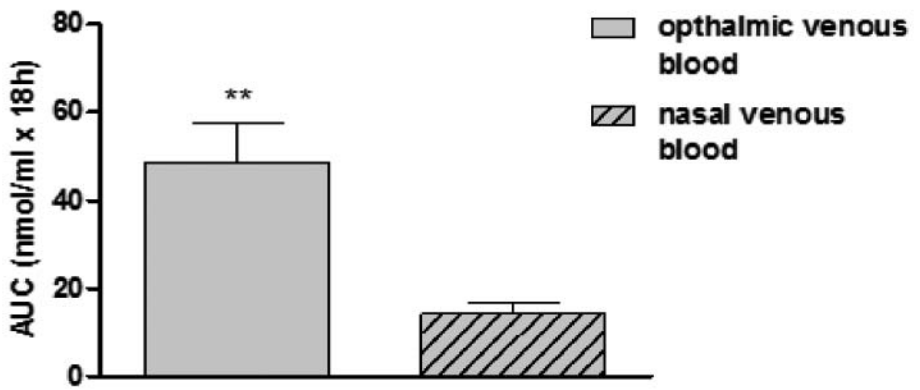

Fig. 3. *CO concentrations in the venous outflow from the eye and nasal areas over the entire collection period during the light phase of the summer presented as the area under the curve (AUC, mean ± SEM) **P<0.01.*

between the day and night (Fig. 4 A, B), and it did not differ from that in the systemic venous blood. A significant difference was not found between the CO concentrations of control nasal venous blood collected in the winter versus the summer. During the winter, the average CO concentration in systemic venous blood was 0.78±0.1 nm/ml and was of similar concentration to that of the night, which was 0.83±0.1 nm/ml.

DISCUSSION

The ability of tissues in many organs, including the eye, to produce CO has been demonstrated by immunohistochemical localization of HO-1 and HO-2 (5-8, 10, 27). In the present study daily measurement of CO concentration in the venous

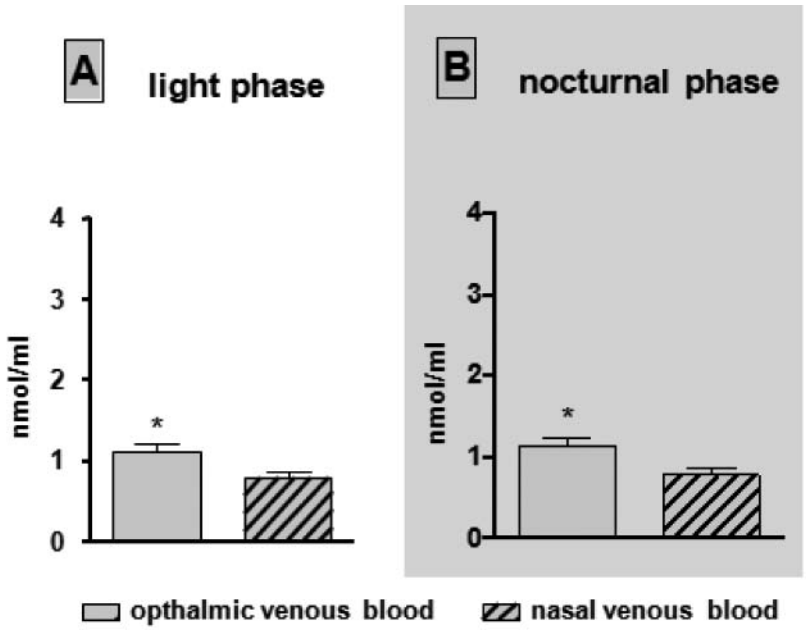

Fig. 4. *The concentration of CO (mean ± SEM) in the venous blood outflow from the eye and nasal areas during the winter. **A**) The light phase of the short days. **B**) The nocturnal phase of the short days. *P<0.05.*

blood flowing out from the eye (and from the nose as the control organ) under physiological condition was performed for the first time to our knowledge. Our results show that CO is not only produced in the eye, but it is also released into the venous blood flowing out from the eye. Furthermore, the amount of CO released from the eye changes during the day and night. The catheters that were inserted into the dorsal nasal vein and into the angularis oculi vein enabled us to repeatedly collect blood samples from the ophthalmic sinus (venous outflow from the eye) and from the nasal vein (venous outflow from nasal area) during the light and nocturnal phases of two consecutive days. It should be emphasized that blood samples were collected in physiological conditions without perturbing the animal. The concentration of CO in venous nasal blood, which was similar to that in systemic venous and arterial blood, was accepted as a control. The localisation of both HO isoforms in the olfactory organ (23, 28) suggested that CO may be produced in this area. Our study demonstrated constant concentration of CO in venous nasal blood during the day and night in both the summer and winter, which potentially resulted from a lack of sensitivity to light in the nasal mucosa.

The results of the present study indicate that during light phase of a summer day with strong illumination reaching the retina (in average of 30 000 lx) the secretion of CO into ophthalmic venous blood was threefold higher comparing to nocturnal phase, during which the CO concentration in ophthalmic venous blood dropped significantly (Fig. 2). In the winter, when the animals were exposed to between 40 and 50 lx during the photophase there was no difference between CO concentration in ophthalmic venous blood during the day and the night. It has been previously demonstrated that light intensity greater than 113 lx during photophase was required for the presentation of melatonin rhythmicity in the pig (29). Moreover, it was postulated that pigs could not differentiate between day and night when the photophase light intensity was 50 lx and the scotophase light intensity 8 lx (30). Thus, it has been hypothesized that pigs may need relatively high photophase light intensity to differentiate between day and night (30). These result could explain why we observed little effect of the light phase on CO release into the ophthalmic venous blood in the winter.

When any result from two seasons are compared

in addition to the difference in light intensity varying ambient temperature should be taken into account. However, the temperature of the blood flow to the retina secreting CO is constant regardless of the season. According to our knowledge there is no information regarding the influence of environmental temperature on the activity of HO and production of CO in the eye.

Venous effluent flow from the eye reaches the ophthalmic sinus (Fig. 1). The high concentration of CO in ophthalmic venous blood and in the venous ophthalmic sinus during the light phase of the summer days couplet with the observed circadian and seasonal changes in this concentration suggest that CO participates in the local regulation of the physiological function of the eye.

It is noteworthy that the concentration of CO in ophthalmic venous blood averaged 3.0 nmol/ml (Fig. 2), whereas the mean concentration of CO in arterial blood, flowing in opposite direction, was in average 1.3 nmol/ml. In the periophthalmic vascular complex (ophthalmic venous sinus and rete mirabile of external ophthalmic artery) the arterial and venous blood stream are closely located to each other (32), making it possible for counter current exchange of particles with the tendency to balance concentrations. We suggest, that under these conditions, after COHb dissociation, CO (size of 28.01 Da) may permeate from venous to arterial blood and be retrograde transferred with ophthalmic arterial blood. It may affect the function of ophthalmic vessels (as exogenous molecule) by influencing the synthesis of cGMP and increasing retinal and choroidal blood flow as it was found after inhaling CO in healthy humans (22). Venous blood from the ophthalmic sinus with high concentration of CO flows to the cavernous sinus (Fig. 2). It is probable that CO, according to Oren's concept (1), may be transferred from venous blood of the cavernous sinus to the arterial blood of rete mirabile of the carotic artery supplying the pituitary and the brain, similarly as it was discovered for numerous neuropeptides and steroid hormones (25).

ACKNOWLEDGEMENTS

The authors dedicate this paper to Professor Tadeusz Krzymowski, who inspired them to perform this research.

This study was supported by the Polish State Committee for Scientific Research (N N 311 1001 33) and Ministry of Science and Higher Education in 2007.

The study was carried out with the use of equipment granted by the project "Centre of Applied Biotechnology and Basic Sciences" supported by the Operational Programme "Development of Eastern Poland 2007-2013", No. POPW.01.03.00-18-018/09

REFERENCES

1. Oren DA. Humoral phototransduction: blood is messenger. Neuroscientist 1996; 2:207-10.
2. Campbell SS, Murphy PJ. Extraocular circadian phototransduction in humans. Science 1998; 279:396-9.
3. Wu L, Wang R. Carbon monoxide: endogenous production, physiological functions and pharmacological application. Pharmacol Rev 2005; 57:585-63.
4. Simonneaux V, Ribelaga C. Generation of the melatonin endocrine massage in mammals: A review of the complex regulation of melatonin synthesis by norepinephrine, peptides, and other pineal transmitters. Pharmacol Rev 2003; 55:325-95.
5. Kutty R.K, Kutty G, Wiggert B, Chader G.J, Darrow RM, Organisciak DT. Induction of heme oxygenase 1 in the retina by intense visible light: suppression by the antioxidant dimetylthiourea. Proc Natl Acad Sci USA 1995; 92:1177-81.
6. Tenhunen R, Marver HS, Schmid R. The enzymatic conversion of heme to bilirubin by microsomal heme oxygenase. Proc Natl Acad Sci USA 1968; 61:748-55.
7. Maines MD. Heme oxygenase: function, multiplicity, regulatory mechanisms and clinical applications. FASEB J 1988; 2:2557-68.
8. Ortiz de Montellano PR. Heme oxygenase mechanism: evidence for an electrophilic, ferric peroxide species. Acc Chem Res 1998; 31:543-49.
9. von Restorff W, Hebisch S. Dark adaptation of the eye during carbon monoxide exposure in smokers and nonsmokers. ASEM 1988; 59:928-31.
10. Cao L, Blute TA, Eldred WD. Localization of heme

oxygenase-2 and modulation of cGMP levels by carbon monoxide and/or nitric oxide in the retina. Vis Neurosci 2000; 17:319-29.
11. Cao L, Eldred WD. Inhibitors of nitric oxide synthase block carbon monoxide-induced increases in cGMP in retina. Brain Res 2003; 988:78-83.
12. Prifitera MG, Potenza M, Bucolo C, Leggio GM, Drgo F. Hemin, an inducer of heme oxygenase-1, lowers intraocular pressure in rabbits. J Ocul Pharmacol Ther 2007; 23:232-9.
13. Goldenberg-Cohen N, Dadon S, Bat-Chen S, Kramer M, Hasanreisoglu M, Eldar M, Weinberger D, Bahar I. Molecular and histological changes following central retinal artery occlusion in a mouse model. Exp Eye Res 2008; 87:327-33.
14. Pannen BH, Bauer M. Differential regulation of hepatic arterial and portal venous vascular resistance by nitric oxide and carbon monoxide in rats. Life Sci 1998; 62:2025-33.
15. Kozma F, Johnson RA, Zhang F, Yu C, Tong X, Nasjletti A. Contribution of endogenous carbon monoxide to regulation of diameter in resistance vessels. Am J Physiol 1999; 276:R1087-R94.
16. Abraham NG, Kappas A. Pharmacological and clinical aspects of heme oxygenase. Pharmacol Rev 2008; 60:79-127.
17. Furchgott RF, Jothianandan D. Endothelium-dependent and independent vasodilatation involving cyclic GMP: relaxation induced by nitric oxide, carbon monoxide and light. Blood Vessels 1991; 28:52-61.
18. Rich A, Farrugia G, Rae JL. Carbon monoxide stimulates a potassium selective current in rabbit corneal epithelial cells. Am J Physiol Cell Physiol 1994; 267:C435-C42.
19. Christodoulides N, Durante W, Kroll MH, Shafer AI. Vascular smooth muscle cell heme oxygenase generate guanyl cyclase stimulatory carbon monoxide. Circulation 1995; 91:2306-9.
20. Morita T, Kourembana S. Endothelial cell expression of vasoconstrictors and growth factors in regulated by smooth muscle cell-derived carbon monoxide. J Clin Invest 1995; 96:2676-82.
21. Wang R, Wang Z, Lingyun W. The direct effect of carbon monoxide on KCa channels in vascular smooth muscle cells. Pflugers Arch 1997; 434:285-91.
22. Resch H, Zawinka C, Weigert G, Schmetterrer L, Garhofer G. Inhaled carbon monoxide increases retinal and choroidal blood flow in healthy humans. Invest Ophthalmol Vis Sci 2005; 46:4275-80.
23. Lo S, Palma SD, Pitkin L, McCombe AW. Localisation of heme oxygenase isoforms in allergic human nasal mucosa. Eur Arch Otorhinolaryngol 2005; 262:595-8.
24. Andersson JA, Uddman R, Cardell LO. Carbon monoxide is endogenously produced in the human nose and paranasal sinuses. J Allergy Clin Immunol 2000; 105:269-73.
25. Krzymowski T, Skipor J, Grzegorzewski W. Cavernous sinus and carotid rete of sheep and sows as a possible place for countercurrent exchange of some neuropeptides and steroid hormone. Anim Reprod Sci 1992; 29:225-40.
26. Kamiński M, Kartanowicz R, Jastrzębski D, Kamiński MM. Determination of Carbon Monoxide, Methane, and Carbon Dioxide in Refinery Hydrogen Gases and Air by Gas Chromatograph. J Chromatogr A 2003; 989:277-83.
27. Maines MD. The heme oxygenase system and its function in the brain. Cell Mol Biol 2000; 46:573-85.
28. Vincent SR, Das S, Maines SD. Brain heme oxygenase isoenzymes and nitric oxide synthase are co-localized in select neurones. Neuroscience 1994; 63:223-31.
29. Griffith MK, Minton JE. Effect of light intensity on circadian profiles of melatonin, prolactin, ACTH and cortisol in pigs. J Anim Sci 1992; 70:492-8.
30. Tast A, Love RJ, Evans G, Andersson H, Peltoniemi OAT, Konnaway DJ. The photophase light intensity does not affect the scotophase metatonin response in domestic pig. Anim Reprod Sci 2001; 65:283-90.

PHARMACOLOGICAL MANIPULATION OF THE DOPAMINERGIC SYSTEM AFFECTS WHEEL-RUNNING ACTIVITY IN DIFFERENTIALLY ACTIVE MICE

A.M. KNAB[1], R.S. BOWEN[2], A.T. HAMILTON[3] and J.T. LIGHTFOOT[4]

[1]Human Performance Laboratory, Appalachian State University, North Carolina Research Campus, Kannapolis, NC, USA; [2]Science and Mathematics Division, Truett-McConnell College, Cleveland, GA, USA; [3]Cannon Research Center, Carolinas Medical Center, Charlotte NC, USA; [4]Huffines Institute for Sports Medicine and Human Performance, Dept. of Health and Kinesiology, Texas A&M University, College Station TX, USA

Received June 17, 2011 – Accepted February 10, 2012

The genetic factors involved in the regulation of physical activity are not well understood. The dopamine system has been implicated in the control of voluntary locomotion and wheel running (WR) in mice and is thus a likely candidate as a genetic/biological system important to the regulation of physical activity. This study evaluated the effects of four different dopaminergic acting drugs on WR in differentially active inbred strains of mice. High active C57L/J (n=7, 3 controls, 4 experimental) and low active C3H/HeJ (n=8, 3 controls, 5 experimental) were analyzed for baseline wheel-running indices of distance (km/day), duration (mins/day), and speed (m/min) for 21 days. Experimental mice received increasing doses over four days of each of the following drugs: SKF 81297 (D1 agonist), SCH 23390 (D1 antagonist), GBR 12783 (DAT inhibitor), and AMPT (tyrosine hydroxylase inhibitor). Each drug dose response treatment was separated by three days of recovery (no drug injections). WR indices were monitored during drug treatments and during drug wash-out phases. SKF 81297 significantly reduced (p=0.0004) WR in the C57L/J mice, but did not affect WR in the C3H/HeJ mice. GBR 12783 significantly increased (p=0.0005) WR in C3H/HeJ mice, but did not affect WR in C57L/J mice. Only duration (not overall WR) was significantly reduced in C57L/J mice in response to SCH 23390 (p=0.003) and AMPT (p=0.043). SCH 23390 (p=0.44) and AMPT (p=0.98) did not significantly affect WR in C3H/HeJ mice. These results suggest that genetic differences in dopamine signaling may play a role in the WR response to dopaminergic-acting drugs in inbred strains of mice. The high activity in the C57L/J strain appears most responsive to D1-like receptor acting drugs, while in the C3H/HeJ strain, dopamine re-uptake appears to have an influence on activity level.

It is well known that physical activity improves human health by decreasing the risk of obesity, cardiovascular diseases, Type II Diabetes, depression, certain types of cancer, and overall mortality (1). Although the physiology of exercise has been well studied over the past 40 years, the genetic and biological regulating factors of physical activity have yet to be fully investigated and understood. It has been estimated that physical inactivity is a leading cause of mortality, and contributes to increasingly

Key words: dopamine, dopamine signaling, physical activity, inbred mice, genetics, regulation

Mailing address: Dr Amy Knab,
Appalachian State University, Human Performance Laboratory,
Plants for Human Health Institute,
North Carolina Research Campus,
600 Laureate Way, Kannapolis, NC 28081,USA
Tel: +1 704 250 5352 Fax: +1 704 250 2509
e-mail: knabam@appstate.edu

0393-974X (2012)

DISCLOSURE: ALL AUTHORS REPORT NO CONFLICTS OF INTEREST RELEVANT TO THIS ARTICLE.

higher health care costs in developed countries (2). Therefore, in order to prevent disease and improve human health it is vital to understand the regulating factors of physical activity.

It has been shown that physical activity patterns are at least moderately inherited and thus partially regulated by genetic factors (3-7). At least two studies have identified both single-gene and epistatic quantitative trait loci (QTL) involved in the regulation of physical activity in mice; in particular, significant single-gene QTL have been found on chromosomes 9 and 13 (8, 9). However, the exact genes involved in regulation of physical activity are yet to be fully elucidated. A different model from inbred mice, selective breeding studies conducted by Garland and colleagues also illustrate a significant genetic component involved in the regulation of physical activity. After 35 generations of selective breeding for running wheel activity, selected animals ran over 170% farther than control mice (10). Selection acting on genetic variation in the original outbred population of mice highlights a definite genetic component to the regulation of voluntary physical activity in mice.

The central nervous system may play a key role in the genetic/biological regulation of physical activity in rodents (11-14). The dopamine system, part of the central nervous system, located in the mid-brain, has two main tracks. The nigrostriatal track mediates locomotion (15) while the mesolimbic track is involved with emotion and motivation (16). For example, it is known that depletion of dopamine neurons in the mid-brain are a major cause of the motor deficits seen in Parkinson's disease (17). Also, the hyperactive phenotype common in Attention Deficit Hyperactivity Disorder (ADHD) is also mediated through dysfunctions in dopamine signaling in the brain (18). Pharmacological studies in rodents confirm dopaminergic involvement in locomotor behavioral responses to stimuli such as psychostimulant drugs (19, 20); however, compelling evidence from wheel running studies in mice also implicates the dopamine system in mediating general voluntary physical activity levels. Specifically, Rhodes and Garland (2003) investigated the effects of Ritalin (a DAT inhibitor), apomorphine (a non-selective dopamine agonist), SCH 23390 (a selective D1-like antagonist), and raclopride (a selective D2-like antagonist) on wheel running in both selected and control animals (12). At high doses of apomorphine, and all doses of raclopride, both control and selected animals markedly decreased their wheel running by the same proportion. However, in response to SCH 23390 control line mice decrease wheel running more than selected animals. A differential response to Ritalin was seen where the selected animals decreased wheel running in response to Ritalin, while the control animals increased wheel running. A differential response to Ritalin, a drug that acts by increasing circulating dopamine (by inhibiting the re-uptake via DAT), indicates genetic differences in dopamine signaling between the selectively bred animals and the controls. Additionally, recent results from our lab exhibiting an independent relationship of dopamine D1 receptors and tyrosine hydroxylase genes with differentially active inbred mice in the nucleus accumbens and striatum area of the brain (21) indicate that D1-like receptors as well as the amount of dopamine present in the mid-brain may influence wheel running in mice.

Wheel running in animals has been suggested as a good model for daily physical activity in humans (22, 23). Thus, studying wheel running responses to dopaminergic drugs may prove useful in elucidating the proposed independent mechanism by which the dopamine system mediates physical activity behavior. Therefore, the purpose of this study was to investigate the wheel running responses to several dopaminergic acting drugs in differentially active inbred mice. This study is another step in the understanding of the central genetic and biological regulation of physical activity, and will be important for future studies investigating the mechanisms of this regulation and importance to human health and performance.

MATERIALS AND METHODS

Animals

Differentially active strains of inbred mice were used in this study: C3H/HeJ mice (n=8 males) previously identified as low active (30), and C57L/J mice (n=6 females, n=1 male) previously identified as high active (30). The use of primarily female C57L/J mice, while not optimal, was unavoidable due to the extremely limited supply of these highly active mice (see below). However, whereas comparisons are made primarily within mouse

and versus control mice of the same sex, appropriate conclusions can be drawn from the use of both male and female mice in this study. The C3H/HeJ mice were purchased from Jackson Laboratories; however, given that C57L/J mice are no longer available from Jackson Laboratories (nor from other suppliers), the C57L/J mice used in this study were taken from a small breeding colony our lab maintains. These mice were the first generation inbred offspring from C57L/J breeder pairs purchased from Jackson Laboratories in Spring 2008.

Running wheel data were collected from the mice beginning at 63 days (9 weeks) of age which corresponds to the most active period in the lifespan for mice (24). All mice were housed in the University Vivarium with 12-hour light/dark cycles (light 6am-6pm, dark 6pm-6am) and were provided with food (Harlan Teklad 8604 Rodent Diet, Madison, WI) and water ad libitum. All procedures were approved by the University of North Carolina Institutional Animal Care and Use Committee. Additionally, all animals were weighed twice weekly.

Measurement of voluntary activity (wheel running)

Daily wheel running was measured using methods described previously (6, 8). Briefly, mice were housed individually in standard rat sized cages, each equipped with a solid surface running wheel (450 mm circumference; Ware Manufacturing, Phoenix, AZ, USA) mounted on the cage top. A magnet was mounted on the outside surface of each wheel and the cage top was equipped with a magnetic sensor (BC500; Sigma Sport, Olney, IL, USA). Each computer was calibrated with wheel dimensions to allow for accurate measurement of distance (km/day) and time (duration-mins/day) each mouse ran on the wheel. Speed of running (m/min) was then calculated from the distance and duration data. Mice were monitored and data was collected every 24 hours at approximately 9am during baseline and drug wash-out phases of the protocol. During drug treatments, data was collected immediately before drug treatment at 6pm (the beginning of the dark/active phase for mice), at 12am (6 h post-drug treatment), and again at 6am (12 h post drug treatment). Negligible running was recorded during the light cycle (6am-6pm) so all data reported is 24 hour data.

Drug treatment

Evidence from our lab (21) and others (12, 14) suggest physical activity in the form of wheel running in mice is at least partially regulated by the D1-like receptors, the dopamine transporter (DAT), as well as possibly the expression and/or function of the tyrosine hydroxylase enzyme. Tyrosine hydroxylase is the enzyme that converts L-dopa into dopamine and thus plays a role in dopamine production. Therefore, in this study, we designed 5 different treatments: SKF 81297 (D1-like agonist; Tocris Bioscience, Ellisville, MO), SCH 23390 (D1-like antagonist; Tocris Bioscience, Ellisville, MO), GBR 12783 (DAT inhibitor; Tocris Bioscience, Ellisville, MO), and DL-2-Methyl-3-(4-hydroxyphenyl) alanine (AMPT) (Tyrosine Hydroxylase inhibitor; Sigma Aldrich, St. Louis, MO), and placebo (saline injections only). All drugs have been shown to be centrally active after intraperitoneal (IP) injection and were administered IP in a volume of 0.3 mL per mouse. Dose responses were investigated using the following consecutive drug doses (mg/kg): SKF 81297 (0.5, 0.75, 1.0, 1.25), SCH 23390 (0.5, 0.75, 1.0, 1.25), GBR 12783 (15, 20, 25, 30), and AMPT (85, 90, 95, 100). All doses were based on previous literature investigating locomotion responses in mice to these particular drugs.

Treatment procedures: At nine weeks of age, mice were housed with a wheel, and baseline activity pattern was assessed for 21 consecutive days in all mice. Five mice from the C3H/HeJ strain and 4 mice (3 females, and 1 male) from the C57L/J strain were randomly chosen for the experimental drug treatment group, leaving three mice in each strain serving as controls. Control mice received saline injections only. The experimental animals received one injection (according to the dose schedule described above) at 6pm, at increasing doses for 4 consecutive days, followed by three full days of drug wash-out (i.e. no injections). Wheel running was monitored at 12am and 6am during drug treatment, and every 24 hours during drug wash-out. This pattern was repeated for all four drugs in succession.

Injection methods: Each drug injection solution was made fresh each day immediately prior to injections and all drugs were dissolved in 0.9% sterile saline. Once the appropriate dose was dissolved, the solution was placed in a sterile syringe and filtered through a 0.2 micron filter during injection. Because drugs were made fresh daily and were kept in sterile conditions, the C57L/J mice received the drugs in the following order: SKF 81297 (83-87 days old), SCH 23390 (90-94 days old), GBR 12783 (97-101 days old), and finally AMPT (103-106 days old). Due to age differences upon arrival and the need to keep drug injections sterile the C3H/HeJ mice received the drug treatments in the following order: GBR 12783 (83-87 days old), AMPT (90-94 days old), SKF 81297 (97-101 days old), and SCH 23390 (103-106 days old).

Statistics

Given the differential drug injections at differing ages, (e.g. the C57L/J mice received SKF 81297 at 83-87 days old, but the C3H/HeJ mice received this drug at 97-101 days old), each strain was analyzed in a separate ANOVA for the effects of the four drugs on wheel running indices.

The alpha value was set *a priori* at 0.05. Within a strain, each drug was analyzed separately with a two-way ANOVA with group (control vs. experimental) and dose (repeated measure) as main effects. Three dependent variables were analyzed including distance (km/day), duration (mins/day), and speed (m/min). Tukey's HSD *post-hoc* tests were used to evaluate main effects and group by dose interactions within the ANOVA model. There were no statistical differences between wheel running indices taken at 6 hours post-injection or 12 hours post-injection (data not shown) and thus, only wheel-running data from 12 hour post-injection will be presented. Differences in weight at baseline measurements between strains, as well as differences in weights between group within strains, were analyzed using independent *t*-tests, and correlation analysis was used to investigate relationships between weight and distance run. Although wheel running in mice has been shown to be highly repeatable (25), whole model *post hoc* power analysis revealed a value of .74.

RESULTS

Weights

Mice were weighed twice weekly during this study to encompass one weight measurement during each drug treatment, as well as one weight measurement during drug wash-out. C3H/HeJ (n=8 males) mice as a whole group were significantly heavier than C57L/J (n=6 females, n=1 male) mice at baseline, and at all time points throughout the study ($p<0.001$). Weight of the control versus the experimental animals did not differ across the treatments (C3H/HeJ, p=0.20; C57L/J, p=0.66). As has been shown in previous studies (6, 8) during baseline activity measurements, weight was not correlated with distance run in either strain (C3H/HeJ: p=0.11, $r^2=0.43$; C57L/J: p=0.12, $r^2=0.36$).

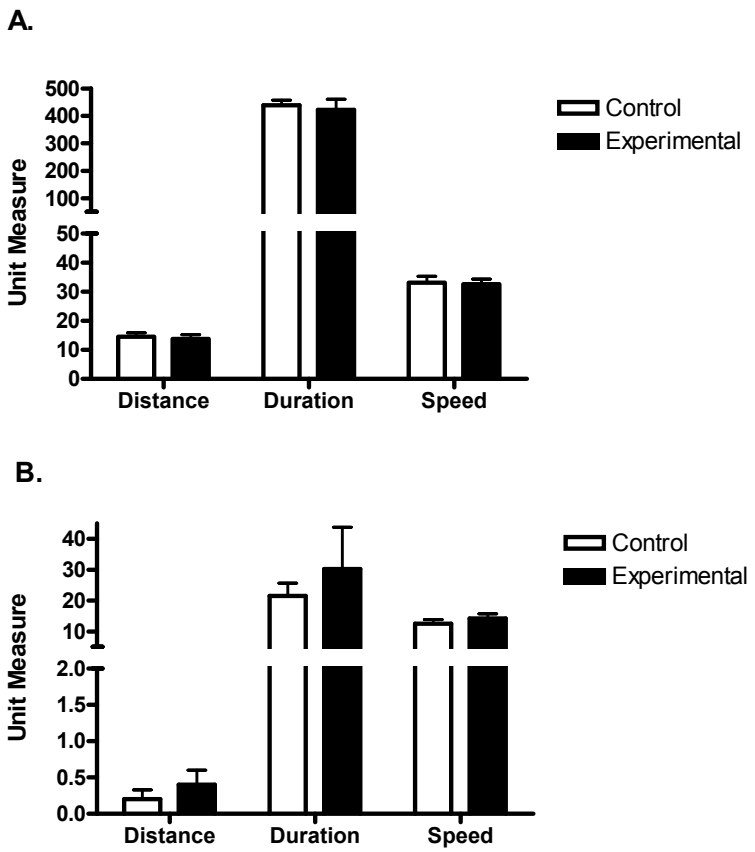

Fig. 1. *Baseline values of distance, duration, and speed in control and experimental mice.* ***A)*** *Running wheel data at baseline for C57L/J mice (n=7) is shown. No differences in distance (km) (p=0.52), duration (mins) (p=0.52), or speed (m/min) (p=0.74) were found between control and experimental groups; however, C57L/J mice ran significantly farther, longer, and faster than C3H/HeJ mice at baseline (p<0.0001).* ***B)*** *Running wheel data at baseline for C3H/HeJ mice (n=8). No differences in distance (p=0.22), duration (p=0.23), or speed (p=0.44) were found between control and experimental groups.*

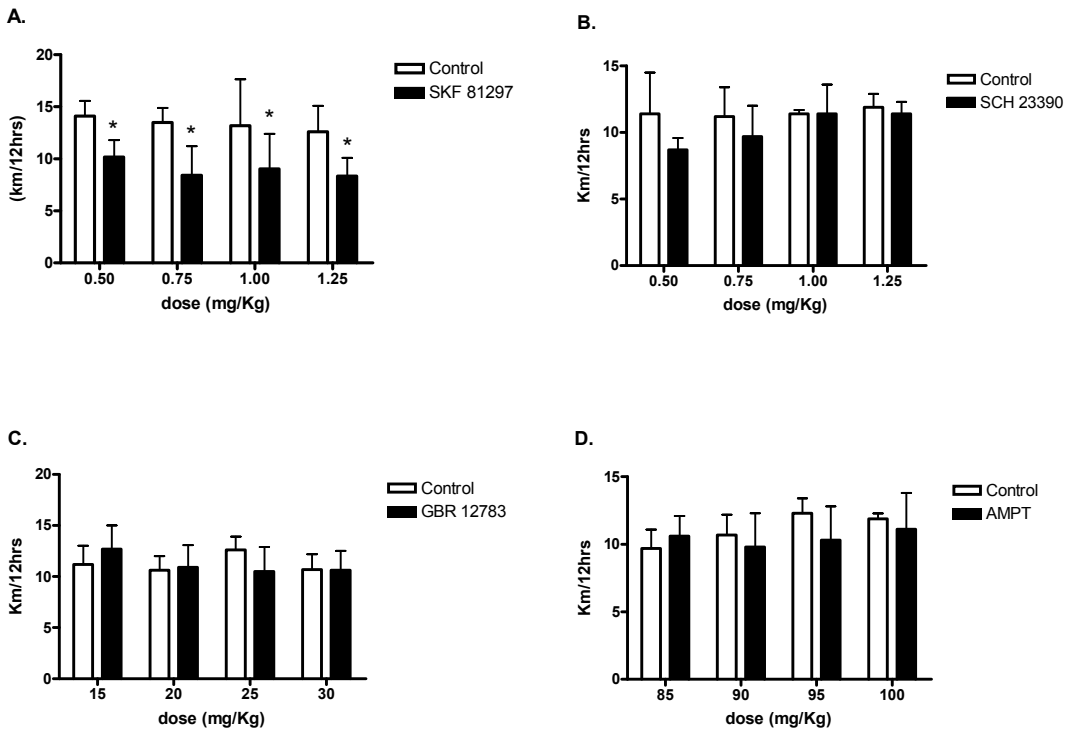

Fig. 2. *Distance responses to all four dopaminergic drugs in C57L/J mice. Distance responses to all four drugs in the C57L/J mice.* ***A****) Dose response after administration of SKF 81297 is shown. No significant dose response was seen; however, all four doses significantly reduced wheel running distance in experimental mice compared to controls (p=0.0004).* ***B****) Dose response to SCH 23390 is shown. No significant changes in distance run between groups were seen for any dose (p=0.12).* ***C****) Dose response to GBR 12783 is shown. No significant differences in distance run were seen between groups for any dose (p=0.89).* ***D****) Dose response to AMPT is shown. No significant differences in distance run between grousp were seen for any of the doses (p=0.37).*

Speed was also not correlated with weight in either strain (C3H/HeJ: p=0.66, r^2=0.03; C57L/J: p=0.93, r^2=0.002). Duration was significantly correlated with weight in both strains (C3H/HeJ: p=0.04, r^2=0.54; C57L/J: p=0.02, r^2=0.69). Weight did not significantly increase over the course of the study in C3H/HeJ mice (p=0.69; beginning: 28.0±1.6g; end: 29.9±2.2g), while weight did significantly increase in C57L/J mice over the course of the study (p=0.02; beginning: 23.6±1.1; end: 25.1±1.0).

Baseline physical activity results

Baseline wheel running indices for both strains of mice are illustrated in Fig. 1. As was expected from previous literature, the C57L/J mice ran 191% farther, 177% longer, and 84% faster than C3H/HeJ mice (p<0.0001). There was no difference between control and experimental mice at baseline in distance (p=0.52), duration (p=0.52), or speed (p=0.74) in the C57L/J mice. Likewise, there was no difference between groups of C3H/HeJ mice at baseline in distance (p=0.22), duration (p=0.33), or speed (p=0.16).

Drug effects on WR in C57L/J mice

Wheel-running distance, the product of duration of activity and speed of activity, responses in C57L/J mice to all four drugs are shown in Fig. 2. No significant dose response was seen in distance run after treatment with the D1 agonist SKF 81297 (p=0.72); however, SKF 81297 significantly reduced wheel running distance regardless of dose (Fig. 2;

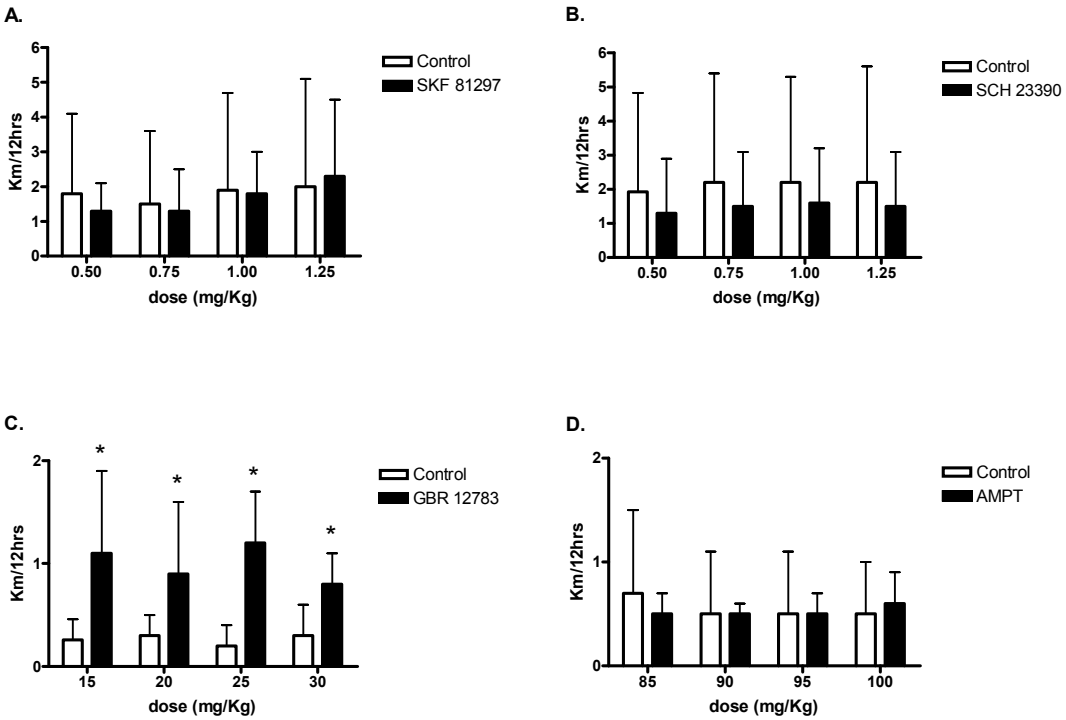

Fig. 3. *Distance responses to all four dopaminergic drugs in C3H/HeJ mice. Distance responses to all four drugs in the C3H/HeJ mice.* ***A)*** *Dose response after administration of SKF 81297 is shown. No significant differences in distance between groups were seen for any dose (p=0.91).* ***B)*** *Dose response to SCH 23390 is shown. No significant changes in distance run between groups were seen for any dose (p=0.44).* ***C)*** *Dose response to GBR 12783 is shown. No significant dose response was observed, however, distance was significantly increased in the experimental group compared to control following treatment with all four doses (p=0.0005).* ***D)*** *Dose response to AMPT is shown. No significant differences in distance run between group were seen for any of the doses (p=0.98).*

p=0.0004). No significant differences in distance were observed between group or by dose for the D1-antagonist SCH 23390 (p=0.12), the DAT inhibitor GBR 12783 (p=0.89), or the TH inhibitor AMPT (p=0.37). Similar responses for duration and speed for all four drugs were observed and are reported in Table I.

Drug effects on WR in C3H/HeJ mice

Wheel-running distance responses in C3H/HeJ mice (low active) to all four drugs are shown in Fig. 3. No significant dose response was seen in distance run after treatment with the DAT inhibitor GBR 12783 (p=0.73); however, injection of GBR 12783 did significantly increase wheel running independent of dose (Fig. 3; p=0.0005). No other drugs used in this study significantly affected wheel running the C3H/HeJ mice: the D1-agonist SKF 81297 (p=0.91), the D1-antagonist SCH 23390 (p=0.44), and the TH-inhibitor AMPT (p=0.98). Data for duration and speed for all four drugs for C3H/HeJ mice showed similar responses as distance and are reported in Table II.

DISCUSSION

This study investigated four different dopaminergic acting drugs on a high active strain of mice and a low active strain of mice to determine the role of D1-like receptors, DAT, and tyrosine

Table I. *Duration and speed responses to dop*

Drug	Dose (mg/Kg)	Duration (mins/12hrs)		Speed (m/min)	
		Control	Experimental	Control	Experimental
SKF 81297	0.5	425±13	358±82	33.3±4.4	29.1±5.7
	0.75	416±17	327±65	32.5±4.5	25.3±4.6
	1	389±50	346±69	33.3±7.7	25.7±5.8
	1.25	401±13	294±45	31.4±5.4	28.3±3.6
			p=0.002*		p=0.015*
SCH 23390	0.5	396±63	312±47	28.5±4.1	28.2±5.4
	0.75	389±45	324±42	28.7±3.7	30.0±5.7
	1	395±29	364±15	29.0±2.8	31.1±5.3
	1.25	402±41	371±24	29.7±3.0	30.7±3.1
			p=0.003*		p=0.54
GBR 12783	15	392±12	382±35	28.4±4.0	33.1±3.5
	20	375±27	339±39	28.4±4.5	31.9±4.2
	25	431±24	369±70	29.3±2.4	28.4±1.3
	30	378±10	373±60	28.5±3.4	28.5±2.0
			p=0.091		p=0.18
AMPT	85	341±28	343±36	28.6±4.6	30.9±4.0
	90	362±27	320±82	29.6±3.4	30.7±2.8
	95	396±25	323±67	31.0±2.4	32.0±3.1
	100	392±37	342±40	30.6±2.5	32.2±4.2
			p=0.043*		p=0.29

Duration and speed data for C57L/J mice. p values reported indicate significant differences between groups within strain.

hydroxylase in regulating physical activity level. We observed strain dependent effects of the D1-like receptor agonist (SKF 81297) and the DAT inhibitor (GBR 12783) (Figs. 1 and 2). The D1-like agonist significantly reduced overall distance, duration, and speed in C57L/J mice (high active), while the DAT inhibitor significantly increased overall distance, duration, and speed in the C3H/HeJ (low active) mice.

It is becoming well accepted that a significant genetic component exists in the regulation of physical activity in both rodents (3-7, 26-28) and humans (29, 30). Using wheel-running as a model of physical activity in mice, both single-gene and epistatic QTL associated with physical activity have been found (8, 9). However, the genes and gene interactions that regulate physical activity behavior are still unclear. Interestingly, haplotype analysis conducted in the study by Lightfoot and colleagues identified a suggestive QTL on chromosome 13 that contains the *Drd1* gene which codes for the D1 receptor (8), and research conducted in our lab (21) indicate C57L/J inbred mice (high active) have significantly lower expression of *Drd1* mRNA compared to low active C3H/HeJ inbred mice. The current study was designed to investigate several aspects of dopamine signaling in relation to physical activity in mice.

Wheel running in response to DAT and tyrosine hydroxylase inhibitors

GBR 12783 and AMPT were used in this study to investigate wheel running responses to drugs

Table II. *Duration and speed responses to dopaminergic drugs in C3H/HeJ mice.*

Drug	Dose (mg/Kg)	Duration (mins/12hrs)		Speed (m/min)	
		Control	Experimental	Control	Experimental
SKF 81297	0.5	97±106	73±33	15.2±4.8	17.2±2.6
	0.75	83±111	75±56	14.4±3.6	16.4±2.6
	1	101±145	103±56	14.5±4.2	16.5±2.8
	1.25	104±150	124±99	15.0±4.4	17.1±2.9
		p=0.95		p=0.11	
SCH 23390	0.5	95±133	74±79	15.7±5.0	16.0±2.8
	0.75	110±141	84±78	15.3±5.5	16.3±2.5
	1	111±142	91±80	15.6±4.6	16.3±2.9
	1.25	110±147	89±80	15.5±5.6	16.1±2.6
		p=0.56		p=0.63	
GBR 12783	15	20±16	66±41	12.5±1.4	16.3±1.7
	20	21±14	53±36	12.5±1.0	15.4±2.0
	25	19±12	69±25	12.1±1.2	16.4±1.8
	30	23±19	53±15	13.1±1.0	15.7±1.1
		p=0.0005*		p<0.0001*	
AMPT	85	39±43	35±12	14.3±3.4	15.3±1.6
	90	34±32	36±6	14.1±2.9	15.0±1.3
	95	33±30	35±10	14.2±2.7	15.3±1.4
	100	29±26	37±15	15.3±3.0	15.5±1.6
		p=0.82		p=0.31	

Duration and speed data for C3H/HeJ mice. p values reported indicate significant differences between groups within strain.

affecting either dopamine re-uptake or dopamine production, respectively. Treatment of low active C3H/HeJ mice with the DAT inhibitor (dopamine re-uptake inhibitor) significantly increased wheel running distance, duration, and speed independent of dose compared to control mice (Fig. 3, Table II). The DAT inhibitor did not affect wheel running in the C57L/J strain. This finding corresponds to previous research with animal models of ADHD and treatment with Ritalin [also a dopamine re-uptake inhibitor] (14). Responses to Ritalin in humans can vary depending on the status of the neurotransmitter systems (31-33). Specifically, it has been proposed that the response to drugs such as Ritalin depends largely on baseline values of the response in question (33).

The only effect of the TH inhibitor was a slight, but significant decrease in duration in the high active C57L/J mice (Table I). We observed no significant group by dose interactions for this drug in C57L/J mice, with no difference reflected in distance or speed (Fig. 2, Table I). In our previous study, we observed decreased expression of tyrosine hydroxylase mRNA in the mid-brain of C57L/J mice compared to C3H/HeJ mice (21). If decreased expression of tyrosine hydroxylase, and subsequent decreased dopamine production and downstream dopamine signaling mediate the high active phenotype, inhibiting this

enzyme further would theoretically lead to further increased physical activity; however, this high active strain may have already been running at a "physiological maximum". Rhodes and Garland (12) have suggested a possible "ceiling effect" in response to high doses of apomorphine in mice selectively bred for high wheel running.

Wheel-running in response to D1-like agonist and antagonist

In contrast to determining the response to generalized alteration in dopamine levels through the use of reuptake inhibitors or dopamine synthesis inhibitors, we used SKF 81297 (D1-like agonist) and SCH 23390 (D1-like antagonist) to investigate the effects of manipulation of dopamine signaling specifically through the D1-like receptors. The D1 agonist caused significant reduction in distance, duration, and speed in the high active C57L/J mice (Fig. 2 and Table I). Observation that high active C57L/J mice in the current study reduced wheel running in response to a D1 agonist supports the hypothesis that decreased function and/or expression of D1-like receptors may mediate running wheel activity in high active inbred strains (21). In contrast, the low active C3H/HeJ mice did not decrease wheel running in response to the D1 agonist used in this study. The largely lack of response to SCH 23390 (a selective D1-like antagonist) would again suggest a possible floor or ceiling effect with these two unique strains of mice (Figs. 2 and 3, Tables I and II).

In summary, strain differences in the response to a D1 receptor agonist demonstrate that D1-like receptors may play a role in mediating the high active phenotype in C57L/J mice. Likewise, differential strain responses to a dopamine re-uptake inhibitor suggest that the amount of dopamine present in the synapse may be important in mediating the low active phenotype in C3H/HeJ mice. However, full elucidation of the role of dopaminergic functioning in these strains purposely selected for their divergent activity responses is difficult because of the possibility of physiological ceiling and floor effects in physical activity levels. Similarly, baseline genetic differences in dopamine signaling between inbred strains are a potential explanation for the differences in wheel running responses to dopaminergic drugs. It is also possible that low activity may be a different phenotype than high activity and regulated by slightly different pathways (JT Lightfoot, personal correspondence). Further investigations should use strains of mice that fall in the middle of the spectrum of voluntary physical activity.

ACKNOWLEDGEMENTS

The authors would like to thank Dr. Trudy Moore-Harrison and David Ferguson for assistance in wheel-running data collection. We also thank the UNC Charlotte Vivarium staff and Dr. Yvette Huet for assistance in preparation of sterile injectables. This work was funded by NIH NIAMS AR050085.

REFERENCES

1. Heitmann BL, Hills AP, Frederiksen P, Ward LC. Obesity, leanness, and mortality: effect modification by physical activity in men and women. Obesity (Silver Spring) 2009; 17(1):136-42.
2. Oldridge NB. Economic burden of physical inactivity: healthcare costs associated with cardiovascular disease. Eur J Cardiovasc Prev Rehabil 2008; 15(2):130-9.
3. Festing MF. Wheel activity in 26 strains of mouse. Lab Anim 1977; 11(4):257-8.
4. Lauderdale DS, Fabsitz R, Meyer JM, Sholinsky P, Ramakrishnan V, Goldberg J. Familial determinants of moderate and intense physical activity: a twin study. Med Sci Sports Exerc 1997; 29(8):1062-8.
5. Lerman I, Harrison BC, Freeman K, et al. Genetic variability in forced and voluntary endurance exercise performance in seven inbred mouse strains. J Applied Physiol 2002; 92(6):2245-55.
6. Lightfoot JT, Turner MJ, Daves M, Vordermark A, Kleeberger SR. Genetic influence on daily wheel running activity level. Physiol Genomics 2004; 19(3):270-6.
7. Stubbe JH, Boomsma DI, De Geus EJ. Sports participation during adolescence: a shift from environmental to genetic factors. Med Sci Sports Exerc 2005; 37(4):563-70.
8. Lightfoot JT, Turner MJ, Pomp D, Kleeberger SR, Leamy LJ. Quantitative trait loci (QTL) for physical activity traits in mice. Physiol Genomics 2008;

32(3):401-8.
9. Leamy LJ, Pomp D, Lightfoot JT. An epistatic genetic basis for physical activity traits in mice. J Hered 2008; 99(6):639-46.
10. Rezende EL, Kelly SA, Gomes FR, Chappell MA, Garland T, Jr. Effects of size, sex, and voluntary running speeds on costs of locomotion in lines of laboratory mice selectively bred for high wheel-running activity. Physiol Biochem Zool 2006; 79(1):83-99.
11. Bronikowski AM, Rhodes JS, Garland T, Jr, Prolla TA, Awad TA, Gammie SC. The evolution of gene expression in mouse hippocampus in response to selective breeding for increased locomotor activity. Evolution Int J Org Evolution 2004; 58(9):2079-86.
12. Rhodes JS, Garland T. Differential sensitivity to acute administration of Ritalin, apomorphine, SCH 23390, but not raclopride in mice selectively bred for hyperactive wheel-running behavior. Psychopharmacology (Berl) 2003; 167(3):242-50.
13. Rhodes JS, Garland T, Jr, Gammie SC. Patterns of brain activity associated with variation in voluntary wheel-running behavior. Behav Neurosci 2003; 117(6):1243-56.
14. Rhodes JS, Hosack GR, Girard I, Kelley AE, Mitchell GS, Garland T, Jr. Differential sensitivity to acute administration of cocaine, GBR 12909, and fluoxetine in mice selectively bred for hyperactive wheel-running behavior. Psychopharmacology (Berl) 2001; 158(2):120-31.
15. Salamone JD. Complex motor and sensorimotor functions of striatal and accumbens dopamine: involvement in instrumental behavior processes. Psychopharmacology (Berl) 1992; 107(2-3):160-74.
16. Salamone JD, Correa M. Motivational views of reinforcement: implications for understanding the behavioral functions of nucleus accumbens dopamine. Behav Brain Res 2002; 137(1-2):3-25.
17. Zhang J, Goodlett DR. Proteomic approach to studying Parkinson's disease. Mol Neurobiol 2004; 29(3):271-88.
18. Arnsten AF. Fundamentals of attention-deficit/hyperactivity disorder: circuits and pathways. J Clin Psychiatry 2006; 67(S):7-12.
19. Gold LH, Swerdlow NR, Koob GF. The role of mesolimbic dopamine in conditioned locomotion produced by amphetamine. Behav Neurosci 1988; 102(4):544-52.
20. Saylor AJ, McGinty JF. Amphetamine-induced locomotion and gene expression are altered in BDNF heterozygous mice. Genes Brain Behav 2008.
21. Knab AM, Bowen RS, Hamilton AT, Gulledge AA, Lightfoot JT. Altered dopaminergic profiles: implications for the regulation of voluntary physical activity. Behav Brain Res 2009; 204(1):147-52.
22. Eikelboom R. Human parallel to voluntary wheel running: exercise. Anim Behav 1999; 57(3):F11-F12.
23. Sherwin CM. Voluntary wheel running: a review and novel interpretation. Anim Behav 1998; 56(1):11-27.
24. Swallow JG, Garland T, Jr, Carter PA, Zhan WZ, Sieck GC. Effects of voluntary activity and genetic selection on aerobic capacity in house mice (Mus domesticus). J Appl Physiol 1998; 84(1):69-76.
25. Knab AM, Bowen RS, Moore-Harrison T, Hamilton AT, Turner MJ, Lightfoot JT. Repeatability of exercise behaviors in mice Physiol Behav 2009.
26. Leamy LJ, Pomp D, Lightfoot JT. A search for quantitative trait loci controlling within-individual variation of physical activity traits in mice. BMC Genet 2010; 11:83.
27. Lightfoot JT. Current understanding of the genetic basis for physical activity J Nutr 2011; 141(3):526-30.
28. Lightfoot JT, Leamy L, Pomp D, et al. Strain screen and haplotype association mapping of wheel running in inbred mouse strains. J Appl Physiol 2010; 109(3):623-34.
29. Rankinen T, Bray MS, Hagberg JM, et al. The human gene map for performance and health-related fitness phenotypes: the 2005 update. Med Sci Sports Exerc 2006; 38(11):1863-88.
30. Garland T, Jr, Schutz H, Chappell MA, et al. The biological control of voluntary exercise, spontaneous physical activity and daily energy expenditure in relation to obesity: human and rodent perspectives. J Exp Biol 2011; 214(Pt 2):206-29.
31. Greenwald MK, Schuster CR, Johanson CE, Jewell J. Automated measurement of motor activity in human subjects: effects of repeated testing and d-amphetamine. Pharmacol Biochem Behav 1998; 59(1):59-65.
32. Robbins TW, Sahakian BJ. "Paradoxical" effects of

psychomotor stimulant drugs in hyperactive children from the standpoint of behavioural pharmacology. Neuropharmacology 1979; 18(12):931-50.

33. Sanger DJ, Blackman DE. Rate-dependent effects of drugs: a review of the literature. Pharmacol Biochem Behav 1976; 4(1):73-83.

LETTER TO THE EDITOR

CORTICOSTEROIDS PROVOKE ACUTE ENDOTHELIAL INJURY – AN IDEAL GROUND FOR THROMBOSIS IN MULTIPLE SCLEROSIS

I. SOSA[1], S. STIFTER[2], S. BAJEK[3], I. STRENJA LINIC[4], D. CUCULIC[1], Z. CRNCEVIC-ORLIC[5], A. GRUBESIC[6] and A. BOSNAR[1]

[1]Department of Forensic Medicine and Criminalistics, University of Rijeka School of Medicine, Rijeka, Croatia; [2]Department of Pathology, University of Rijeka Medical School, Rijeka, Croatia; [3]Department of Anatomy, University of Rijeka Medical School, Rijeka, Croatia; [4]Neurology Clinic, Rijeka University Hospital, Rijeka, Croatia; [5]Department of Internal Medicine, University of Rijeka Medical School, Rijeka, Croatia; [6]Rijeka Emergency Medicine Institute, Rijeka, Croatia

Received September 6, 2011 – Accepted December 6, 2011

Despite the effect corticosteroids exert on blood clotting and the irrefutable impact of intracranial pressure decreasing shortly after lumbar puncture, a certain number of intracranial thromboses remain unexplained. Corticosteroids are useful in reducing the severity and duration of relapses of multiple sclerosis (MS). Several questions emerge concerning the reasons behind thrombosis occurring so sporadically, not pertaining to any rule, the most important of which regard the location and timing. We developed this hypothesis as an obverse to chronic endothelial injury theory which, only partially explains atherosclerosis development. We followed Virchow's classical triad of conditions which are believed to be connected to the development of thrombosis. Although corticosteroids affect more than vessel wall injury, component of Virchow's triad that has been our narrowest interest is exactly vessel wall injury.

Multiple sclerosis (MS) is an inflammatory disease of the central nervous system. Even if the etiological agent is unknown, it is presumed that the inflammatory reaction is directed against, or is mediated by, this elusive agent. Some pathogens by their nature tend to directly provoke chronic (1) rather than acute inflammation (2). MS usually appears in adults in their thirties but it can also appear in children. The primary progressive subtype is more common in people in their fifties. The disease is more common in women, and the trend may be increasing. In children, the sex ratio difference is higher, while in people over fifty, MS affects males and females almost equally (3). Thus, MS is a disease of young adults, with long-term implications for both their personal and professional lives. The economic impact of the condition is particularly significant as the majority of patients are of working age, with hardly negligible expenses for society. By retrospective analysis, in 240 MS relapses, only one case of deep vein thrombosis was documented following lumbar puncture and/or high-dose parenteral corticosteroid treatment (4). Commonly, thrombosis in unusual sites refers to all

Key words: acute endothelial injury, perivascular compartments, multiple sclerosis, corticosteroids

Mailing address: I. Sosa, MD
Department of Forensic Medicine and Criminalistics,
University of Rijeka School of Medicine,
Brace Branchetta 20,
51 000 Rijeka, Croatia
Tel: +38 5916996969
Fax: +38551215227
e-mail: ivan.sosa@vip.hr

0393-974X (2012)

DISCLOSURE: ALL AUTHORS REPORT NO CONFLICTS OF INTEREST RELEVANT TO THIS ARTICLE.

venous thromboses in sites other than the veins of the limbs. Such are thrombosis of the cerebral sinuses; portal system; renal veins; suprahepatic veins and venae cavae (5, 6). Prevalence of MS ranges between 2 and 150 per 100,000 depending on the country or specific population (7). There is a north-to-south gradient in the northern hemisphere and a south-to-north gradient in the southern hemisphere, with MS being much less common in people living near the equator (3). However, there are important exceptions to the north–south pattern and changes in prevalence rates over time; in general, this trend might be disappearing (8). MS is also more common in regions with northern Europe populations. But even in regions where MS is common, some ethnic groups are at low risk of developing the disease. Environmental factors during childhood may play an important role in the development of MS later in life.

Nature of multiple sclerosis

As discussed earlier, MS is said to be an inflammatory disease where immune cell invasion leads to focal as well as axonal damage. Traditionally, any active and chronic active MS lesion throughout the course of MS is featured by axonal damage. These mechanisms involve immune attack directed at axonal components causing secondary axonal degeneration. Progression of these lesions is the major cause for irreversible damage in the central nervous system (9).

Primarily, the activation of T cells occurs in the peripheral lymphoid compartment. Previously activated immune cells require re-stimulation (10). Re-stimulation takes place in perivascular compartment (PC) by antigen-presenting cells. PCs surrounding small blood vessels as they penetrate the brain parenchyma are not a unique feature of MS (11). Perivascular spaces in normal brain are anatomical routes for the bulk flow drainage of fluid from the gray matter to the subarachnoid space. Perivascular cuffing and PC enlargements have been observed in MS. The question remains whether the MS patients have more numerous and/or larger perivascular compartments than healthy controls? Prominent perivenular spaces as a sign of perivascular inflammation are seen as a result of autoimmune processes and are a critical event in the pathogenesis and evolution of MS lesions. Additionally, their unavoidable role in leukocyte trafficking was not appreciated until very recently. To date, relation of MS lesions to venules and small veins has been confirmed only by post-mortem studies of central nervous system tissue. MS lesions have a perivenous location and their form is determined by location and orientation of veins. Initial inflammatory process of MS starts around small veins (12). Therefore, the mere presence of (small) veins in MS lesions may not be more than a coincidence.

Action of corticosteroids

During a MS relapse, patients are prescribed corticosteroids to reduce its severity and duration. Methylprednisolone is a corticosteroid drug typically used for its anti-inflammatory effects. In MS this is employed to reduce the inflammation in the central nervous system (13). On the whole, high-dosage methylprednisolone treatment can be considered as safe. The main effect of methylprednisolone consists of reducing the severity and shortening the length of attacks, as well as a slight lessening in spasticity (14). Methylprednisolone is an excellent treatment for attacks, but not for continuous therapy. In repeated studies, a therapeutic effect of a longer-lasting, lower oral dosage of steroids could not be confirmed (15). Methylpre- dnisolone's anti-inflammatory effect is five times greater than that of natural cortisone and persists at least twice as long (16). In 1980, a study was carried out on the effect of administering intravenous high-dose methylprednisolone, which demonstrated a powerful anti-exacerbative effect (13).

Evidence of the efficacy of high-dose corticosteroids in conditions such as acute spinal cord injury, traumatic optic neuropathy, or relapsing phase of MS supports its application. On the other hand, there are studies according to which no benefit of high-dose corticosteroid treatment in acute traumatic optic neuropathy, or acute spinal cord injury has been achieved. Recent experimental studies decline basis for treating and suggest the harmfulness of the treatment if corticosteroids are administered more than eight hours following spinal cord injury (17).

To date, only intravenous administration of methylprednisolone has been confirmed as effective in controlled studies. In order to prevent another rapid flare-up of inflammatory activity during

an attack, after the intravenous administration of methylprednisolone nowadays prednisone is administered in tablet form in decreasing dosages for about 2-3 weeks (18).

Adverse reactions from high dosages of intravenously administered methylprednisolone are arrhythmias and, occasionally, also a clear rise in blood pressure in patients already suffering from high blood pressure has been described (19). Also, some cases of psychological changes and, rarely, epileptic attacks. Bone necrosis, although feared as a result of high dosages of steroids, is extremely rare.

Vessel walls in the brain – hypothesis of acute endothelial injury in MS

Corticosteroids are known to suppress inflammation. Because veins and venules are ubiquitous, they traverse most other types of disease processes. We presume that abrupt reduction of parenteral corticosteroid treatment might serve as a trigger of thrombosis. The study of Bousser et al. shows that cerebral venous thrombosis is not rare and that it is difficult to diagnose because it manifests differently, that most CT findings are non specific and that angiography remains the best diagnostic tool (20). Namely, for thrombosis to occur, by classic pathological criteria, three principal factors are required: venous stasis (reduced or stagnant blood flow, injury to the blood vessel wall, or an increase in the activity of those substances in the blood that are part of the normal clotting mechanism (21). The role that the vessel wall itself plays in the development of venous thrombosis is less clear. The findings of Brooks et al. re-direct our attention to venous valves as they bring alterations of the vessel walls into focus when considering the multiple pathomechanisms leading to venous thrombosis.

Therefore, we hypothesize cascade of events (perivascular edema – space expansion/ retraction) that finally results in vascular injury precipitating coagulation/endothelium "springs back" and damage (22). Ultra-structural endothelial cell dysfunction involving membrane damage, increased permeability, swelling and necrosis usually precedes vascular wall disorders. Dysfunction of endothelial cells could be a result of changes due to immune-mediated mechanisms e.g. triggering inflammatory signaling cascades, enhancing expression of cellular adhesion molecules, activation of cytotoxic T cells and/or auto antibodies directed against endothelial cell membranes. Considering the role of the endothelium in the initiation and propagation of the vascular wall injury, the role of acute endothelial injury should be articulated as a hypothesis and confirmed in praxis.

Atherosclerosis is but a lipid deposition within the artery wall. A complex theory in which the presence of a dysfunctional endothelium plays a pivotal role has been implied. Unlike the hypotheses on chronic endothelial injury in which an etiology of atherosclerosis is imprinted, we offer a new, interesting and reasonable explanation of development of thrombosis in patients treated with high doses of corticosteroids.

Nevertheless, whether particular sections of the endothelium will emerge as a novel risk factor of venous thrombosis is still an open question as there are some limitations to the study.

REFERENCES

1. Bottasso O, Docena G, Stanford JL, Grange JM. Chronic inflammation as a manifestation of defects in immunoregulatory networks: implications for novel therapies based on microbial products. Inflammopharmacology 2009; 17:193-203.
2. Rankin JA.Biological mediators of acute inflammation. AACN Clin Issues 2004; 15:3-17.
3. Compston A, Coles A. Multiple sclerosis. Lancet 2008; 372:1502-17.
4. Maurelli M, Bergamaschi R, Candeloro E, Todeschini A, Micieli G. Cerebral venous thrombosis and demyelinating diseases: report of a case in a clinically isolated syndrome suggestive of multiple sclerosis onset and review of the literature. Mult Scler 2005; 11:242-4.
5. Girolami A, Simioni P, Scarano L, Girolami B. Venous and arterial thrombophilia. Haematologica 1997; 82:96-100.
6. Joist JH. Hypercoagulability: introduction and perspective. Semin Thromb Hemost 1990; 16:151-7.
7. Rosati G. The prevalence of multiple sclerosis in the world: an update. Neurol Sci 2001; 22:117-39.
8. Alonso A, Hernán MA. Temporal trends in the incidence of multiple sclerosis: a systematic review. Neurology 2008; 71:129-35.

9. Silber E, Sharief MK. Axonal degeneration in the pathogenesis of multiple sclerosis. J Neurol Sci 1999; 170:11-8.
10. Bouchonnet F, Lecossier D, Bellocq A, Hamy I, Hance AJ. Activation of T cells by previously activated T cells. HLA-unrestricted alternative pathway that modifies their proliferative potential. J Immunol 1994; 153:1921-35.
11. Ge Y, Law M, Herbert J, Grossman RI. Prominent perivenular spaces in multiple sclerosis as a sign of perivascular inflammation in primary demyelination. AJNR Am J Neuroradiol 2005; 26:2316-9.
12. Chaynes P. Microsurgical anatomy of the great cerebral vein of Galen and its tributaries. J Neurosurg 2003; 99:1028-38.
13. Dowling PC, Bosch VV, Cook SD. Possible beneficial effect of high-dose intravenous steroid therapy in acute demyelinating disease and transverse myelitis. Neurology 1980; 30:33-6.
14. Nos C, Sastre-Garriga J, Borràs C, Río J, Tintoré M, Montalban X. Clinical impact of intravenous methylprednisolone in attacks of multiple sclerosis. Mult Scler 2004; 10:413-6.
15. Sellebjerg F, Barnes D, Filippini G, et al.; EFNS Task Force on Treatment of Multiple Sclerosis. EFNS guideline on treatment of multiple sclerosis relapses: report of an EFNS task force on treatment of multiple sclerosis relapses. Eur J Neurol 2005; 12:939-46.
16. Benedek TG. History of the development of corticosteroid therapy. Clin Exp Rheumatol 2011; 29(S):5-12.
17. Steinsapir KD. Treatment of traumatic optic neuropathy with high-dose corticosteroid. Neuroophthalmol 2006; 26:65-7.
18. Anlar O. Treatment of multiple sclerosis. CNS Neurol Disord Drug Targets 2009; 8:167-74.
19. Lyons PR, Newman PK, Saunders M. Methylprednisolone therapy in multiple sclerosis: a profile of adverse effects. J Neurol Neurosurg Psychiatry 1988; 51:285-7.
20. Bousser MG, Chiras J, Bories J, Castaigne P. Cerebral venous thrombosis--a review of 38 cases. Stroke 1985; 16:199-213.
21. Verhamme P, Hoylaerts MF. The pivotal role of the endothelium in haemostasis and thrombosis. Acta Clin Belg 2005; 61:213-9.
22. del Zoppo GJ. Virchow's triad: the vascular basis of cerebral injury. Rev Neurol Dis 2008; 5:S12-21.

JOURNAL OF BIOLOGICAL REGULATORS & HOMEOSTATIC AGENTS Vol. 26, no. 1, 135-138 (2012)

LETTER TO THE EDITOR

ACTH AND AZATHIOPRINE: ANTIPROTEINURIC AND LIPID-LOWERING EFFECT IN THE COURSE OF IDIOPATHIC MEMBRANOUS GLOMERULONEPHRITIS

A. GIGANTE[1], E. ROSATO[2], M. LIBERATORI[1], M.L. GASPERINI[1], K. GIANNAKAKIS[3], B. BARBANO[1], R. CIANCI[1], F. SALSANO[2] and A. AMOROSO[1]

[1]Department of Clinical Medicine, [2]Department of Clinical Immunology, [3]Department of Experimental Medicine[2], Sapienza, University of Rome, Italy

Received April 21, 2011 – Accepted December 5, 2011

Idiopathic membranous glomerulonephritis is a frequent cause of nephrotic syndrome and may have a variable course, from spontaneous remission to progression on renal failure. The therapy is based on alternating steroids and chlorambucil or cyclophosphamide (Ponticelli protocol) for six months. In absence of complete or partial remission after protocol, cyclosporine, adrenocorticotropic hormone, mycophenolate mofetil, rituximab can be used for potential therapy. We report here the case of a woman with idiopathic membranous glomerulonephritis unresponsive to the Ponticelli regimen and treated with adrenocorticotropic hormone in association with azathioprine, showing a dramatic decrease of proteinuria and beneficial effects on lipid profile. After 36 months, no relapse of disease has occurred. Although larger cohorts of patients are needed to evaluate the long-term effects, adrenocorticotropic hormone plus azathioprine in association could be a possible therapeutic option for unresponsive idiopathic membranous glomerulonephritis.

Idiopathic membranous glomerulonephritis (IMN) is the most common cause of nephrotic syndrome in adults and it is characterized histologically by uniform thickening of the glomerular capillary due to the presence of subepithelial immune deposits or the subsequent changes of the glomerular basement membrane (1). Recently, Beck et al. found in most of patients affected by IMN, autoantibodies against M-type phospholipase A2 receptor, normally expressed on podocytes (2).

IMN exists in idiopathic or secondary forms and some studies have demonstrated that many patients have a spontaneous recovery while others show persistent proteinuria or progressive end-stage renal disease (3).

Treatment is still controversial and proteinuria is the important determining factor for renal outcome (4). We report the case of a woman with IMN treated with adrenocorticotropic hormone (ACTH) plus azathioprine (AZA), achieving good outcome in terms of proteinuria reduction and lipid-lowering profile.

Case report

A 69-year-old Caucasian woman was admitted to the Department of Clinical Medicine, Sapienza, University of Rome, Italy, with generalized edema. Her medical history included diagnosis of hypertension in treatment with amlodipine 10 mg daily and ramipril 5 mg daily. Laboratory studies showed: creatinine 0.8mg/dL (MDRD-4 formula creatinine clearance 71mL/min), urea

Key words: idiopathic membranous glomerulonephritis, nephrotic syndrome, adrenocorticotropic hormone, azathioprine

Mailing address: Gigante Antonietta, MD
Sapienza, University of Rome,
Department of Clinical Medicine,
Viale dell'Università 37,
00185 Rome, Italy
Tel/Fax: +39 06 49972046
e-mail: antonietta_gigante@yahoo.it

0393-974X (2012)

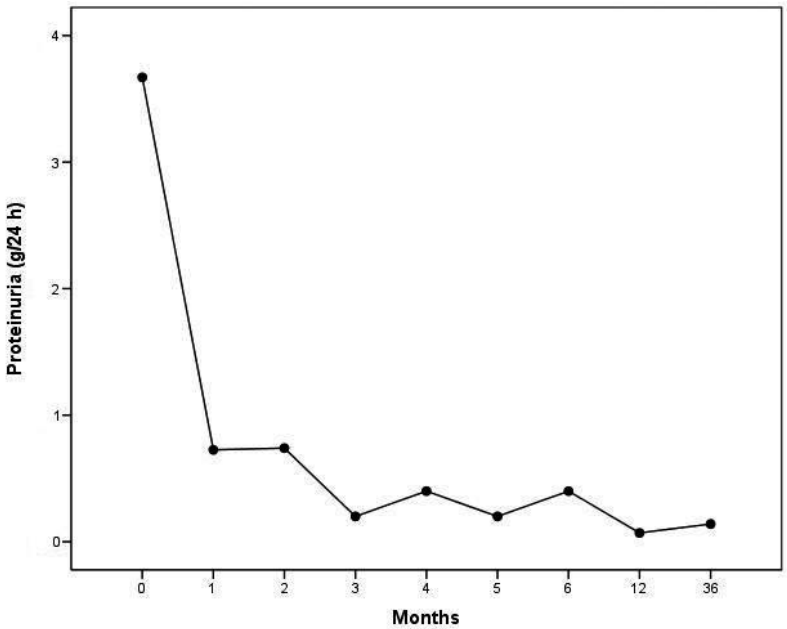

Fig. 1. *Proteinuria after ACTH-AZA treatment and during follow-up.*

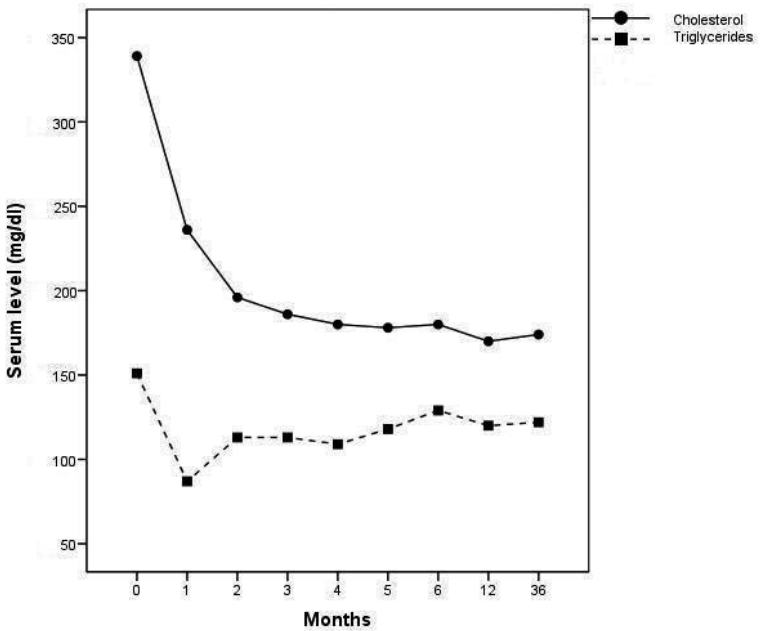

Fig. 2. *Serum cholesterol and triglycerides after ACTH-AZA treatment and during follow-up.*

38mg/dL, uric acid 7.7mg/dL, total proteins 4.3g/dL, albumin 1.8g/dL, total cholesterol 275mg/dL, triglycerides 202mg/dL, LDL cholesterol 151mg/dL, HDL cholesterol 74mg/dL, ESR was 35mm/h, haemoglobin 14.2g/dL. Serum complement C3-C4 and immunoglobulin levels were normal, antinuclear antibodies, extractable nuclear antigens antibodies, anti-dsDNA antibodies were absent. Serology for hepatitis B and C antigens was negative. Urinalysis revealed microscopic hematuria and proteinuria was 5.6g/24h.

These findings were compatible with nephrotic

syndrome and percutaneous renal biopsy was performed. Possible secondary causes of nephrotic syndrome were ruled out and tumoral markers were negative.

Renal tissue was processed and 47 glomeruli were found, two of which showed global sclerosis, whereas all the others did not show proliferative features and there was no evidence of crescents, fibrinoid necrosis or endocapillary proliferation. Moderate subepithelial deposits were present on the basement membrane. Infiltration of inflammatory cells and fibrosis were visible in the tubule and interstitium. Arteries were unremarkable, while arterioles showed mild hyaline deposition. Along capillary walls, immunofluorescence microscopy showed granular staining for IgG 3+, C3 2+, κ light chains 3+ and λ light chains 3+. Thus, IMN with mild arteriolosclerosis was diagnosed. Therefore a treatment (Ponticelli protocol) based on 3 intravenous pulses of methylprednisolone at months 1, 3, 5 followed by oral prednisone 0.5mg/Kg per day in a single morning dose for 27 days was started; then steroids were stopped and chlorambucil 0.2mg/Kg per day at months 2, 4, 6 was administrated. Symptomatic therapy with dietary salt restriction, irbesartan 300 mg daily and ezetimibe/ simvastatin 10/40mg daily was also started. After six months of treatment, remission was not obtained and laboratory tests showed: creatinine 1mg/ dL (MDRD-4 formula creatinine clearance 55 ml/min), urea 42mg/dl, cholesterol 281mg/ dL, triglycerides 242mg/ dL, LDL total cholesterol 190mg/ dL, HDL cholesterol 43mg/dL and proteinuria 4.3g/24h. Because of hypertension, cyclosporine treatment was not recommended and we decided to treat IMN with synthetic ACTH 1 mg administered by two intramuscular injection per week for 5 weeks, in gradually reduced doses (1 injection per week for 3 weeks, then 1 injection every two weeks for a total treatment period of six months) in association with AZA 2mg/Kg daily for a period of three months, then a decreased dose at 1 mg/kg daily in the following months, for a total treatment period of six months. After six months of the new treatment, we noticed a dramatic decrease of proteinuria (0.4g/24h), total cholesterol (186mg/dL), LDL cholesterol (81mg/ dL), triglycerides (113mg/dL) with an increase of HDL cholesterol (64mg/dL); renal function was in normal range (creatinine 0.8mg/dL, urea 38mg/dL, MDRD-4 formula creatinine clearance 71mL/min). During 36 months of follow-up, carried out every 3 months, laboratory tests showed: creatinine 0.8mg/ dL, urea 29mg/dL, total cholesterol 179mg/dL, triglycerides 110mg/dL, LDL cholesterol 73mg/dL, HDL cholesterol 72 mg/dL, and proteinuria value was stable on 0.14g/24h (Figs. 1 and 2).

DISCUSSION

IMN treatment remains controversial and it is well known that corticosteroids alone are not efficient, while Ponticelli protocol, alternating steroids and chlorambucil (0.2mg/kg/die) or cyclophosphamide (2-2.5mg/kg/die) for six months is recommended with good results. In absence of complete or partial remission after Ponticelli protocol, cyclosporine, ACTH, mycophenolate mofetil, rituximab can be used as second-line therapy (5).

Prolonged use of these agents may cause dangerous adverse effects and cyclosporine was not recommended for hypertension and mild renal arteriosclerosis found in biopsy. Thus, we decide to treat the unresponsive nephrotic syndrome of our patient with ACTH in association with AZA for six months. Synthetic ACTH is tetracosactide acetate synthetic peptide containing the first 24 amino acids of ACTH.

After administration of 0.25 mg of synthetic ACTH in patients with normal adrenocortical function, the peak plasma concentration of cortisol is achieved within 1 h and begins to decrease after 2-4 h. Then, ACTH is rapidly removed from the plasma by many tissues resulting in short action duration (6). The mechanism responsible for the beneficial effect of ACTH is unknown. It is unlikely that it may depend on the enhanced secretion of endogenous glucocorticoids. A possible speculation is that by modifying apolipoprotein metabolism, ACTH might restore podocyte expression of apolipoprotein J, which competes with terminal components of complement, C5b-C9, for the same receptor in podocytes. Thus, ACTH therapy may be functionally equivalent to *in situ* down-modulation of complement-mediated podocyte injury (6). Some studies have demonstrated that short-term treatment with ACTH has beneficial effects on the serum

lipoprotein profile (inducing an increase of serum HDL level and a reduction of serum lipoprotein concentration), the reduction of proteinuria and the improvement of glomerular function in the course of IMN.

In fact, ACTH is able to modify the metabolism of apoliprotein B containing lipoproteins, whereas the influence on HDL and lipoprotein metabolism may be mediated by steroids (7). Regarding clinical use of ACTH monotherapy in glomerulonephritis, further studies are needed to confirm the preliminary data based on a small number of patients with short-term follow-up (6). Although there is no consensus regarding treatment in the course of IMN, especially for unresponsive patients to Ponticelli protocol, several studies have been carried out to find other therapeutic options. Regarding AZA therapy, Ahuia et al., in a clinical study, reported no significant beneficial effects on the progression of IMN in patients treated with prednisone 1mg/kg/die and AZA 2mg/Kg/die (8). Naumovic et al. reported a prospective study on IMN patients who did not react to Ponticelli protocol. This treatment with small doses of prednisone and cyclosporine at 3 mg/Kg/die or AZA at 1.5 to 2mg/Kg/die for six months showed no beneficial long-term effects regarding renal function preservation in patients treated with AZA (9). However, no cases have been reported regarding simultaneous treatment of ACTH and AZA.

In our case, because the patient did not react to classic treatment with cytotoxic drugs (Ponticelli protocol), we used ACTH to reduce proteinuria and lipid profile which acted in a short period of time, in combination with the immunosuppressive drug (AZA) to alleviate the pathogenesis of glomerulonephritis and delay the progress of sclerosis.

Therefore, randomized clinical trials with a large cohort of patients are needed to evaluate the long-time effect of AZA-ACTH association.

REFERENCES

1. Jennette CJ, Olson JL, Schwartz MM, Silva FG. Membranous Glomerulonephritis. In Heptinstall's Pathology of the Kidney, 6th Edition. Lippincott Williams & Wilkins, 2007; p. 206-53.
2. Beck LH Jr, Bonegio RG, Lambeau G, Beck DM, Powell DV, Cummins TD, Klein JB, Salant DJ. M-type phospholipase A2 receptor as target antigen in idiopathic membranous nephropathy. N Engl J Med 2009; 361:11-21.
3. Ponticelli C, Passerini P. Can prognostic factors assist therapeutic decisions in idiopathic membranous nephropathy? J Nephrol 2010; 23(02):156-63.
4. Aaltonen S, Honkanen E. Outcome of idiopathic membranous nephropathy using targeted stepwise immunosuppressive treatment strategy. Nephrol Dial Transplant 2011; 0:1-7.
5. Ponticelli C. Membranous nephropathy. J Nephrol 2007; 20(3):268-87.
6. Ponticelli C, Glassock RJ. Membranous nephropathy. In Treatment of primary glomerulonephritis, Second Edition. Oxford University Press, 2009, p. 261-308.
7. Berg AL, Nilsson-Ehle P, Arnadottir M. Beneficial effects of ACTH on the serum lipoprotein profile and glomerular function in patients with membranous nephropathy. Kidney Int 1999; 56(4):1534-43.
8. Ahuja M, Goumenos D, Shortland JR, Gerakis A, Brown CB. Does immunosuppression with prednisolone and azathioprine alter the progression of idiopathic membranous nephropathy? Am J Kidney Dis 1999; 34(3):521-9.
9. Naumovic R, Jovanovic D, Pavlovic S, Stosovic M, Marinkovic J, Basta-Jovanovic G. Cyclosporine versus azathioprine therapy in high-risk idiopathic membranous nephropathy patients: A 3-year prospective study. Biomed Pharmacother 2011; 65(2):105-10.

LETTER TO THE EDITOR

SKELETAL MODIFICATIONS IN MUCOPOLYSACCHARIDOSES: AN OVERVIEW

L. SCARAMUZZO[1], C. PERISANO[1], A. LEONE[2], C. GRACI[1], M.S. SPINELLI[1], G. DI GIACOMO[1], E. VENANZI[1], A. SCHIAVONE PANNI[3] and G. MACCAURO[1]

[1]Department of Orthopaedics and Traumatology, Catholic University, Rome, Italy;
[2]Department of Bioimaging and Radiological Sciences, Catholic University, Rome, Italy;
[3]Science of Health Department, Molise University, Campobasso, Italy

Received August 8, 2011 – Accepted January 23, 2012

The mucopolysaccharidoses (MPS) are a group of rare diseases characterized by deficiencies in different enzymes required for degradation of complex carbohydrates. The enzymatic deficiencies lead to lysosomal accumulation of dermatan sulphate, heparan sulphate, and keratan sulphate in different tissue resulting in multi-system complications. Six different principal types are described. Most MPS types, with the exception of MPS III, are associated with widespread skeletal abnormalities and joint disease. Authors analyzed clinical pathological and radiographycal features of mucopolissacaridoses focusing on pelvic and spine pathologies that generally limit activity and normal life so they have to be treated at the beginning of their manifestations in order to avoid major complication and improve quality of life.

The mucopolysaccharidoses (MPS) are a group of diseases characterized by deficiencies in different enzymes required for degradation of complex carbohydrates. The enzymatic deficiencies result in the lysosomal accumulation of dermatan sulphate (DS), heparan sulphate (HS), and keratan sulphate (KS) in different tissue resulting in multi-system complications (1). All MPS types are very rare heritable disorders with prevalence data varying considerably between regions. They have a chronic and progressive course, with a wide spectrum of progression rate and clinical manifestations, according to different mutations, also in the same enzyme (3). In medical literature six different principal types of MPS are described, MPS I, II, III, IV, VI, VII, IX, differentiated by the qualitative and quantitative enzyme deficiency, the type of affected GAG and the presence of mental retardation, and the different skeletal abnormality (2) (Table I). Typical features of MPS are short stature, secondary to a combination of structural, metabolic and endocrine abnormalities (3), coarse facial features, loss of hearing, organomegaly, secondary to GAG accumulation and organ dysfunction, respiratory and cardiovascular complications. An exception is represented by MPS type III in which patients usually do not show severe somatic manifestations but a profound mental retardation (2). A mental retardation is present also in MPS VII and in severe forms of MPS I and MPS II. Most MPS types, with the exception of MPS III, are also associated with widespread skeletal abnormalities and joint disease. The presence of these signs and symptoms occurring in concert can usually suggest the diagnosis of MPS.

Key words: mucopolyssacaridosis, skeletal abnormalities, dysostosis, bone remodelling disorder

Mailing address: Dr. Giulio Maccauro,
Department of Orthopaedics and Traumatology,
Catholic University,
Agostino Gemelli Hospital,
L.go F. Vito, 8 00168 Rome, Italy .
Tel: +39 06 30154353; Fax: +39 06 3051161
e-mail: giuliomac@tiscali.it

0393-974X (2012)

DISCLOSURE: ALL AUTHORS REPORT NO CONFLICTS OF INTEREST RELEVANT TO THIS ARTICLE.

Table I. *Table showing the classification of different types of mucopolysaccaridosis.*

Type	Enzyme deficiency	GAG affected	Mental status	Skeletal manifestations
MPS I (mild and severe)	α –L Idurosinase	Dermatan and heparan sulfate	From normal intelligence to mental retardation	Short stature, dysostosis multiplex
MPS II (mild and severe)	Iduronate sulfatase	Dermatan and heparan sulfate	From normal intelligence to mental retardation	Short stature, dysostosis multiplex
MPS III A	Heparan – N - sulfatase	Heparan sulfate	Profound mental retardation	Mild somatic manifestations
MPS III B	α-N-acetilglucosaminidase	Heparan sulfate	Profound mental retardation	Mild somatic manifestations
MPS III C	Acetyl-CoA- α-glucosaminide acetyltransferase	Heparan sulfate	Profound mental retardation	Mild somatic manifestations
MPS III D	N- acetylglucosamine 6 sulfatase	Heparan sulfate	Profound mental retardation	Mild somatic manifestations
MPS IV A	Galactose -6-sulfatase	Keratan sulphate, chondroitin 6-sulfatase	Normal intelligence	Short-trunk dwarfism
MPS IV B	β -galactosidase	Keratan sulfate	Normal intelligence	Short-trunk dwarfism
MPS VI	Arylsulfatase B	Dermatan sulfate	Normal intelligence	Short stature, dysostosis multiplex
MPS VI	β -glucurunidase	Dermatan sulfate heparan sufate chondroidin 4-6-sulfates	Mental retardation	Short stature, dysostosis multiplex
MPS IX	Hyaluronidase	Hyaluronan	Normal intelligence	Short stature

Severe cases are generally recognised early in life, but in presence of more attenuated phenotypes, it can take many years before identifying a metabolic origin of the symptoms (2). A first diagnosis of MPS can be obtained with an analysis of urinary GAG, but this technique cannot discriminate between different MPS subtypes and may fall in the normal range for the mild and non-progressive forms. A definite diagnosis can only be made by measuring enzyme activity; a very reduced or absent enzyme activity together with clinical signs of the disease establishes the presence of the pathology (4). The diagnosis can be supported by mutational analysis of the affected gene, which could be useful in the beginning of a genetic counselling of the patients and their families (Table II). In MPS II, which is an X-linked disease, it is the only way to identify female carriers with certainty (5). The introduction of new, specific therapies for several MPS types has increased the need for early diagnosis.

Radiologic findings in mucopolysaccharidoses

Radiologic findings generally play an important role in diagnosing MPS. Radiologic imaging does not

Table II. *Table showing the main diagnostic exam in mucoplysaccaridosis.*

Exam type	Result	Differential diagnosis between subtypes
Analysis of urinary GAG	High urinary GAG levels	No
Analysis of enzyme activity	Reduced or absent enzyme activity	Yes
Mutational analysis of the affected gene	Identification of the mutation type	Yes
Analysis of serum levels of heparin cofactor- II- thrombin	Increased levels	No
Quantitative measurement (height and head circumference)	Decreased height, increased head circumference	Partially
Radiological exam	Dysostosis, hip dysplasia, claw hands, scoliosis and kyphosis etc.	Partially
Functional tests	Evaluation of body and mental function	Partially

permit to accurately differentiate between MPS types based on specific skeletal X-ray or neuroimaging characteristics (6). A genetic skeletal survey generally includes skull, antero-posterior (AP) and lateral view, chest AP view, spine AP and lateral view, pelvis AP view, long bones AP view and hands and feet views, in order to individuate characteristic dysostosis multiplex. Another characteristic radiological sign to evaluate soon after MPS diagnosis is cervical spine instability, in which case lateral cervical spine X-ray with flexion and extension views could be useful, especially after enzyme replacement therapy or hematopoietic cell transplantation, which may increase joint or ligament flexibility (6). Further skeletal X-ray follow-up examinations may be required to evaluate specific clinical problems such as hip pain, scoliosis/kyphosis or genu valgum. Skeletal X-rays are generally sufficient to make MPS diagnosis, but in the more severe forms in which a mental component is present also more sophisticated radiologic exams are very important. More subtle osseous anomalies can be identified using CT, which give also a 3-dimensional view of the skeletal part being examined and permits a more complete surgical planning when necessary. MRI of the brain and spinal cord is essential in order to evaluate MPS complications such as cervical spine compression or hydrocephalus. These evaluations should be initiated at diagnosis for baseline assessment and then only repeated every one to three years according to clinical severity 6). When mental artefacts preclude high quality MRI, then CT may be the preferred imaging technique. MPS patients are in fact the most difficult patients for performing advanced imaging studies for different reasons: many patients present an important mental retardation and are not very cooperative; airway problems, very common in these patients, make performing general anaesthesia difficult. CT and MRI imaging of the thoracic spine is also complicated by both cardiac and respiratory motion. A regular and systematic evaluation of MPS patients using a radiologic reproducible scoring system could be very useful for evaluating and monitoring these patients for surgical treatment, and for measuring the impact of treatment. A scoring system could also be useful in evaluating the dysostosis multiplex, the typical skeletal alterations of MPS, characterized by a great variety in bone shapes among individuals, including even interfamilial variability.

Bone quality

A typical characteristic of patients affected by MPS, though there is a paucity of research focused on this, is a defect in bone mineralization. Generally

60-80% of the variability in peak bone mass depends on heritable factors (7). Many modifiable factors can contribute to the development of peak bone mass, such as weight bearing, physical activity, calcium, vitamin D intake (8). Several factors negatively influence bone mineralization in MPS: small frame, abnormal gait or limited mobility and decreased physical activity or post-surgical non-weight bearing. Additionally, the presence of nutritional deficiencies, particularly of vitamins, may also negatively affect bone accumulation. An accurate interpretation of the data regarding bone mineral density of these patients is also very difficult. These data are important, especially in order to monitor patients on enzyme replacement therapy (ERT). Patients with MPS have considerable height deficits, often accompanied by large heads and dense skulls, therefore for these patients an MOC DXA excluding head in respect to total body is generally recommended. Size considerations are very important when interpreting aBMD measurements (9). The relationship between the change in aBMD and growth should be closely monitored and considered in the interpretation of DXA scan especially in patients on ERT, where the induced growth brings a decrease in bone mineral density Z-score (10). A similar pattern is reported in healthy children during the adolescent growth spurt when bone growth precedes mineralization and bone density decrease. Adolescence is in fact the second peak in fracture incidence, which is more common in males than females, with the peak of age around 14 years for males and around 12 years for females, similar to the age of peak high velocity. Fracture incidence is elevated during this period of rapid growth due to the lack of mineralization of bone following skeletal growth (11). The same process takes place in MPS patients on ERT in which skeletal growth is present but not consequent bone mineralization, so these patients become at elevated risk of pathologic fractures (12). ERT therapy is generally a long-term treatment administered indifferently in childhood or in adult age, but its clinical impact is greatest in patients aged under 16 years. The poor mineralization becomes an adjunctive risk factor in these patients as well as abnormal length and diameter of long bones, especially femoral neck and hip dysplasia. This increased risk however does not affect the outcome of these patients after surgical treatment.

Skeletal manifestations

Three mechanisms probably affect skeletal development in mucopolysaccharidoses, with a systemic disturbance of bone modelling, the presence of focal failures of ossification and with the development of an avascular disorder of the femoral head (13). The disturbance of bone modelling is seen in both primary ossification and modelling of the skeleton, resulting in very short stature and poor diaphyseal modelling. The focal failure is seen especially in the anterosuperior quarters of the lowest thoracic and in the upper two lumbar vertebral bodies, in the roof of the acetabulum and the lateral margin of the proximal tibial metaphysic. In all these sites it is possible to identify the cartilage elements, but the ossification is lacking (13). Failure of ossification in the thoraco-lumbar junction is present in all types of mucopalysaccharidoses, and is probably responsible for the kyphosis deformity seen in these diseases. The process results in anterior wedging, retrolisthesis of the apex vertebrae and anterior herniation of the intervertebral discs at the thoracolumbar junction, causing the development of severe scoliosis and kyphosis in which surgical fusion is required (14). The criteria for fusion follow the traditional indications for intervention in complex deformity, including the need for a combined anterior and posterior fusion in severe deformity and in less mature children in order to prevent crankshaft phenomenon (15).

Hip problems are present in all MPS and can be divided in two major categories: hip dysplasia due to ossification failure and osteonecrosis-like epiphyseal dysplasia (15). The disorder of the acetabulum is similar to that in the vertebral bodies and the developmental failure of the lateral part of the acetabulum precludes the ossification of this tissue, and in the lateral margin of the acetabulum it is possible to see a significant cartilaginous anlage in the MRI or arthrogram. This defect results in hip instability and late dislocations. Another important cause of hip dysplasia is an epiphyseal dysplasia, assimilable to the osteonecrosis or to the Perthes disease. In MPS patients, this disease could be the final result of an inflammatory apoptosis (16), and is characterized by partial fragmentation of the medial epiphysis, followed by remodelling and thinning of the affected segment (13). In these

patients two local abnormalities may contribute to the development of this pathological situation: the failure of the lateral portion of the acetabular roof, which causes an increase of load on the medial part of the femoral head, and also the valgus angulation of the femoral neck, which compromises the medial ascending retinacular vessels (13). Hip dysplasia in MPS patients generally requires a surgical treatment which, for these patients, is a combination of osteotomies in order to reposition the bone and optimize hip mechanics. Generally two osteotomies are performed: a pelvic osteotomy to reduce the global acetabular deficiency, and a proximal femoral osteotomy to reduce the valgus deformity of the neck (17). When the hip is dislocated a capsulorrhaphy is also necessary. In most severe and advanced cases also a prosthetic replacement could be required. This solution has to be carefully evaluated, taking into account the general complications of these patients. Another side of incomplete ossification in MPS patients is the lateral margin of the proximal tibial metaphysis. At this site, generally, a valgus deformity may be seen, due to an altered transmission of load. The greater part of the load is normally transmitted through the medial side of the knee, so structural failure is delayed until the end of the first decade of life (13). Some patients may also show typical knock-knees that often require surgery. Indication for surgery is a tibial-femoral angle greater than 15° (15). Surgical treatment is represented by femoral or tibial osteotomies near the knee. In these patients osteotomies are generally invasive and painful, but often necessitate obtaining and maintaining a good result that staple or tension band plate could not be able to achieve in such small patients, who do not have enough growth remaining to modulate. At the level of the knee, patients generally present also a typical stiffness, which prevents full straightening and results in a crouched gait. Medical and genetical therapy could generally improve this condition (17). A typical stiffness may be also recognized in the upper extremities, especially in shoulder and elbow. Also this stiffness showed a good responsivity to ERT therapy, also when it was evident after several years. (17) Forearm pronation and supination may also be limited in Madelung's deformity, especially in MPS type II (18). Other typical manifestation of MPS in the upper extremities are periferical neuropathy; primary neuropathy or secondary neuropathy due to GAG accumulation in the synovial tissue, known as "trigger digits". These neuropathies interest the median nerve at the level of the carpal tunnel, and are generally unrecognized in such patients, resulting in loss of function. For both conditions in MPS a fast surgical release is recommended, that may be carried out also in the same surgical procedure. A delayed treatment of trigger digits may result in fixed flexion contractures.

Another typical site of accumulation of GAG is represented in MPS by the retro-odontoid space, resulting in progressive stenosis and compression of the spinal cord at the occipito-cervical junction (19). At this site a delayed ossification is also recognized of the odontoid process, with the persistence of a cartilagineous anlage, prone to repetitive trauma, and consequent fracture. These repetitive traumas cause two major problems - an atlanto-axial instability, due to dens fracture associated to ligamentous instability, commonly visible in flexion-extension radiographs, and a cartilage/fibrocartilage reactive hypertrophy around the odontoid process, with a thickening of the dura and ligamentum flavum hypertrophy, resulting in a complex cervical stenosis (19). This combination of pathological factors may also be seen at subaxial cervical level resulting in a severe myelopathy. These complicaton can only be treated by surgery. A cervical decompression could be performed with fusion of the atlo-axial joint, or in absence of an evident instability only a wide decompression. Indications for surgery to be considered are: a cord space < 14 mm, also in asymptomatic patients; a cervical instability of >8 mm, with an instability from 5 to 8 mm; the presence of a spinal cord impingement or deteriorating neurological conditions (20).

CONCLUSIONS

MPS presents a significant muscoloskeletal involvement which involves several areas such as spine, hip, knee, and hands, resulting in severe disabilities. The skeletal pathologic conditions, except for cervical spine, are rarely life threatening but generally limit a child's functioning, activity and normal life therefore they have to be treated at the beginning of their manifestations in order to avoid major complications and improve quality of life.

REFERENCES

1. Neufeld E. The mucopolysaccharidoses, in : The metabolic and molecular basis of inherited disease. C. Scriver, McGraw-Hill, 2001; 3421-52.
2. Beck M, Muenzer J, Scarpa M. Evaluation of disease severity in mucopolysaccharidoses. J Ped Rehab Med 2010; 3:39-46.
3. Polgreen LE, Tolar J, Plog M, et al. Growth and endocrine function in patients with Hurler syndrome after hematopoietic cell transplantation. Bone Marrow Transplant 2009; 44:279-85.
4. Giugliani R, Harmatz P, Wraith JE. Management guidelines for mucopolysaccharidosis VI. Pediatrics 2007; 120:405-18.
5. Martin R, Beck M, Eng C, et al. Recognition and diagnosis of mucopolysaccharidosis II (Hunter syndrome). Pediatrics 2008; 121:e377-e86.
6. Lachman R, Martin KW, Castro S, Basto MA, Adams A, Teles EL. Radiologic and neuroraiologic findings in the mucopolysaccharidoses. J Ped Rehab Med 2010; 3:109-18.
7. Heany RP, Abrams S, Dawson-Hughes B, et al. Peak bone mass. Osteoporosis Inter 2000; 11:985-1009.
8. Misra M, Pacaud D, Petryk A, et al. Vitamin D deficiency in children and its management: review of the current knowledge and recommendations. Pediatrics 2008; 122:398-417.
9. Fewtrell MS, Gordon I, Biassoni L, Cole TJ. Dual X-ray absorptiometry (DXA) of the lumbar spine in a clinical paediatric setting: does the method of size-adjustment matter? Bone 2005; 37:413-9.
10. Fung EB, Johnson JA, Madden J, Kim T, Harmatz P. Bone density assessment in patients with mucopolysaccharidosis: a preliminary report from patients with MPS II and VI. J Ped Rehab Med 2010; 3:13-23.
11. Bailey DA, McKay, Minwald RL, Corcker PRE, Faulkner RA. A six-year longitudinal study of the relationship of physical activity to bone mineral accrual in growing children: The University of Saskatchewan bone mineral accrual study. J Bone Miner Res 1999; 14:1672-9.
12. Ichikawa T, Nishimura G, Tsukune Y, Dezawa A, Miki H. Progressive bone resorption after pathological fracture of the femoral neck in Hunter's syndrome. Pediatr Radiol 1999; 12:914-6.
13. Field RE, Buchanan JAF, Copplemans MGJ, Ajchroth PM. Bone-marrow transplantation in Hurler's syndrome. J Bone Joint Surg Br 1994; 76-B:975-81.
14. Levin TL, Berdon WE, Lachman RS, Anyane-Yeoba K, Ruzal-Shapiro C, Roye DP Jr. Lumbar gibbus in storage diseases and bone dysplasias. Pediatr Radiol 1997; 27:289-94.
15. White KK, Harmatz P. Orthopedic management of mucopolysaccharide disease. J Pediatr Rehab Med 2010; 3:47-56.
16. Simonaro CM, D'Angelo M, He X, et al. Mechanism of glycosaminoglycan-mediated bone and joint disease: implications for the mucopolysaccharidoses other connective tissue diseases. Am J Pathol 2008; 172:112-22.
17. Muenzer J, Guksavas-Calikoglu M, McCandless SE, Schuetz TJ, Kimura A. A phase I/II clinical trial of enzyme replacement therapy in mucopholysaccharidosis II (Hunter syndrome). Mol Genet Metab 2007; 3:329-37.
18. White KK, Raff HSM, Goldberg MJ. Muskoloskeletal Health in MPS II: Pediatric outcome data collection instrument (PODCI), demonstrated functional improvement in patients on ERT, in World Symposium 2009, San Diego CA.
19. Stevens JM, Kendall BE, Crockard HA, Ransford A. The odontoid process in Morquio-Brailsford's disease. The effects of occipitocervical fusion. J Bone Joint Surg Br 1991; 73:851-8.
20. White KK, Steinman S, Mubarak SJ. Cervical stenosis and spastic quadriparesis in morquio disease (MPS IV). A case report with twenty-six years follow-up. J Bone Joint Surg Am 2009; 91:438-42.

JOURNAL OF BIOLOGICAL REGULATORS & HOMEOSTATIC AGENTS Vol. 26, no. 1, 145-149 (2012)

LETTER TO THE EDITOR

ADVERSE REACTION TO IRRIGATION WITH POVIDONE-IODINE AFTER DEEP-IMPACTED, LOWER THIRD MOLAR EXTRACTION

G. SAMMARTINO[1], M. TIA[1], S. TETÉ[3], L. PERILLO[2] and O. TROSINO[1]

[1]Department of Oral Surgery, University of Naples "Federico II", Italy; [2]Department of Orthodontics, Second University of Naples, Italy; [3]Department of Oral Surgery, University of Chieti, Italy

Received August 5, 2011 – Accepted January 19, 2012

Povidone-iodine is most commonly used worldwide because of its germicidal activity, relatively low irritancy or toxicity and low cost. Frequently, povidone-iodine is used as a topical antiseptic for treating and preventing wound infection. In rare cases skin irritation or iododerma-like eruption could represent possible adverse effects due to the oxidative effects of iodine and allergic hypersensitivity reaction. In this report we describe a case of a massive adverse reaction to the irrigation of surgical wound dehiscence with 10% povidone-iodine solution after deep-impacted, lower third molar extraction. This reaction was related to a central neurotrophic reflex involving three trigeminal branches and probably due to a peripheral chemical insult of mandible nerve. This adverse reaction determined a severe edema and diffuse skin lesions, involving the whole left side of the face mimicking an iododerma-like eruption. These violent symptoms were solved after 60 days. Furthermore, we report a small permanent skin scar in the zygomatic area and transient alterations of facial sensitivity on the affected side which completely disappeared in 6 months.

Iodine compounds have been widely used as antiseptics and disinfectants for the skin before surgical procedures. Povidone iodine (PI) is a water-soluble combination of molecular iodine and the solubilizing agent polyvinyl-pyrrolidone (PVP-iodine). PVP-iodine is most commonly used worldwide because of its germicidal activity, relatively low irritancy or toxicity and low cost. Frequently, povidone-iodine is used as a topical antiseptic for treating and preventing wound infection (1). The iodine compounds are available in aqueous solution, tincture, aerosol, ointment or foam (2, 3). In rare cases skin irritation or iododerma-like eruption could represent possible adverse effects, even if less frequent, due to the oxidative effects of iodine and allergic hypersensitivity reaction (4, 5). Sometimes 10% povidone iodine solution can cause primary irritant dermatitis and allergic contact dermatitis (6-8). In literature the local irrigation before the tooth extractions by means of 10% PI solution of the gingival sulcus was described which is considered an important source of bacteremia following dental procedures (9, 10). The iodine compound is considered most effective in prevention of post-treatment bacteremia compared to chlorexidine or hydrogen peroxide. PI is also topically used during subgingival instrumentation in order to improve the outcome of non-surgical periodontal therapy (11). PVP-iodine has been used in a mouthwash to inhibit the development of gingivitis, for subgingival

Key words: povidone-iodine, neurotrophic reaction, dehiscence, lower third molar, neurologic damage

Mailing address: Prof. Gilberto Sammartino,
Dipartimento di Scienze Odontostomatologiche
e Maxillo-Facciali (Ed. 14),
Università degli Studi di Napoli "Federico II"
Via S. Pansini, 5 80131 Napoli, Italy
Tel/Fax: +39 0817462118
e-mail: gilberto.sammartino@unina.it

0393-974X (2012)

DISCLOSURE: ALL AUTHORS REPORT NO CONFLICTS OF INTEREST RELEVANT TO THIS ARTICLE.

a

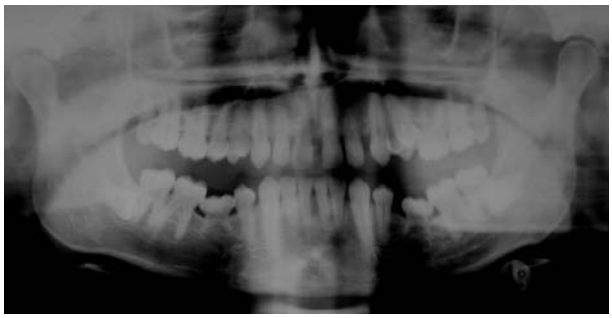

b

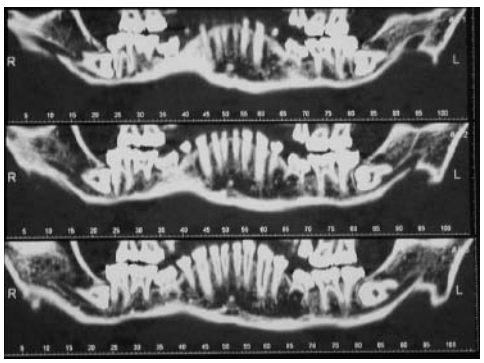

Fig. 1. a,b) *Orthopantomograpy and CT images for the correct evaluation before deep-impacted lower third molar extractions.*

irrigation in periodontal maintenance and in patients with recurrent periodontitis (12-14). In this report we describe a case of a massive adverse reaction to the irrigation of the dry alveolar socket with 10% povidone-iodine solution after impacted, lower third molar extraction.

Case report

At the Oral Surgery Division of the University of Naples "Federico II" we admitted a 31-year-old man without a past medical history of allergic events or other pathologies in order to perform an intervention for orthognatic surgery to correct a second skeletal class. Before the major surgery we planned the extraction of both lower third molars in deep impaction (Fig. 1). Following the lower, deep-impacted third molar extraction on the left side the patient had a surgical wound dehiscence (Fig. 2). After suture removal, irrigation with 10% povidone-iodine (PI) solution was used in order to clean and disinfect the post-extractive site and was repeated every week. After 2 weeks, during the irrigation with PI, unexpected and diffuse edema developed on the left side of the face involving the zygomatic, temporal, parietal and frontal area. The chin area was also involved in the edema. Severe alterations of neurological sensitivity on the affected facial side were immediately noted, related to the massive edema involving the facial nerve, associated to the transient damage on the lower and upper alveolar nerves with consequent hypoesthesia in the correspondent areas. The patient was admitted to hospital in order to begin a clinical follow-up and adequate medical therapy. A therapy with cortisone, antibiotics, enzymatic anti-inflammatories and B1, B6, B12 vitamins (Betametasone 4mg i.v./once in a day; Ceftriaxone 1g i.v./twice in a day; Escine 5mg i.v./twice in a day) was prescribed under gastric protection (Zantac i.v 50mg/day). Laboratory data showed elevated CK (1807 U/l) and AMS (1196 U/l) values, IgE value was modified (183 KU/l); the white blood cell count was within the normal limits. The ecography and CT images showed normal conditions of parotid gland and other facial structures; only a massive mandible lymphoadenopathy was noted. After 4 days the partial resolution of the edema began but multiple bullous lesions evolving in erosions and ulcerations were noted on the left side facial skin: these symptoms were compatible with an iododerma-like eruption. After 5 days, according to the consulting dermatologist, we prescribed the substitution of parenteral cortisone therapy with oral cortisone therapy (prednisone 25 mg, twice in a day) and the application of fucsid acid gel on the skin lesions (twice a day for 15 days). Work-up included lesion bacterial culture, which revealed normal skin flora, a Gram stain that showed no organisms and blood cultures that were negative. After consulting the neurologist we related this abnormal reaction to a central neurotrophic reflex of the trigeminal branches caused by a peripheral irritation of exposed mandibular nerve after the lower third molar extraction. After 15 days we also noted herpes-like lesions involving the hard and soft palate area. The ophthalmologic control pointed out left conjunctive hyperaemia, resolved after local therapy with nebicin

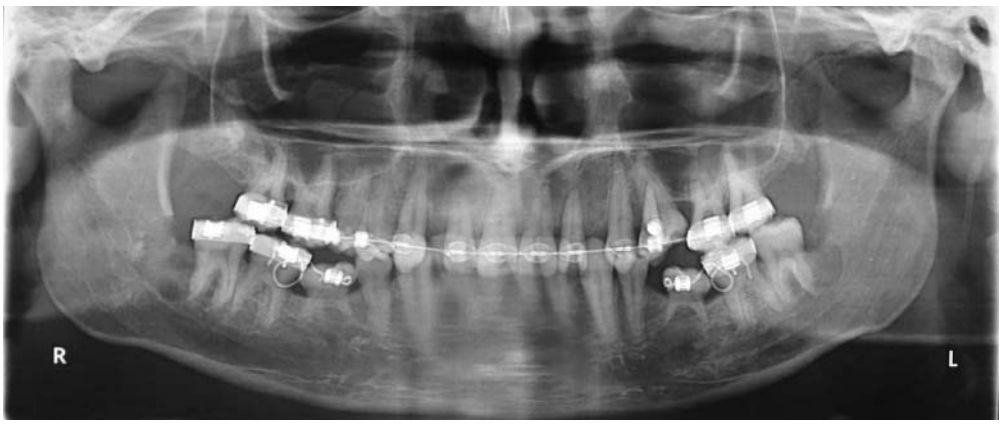

Fig. 2. *Radiographic control 20 days after the lower third molar extractions. On the left side we reported a dry alveolar pot-extractive socket.*

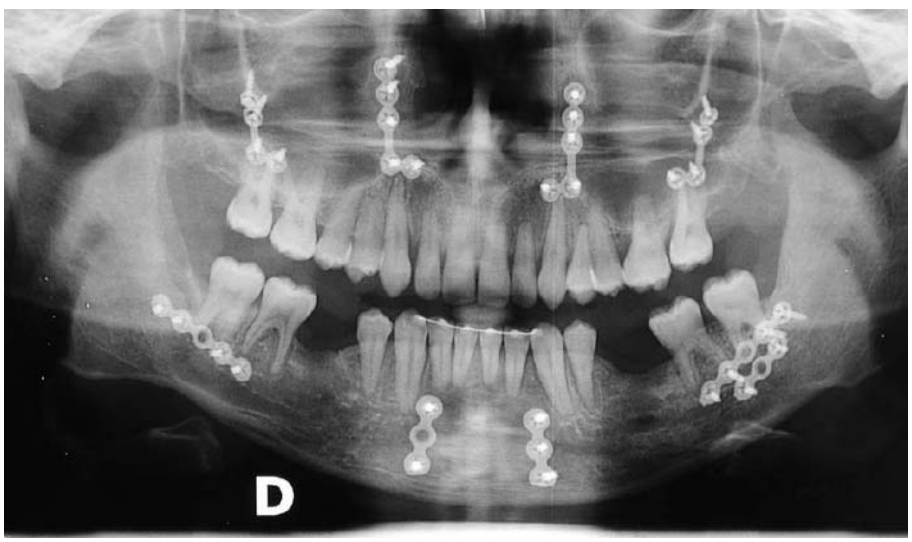

Fig. 3. *Radiographic image after the orthognatic surgery for a second skeletal class.*

for 2 weeks. After 30 days the altered laboratory data (CK, AMS and IgE) returned within normal limits. After 60 days the edema and skin lesions were completely resolved, only a small scar remained in the zygomatic area; while the alterations of facial sensitivity and the neurological damage to the lower and upper alveolar nerves completely disappeared after 6 months. After 1 year the same patient was submitted to the previously planned orthognatic surgery with excellent clinical and esthetic outcomes (Fig. 3).

DISCUSSION

The unexpected, unusual and massive reaction to the irrigation with 10% PI solution after the lower third molar extraction described in this report could be justified by the direct contact of the chemical agent with the exposed alveolar nerve after the deep-impacted lower third molar avulsion. We related this abnormal reaction to a central neurotrophic reflex of three trigeminal branches caused by an iodine peripheral irritation of exposed mandibular nerve

after deep-impacted lower third molar extraction. Following the povidone-iodine chemical insult to the mandibular nerve, a severe edema, several skin lesions, mimicking an iododerma-like eruption and herpes-like lesions at the hard and soft palate were reported in association of transient neurologic alterations of facial sensitivity. We related the high values of CK and AMS to the initial chemical necrosis of facial muscles; while the high value of IgE could be related to the afore-mentioned pseudo-allergic response. The diagnosis of iododerma rests on history and clinical findings, because no laboratory or histopathological finding is pathognomonic (15).

In literature patients have presented with polymorphous lesions that may mimic Sweet's syndrome, pemphigus vegetans, mycosis fungoides and blastomycosis (16, 17). The main histological features of iododerma are hyperkeratosis in epidermis, pseudoepitheliomatous hyperplasia and a dermal-epidermal separation with epidermal necrosis underlying abscess formation. A superficial and deep perivascular, interstitial and perifollicular infiltrate containing numerous neutrophils with abscess formations and eosinophils have also been noted. Histology of early lesions shows superficial microabscesses and macroabscesses within the epidermis and dermis. Upon discontinuation of iodide use, lesions resolve typically within 4-6 weeks, leaving only mild post-inflammatory pigment changes and possibly dermal atrophy. Treatment of iododerma has been attempted with systemic corticosteroids, which may be helpful. However, iododerma is generally a self-limited condition following cessation of iodide exposure (18). Iododerma is a rare skin eruption that is usually induced by the systemic use of iodide-containing radiographic contrast medium or treatment with oral potassium iodide therapy. Iododerma has also more rarely been reported to occur following topical application of iodine. Review of the literature yielded 18 cases of povidone-iodine-induced burn. This adverse effect of povidone-iodine application typically occurs when the povidone-iodine has not been allowed to dry or has been trapped under the body of a patient in a pooled-dependent position. All patients with a history of iododerma should avoid iodine in their diet, medications and radiographic studies. However, the adequate clinical management of our patient allowed to resolve the case without relevant consequences; in fact, the small permanent skin scar in the patient's zygomatic area is not serious, considering the violent and massive adverse reaction to the topical use of 10% PI solution.

Our case report shows a rare massive adverse reaction to the topical irrigation of surgical wound dehiscence after rinsing with 10% povidone-iodine solution after a left, deep-impacted, lower third molar extraction. This reaction was related to a central neurotrophic response involving three trigeminal branches and probably due to a peripheral chemical insult of exposed mandible nerve after the surgical dehiscence. This adverse reaction induced a severe edema and diffuse skin lesions, involving the whole left side of face, mimicking an iododerma-like eruption. These violent symptoms were resolved after 60 days. Furthermore, we report the small permanent skin scar in the zygomatic area, and transient alterations of facial sensitivity on the affected side which completely disappeared in 6 months. This report showed an unusual but aggressive complication which can occur when a chemical agent such as the 10% povidone-iodine solution comes into contact with the exposed mandible nerve after recent surgery. In this case the oral surgeon must avoid the use of this chemical agent in the oral cavity.

REFERENCES

1. Flynn J. Povidone-iodine as a topical antiseptic for treating and preventing wound infection: a literature review. Br J Community Nurs. 2003; 8(S):36-42.
2. Chambers HF. Miscellaneous antimicrobial agents; disinfectants, antiseptics and sterilants. In: Basic and Clinical Pharmacology, 8th edition, Katzung BG (ed.): New York, NY, Lange Medical Books/ McGraw-Hill, 2001:852.
3. Lee S, Zhai H, Maibach H. Allergic contact dermatitis from iodine preparations: a conundrum. Contact Dermatitis 2005: 52:184-7.
4. Velázquez D, Zamberk P, Suárez R, Lázaro P. Allergic contact dermatitis to povidone-iodine. Contact Dermatitis 2009; 60:348-9.
5. Massé M, Falanga V, Zhou LH. Use of topical povidone-iodine resulting in an iododerma-like

eruption. J Dermatol 2008; 35:744-7.
6. Happle R. Chemical burn: a risk with outdated povidone-iodine. Pediatric Dermatology 2007; 24(4):449-50.
7. Lachapelle JM. Allergic contact dermatitis from povidone-iodine: a re-evaluation study. Contact Dermatitis 2005; 16:9-10.
8. Okamo M. Irritant dermatitis caused by povidone-iodine. J Am Acad Dermatol 1989; 5:860-3.
9. Yamalik MK, Yucetas S, Abbasoglu U. Effects of various antisepetics on bacteremia following tooth extraction. J Nihon Univ Sch Dent 1992; 34(1):28-33.
10. Rahn R, Schneider S, Diehl O, Schäfer V, Shah PM. Preventing post-treatment bacteremia: comparing topical povidone-iodine and chlorhexidine. J Am Dent Assoc 1995; 126(8):1145-9.
11. Rosling B, Hellström MK, Ramberg P, Socransky SS, Lindhe J. The use of PVP-iodine as an adjunct to non-surgical treatment of chronic periodontitis. J Clin Periodontol 2001; 28:1023-31.
12. Clark WB, Magnusson I, Walker CB, Marks RG. Efficacy of Perimed® antibacterial system on established gingivitis. Clinical results. J Clin Periodontolol 1989;16:630-635.
13. Wolff LF, Bakdash MB, Pilhlstrom BL, Bandt CL, Aeppli DM. The effect of professional and home sub-gingival irrigation with antimicrobial agents on gingivitis and early periodontitis. J Dent Hygiene 1989; 63:222-5.
14. Collins JG, Offenbacher S, Arnold RR. Effects of a combination therapy to eliminate Porphyromonas gingivalis in refractory periodontitis. J Periodontol 1993; 64:998-1007.
15. Chang MW, Miner JE, Moiin A, Hashimoto K. Iododerma after computed tomographic scan with intravenous radiopaque contrast media. J Am Acad Dermatol 1997; 36:1014-16.
16. Boudoulas O, Siegle RJ, Grimwood RE. Iododerma occurring after orally administered iopanoic acid. Arch Dermatol 1987;123:387-8.
17. Noonan MP, Williams CM, Elgart ML. Fungating pustular plaques in a patient with Graves' disease. Arch Dermatol 1994; 130:786-787,789-790.
18. Paul AK, Al-Nahhas A, Ansari SM, Islam N. Skin eruption following treatment with IOdine-131 for hyperthyroidism: a rare and un-reported early/ intermediate side effect. Nucl Med Rev Cent East Eur 2005; 8:125-7.

LETTER TO THE EDITOR

PLATELET-RICH PLASMA IMPROVES WOUND HEALING IN MULTIPLE MYELOMA BISPHOSPHONATE-ASSOCIATED OSTEONECROSIS OF THE JAW PATIENTS

V. COVIELLO[1], F. PELUSO[2], S.Z. DEHKHARGANI[1], F. VERDUGO[3], L. RAFFAELLI[1], P.F. MANICONE[1] and A. D'ADDONA[1]

[1]Department of Oral Sciences, Catholic University, Rome, Italy; [2]Department of Oral and Maxillofacial Surgery and Odontostomatology, A.O.R.N. "Sant'Anna and San Sebastiano", Caserta, Italy; [3]VA Hospital, Greater Los Angeles, Private Practice Altadena, Los Angeles, CA, USA

Received April 29, 2011 – Accepted December 12, 2011

Bisphosphonates are drugs used to treat various metabolic and malignant bone diseases. In the past 10 years intravenous bisphosphonates have been associated with increased risk of osteonecrosis of the jaw (ONJ). The aim of the present study is to evaluate platelet-rich plasma (PRP) wound healing benefits in multiple myeloma (MM) patients who developed ONJ after surgical tooth extraction. The study included 7 patients, 2 males and 5 females. All individuals had been taking zoledronate or pamidronate followed by zoledronate for an average of 5 years. Four subjects had only standard surgical debridement and sequestrectomy to treat the ONJ and three had additional autologous PRP. The patients were followed-up for 3 months. The use of PRP to enhance wound healing and reduce bone exposure seems to be a good treatment protocol in ONJ MM subjects.

Bisphosphonate drugs are synthetic analogs of inorganic pyrophosphate developed more than 30 years ago. They are used to treat various metabolic and malignant bone diseases (1-17). In the past 10 years bisphosphonate use has been associated with increased risk of ONJ (5). Marx et al. (2) and Ruggiero et al. (3) were the first to report ONJ episodes after tooth extractions, traumatic dental procedures and other oral injuries. They concluded that the aforementioned events can represent important risk factors for the development of ONJ. The majority of patients affected by ONJ had had history of malignancies and the only factor in common was the long-term intravenous administration of bisphosphonates, primarily zoledronate and/or pamidronate (4-7). Although the etiopathogenesis is unclear, a decreased osseous blood supply together with a hypercoagulable state and subsequent infection may be key factors in the progression of ONJ. Bone disease affects approximately 70% of MM patients and is associated with pain and/or pathologic fractures. Bone destruction could occur as a result of an osteoclast/osteoblast imbalance so that the increased osteoclast activity would favor osseous resorption (8). Treatment of avascular ONJ involves a variety of extensive therapies that remain controversial and challenging. The use of growth factors has been proposed to favor osseous wound healing in ONJ subjects treated with conventional surgical protocols (9, 15, 17, 18). PRP enhances the production of high platelet concentrations and it can therefore promote wound healing (9, 17-19). The

Key words: bisphosphonates, osteonecrosis of the jaw, multiple myeloma, platelet-rich plasma

Mailing address: Dr L. Raffaelli,
Catholic University of the Sacred Heart,
Department of Oral Sciences,
Largo A.Gemelli, 8
00168 Rome, Italy
Tel: +39 06 30154079 Fax +39 06 30154079
e-mail: lraffaelli@rm.unicatt.it

0393-974X (2012)

DISCLOSURE: ALL AUTHORS REPORT NO CONFLICTS OF INTEREST RELEVANT TO THIS ARTICLE.

aim of the present study is to evaluate PRP healing benefits for the treatment of ONJ occurring after surgical tooth extractions in MM patients taking zoledronate and/or pamidronate.

MATERIALS AND METHODS

From March 2008 to April 2009, seven patients were diagnosed with ONJ after tooth extractions. All individuals had MM and were in therapy with zoledronate (Zometa®) or pamidronate (Aredia®) followed by zoledronate for an average of 5 years. All subjects presented clinically with localized osteolytic bone lesions confirmed by panoramic radiographs and computed tomography (CT) scan evaluation. None of the patients had previously received radiation therapy to the head and neck region or chemotherapy (Table I).

Subjects were divided into two groups, A and B, according to the surgical treatment protocol. Group A patients (n=4) received only standard surgical therapy of debridement and sequestrectomy. Group B patients (n=3) received additional autologous PRP as proposed by Marx's et al. (19). Both treatment protocols followed included cessation of bisphosphonate therapy from 14 to 21 days before surgical therapy and administration of amoxicillin/clavulanic acid 1g (Augmentin®) twice daily for 14 days, itroconazolo 100 mg (Sporanox®) once daily 14 days, prednisone 5 mg (Deltacortene®) once daily for 10 days and Naproxene sodico 550 mg (Synflex Forte550®) twice daily as needed for pain. Tissue healing was further evaluated by measuring in millimeters (mm) the size of the lesion before and after surgical therapy and during the 3-month follow-up. Measurements were made with a Williams color-coded probe by the same calibrated examiner. Clinical examination was undertaken to detect exposed necrotic bone, edema, suppuration and signs of infection. Follow-up examinations were performed at 15,

Table I. *ONJ MM patients' characteristics.*

	GROUP A				***GROUP B***			
N° PZ	**1**	**2**	**3**	**4**	**5**	**6**	**7**	
SEX								***Sex ratio***
F	●	●	●		●		●	***1:2.5***
M				●		●		
AGE	**80**	**66**	**80**	**75**	**75**	**84**	**69**	***Median age*** ***75.57***
DIAGNOSIS	**MULTIPLE MYELOMA**							
BISPHOSPHONATE								
Zoledronate				●	●	●	●	***Median duration therapy*** ***8.5 years***
Pamidronate/ zoledronate	●	●	●					***Median duration therapy*** ***2.45 years***
LOCATION								
Mandible	●		●	●		●	●	
Mandible + Maxilla		●			●			

Table II. *Therapy and results.*

		GROUP A				*GROUP B*		
N° PZ		**1**	**2**	**3**	**4**	**5**	**6**	**7**
DISCONTINUATION OF BISPHOSPHONATES (days)		**16**	**20**	**14**	**15**	**21**	**21**	**20**
THERAPY		**DEBRIDEMENT/ SEQUESTRECTOMY**				**DEBRIDEMENT/ SEQUESTRECTOMY + PRP**		
FOLLOW UP (days)	**t0**	I. N.B E. F.	I. N.B. E.	I. N.B. E.	I. N.B. E.	I. N.B. E.	I. N.B. E.	I. N.B. E.
	15	N.B. E.	N.B. E.	N.B.	N.B.	N.B. E.	—	N.B. E.
	30	N.B. E.	N.B E.	N.B. E.	N.B. E.	E.	—	E.
	60	N.B. E.	N.B.	N.B.	N.B.	—	—	—
	90	N.B. E.	N.B.	N.B.	N.B.	—	—	—
OUTCOME/ HEALING		R. + left Hemi-mandibulectomy	S.B. N.	P.H. + ONJ right hemi-mandible	P.H.	S.H.	S.H.	S.H.

I: Infection; N.B.: Necrotic Bone; E: Edema: F: Fistula; R: Recurrence; S.B.N.: Stabilized Bone Necrosis; P.H.: Partial Healing; S.H.: Satisfactory Healing

30, 60 and 90 days thereafter (Table II).

RESULTS

Five patients presented mandibular bone exposure. Patients 2 and 5 of group A and B, respectively, presented radiographic osteolytic bone lesions both in the maxilla and mandible. In all cases, panoramic and CT scan evaluations revealed regions of osteolysis at the tooth extraction sites except for patient 3A who presented additional spontaneous mandibular ONJ on the buccal and crestal aspects of 36-37 areas.

Clinical examination revealed signs of infection, necrotic bone exposure and edema at the ONJ area before surgical therapy, in all seven patients (t0). Patient 1A had an additional abscess formation that developed into a trans-cutaneous fistula.

Post-surgical follow-up observations at 15, 30, 60 and 90 days, in group A subjects, revealed necrotic bone exposure and edema surrounding the treated area.

Group A patients showed clear signs of incomplete osseous healing with bone exposure > 1-2 mm. Patient 3A had also spontaneous necrotic lesions at the right hemi-mandible. Patient 2A presented a

stable in size necrotic bone exposure. Patient 1A had clinical worsening and the recurrent osseous lesion required a left hemi-mandibulectomy procedure. The 15 day follow-up in group B patients revealed significantly smaller exposed areas of bone and less edema. At 30, 60 and 90 days of follow-up, osseous lesions had progressively resolved displaying satisfactory healing and less than 1-2 mm of exposed bone (Table II).

DISCUSSION

ONJ is a rising dilemma in MM patients who have received long-term intravenous bisphosphonate therapy and dental surgery (5-8,11-12). Hoff et al. reported a 2.4% incidence of ONJ in MM patients (10). The management of MM patients with bisphosphonate-associated osteonecrosis of the jaw is challenging and can take long healing times (13-14).

Current therapy protocols entail bisphosphonate use discontinuity, surgical site debridement to obtain fresh wound bleeding margins and long-term antibiotic therapy (14-15). It is still unclear whether or not there is any benefit from interrupting bisphosphonate therapy (9). The clinical decision of interrupting bisphosphonate use, in the present study, was at the discretion of the treating physicians, surgeon and oncologist, and was based on the patients' symptoms and severity of the osseous lesions.

A variety of different treatment modalities has been proposed to enhance bone wound healing using growth and differentiation factors in ONJ surgical patients taking long-term intravenous bisphosphonates. Experimental and clinical studies have shown the effectiveness of various cellular mediators (bone morphogenetic proteins, interleukins, angiogenic growth factors) in bone wound healing (9, 16-19).

PRP is an autologous concentration of human platelets that provide a source of growth factors obtained by gradient density centrifugation. It may improve wound healing and bone regeneration (9, 16-18). PRP is a platelet concentrate that contains at least 1.000.000/mL in a 5-mL volume of plasma and contains 4 to 6 times the normal level of growth factors compared with peripheral platelet counts (17, 19).

The findings of the present study are not conclusive. However, the positive clinical outcomes after PRP use seem promising in the treatment of MM bisphosphonate-associated ONJ patients. Cetiner et al. (7) and Curi et al. (9) treated refractory cases of ONJ combining surgical necrotic bone resection and growth factors. They applied PRP topically onto the affected exposed bone achieving excellent osseous and mucosa healing in 6-8 months. Lee et al. (17) described the effects of PRP application plus hyperbaric oxygen (HBO) in 2 patients who were taking oral bisphosphonates to treat osteoporosis and who showed complete ONJ remission in 6-9 months.

The present study confirms the enhanced healing effects of PRP use in ONJ patients. Within the limitations of the present study, the use of PRP in ONJ MM patients seems to be a good treatment alternative to foster osteogenesis and accelerate wound healing.

ONJ is a rising dilemma in MM patients and appears to be a time-dependent process. Long-term intravenous bisphosphonate use can pose a serious of developing ONJ in MM patients after oral surgical procedures. The use of growth factors has been proposed to favor osseous wound healing in ONJ subjects treated with conventional surgical protocols. The mechanism of PRP for enhancing wound healing is not fully understood. High concentrations of specific growth factors may be responsible for the beneficial effects in soft and hard tissue wound healing. PRP may enhance the production of high platelet concentrations therefore promoting wound healing.

The present case series shows the potential beneficial effects of PRP on wound healing in MM ONJ-associated subjects and could be an integral part of future standard surgical protocols.

REFERENCES

1. Merigo E, Manfredi M, Meleti M, Corradi D,Vescovi P. Jaw bone necrosis without previous dental extractions associated with the use of bisphosphonates (pamidronate and zoledronate): a four-case report. J Oral Pathol Med 2005; 34:613-7.
2. Marx RE. Pamidronate (AREDIA) and Zoledronate (ZOMETA) induced avascular necrosis of the jaws: a growing epidemic. J Oral Maxillofac Surg 2003; 61:1115-8.

3. Ruggiero S, Mehrotra B, Rosenberg T, Engroff S. Osteonecrosis of the jaws associated with the use of bisphosphonates: a review of 63 cases. J Oral Maxillofac Surg 2004; 62:52-34.
4. Statz TA, Guthmiller JM, Humbert LA, Johnson GK. Intravenous bisphosphonate-associated osteonecrosis of the jaw. J Periodontol 2007; 78:2203-8.
5. Silverman SL et al. Osteonecrosis of the jaw and the role of bisphosphonates: a critical review. Am J Med 2009; 122:33-45.
6. Raffaelli L, Scaramuzzo L, Rossi Iommetti P, Graci C, Maccauro G, Manicone PF. Jaw osteonecrosis related to bisphosphonate treatment of bone metastasis. J Biol Regul Homeost Agents 2010; 24:115-21.
7. Cetiner S, Sucak GT, Kahraman SA, Aki SZ, Kocakahyaoglu B, Gultekin SE, Cetiner M, Haznedar R. Osteonecrosis of the jaw in patients with multiple myeloma treated with zoledronic acid. J Bone Miner Metab 2009; 27:435-43.
8. Badros A, Weikel D, Salama A, et al. Osteonecrosis of the jaw in multiple myeloma patients: Clinical features and risk factors. J Clin Oncol 2006; 24:945-52.
9. Curi MM, Cossolin GS, Koga DH, Araújo SR, Feher O, dos Santos MO, Zardetto C. Treatment of avascular osteonecrosis of the mandible in cancer patients with a history of bisphosphonate therapy by combining bone resection and autologous platelet-rich plasma: Report of 3 cases. J Oral Maxillofac Surg 2007; 65:349-55.
10. Hoff AO, Toth BB, Altundag K, et al. Frequency and risk factors associated with osteonecrosis of the jaw in cancer patients treated with intravenous bisphosphonates. J Bone Miner Res 2008; 23:826-36.
11. Jadu F, Lee L, Pharoah M, et al. A retrospective study assessing the incidence, risk factors and comorbidities of pamidronate-related necrosis of the jaws in multiple myeloma patients. Ann Oncol 2007; 18:2015-9.
12. Walter C, Al-Nawas B, Frickhofen N, Gamm H, Beck J, Reinsch L, Blum C, Grötz KA, Wagner W. Prevalence of bisphosphonate associated osteonecrosis of the jaws in multiple myeloma patients. Head Face Med 2010; 6:11.
13. Terpos E, Sezer O, Croucher PI, et al. European Myeloma Network. The use of bisphosphonates in multiple myeloma: recommendations of an expert panel on behalf of the European Myeloma Network. Ann Oncol 2009; 20:1303-17.
14. Dimitrakopoulos I, Magopoulos C, Karakasis D. Bisphosphonate-induced avascular osteonecrosis of the jaws: a clinical report of 11 cases. Int J Oral Maxillofac Surg 2006; 35:588-93.
15. Ruggiero SL, Thomas B, Dodson, Leon A. Assael, Regina Landesberg, Marx RE, Mehrotra B. American Association of Oral and Maxillofacial Surgeons Position Paper on Bisphosphonate-Related Osteonecrosis of the Jaws – 2009 Update. J Oral Maxillofac Surg 2009; 67:2-12.
16. Oyama T, Nishimoto S, Tsugawa T, Shimizu F. Efficacy of platelet-rich plasma in alveolar bone grafting. J Oral Maxillofac Surg 2004; 62:555-8.
17. Lee CY, David T, Nishime M. Use of platelet-rich plasma in the management of oral bisphosphonate-associated osteonecrosis of the jaw: a report of 2 cases. J Oral Implantol 2007; 33:371-82.
18. Marx RE. Platelet-rich plasma: evidence to support its use. J Oral Maxillofac Surg 2004; 62:489-96.
19. Marx RE, Carlson ER, Eichstaedt RM, Schimmele SR, Strauss JE, Georgeff KR. Platelet-rich plasma: Growth factor enhancement for bone grafts. Oral Surg Oral Med Oral Pathol Oral Radiol Endod 1998; 85:638-46.

JOURNAL OF BIOLOGICAL REGULATORS & HOMEOSTATIC AGENTS Vol. 26, no. 1, 157-163 (2012)

LETTER TO THE EDITOR

SCLEROSTIN CONCENTRATIONS IN ATHLETES: ROLE OF LOAD AND GENDER

G. LOMBARDI[1], P. LANTERI[1], A. COLOMBINI[1], M. MARIOTTI[1,2] and G. BANFI[1,2]

[1]I.R.C.C.S. Orthopedic Institute Galeazzi, Milan, Italy;
[2]School of Medicine, University of Milan, Milan, Italy

Received October 12, 2011 – Accepted December 12, 2011

Bone mass is the net product of formation and resorption, which are closely regulated by the equilibrium between endogenous/exogenous factors. Sclerostin inhibits the Wnt canonical signaling and is considered an anti-anabolic factor. We compared sclerostin serum concentrations between genders in athletes belonging to different sport disciplines, characterized by a different weight-bearing, and in their sedentary counterparts in order to study the possible link between bone metabolism in athletes and its peripheral concentration. We also compared sclerostin levels with bone alkaline phosphatase activity, a marker of bone formation. Sixty-one elite athletes, belonging to weight-bearing (15 male rugby players, 11 male enduro racers, 8 female basketball players), high-impact (6 male tennis players, 8 female ice skaters), non weight-bearing sports (13 male cyclists) and 16 sedentary controls were enrolled. Higher levels of sclerostin were found in females. Sclerostin was higher in weight-bearing than in non-weight-bearing disciplines in males. Significant inverse age-related correlation was found. Higher bone alkaline phosphatase activity was observed in females. The young adult elite athlete represents a peculiar physiologic model for studying sclerostin behavior: the applied load increased the marker concentrations, testifying a high bone turnover rate; however, a gender effect is evident.

Bone mass can be considered as the product of two counteracting metabolic processes, formation and resorption, which are closely regulated by the relative equilibrium between endogenous (i.e., hormones, growth factors and cytokines) and exogenous (mechanical loading) factors (1). The importance of mechanical stress in maintaining the balance between bone formation and resorption becomes evident during weightlessness and prolonged bed rest, when rapid bone loss occurs. Road cycling has also a similar effect because of the type of forces exerted on the skeleton: bone resorption is reportedly increased in cyclists, at least transiently, while bone formation is not modified (2).

Several blood and urinary molecules have been proposed and introduced in diagnostics as markers of bone metabolic activity for evaluating the biological activities governing bone turnover, although they are characterized by high biological variability. Despite of the discrepant results reported by different studies, short exercise could not be able to modify serum concentrations of these markers. After prolonged training and competition, bone formation markers were changed in athletes as well as in sedentary trained subjects, whereas bone resorption markers were not modified. Moreover, the characteristics of exercise (i.e., weight-bearing, impact) are crucial

Key words: sclerostin, bone alkaline phosphatase, workload, sedentary, gender, young adults

Mailing address: Patrizia Lanteri, PhD
I.R.C.C.S. Istituto Ortopedico Galeazzi,
via R. Galeazzi, 4
20161, Milano, Italia
Tel: +39 0266214068
Fax: +39 0266214060
e-mail: patrizia.lanteri@grupposandonato.it

0393-974X (2012)

DISCLOSURE: ALL AUTHORS REPORT NO CONFLICTS OF INTEREST RELEVANT TO THIS ARTICLE.

in long term training for bone turnover (1). Thus, different levels of weight-bearing activities imply different levels of anabolic effects on skeletal tissue and alterations in bone turnover markers are useful for evaluating the impact of physical exercise on bone metabolism.

Formation markers are products of active osteoblasts released during different phases of development and measured in terms of concentration or enzymatic activity in serum. We have already demonstrated (3) that in a group of top-level female skiers, serum levels of formation markers, as bone-specific alkaline phosphatase (bone ALP) and osteocalcin (OC), and the resorption marker tartrate-resistant acid phosphatase (TRAP5b) activity, moved across the training year with a net significant increase during the more physically stressful competitive period (3).

Among these bone markers, sclerostin (SOST) has not yet been evaluated in athletes, nor has its physiology been deeply elucidated: a few papers have reported its concentration in pathologies (4-6). Only one paper concerning SOST physiology reports concentrations in children: higher levels in males are reported during puberty, whilst concentrations decreased in both sexes after puberty (7).

Sclerostin is a protein involved in the regulation of Wnt signaling, primarily expressed in bone tissue, predominantly by osteocytes and premature osteoclasts (8). This molecule potently inhibits the Wnt canonical signaling by binding the low-density lipoprotein receptor-related protein 5 (LRP5) receptor (9, 10) and it is believed to act through the thick network of osteocyte canaliculi to reach the surface of bone, where the target cells, the osteoblasts, are resident (11). The localization of osteocytes can affect the production of sclerostin: osteocytes closer to the surface, that probably undergo a more intense mechanical stimulation, are more often sclerostin-negative than the deeper osteocytes (11). In order to study the physiology of this molecule, we compared the serum concentrations of sclerostin and bone ALP in female and male athletes practicing different sport disciplines, characterized by different levels of load, and in sedentary controls. Furthermore, we compared sclerostin levels and bone ALP activity, in order to verify a correlation.

MATERIALS AND METHODS

Study population

A total number of 77 subjects were recruited for this study. An informed consent was obtained from each subject according to international standards and following the ethical standards reported in the paper of Harriss and Atkinson (12). The study was approved by the local Ethics Committee.

All subjects were submitted to venous blood sampling and physician examination to evaluate healthy status. Either endocrine or metabolic disorders and recent bone fractures (not less than 1 year) were the exclusion criteria. Noteworthy, all athletes were tested at the end of the relative rest period, before the starting of the training and competitive season.

The recruited professional athletes (mean age: 27.2±6.8 years) were: 15 males from the Italian national rugby team (29.1±1.7 years), 13 males from a professional cycling team (31.1±2.7 years), 6 professional male tennis players (23.2±6.2), 11 males from a professional enduro motorcycling team (29.1±11.8 years), 8 professional female basketball players belonging to a first Italian league division team (27.0±3.0 years) and 8 female figure ice skaters from the Italian national team (19.5±4.9 years). Different sports were classified into three categories based on the exerted work-load, as already defined (1): weight-bearing (WB: basket, enduro and rugby), non-weight-bearing (NWB: cycling) and high impact sports (HI: ice skating, owing to jumps, and tennis, owing to the high impact with the ground).

A cohort of 16 non-athletic age-matched control subjects (8 males and 8 females, mean age 26.6±4.21 years) were also recruited, none of whom practiced physical activity for more than 3 hours per week.

Blood sampling

Blood samples were taken by standard antecubital venipuncture after overnight fasting from subjects in sitting position, after 10 minutes resting, in plain tubes (SST™ II Advance, BD Vacutainer, Becton Dickinson, Franklin Lakes, NJ, USA). Blood samples were kept at rest for 30 minutes, allowing them to clot, centrifuged at 1200 g for 10 minutes at 4°C, aliquoted and immediately stored at -80°C until assayed.

Biochemical assays

Serum SOST levels were assayed through an ELISA test (TECO® Sclerostin, TECO*medical* Group, Sissach, Switzerland), according to the manufacturer's specifications. Absorbance reading was performed at λ= 450nm, while reference reading was set at λ= 620nm. Each sample was evaluated in duplicate. The detection

limit of the test was < 0.13 ng/mL. Maximum intra- and inter-assay CVs were 6.0 and 7.0%, respectively.

Serum activity of bone ALP were measured with a Metra® BAP EIA Kit (Quidel Corporation, San Diego, CA, USA), according to the manufacturer's specifications. Absorbance reading was performed at λ= 405nm. Each sample was evaluated in duplicate. Intra- and inter-assay CVs were 3.9 and 7.6%, respectively, and the detection limit of the test was < 0.7 U/L. Absorbance readings were performed with Victor X³ (PerkinElmer Inc., Waltham, MA, USA).

Statistical analysis

All values were expressed as mean ± SD: paired comparisons males/females and athletes/sedentaries were performed by Mann-Whitney test. Comparisons between different sports or classes of sports were performed by Kruskal-Wallis test. Correlations were assayed by Spearman's coefficient of rank correlation. Parametric or non-parametric test were used on the basis of normal or non-normal distribution within the different cohorts. Statistical analyses were performed with GraphPad Prism v5.00 program (GraphPad software, USA).

RESULTS

Mean sclerostin serum levels were the same for the whole population, athletes and sedentaries (0.42±0.09 ng/mL). No significant differences were found comparing these groups. Significant inverse age-related correlation (p=0.0037; r=-0.34) was found between age and sclerostin levels. Concentrations of sclerostin were significantly different within the whole cohort of males and females (0.40±0.09ng/mL and 0.45±0.07ng/mL, respectively) (p=0139) and sedentaries (males: 0.36±0.05ng/mL; females: 0.46±0.09ng/mL) (p=0.0378). However, no differences were found among genders in athletes (males: 0.41±0.09ng/mL, females: 0.45±0.07ng/mL).

No differences were found within the female cohort by comparing athletes' values of different

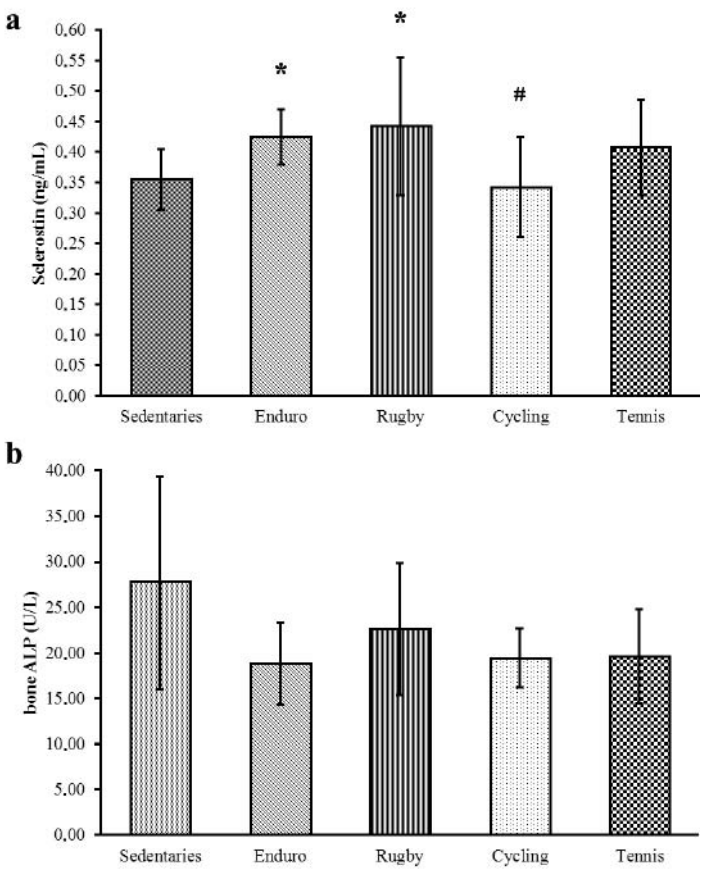

Fig. 1. *Differences in serum sclerostin concentrations (**a**) and bone ALP activity (**b**) within the male cohort. Data are reported as mean ± SD. Bars bearing different symbols in apex are significantly diffe*

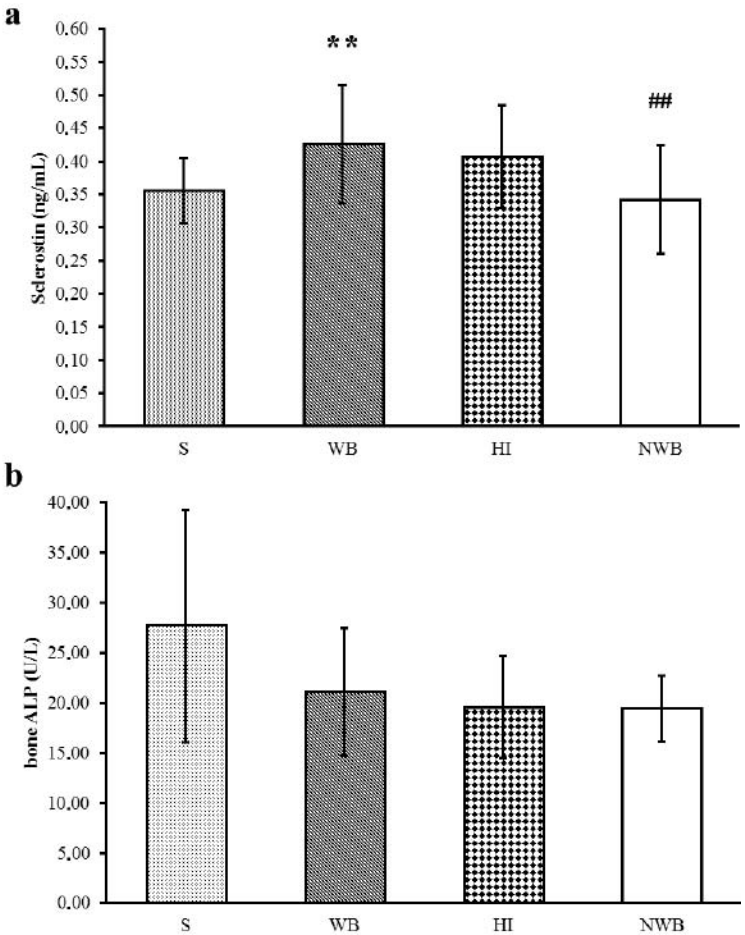

Fig. 2. *Differences in serum sclerostin concentrations (**a**) and bone ALP activity (**b**) within the male sport categories. Data are reported as mean ± SD. Bars bearing different symbols in apex are significantly different (p<0.005). S: sedentaries; WB: weight-bearing sports; HI: high impact sports; NWB: non-weight-bearing sports rent (p<0.05).*

sports and by comparing athletes' values with those of the sedentary group. On the contrary, differences were observed analyzing the male cohort: sclerostin concentrations of enduro athletes (0.42±0.04ng/mL) and rugby players (0.44±0.11ng/mL) were significantly higher than those of cyclists (0.34±0.08ng/mL) (Fig. 1a; p=0.0057).

Furthermore, we did not observe a correlation between serum sclerostin concentrations and sport category in female athletes while, in males, sclerostin concentrations in WB sports were significantly higher (0.43±0.0 ng/mL) than in NWB sport (0.34 ± 0.08ng/mL) (Fig. 2a; p=0.0024). No significant differences were observed among these two categories and HI sports or non-athletes.

Mean serum bone ALP activity was: 22.8±7.8U/L in the whole population, 22.4±7.6U/L in athletes and 24.3±8.5U/L in sedentaries. No significant differences were found comparing these groups, nor was significant correlation found between age and bone ALP activities.

Bone ALP activity was significantly different within the whole cohort of males and females (21.3±6.8U/L and 26.1±8.8U/L, respectively) (p=0.0030) and athletes (males: 20.4±5.5U/L; females: 28.4±9.8U/L) (p=0.0005). However, no differences were found between sedentary males (27.7±11.6U/L) and females (21.7±4.6U/L). No differences were found comparing different groups of the female cohort, nor comparing male bone

ALP values of different sports (Fig. 1b) or between sport category in male athletes (Fig. 2b). Significant inverse correlation (p=0.0458; r=-0.7) was found between sclerostin and bone ALP activity, but only in sedentary females.

DISCUSSION

Literature lacks studies on the *in vivo* behavior of sclerostin, particularly regarding its concentrations in different sport disciplines or physical activities that can be assumed as different prototypes of physiological workload (1). Indeed, we did not find any report on sclerostin concentrations in athletes: the physiology of this protein is not well known, despite some reviews concerning this protein; moreover, few studies concerning its behaviour in pathologies have been published (4-6). *In vitro* studies demonstrated that sclerostin is a potent Wnt antagonist and, thus, it is a mediator of the bone formation cascade (9, 10). In this study, we compared Sclerostin serum concentrations between genders in different sport disciplines, using as study models cohorts of young (mean age: 27.2±6.83 years) and healthy subjects of both genders. Moreover, we measured bone ALP activity in the same subjects to discover whether they correlate with those of sclerostin.

A major distinction between sports disciplines could be based on load or impact. Actually, cycling is commonly considered a non-weight-bearing discipline: thus, cyclists have a lower bone mineral density (BMD) than runners (2). Male athletes engaged in rugby, soccer and martial arts have higher BMD than other practicing non-weight-bearing disciplines (13). Differences between sport disciplines also depend on impacts and jumps: female athletes practicing impact sports (i.e., volleyball) have higher BMD and osteocalcin concentration than swimmers (14). An increased BMD in comparison to controls has been described also in ice skaters (15), as well as in tennis players (16).

No data exist on enduro motorcyclists. Noteworthy, these athletes are typically submitted for lengthy times, i.e., 10-12 hours per day, during competitions, and 2-3 hours per day during training, to strong mechanical stress and vibrations, due to the continuous impacts with the rambling ground, transmitted to legs and back throughout the motorcycle, possibly affecting the bone metabolism homeostasis.

Significant correlation was found in our population between age and sclerostin concentrations; besides, there were evident differences between genders: serum sclerostin significantly differed between the whole cohort of males and females, as well as between sedentary males and females. Even among male and female athletes a trend in sclerostin levels was found, but in this case it was not significant.

All the athletes were tested at the end of the specific relative rest period, before the starting of training and competitive season because, as previously reported (3), bone marker concentrations are affected by the timing of sampling during the sport season. Thus, we recruited athletes during the resting period, when only the consolidated bony effects of the past training and competition period were stabilized, allowing the comparison with non-athletes.

Despite the lack of differences within the different categories of female athletes and between these athletes and their sedentary counterparts, we observed significant differences within the male cohort. When compared with cyclists, higher values of sclerostin in enduro racers and rugby players were found, while there were no differences in comparison with tennis players and sedentaries. Moreover, the sport disciplines characterized by WB sports were linked to significantly higher levels of sclerostin compared to NWB sports.

As previously reported, exercise influences bone turnover (3). Therefore, we evaluated bone ALP levels in all the subjects who were submitted to the sclerostin measurement. Although significant correlation between age and bone ALP was not found, there were differences between genders: bone ALP significantly differed between the whole cohort of males and females, as well as between male and female athletes.

However, no differences were found in any other comparison. Finally, we correlated sclerostin and bone ALP levels: a significant inverse correlation was found only in the sedentary females; current researches are investigating this finding.

The main remark of this study resides in the report of results very different from those already published (4-6), where higher levels of sclerostin

were found in females and in conditions of bone stasis. However, we studied a completely different physiological model: young athletes and sedentaries instead of postmenopausal women and/or immobilized subjects. The increased sclerostin levels in females could be correlated with the estrogen concentrations. Possibly, the slight sclerostin increase in basal values reported in women is related to age, while we recruited females younger than those previously studied. Moreover, we outline that in properly-trained athletes the applied load increased the marker concentrations, probably induced by a higher bone turnover (3). In athletes, a confounding effect may derive from the type of sport (i.e., high impact) performed by females. It could be suggested that the combination of young age and high impact exercise in women enhances sclerostin release.

We can finally speculate that a kind of feedback regulation exists, although the serum concentrations of sclerostin should not completely represent its local concentration and activity in bone. When the loading stimulus exceeds the threshold, the anabolic response in the bone is slowed down throughout the increase of anti-anabolic factors, i.e., sclerostin. To better clarify the physiology of this marker, our studies are currently proceeding to define the molecular mechanisms regulating this putative feedback pathway.

ACKNOWLEDGEMENTS

The authors are indebted with Dr. Alessandro Degrate for his help in statistical analysis.

This work was funded by the Italian Ministry of Health.

REFERENCES

1. Banfi G, Lombardi G, Colombini A, Lippi G. Bone metabolism markers in sports medicine. Sports Med 2010; 40:697-714.
2. Rector RS, Rogers R, Ruebel M, Hinton PS. Participation in road cycling *vs* running is associated with lower bone mineral density in men. Metabolism 2008; 57:226-32.
3. Lombardi G, Colombini A, Freschi M, Tavana R, Banfi G. Seasonal variation of bone turnover markers in top-level female skiers. Eur J Appl Physiol 2011; 111(3):433-40.
4. Gaudio A, Pennisi P, Bratengeier C, et al. Increased sclerostin serum levels associated with bone formation and resorption markers in patients with immobilization-induced bone loss. J Clin Endocrinol Metab 2010; 95(5):2248-53.
5. Mirza FS, Padhi ID, Raisz LG, Lorenzo JA. Serum sclerostin levels negatively correlate with parathyroid hormone levels and free estrogen index in postmenopausal women. J Clin Endocrinol Metab 2010; 95(4):1991-7.
6. Modder UI, Hoey KA, Amin S, McCready LK, Achenbach SJ, Riggs BL, Melton LJ, 3rd, Khosla S. Relation of age, gender, and bone mass to circulating sclerostin levels in women and men. J Bone Miner Res. 2011; 26(2):373-9.
7. Kirmani S, Amin S, McCready LK, Atkinson EJ, Melton LJ, 3rd, Muller R, Khosla S. Sclerostin levels during growth in children. Osteoporos Int 2011; 23(3):1123-30.
8. Hoeppner LH, Secreto FJ, Westendorf JJ. Wnt signaling as a therapeutic target for bone diseases. Expert Opin Ther Targets 2009; 13(4):485-96.
9. Li X, Zhang Y, Kang H, Liu W, Liu P, Zhang J, Harris SE, Wu D. Sclerostin binds to LRP5/6 and antagonizes canonical Wnt signaling. J Biol Chem 2005; 80(20):19883-7.
10. Veverka V, Henry AJ, Slocombe PM, et al. Characterization of the structural features and interactions of sclerostin: molecular insight into a key regulator of Wnt-mediated bone formation. J Biol Chem 2009; 284(16):10890-900.
11. Poole KE, van Bezooijen RL, Loveridge N, Hamersma H, Papapoulos SE, Lowik CW, Reeve J. Sclerostin is a delayed secreted product of osteocytes that inhibits bone formation. FASEB J 2005; 19(13):1842-4.
12. Harriss DJ, Atkinson G. International Journal of Sports Medicine - ethical standards in sport and exercise science research. Int J Sports Med 2009; 30(10):701-2.
13. Morel J, Combe B, Francisco J, Bernard J. Bone mineral density of 704 amateur sportsmen involved in different physical activities. Osteoporos Int 2001; 12(2):152-7.

14. Creighton DL, Morgan AL, Boardley D, Brolinson PG. Weight-bearing exercise and markers of bone turnover in female athletes. J Appl Physiol 2001; 90(2):565-70.
15. Oleson CV, Busconi BD, Baran DT. Bone density in competitive figure skaters. Arch Phys Med Rehabil 2002; 83(1):122-8.
16. Ducher G, Tournaire N, Meddahi-Pelle A, Benhamou CL, Courteix D. Short-term and long-term site-specific effects of tennis playing on trabecular and cortical bone at the distal radius. J Bone Miner Metab 2006; 24(6):484-90.

ERRATA CORRIGE

JBRHA Vol. 25 No. 4.
Page 603. M. Dipalma should read G. Dipalma.